Relationship Between Body Surface Potential Maps and Atrial Electrograms in Patients with Atrial Fibrillation

Marjan Bojarnejad

23th August 2013

Supervisors:

Dr. Philip Langley, Dr James Blake, Dr. John Bourke, Prof. Alan Murray

Department of Medical Physics

Institute of Cellular Medicine, Faculty of Medical Sciences

Newcastle University

Registration Date: 19th November 2009

Degree: PhD

Declaration

I declare that this thesis has been written by me and has not been submitted or accepted for any other degree. Except where specifically acknowledged, the data were collected, analysed and interpreted by myself.

Marjan Bojarnejad

Contents

List of Figures

List of Tables

Abbreviations and Notations

AA	Atrial Activity
ABS	Average Beat Subtraction
ACC	American College of Cardiology
ACL	Anterior Central Left
ACR	Anterior Central Right
AF	Atrial Fibrillation
AHA	American Heart Association
ALL	Anterior Lateral Left
ALR	Anterior Lateral Right
ANOVA	Analysis of Variance
AP	Action Potential
ASCII	American Standard Code for Information Interchange
AT	Atrial Tachycardia
AU	Arbitrary Unit
AV	Atrioventricular
BMI	Body Mass Index
BSPM	Body Surface Potential Map
BSS	Blind Source Separation
CFAE	Complex Fractionated Atrial Electrogram
CI	Confidence Interval
CL	Cycle Length
CS	Coronary Sinus
DC	Direct Current
DF	Dominant Frequency
ECG	Electrocardiogram
EGM	Electrogram
EP	Electrophysiology
ESC	European Society of Cardiology
ICA	Independent Component Analysis
IIR	Infinite Impulse Response
IQR	Inter-Quartile Range
IVC	Inferior Vena Cava
kΩ	Kilo-Ohm
LA	Left Atrium
LAr	Left Arm
LAA	Left Atrium Activity
LL	Left Leg
LOA	Limits of Agreement
LSB	Least Significant Bit
LSD	Least Significant Difference
LV	Left Ventricle
MAW	Main Atrial Wave
MCL	Mean Cycle Length
ms	Milliseconds

mV	Millivolts
N.S.	No Statistically Significant Difference
PCA	Principal Component Analysis
PCL	Posterior Central Left
PCR	Posterior Central Right
PLL	Posterior Lateral Left
PLR	Posterior Lateral Right
PSD	Power Spectral Density
PVs	Pulmonary Veins
RA	Right Atrium
RAr	Right Arm
RAA	Right Atrium Activity
RF	Radiofrequency
RL	Right Leg
RMSE	Root Mean Square Error
RV	Right Ventricle
SA	Sinoatrial
SampEn	Sample Entropy
SC	Spectral Concentration
SD	Standard Deviation
SR	Sinus Rhythm
SVC	Superior Vena Cava
VA	Ventricular Activity
WCT	Wilson Central Terminal
F_r	Frequency Resolution
F_{S-B}	BSPM Sampling Frequency
F_{S-E}	EGM Sampling Frequency
F_s	Sampling Frequency
H_0	Null Hypothesis
H_1	Alternative Hypothesis
β_0	Intercept of a Linear Fit
β_1	Slope of a Linear Fit
t_E	Time of the EGM Signal
t_B	Time of the BSPM Signal
δt	Time Difference Between the BSPM and EGM Recording
s	Scaling Parameter to Adjust BSPM and EGM Recording Systems Different Clock Speed
E	Lead I Signal from the EP Recording System
B	Lead I Signal from the BSPM Recording System
ϵ	Sum of Squares Differences
R	Temporal Location of the R-waves
t_1	Start of the Q-wave
t_2	End of the T-wave
TQ	Segment Between End of the T-wave and Start of the Q-wave of Neighbouring Beats
$\tilde{q}$	Average QRST Window Morphology
q_j	j^{th} QRST Window Within Two Minute BSPM Recording

y	A Sinusoidal Model
A	Amplitude of the Sinusoidal Model
T	Period (Inverse of the Sampling Frequency)
t	Time of the BSPM Signal
y^M	Sinusoidal Model Response
M	Number of Samples Within the Frequency Band of Interest
P	EGM DF Power Distribution on Body Surface Spectra
P_{CS}	CS DF Power
P_{PVAC}	PVAC DF Power
f_{EGM}	EGM DF
f_{BSPM}	BSPM DF
PSD_{BSPM}	BSPM Spectrum
PSD_{EGM}	EGM Spectrum
r	Pearson Correlation Coefficient
R^2	Coefficient of Determination

Acknowledgement

I would like to express my gratitude to Dr Philip Langley for his valuable advice and guide on my research work and also on presenting this thesis. I would like to thank Professor Alan Murray for his advice on how to present scientific research. Thanks to Dr John Burke and Dr Ian Shepherd for kindly helping me on data collection. Warmest thanks to Dr James Blake for his encouragement, supervision on computer programming, and advice on scientific research.

Thanks to Dr Jim Lloyd and Professor Azfar Zaman who assessed my progress and gave me their scientific comments to construct this work. Special thanks to Dr Chris Ward, and Dr Alison Tyson-Capper for their kind advice and support. Sincere thanks to the many volunteers from the Freeman Hospital who kindly participated in this work in the name of science. Also thanks to all the staff in the Regional Medical Physics Department, Cardiology Ward, and Electrophysiology Laboratory in particular Donald Greenhalgh and Susan King.

I would like to express my most special thanks to my dearest parents in Iran for their love and support. I deeply regret that I could not share this proud moment of accomplishing this scientific work with my late father. I am honoured to dedicate this work to the best parents in the world my mother and my late father, and to my sisters Maryam and Elham, and my brother Mohsen.

Friends who I will remember; Robberto Giovannini, Dr Luigi Di Marco, Dr Dingchang Wang, Costanzo Di Maria, Dr Alison Bray, Dr Wengfeng Duan, Dr Kun Wang, Philip McGonigle, Danielle Giacopelli, Dr Svetlin Nedkov Tsonev, Dr Ghazaleh Hosseini, Shina Cheraghi, Mehrnoosh Atashbiz, Kave Farahmand, Dr Amin Rezaienia, Dr Nima Sattari, Aida Nabi, Dr Nushin Moharami, Dr Dena Ghiyasi, Shirin Pourhasan, Dr Parisa Javadian, Maryam Saghafi, Dr Elmira Jalilian, Dr Sadaf Atarod, Dr Shirin Amirian, Dr Somaye Mohammadi, Dr Kamyar Mehran, Dr Amin Gangian, Dr Kianoush Nazarpour, Dr Amir Enshaie, Hossein Tasadogh, Omid Sayadi, Dr Kambiz Faramarz and Dr Ali Shariat.

Last but not least, very special thank to Dr Gavin Venchard for his invaluable support and help.

Publications

- *Bojarnejad M.*, Blake J., Bourke J., Murray A., Langley P., (2013). Comparison of body surface and intracardiac ECG recordings in patients with atrial fibrillation during electrophysiological studies. IFMBE Proceedings; 39: 612-615.

- *Bojarnejad M.*, Blake J., Bourke J., Murray A., Langley P., (2012). Comparing power spectral density of 64 channel surface ECG with left atrium electrogram in patients in atrial fibrillation. Computing in Cardiology; 39: 713-716.

- *Bojarnejad M.*, Blake J., Bourke J., Murray A., Langley P., (2011). Atrial fibrillation dominant frequency changes during ablation. Computing in Cardiology; 38: 185−188.

- Di Maria C., Duan W., *Bojarnejad M.*, Pan F., King S., Zheng D., Murray A., Langley P., (2013). An algorithm for the analysis of foetal ECG from 4-channel non-invasive abdominal recordings. Computing in Cardiology.

- Langley P., Di Marco L.Y., King S., Duncan D., Di Maria C., Duan W., *Bojarnejad M.*, Zheng D., Allen J., Murray A., (2011). An algorithm for assessment of quality of ECGs acquired via mobile telephones. Computing in Cardiology; 38: 281−284.

- Langley P., King S., Wang K., Zheng D., Giovannini R., *Bojarnejad M.*, Murray A., (2010). Estimation of missing data in multi-channel physiological time-series by average substitution with timing from a reference channel. Computing in Cardiology; 37: 309−312.

Abstract

Atrial fibrillation (AF) is the most common cardiac arrhythmia. It is distinguished by fibrillating or trembling of the atrial muscle instead of normal contraction. Patients in AF have a much higher risk of stroke. AF is often driven by the left atrium (LA) and the diagnosis of AF is normally made from lead V1 in a 12-lead electrocardiogram (ECG). However, lead V1 is dominated by right atrial activity due to its proximal location to the right atrium (RA). Consequently it is not well understood how electrical activity from the LA contributes to the ECG. Studies of the AF mechanisms from the LA are typically based on invasive recording techniques. From a clinical point of view it is highly desirable to have an alternative, non-invasive characterisation of AF.

The aim of this study was to investigate how the LA electrical activity was expressed on the body surface, and if it could be observed preferentially in different sites on the body surface. For this purpose, electrical activity of the heart from 20 patients in AF were recorded simultaneously using 64-lead body surface potential mapping (BSPM) and bipolar 10-electrode catheters located in the LA and coronary sinus (CS). Established AF characteristics such as amplitude, dominant frequency (DF) and spectral concentration (SC) were estimated and analysed. Furthermore, two novel AF characteristics (intracardiac DF power distribution, and body surface spectral peak type) were proposed to investigate the relationship between the BSPM and electrogram (EGM) recordings.

The results showed that although in individual patients there were body surface sites that preferentially represented the AF characteristics estimated from the LA, those sites were not consistent across all patients. It was found

that the left atrial activity could be detected in all body surface sites such that all sites had a dominant or non-dominant spectral peak corresponding to EGM DF. However, overall the results suggested that body surface site 22 (close to lead V1) was more closely representative of the CS activity, and site 49 (close to the posterior lower central right) was more closely representative of the left atrial activity. There was evidence of more accurate estimation of AF characteristics using additional electrodes to lead V1.

Structure of the Thesis

This doctoral thesis focuses on comparing the body surface potential maps (BSPM) and atrial electrograms (EGM) in patients with atrial fibrillation (AF). The presentation of this work is structured as shown below.

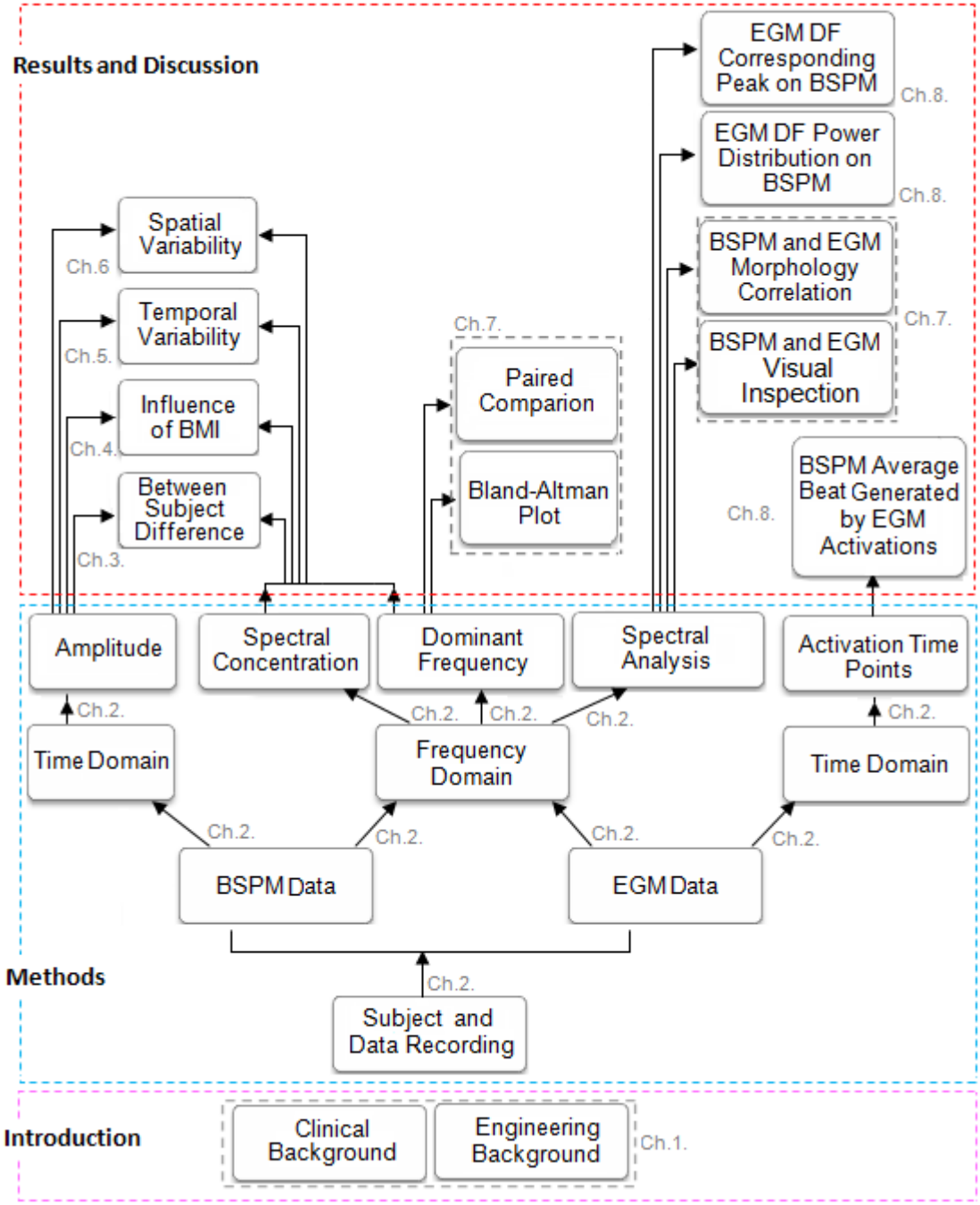

Figure i. A schematic representation of the thesis outline. The chapter (ch) number are identified for each analysis. The pink box represents introduction (Chapter 1), the blue box represents methods (Chapter 2), and the red box represents results and discussion (Chapter 3 to Chapter 8).

This thesis is comprised of four main parts of introduction, methods, results and discussion, and conclusion which are presented in nine chapters:

Introduction (Chapter 1): This chapter provides a clinical background of the heart and atrial fibrillation, as well as a review of the current signal processing 'state of the art' from which the methods used in this work are advanced.

Methods (Chapter 2): This chapter describes the body surface and intracardiac recording equipment, patient recruitment, data collection, signal processing and statistical methods. In the signal processing section, characterisation of the atrial activity from the body surface and intracardiac recordings are performed in two domains: time and frequency. AF amplitude from the body surface recordings and atrial activation time points from the intracardiac recordings are estimated in the time domain. Spectral analysis, and estimation of dominant frequency (DF) and spectral concentration (SC) are performed in the frequency domain. Moreover, in this chapter two novel AF characteristics for examining the body surface and intracardiac recordings are described.

Results and Discussion (Chapter 3 to Chapter 8): In these chapters the AF characteristics estimated from the body surface and intracardiac recordings are analysed and compared, and the results are discussed. In chapters 3, 4, 5, and 6, the data analysis is performed with limited aims to provide overview of the data. The intention at the end of each chapter is to find the linear relationship between the body surface and intracardiac recordings between subjects using selected body surface sites and/or using the median across the body surface sites for the characteristics of interest. In chapters 7 and 8, the body surface and intracardiac recordings are compared in more detail at individual body surface site with different approaches.

Chapter 3 focuses on between subject differences in the AF characteristics estimated from the body surface (AF amplitude, DF and SC) and inside the heart (DF and SC). Moreover, the linear relationships between subjects are investigated linking body surface and intracardiac DF and SC.

Chapter 4 focuses on the influence of subject BMI on the AF characteristics estimated from the body surface recordings. It also investigates whether there is a relationship between subject BMI and the differences in the AF characteristics estimated from the body surface and inside the heart.

Chapter 5 focuses on the temporal variability of the AF characteristics during the two minute recordings to assess repeatability over this duration of recording. Moreover, the linear relationship between temporal variability estimated from the body surface and intracardiac recordings are studied for AF characteristics.

Chapter 6 focuses on the spatial variability of the AF characteristics across the 64 body surface sites, and at different groups of electrode sites. It also explores the spatial variability of the AF characteristics along the CS and PVAC catheters sites. Moreover, the linear relationship between all body surface sites and selected intracardiac sites are investigated across all subjects.

Chapter 7 then provides a more detailed comparison of individual body surface and intracardiac spectra using five approaches: visual interpretation; spectral morphology correlation; comparison using Bland-Altman plot; paired comparison of DF at individual sites; paired comparison of DF at the body surface site with the largest SC.

Chapter 8 focuses on the comparison of the body surface and intracardiac recordings using novel methods previously not presented in the literature. Firstly, quantifying the intracardiac DF power distribution on the body surface spectra. Secondly, specifying the body surface spectral peak corresponding to the intracardiac DF. Thirdly, identifying any distinct F-wave on the AF segment corresponding to intracardiac atrial activity.

Conclusion (Chapter 9): In this chapter the main scientific contributions of this work are summarised.

Results Summary

Differences in Atrial Fibrillation Characteristics Between Subjects (Chapter 3):

1. Atrial Fibrillation (AF) characteristics estimated from the body surface and inside the heart were significantly different between subjects ($p<0.001$).

   From the body surface:

   - Median amplitude ranged from 19.2 µV (subject 18) to 90.0 µV (subject 3) with median and inter-quartile range (IQR) of 35.9 (21.0 – 57.3) µV across subjects.
   - Median dominant frequency (DF) ranged from 4.1 Hz (subject 12) to 7.5 Hz (subject 11) with median and IQR of 5.9 (5.1– 6.2) Hz across subjects.
   - Median spectral concentration (SC) ranged from 19.0 % (subject 13) to 60.5 % (subject 3) with median and IQR of 31.0 (27.8 – 43.8) % across subjects.

   From inside the heart:

   - Median DF estimated from the coronary sinus (CS) ranged from 4.3 Hz (subject 9) to 7.1 Hz (subjects 5 and 7) with median and IQR of 5.9 (5.1– 6.4) Hz across subjects.
   - Median DF estimated from the pulmonary vein ablation catheter (PVAC) ranged from 4.3 Hz (subject 18) to 7.1 Hz (subjects 7) with median and IQR of 5.6 (5.1– 6.0) Hz across subjects.
   - Median SC estimated from CS ranged from 21.1 % (subject 9) to 86.0 % (subjects 3) with median and IQR of 47.5 (39.5 – 56.8) % across subjects.
   - Median SC estimated from PVAC ranged from 36.3% (subject 18) to 90.0% (subject 3) with median and IQR of 63.0 (53.3 – 70.0) % across subjects.

2. There was a strong positive linear relationship between DF of the body surface and CS ($p<0.001$, R^2 = 54.3%), and between DF of the body surface and PVAC ($p<0.001$, R^2= 70.1%).

3. There was a positive but weak linear relationship between SC of the body surface and CS ($p=0.004$, R^2= 38.4%), and between SC of the body surface and PVAC ($p=0.006$, R^2= 35.0%).

Effect of Body Mass Index on Atrial Fibrillation Characteristics (Chapter 4):

1. Body surface amplitude was negatively correlated to BMI ($p=0.043$, R^2= 20.2%).

2. Body surface DF was positively correlated to BMI ($p=0.046$, R^2= 20.0%).

3. The DF difference (BSPM site 22 - EGM) was negatively correlated to BMI (p=0.022 BSPM vs. CS, and p=0.019 BSPM vs. PVAC), with R^2 =30.0 %.

4. There was no correlation between SC estimated from either the body surface or inside the heart and BMI ($p>0.05$, R^2= 9.0%).

Temporal Variability of Atrial Fibrillation Characteristics (Chapter 5):

1. AF characteristics estimated from the body surface and from inside the heart did not change significantly over the two minute recordings ($p>0.05$).

2. There was no evidence that subjects with the large AF amplitude and high SC had more stable amplitude over the two minute recordings.

3. There was no evidence that subjects with the small DF had more stable DF over the two minute recordings.

4. There was no correlation between DF temporal changes estimated from the body surface or from inside the heart ($p>0.05$, R^2= 3.0%).

5. There was no correlation between SC temporal changes estimated from the body surface or from inside the heart ($p>0.05$, R^2= 16.2%).

Spatial Variability of Atrial Fibrillation Characteristics (Chapter 6):

1. AF characteristics exhibited significant differences between body surface sites ($p<0.001$).

    - Median amplitude ranged from 21.8 µV (site 60) to 77.4 µV (site 22), with median and IQR of 34.4 (29.2– 44.9) µV across the sites.
    - Median DF ranged from 5.5 Hz (site 45) to 6.1 Hz (site 22), with median and IQR of 5.6 (5.3 – 6.0) Hz across the sites.
    - Median SC ranged from 22.0 % (site 5) to 44.5 % (site 23) with median and IQR of 31.0 (28.5 – 36.0) % across the sites.
    - AF amplitude estimated from the body surface changed significantly (least significant $p=0.001$) between the anterior and posterior (22.1 µV), left and right (8.0 µV), vertical electrode lines (35.4 µV), and horizontal electrode lines (78.0 µV).
    - DF estimated from the body surface did not change significantly ($p>0.05$) between the anterior and posterior, left and right, or vertical electrode lines.
    - DF estimated from the body surface changed significantly between the horizontal electrode lines 4 and 8 which were the anterior central and anterior upper sites ($p=0.035$, 0.2 Hz), and also between lines 8 and 13 which were the anterior upper and posterior central sites ($p=0.032$, 0.3 Hz).
    - SC estimated from the body surface did not change significantly between the anterior and posterior, or between the horizontal electrode lines ($p>0.05$).
    - SC estimated from the body surface changed significantly between the left and right ($p=0.008$, 5.0 %), and between the vertical electrode lines ($p=0.008$, 14.8 %).
2. The anterior upper central right body surface sites had the largest amplitude, DF and SC.

3. DF estimated from inside the heart did not change significantly from any of the electrodes of the same catheter, either CS or PVAC ($p>0.05$). However, there was a significant difference in DF between the CS and

PVAC catheters ($p<0.001$, the median DF was 0.5 Hz greater in PVAC than CS).

4. SC estimated from inside the heart did not change significantly from any of the electrodes of the same catheter, either CS or PVAC ($p>0.05$). However, there was a significant difference in SC between the CS and PVAC catheters ($p<0.001$, the median SC was 21.5 % greater in PVAC than CS).

Relationship Between Frequencies Derived from Individual and Groups of Body Surface Sites and Those Derived from Intracardiac Sites (Chapter 7):

1. Visual comparison of frequency spectra estimated from the body surface and inside the heart showed that there was agreement between the spectral peaks which may or may not necessarily be the dominant one. In other words, the body surface sites may reflect all or some of the frequency components presented on the intracardiac spectrum.

2. Spectra from body surface sites close to the anterior upper central right and the posterior lower sites had highest morphology correlation (75.0 %) with the CS recordings.

3. Bland-Altman plot showed no significant differences between DF estimated from body surface and inside the heart ($P_{Trend} > 0.05$, limits of agreement (LOA) < 1.2 Hz).

4. There was no significant difference between paired comparisons of DF of each BSPM site with each EGM site.

5. There was no evidence that the body surface sites with the largest SC had closer DF to the intracardiac recordings.

Innovative Methods for Examining the Relationship Between Body Surface and Intracardiac Signals (Chapter 8):

1. The anterior upper body surface sites expressed the largest power at CS DF. Moreover, the posterior lower body surface sites expressed the largest power at PVAC DF.

2. DF estimated from inside the heart was likely to be seen as a dominant or non-dominant frequency peak on any of the body surface sites.

3. Visual comparison of the body surface average beat generated by the intracardiac activations showed morphology of the peak or trough on the majority of the sites. This may suggest that the EGM activations were consistent on each body surface site.

Chapter 1. Introduction

1.1. Clinical Background

1.1.1. The Heart

The heart consists of four chambers; the upper chamber on each side of the heart is called the atrium, which receives the blood coming to the heart. The atrium then delivers the blood to the powerful lower chamber on the same side, called the ventricle. The ventricle pumps the blood away from the heart through rhythmic contractions, see Figure 1. The right atrium (RA) receives de-oxygenated blood from the body and the right ventricle (RV) pumps it into the lungs to add oxygen and remove the carbon dioxide. The left atrium (LA) receives the oxygenated blood from the lungs. The left ventricle (LV) pumps fresh blood to the organs and tissues of the body and provides the oxygen and nutrients.

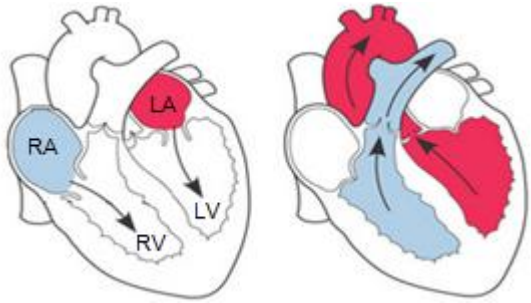

Figure 1. Mechanical function of the heart (Cardiac Health, 2009, [Online image]. Available from: http://www.cardiachealth.org).

The heartbeat consists of two stages, named systole and diastole. Systole is the stage when the ventricles are contracting and pump the blood out to the lungs and the rest of the body. Diastole is the stage when the ventricles are relaxed. During this stage, the atria are filled with blood and pass it into the ventricles. Oxygen-rich blood (arterial blood) flows from the heart to the body to

provide oxygen and nutrients. Oxygen-poor blood (venous blood) returns from the body to the heart. The blood then exchanges carbon dioxide with new oxygen in the lungs. The coronary sinus (CS) is a collection of veins joined together, which form a large vessel and collects blood from the heart muscle. It delivers this oxygen-poor blood to the RA, as do the superior and inferior vena cava (SVC, IVC). The pulmonary veins (PVs) are large blood vessels that carry oxygen-rich blood from the lungs to the LA of the heart, see Figure 2.

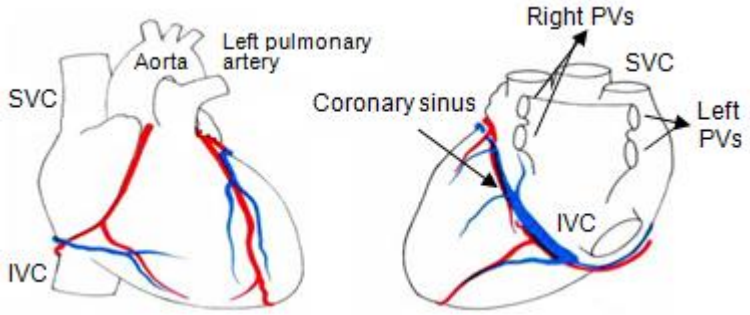

Figure 2. The coronary arteries and pulmonary veins. Red: oxygen-rich blood, and blue: oxygen-poor blood (Expressions in cardiology, 2011, [Online image]. Available from: http://www.dartmouth.edu).

The contraction of the heart as a whole is as a direct result of the systematic contraction of all of the microscopic cells of the heart muscle. The mechanical force (contraction) of the heart muscle cells is triggered by electrical impulses known as the action potentials (AP). A conduction system of specialized cells in the myocardium spreads an electrical impulse throughout the heart. The conduction system includes sinoatrial node (SA node), atrial internodal areas, atrioventricular node (AV node) and the bundle of His, which divides into left and right bundle branches made up of specialized cells called Purkinje fibres. The SA node normally acts as the essential cardiac pacemaker that spontaneously generates the AP. The AP travels through atrial muscle fibres to the AV node, then to the bundle of His and then the right and left

bundles made up of large Purkinje fibres. These specialised fibres rapidly conduct the impulse to the ordinary muscle cells resulting in fast and rhythmic simultaneous excitation of all ventricular cells. The speed with which an electrical impulse can be transmitted through excitable tissue is called the conduction velocity. The period of time during which the cardiac cell is unable to initiate another AP is called refractory period (RP), which typically is 250 ms in duration (Fagan, 2002). The AV node receives two inputs from the atria through two different pathways: anteriorly, which has a slow conduction velocity but shorter RP, and posteriorly, which has a faster conduction velocity but longer RP. Figure 3 shows the conduction pathway of the heart.

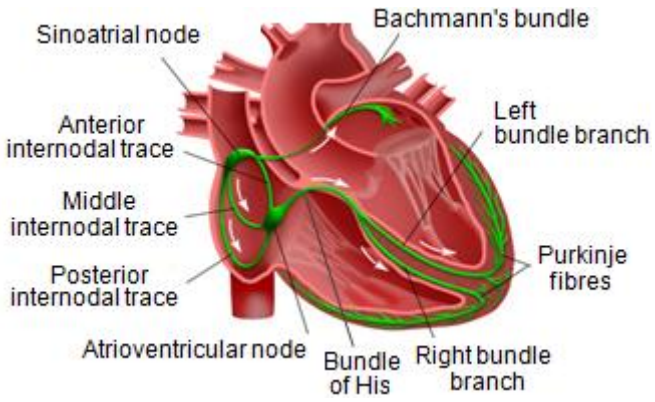

Figure 3. Conduction pathway of the heart. The white arrows demonstrate major electrical signal pathways (The Nebraska Medical Centre, ND, [Online image]. Available from: http://www.nebraskamed.com).

The electrical activity of the heart comes from the electrophysiology of single cells. At rest, the myocardial cell has a trans-membrane potential of about -80 to -90 mV. The cell membrane controls permeability to a number of ions, including sodium, potassium, calcium and chlorine. These ions pass across the membrane through specific channels that open and close in response to voltage changes. The variation of membrane conductance due to the opening and closing of ion channels generates changes in the AP over time (Wanger, 2008). An electrical impulse arriving at the cell allows positively

charged ions to cross the cell membrane causing depolarisation. The rapid depolarisation is caused by a transient fast increase in sodium channel conductance. The repolarisation occurs when potassium conductance increases. Calcium conductivity also contributes to the repolarisation of the cell and it is fundamental for the mechanism of muscle contraction. Therefore, both depolarisation and repolarisation of the myocardium are electrical phenomena caused by the movement of ions, see Figure 4.

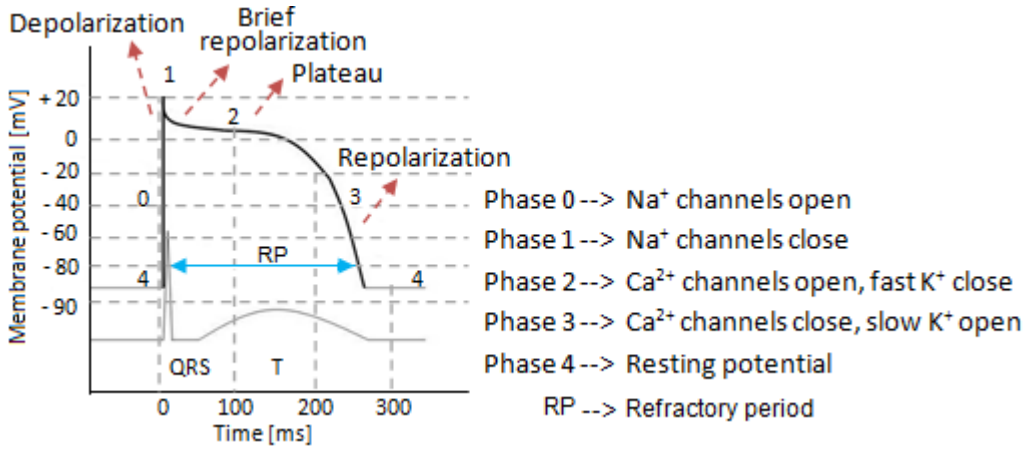

Figure 4. The action potential of a myocardial cell. In phase 0 a fast increase of sodium channel conductance causes the depolarisation. Then during plateau calcium ions enter and the contraction starts. Finally repolarisation is due to the exit of potassium ions. Cardiac action potential lasts 250 to 300 ms, which during this time the cell is unable to respond to new stimulations, known as refractory period.

As the body is conductive, the electrical activity of the heart can be detected, recorded, and interpreted from the skin surface. This can be performed through the use of sensitive monitoring equipment to obtain the Electrocardiogram (ECG). As shown in Figure 5, each heartbeat captured by the ECG signal during normal resting heart rate (known as sinus rhythm (SR)), consists of a P-wave (atrial activation), a QRS complex (contraction of the ventricles), and a T-wave (ventricular recovery). The conduction from the SA node in a wave travels downwards through both atria. This causes each cell to

depolarise in turn, and contracts the atria (the P-wave on the ECG). This conduction reaches the AV node and causes a delay in conducting the impulse from the atria to the ventricles. This delay allows the blood to fill the ventricles before they contract. The depolarisation travels down along the bundle of His. The left bundle branch is activated first, the depolarisation proceeds from left to right and gives rise to a small negative deflection on the ECG (the Q-wave). At the same time that the atria start to repolarise and relax, the wave of depolarisation continues down into the ventricular wall. The depolarisation takes place quickly and causes the ventricles to contract (the R-wave on the ECG). The RR interval is the distance between two following R-waves. The atria, AV nodal, and bundle of His are relaxed, and depolarisation ends with the S-wave on the ECG.

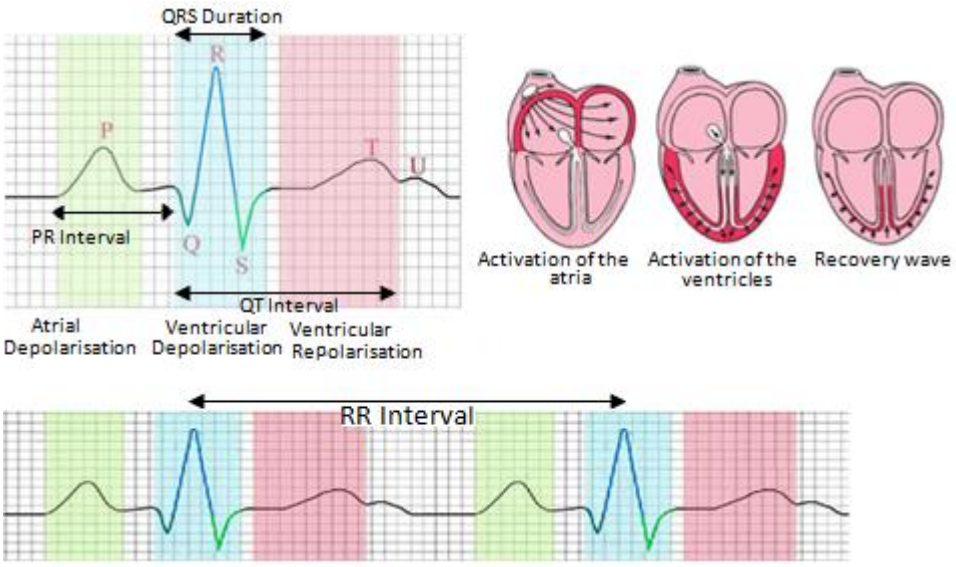

Figure 5. A presentation of an ECG. Typically the PR duration is 120-200 ms, the QRS duration is 120 ms, and the QT interval (or QRST) is up to 420 ms in heart rate of 60 beat per minute (IVLine, 2010, [Online image]. Available from: http://www.ivline.info).

The ST segment represents completed ventricular depolarisation as a plateau on the ECG, followed by a deflection in the same direction as depolarisation (T-wave) and represents the recovery of the ventricles. When the

heart has repolarised, the chambers are relaxed until the SA node triggers the start of the next heartbeat.

1.1.2. Atrial Fibrillation

Cardiac arrhythmia is a term for any condition in which there is abnormal electrical activity in the heart. The heartbeat may be too fast (tachycardia) or too slow (bradycardia), and may be regular or irregular. Atrial fibrillation (AF) is the most common cardiac arrhythmia, which is distinguished by fast and irregular electrical activity of the atria. Its name comes from the fibrillating or trembling of the atria muscle, instead of the normal contraction. In AF, control of the heart rhythm is taken away from the SA node by other electrical activities in different areas of the atria such as PVs (see Figure 6). Therefore, the ventricular rate during AF is no longer under physiological control of the SA node (Klabunde, 2005).

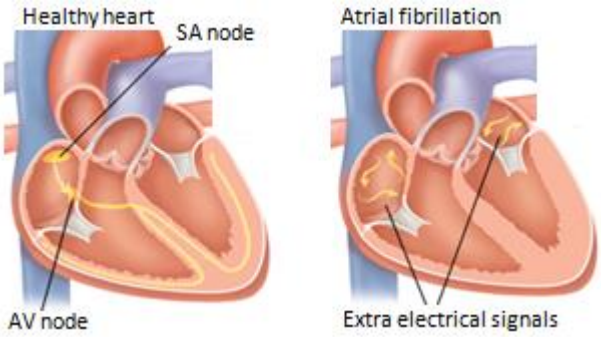

Figure 6. Simple illustration of electrical activities in the heart during AF (Harvard Medical School, 2013, [Online image]. Available from: http://www.patienteducationcenter.org).

Normally, the heart rate is adjusted to suit the body's metabolic needs through physiological control of the SA node, which is typically ranged from 60-80 beats per minute at rest. This can be increased to a typical maximum of 180–200 beats per minute to cope with the increased oxygen demands of peak exercise. In AF, the atria contract rapidly and irregularly typically ranged from

400-600 beats per minute. If each atrial impulse were conducted to the ventricles, the rapid ventricular rate would lead to ineffective cardiac contraction and death. In AF, the AV node limits the impulses that reach the ventricles; typically between 110 and 180 beats per minute, thus the coordination between atria and ventricles is lost (Waktare, 1998), see Figure 7. In this case, the amount of blood pumped out of the ventricles to the body would change randomly. The volume of blood (cardiac output) which is pumped to the body by the normal heart is about 5 litres per minute in an average person. In the case of AF, the body may receive smaller and occasionally larger amounts of blood (Milnor, 1990).

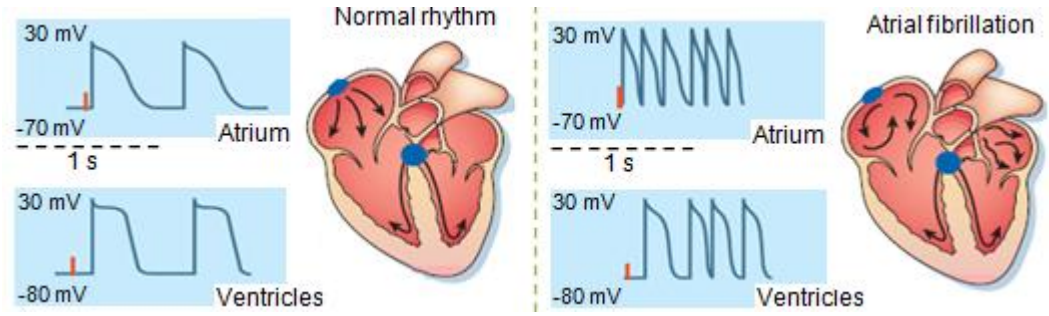

Figure 7. Simple illustration of action potentials from the atrium and ventricles during normal rhythm and atrial fibrillation. The red vertical line on each action potential recording corresponds to a common time reference (Nattel, 2002a).

1.1.3. Theories on Concept of Atrial Fibrillation Mechanism

In 1874, the electrical stimulation of animal hearts led to the discovery of AF. By 1909 simultaneous recordings of the human heart and ECG activity had revealed the common origin of AF events. Subsequently, attention focused on whether AF was sustained by an abnormal focus or by a closed circuit. The debate has advanced as electrophysiological measurement techniques have become more sophisticated (Kenneth, 1995).

I. Circus Movement Theory

Garrey in 1914 discussed a hypothesis that concerned pathway conduction block. The assumption was that impulses can travel in any direction but they become limited by localised blocks in the tissue mass, which cause a series of ring-like circuits (Garrey, 1914). The hypothesis was called circus movement theory and came to prevail for the next 30 years. Figure 8 demonstrates simple example of circus movement theory.

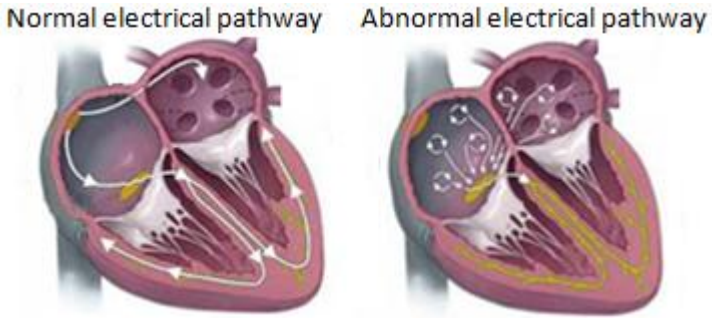

Figure 8. Illustration of circus movement theory of AF (Wellsphere, Health knowledge, 2009, [Online image]. Available from: http://www.wellsphere.com).

II. Multiple Wavelet Hypotheses

The circus movement theory was later tested by cutting or burning the route of the specific circus pathway, and it was found to have no effect on the propagation of the fibrillation wave (Mansour, 2006). Prinzmetal in 1950 used multiple site electrocardiography to investigate the AF mechanism. He showed that the electrically stimulated fibrillation wave proceeded uniformly in all directions from the point of stimulation. No circus movement could be shown, the waves moved into different paths, weaving, crossing and re-crossing old paths (Prinzmetal et al. 1950). The theory of circus movement as the mechanism of AF was no longer acceptable. A new mechanism of AF was proposed in 1959 as a self-sustaining arrhythmia and called the multiple wavelet hypotheses (Moe and Abildskov, 1959). In this proposal it was thought

that although the fibrillation may have originated from one focus, it did not depend on it to persist and propagate, but rather depended on a random fractionation of the wave front around tissue. In 1962 this theory was explained in more detail: *"during AF, many independent wavelets propagate in an ever-changing pattern around continuously shifting areas of conduction block"* (Moe et al. 1962). Figure 9 shows simple illustration of multiple wavelet theory.

Figure 9. Simple illustration of the multiple wavelet hypothesis. Wavelets indicated by arrows randomly enter tissue that was previously activated by the same or another wavelet (Health from Trusted Sources, 2008, [Online image]. Available from: http://health-fts.blogspot.co.uk).

III. Re-entry Theory

Modern electrophysiological evidence for block with re-entry began in 1977. Of particular interest in the explanation of AF is the type called "leading circle". In this type, the initiation of re-entry takes place because of non-uniform RP in atrial fibres in close proximity to one another. The initiating impulse propagates along fibres with short RP and is blocked in those with longer ones, allowing re-entry into them before the impulse has died out. The size of the circle is determined by the recovery time of the tissue forming the circuit, as tissue on both sides is kept depolarised by the leading circle, *"It is said that what goes around, comes around"* (Allessie et al. 1977).

By mapping the heart electrical activity during AF, in 1985, Allessie provided the first experimental evidence supporting Moe's multiple wavelets hypothesis. According to this evidence, AF is associated with multiple indirect

activation waves, which propagate randomly within the atria. The fractionation of the wavefronts as they propagate, results in self-continuing independent wavelets, called re-entries (Allessie et al. 1985). Re-entry arises from abnormal impulse propagation between different zones of tissue. Figure 10 shows re-entry occurring between two tissue zones (I and II) which are connected. An ectopic activation (2) arising in zone II during the RP of AP in zone I, which fails to initiate firing in zone I. However, it may propagate (red dashed line) through an alternative pathway to zone I (3). The impulse then leaves zone I and move towards zone II (4) and the process can continue indefinitely (Nattel, 2002a).

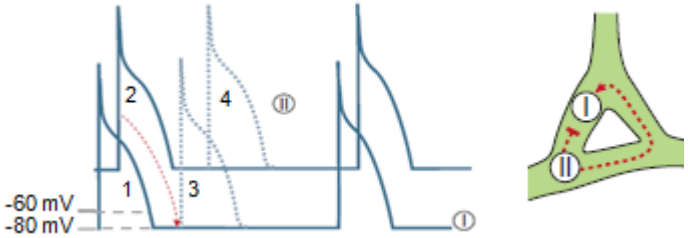

Figure 10. Re-entry occurring between two tissue zones, I and II, which are connected as shown on the right. A premature activation (2) in zone II fails to initiate firing in zone I because zone I is still refractory. It may conduct back (red dashed line) to zone I at a time when it can respond with an action potential (3). This action potential may propagate to initiate (4) in zone II, and the process can continue indefinitely (Nattel, 2002a).

A more detailed model of re-entry is shown in Figure 11. In normal tissue (A), if a single fibre forms two branches (1 and 2) the AP will travel down each branch. An electrode (indicated by a green star) in a side branch would record single, normal APs as they are conducted down branch 1 and into the side branch. If branches 1 and 2 are connected together by a common pathway (branch 3), the APs that travel into branch 3 will cancel each other out. Re-entry (B) can occur in a branch that has an unidirectional block. In such a block, impulses can travel retrograde (from branch 3 into branch 2) but not orthograde. With this condition, an AP will travel down branch 1, into the common distal path (branch 3), and then travel retrograde through the

unidirectional block in branch 2 (blue line). Within the block (grey area), the conduction velocity is reduced because of depolarisation. When the AP exits the block, if it finds the tissue excitable, then the AP will continue by travelling down (re-enter) the branch 1.

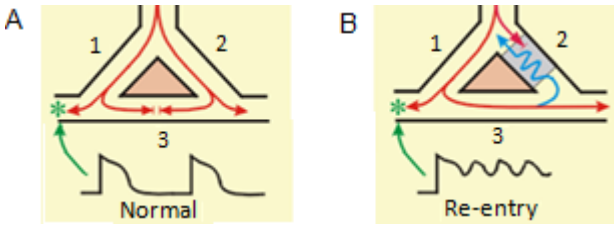

Figure 11. Illustration of re-entry model of AF. Normal tissue (A), tissue with re-entry (B), green star indicates an electrode and gray area indicates a block. (Cardiovascular Physiology Concepts, 2007, [Online image]. Available from: http://www.cvphysiology.com).

If the AP exits the block in branch 2 and finds the tissue unexcitable (within its RP) then the AP will cease. If it can re-excite the tissue, a circular (counter-clockwise in this case) pathway of high frequency impulses will become the source of APs. They may spread throughout a region of the atria (e.g. lone AF, see section 1.1.8) which is called local re-entry, or occur between the atria and ventricles (e.g. Wolf Parkinson White) which called global re-entry, see Figure 12.

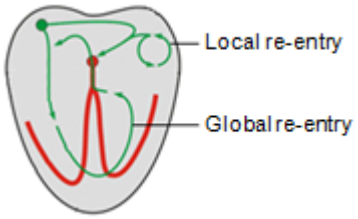

Figure 12. Simple illustration of re-entry of AF (Cardiovascular Physiology Concepts, 2007, [Online image]. Available from: http://www.cvphysiology.com).

While supporting re-entry as the major mechanism of AF, an idea was put forward arguing that AF could be produced by several factors including a

single rapidly discharging ectopic focus, multiple rapidly discharging foci, or rapidly circulating circus movement (Ziad et al. 2008).

IV. Electrophysiological Remodelling

A further development in understanding AF came through consideration of the electrophysiological mechanisms, which confirmed AF alters the atrial electrophysiological properties in a way that promotes its own maintenance. Wijffels demonstrated that, when AF is induced in goats by electrical-burst stimulation, the interval of spontaneous reversions increases progressively from several seconds to hours or days. He described this phenomenon “AF begets AF” (Wijffels et al. 1995). It was also demonstrated by Biffi that atrial remodelling is a time-dependent process that develops as an adaptive regulation of cardiac myocytes to maintain cell homeostasis against external tachycardia. This ‘structural remodelling’ adds the abnormalities of refractoriness and may explain the reduced efficiency of the AF therapy in patients with enlargement of the atria (Biffi and Boriani, 2003).

V. Complexity

AF posses different degrees of complexity and may be organised or disorganised. Organised AF may have one re-entrant circulating round the atria, with regular fibrillatory rate and localised frequency spectrum. Disorganised AF may have several re-entrant pathways circulating round the atria, taking different paths, with possible variations in frequency, or directional switches in time. In addition they have irregular fibrillatory rate and wider frequency spectrum compared to organised AF. A simplified model (ideal sphere) of the atrial wall will be adopted to demonstrate AF rhythms organisation. Based on the assumption that a well organised AF is characterised by a single dominant

re-entrant circuit of electrical propagation (Moe et al. 1962), the spectral distribution of intracardiac signals is synchronously recorded at multiple sites (S_1,S_2,…, S_N). This will exhibit a dominant peak. On the other hand, disorganised AF will exhibit multiple re-entrant pathways, generating different spectral distributions for different points of observation, see Figure 13.

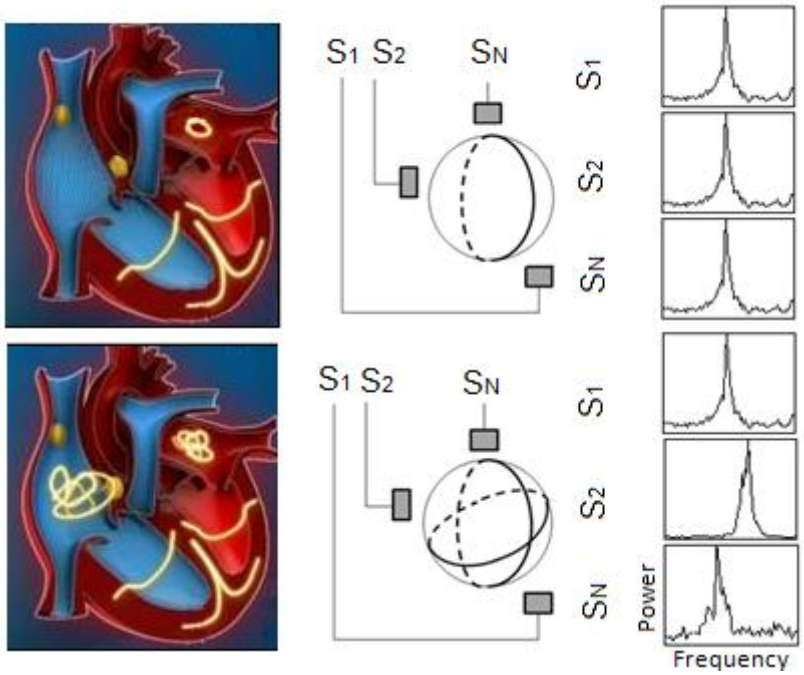

Figure 13. Illustration of organised (top) and disorganised AF (bottom). (Left figures: Atrial Fibrillation Press Office, 2012, [Online image]. Available from: http://www.dronedarone-atrial-fibrillation-pressoffice.com)

VI. Atrial Fibrillation Propagation

In order to characterize the rotation path of the AF non-invasively, wavefront propagation maps have been introduced (Kim 2012; Guillem 2009; Sanchez 2008). The wavefront propagation maps show irregular pattern, with multiple simultaneous wavefronts on the anterior sites of the torso. These activation patterns reflect different degrees of AF complexity (Sanchez, 2008). Two opposite rotation directions are observed in typical organised AF: (1) compatible with counter-clockwise activation (see Figure 14, A), downward

propagation on the anterior sites of the torso, moving towards the posterior torso and then continuing with an upward propagation on the posterior torso, and final downward propagation that ends at the same point at which the wavefront propagation map started. (2) Compatible with clockwise activation (see Figure 14, B), upward propagation on the anterior torso that spreads towards the superior part of the posterior torso and ends with a downward propagation on the back. Patients with less organised AF present varying propagation directions (Guillem et al. 2009).

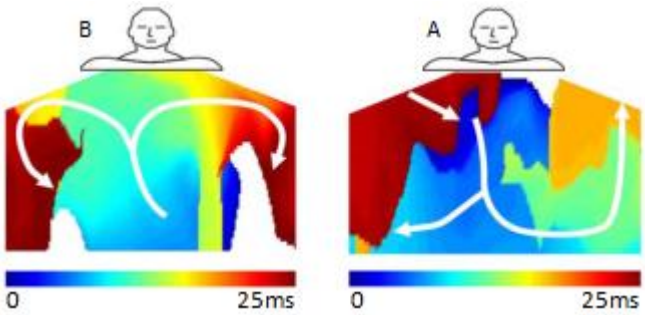

Figure 14. Wavefront propagation maps of two different patients in organised AF (Guillem et al. 2009).

1.1.4. Epidemiology

AF is age-dependent, affecting 4% of persons older than 60 years and 8% older than 80 years. Approximately 25% aged 40 years and older will develop AF during their lifetime. The prevalence of AF is 0.1% in persons younger than 55 years. The incidence of AF is significantly higher in men than in women in all age groups (Cotter et al. 2013).

1.1.5. Causes

AF may happen with or without evidence of heart disease. Some of the causes of AF not involving disease of the heart are: hyperthyroidism (overactive thyroid), acute infection, excess alcohol intake, intra-thoracic pathology (e.g. lung cancer), postoperative problems, and pulmonary embolism (a blood clot in

the lungs). Most commonly, AF occurs as a result of some other cardiac condition such as, sick sinus syndrome, ischaemic heart disease, pre-excitation syndromes, heart valve disease, rheumatic heart disease, enlargement of the left ventricle walls, coronary heart disease, and high blood pressure. Less common causes of AF are cardiomyopathy (disease of the heart muscle), atrial septal defect, atrial myxoma, and pericardial disease (Lip and Beevers, 1996).

1.1.6. Symptoms

AF may be asymptomatic (Wattigney et al. 2002). Usually the associated symptoms of AF are related to a rapid heart rate. The common symptoms are: chest discomfort, palpitation, exercise intolerance, light-headedness, dyspnea, fatigue, syncope, pulmonary oedema, pedal oedema, cerebral under-perfusion, dizziness, shortness of breath, and irregular fluttering in the chest (Alpert, 2005).

1.1.7. Screening and Diagnosis

Screening of AF could be performed through a simple check of the arterial pulse (e.g. radial pulse) to assess the pulse rate and rhythm. The AF rhythm is usually described as “irregularly irregular” (Walsh and King, 2007). The diagnosis of AF typically is confirmed through a 12-lead ECG, Holter monitoring, or implantable loop recorder.

I. 12-lead ECG

When an irregular heartbeat is suspected, a 12-lead ECG test is performed. The 12-lead ECG system consists of twelve leads (I, II, III, aVR, aVL, aVF, V1, V2, V3, V4, V5, and V6). The first three leads are the Einthoven limb leads, and then three Goldberger augmented leads and, finally six

precordial leads. The first three leads are defined as bipolar leads, and the others are defined as unipolar leads. The precordial leads are measured with respect to a reference. The Wilson Central Terminal (WCT) is chosen as reference, and it approximates the potential at infinity. It is formed by averaging the voltage from each limb lead. The WCT represents the average of the limb potentials. The 12-lead ECG is the most common non-invasive technique in cardiology, due to its capability to assess the cardiac disorders in a simple low-cost manner. Figure 15 demonstrates the placement of the 12-lead ECG electrodes on the torso.

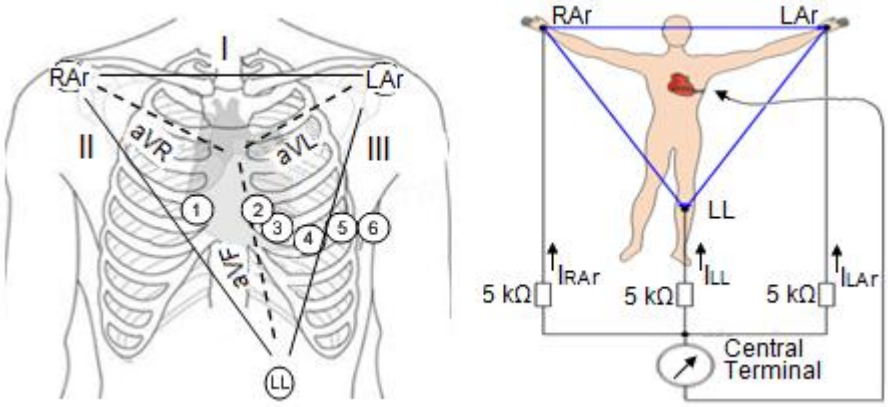

Figure 15. Left: Position of the 12-lead ECG on the torso (ECG exercise positioning). RAr: right arm, LAr: left arm, and LL: left leg. Right: The Wilson Central Terminal, I: electrical current (Geeky Medics, 2013, [Online image]. Available from: http://www.geekymedics.com and http://www.bem.fi).

The characteristic ECG findings of AF are as follows: (1) the absence of P-wave, (2) irregular electrical activity instead of P-wave known as fibrillatory wave or F-wave, (3) irregular RR interval due to the irregular conduction of the impulses to the ventricles. The F-wave is displayed as small rapid activity on the baseline of the ECG leads (Fuster et al. 2006). Figure 16 demonstrates ECG of a normal heart rhythm and AF with irregular rhythm.

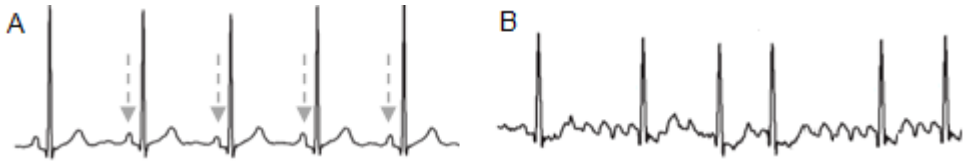

Figure 16. A: ECG of a normal heart rhythm, the arrows display P-waves. B: ECG showing AF, in contrast F-waves (irregular electrical activity) are present instead of P-waves (Nattel, 2002b).

II. Holter Monitoring

When irregular heartbeats are intermittent, it is likely that they will not be recorded on the ECG. In this case a small portable ECG, called a Holter Monitor, is worn for 24-48 hours in order to capture the episodes, see Figure 17. The heart electrical activity are continuously recorded and stored in the monitor. After the monitor is removed, a technician uses a computer to analyse the recorded signal to evaluate the heart's rhythm.

Figure 17. Illustration of a 12-lead Holter monitor (DM Systems, 2013, [Online image]. Available from: http://www.dmsmed.en.alibaba.com).

III. Implantable Loop Recorder

The implanted recorder continuously monitors the heartbeat, 24 hours a day, 7 days a week. The recorder is implanted under the skin, below the collarbone. This device is used for patients who occasionally feel palpitations, light-headedness or fainting, to assess whether the heart is causing these symptoms.

1.1.8. Classification

Guidelines of the American College of Cardiology (ACC), American Heart Association (AHA), and the European Society of Cardiology (ESC) recommend the following classification of AF based on simplicity and clinical application;

- Acute AF with new-onset of AF and lasting less than two days.
- Lone AF: with absence of clinical findings of any cardiovascular disease. The frequency of attacks in lone AF may vary from less than one a year to three per year or more.
- Paroxysmal (intermittent): if there are recurrent episodes of AF that come and go spontaneously. Each episode stops just as suddenly as it starts without treatment within seven days. The period of time between each episode (each paroxysm) can vary greatly from case to case.
- Chronic Persistent: if lasting longer than seven days, and is unlikely to revert back to normal without treatment, such as cardioversion. Persistent AF is likely to be recurrent so it may come back again even after successful cardioversion treatment.
- Permanent (established): if there is an ongoing long-term episode. This means that the AF is presenting long-term. This may be because cardioversion treatment was not successful, or because cardioversion has not been tried. In permanent AF, it should be tried to bring the heart rate back to normal although the rhythm may remain irregular. Figure 18 shows a schematic representation of AF classification.

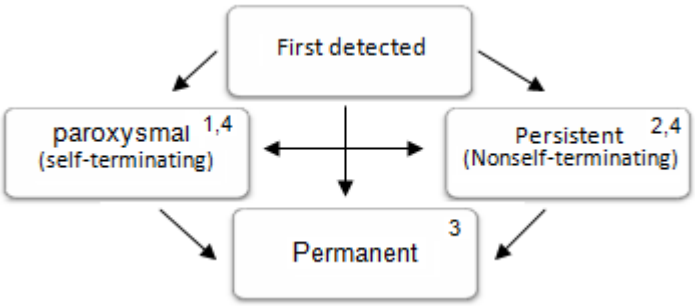

Figure 18. Patterns of atrial fibrillation types. 1: episodes that last ≤ 7 days. 2: episodes that last > 7 days. 3: cardioversion failed. 4: either paroxysmal or persistent AF may be recurrent (ACC/AHA Practice Guidelines, Available from: http://www.circ.ahajournals.org).

1.1.9. Complications

The main complication of AF is an increased risk of systemic thrombo-embolism. This is because in AF, blood is pumped into the ventricles randomly, and the amount of blood pumped out of the ventricles is based on the randomness of the atrial beats, subsequently a blood clot forms. The clot can block blood supply in the heart and cause a heart attack, or travel to the brain and cause a stroke. Other complications of AF include the following (Cohn, 2008):

- Heart failure
- Cardiomyopathy; atrial fibrillation can decrease the heart's pumping ability and efficiently. In addition, atrial fibrillation occurs over a long period of time and can lead to weakening of the heart muscle
- Other organ damage due to systemic emboli.

1.1.10. Management and Therapy

The management of AF can be broken down into management of new-onset and long-standing AF. The new-onset AF management is rhythm control, with pharmacological or/and electrical cardioversion. Rhythm control is restoration and maintenance of the normal rhythm of the heart. The long-

standing AF management is rhythm control or rate control strategy. Rate control is used to minimise symptoms associated with excessive heart rates. This involves the use of drugs or electrophysiological/surgical approach to reduce the rapid ventricular rate. Choosing each strategy requires integration of several factors, including degree of symptoms, and likelihood of restoration of SR. In respect to management and treatment of AF there are pharmacological and non-pharmacological therapies (Zimetbaum and Josephson, 2003).

I. Pharmacological

Antiarrhythmic therapy is used for the following purposes: to convert AF into SR, to prevent recurrence after electrical cardioversion, or to achieve rate control in patients with permanent AF. *Anticoagulation* (antithrombotic) therapy is used to prevent thromboembolic complications. *Antithrombotics* therapy is used to reduce the risk of stroke. They include anti-platelet agents (e.g. Aspirin, Clopidogrel) and anti-coagulant agents (e.g Warfarin) (Anfinsen, 2002).
Some of the pharmacological agents used for management of AF are:

- Rate control agents: control the ventricular rate in response to AF. These include Digoxin, Calcium channel blockers (e.g. Verapamil, Diltiazem), and Beta-blockers (e.g. Atenolol, Metoprolol, Esmolol, Propranolol).
- Rhythm control agents: maintain the SR and prevent the recurrence of AF. They include Quinidine, Disopyramide, Flecainide, Propafenone, Dofetilide, Ibutilide, Procainamide, and Amiodarone.

II. Non-Pharmacological

Some choices of non-pharmacological treatments are: surgical therapies, electrical cardioversion, and catheter ablation, which are explained in the following sections:

Surgical Therapies

The corridor procedure: in this procedure a strip of myocardium tissue connects the SA node to the AV node. This results in the isolation of the remainder of both left and right atrium, see Figure 19. The SR is restored in 69% of patients. However, the left atrioventricular synchrony could not be re-established in the majority of the patients, so the heart remained still a source of thromoboembolism (Liem, 2001).

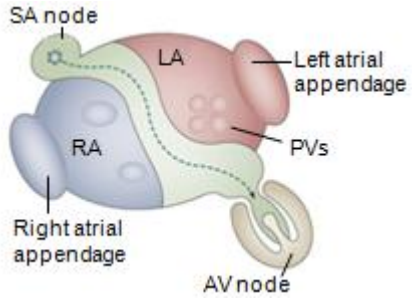

Figure 19. Illustration of the corridor procedure (Medscape education, 2009, [Online image]. Available from: http://www.med-scape.org).

The maze procedure: a series of specific lesions are made in the left and right atrium to confine the electrical impulses and define pathways to reach the AV node, see Figure 20. These lesions block the abnormal electrical impulses from being conducted through the heart. Early results of the maze procedure were 89% SR restoration. However follow-up showed that up to 40% of patients required a pacemaker (Cox 1995 and 1993; McCarthy 1993).

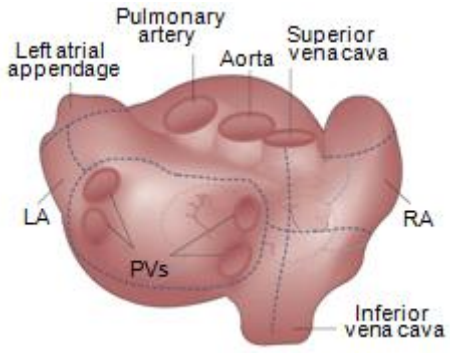

Figure 20. Illustration of the maze procedure. (Medscape education, 2009, [Online image]. Available from: http://www.med-scape.org).

Electrical Cardioversion

Electrical cardioversion (atrial defibrillator) is a procedure where an electrical shock (low-voltage electric current) is delivered to the heart through metal patches to convert an abnormal heart rhythm back to a normal rhythm, see Figure 21. It is used to stop AF that has not stopped after catheter ablation or a trial of pharmacological cardioversion has failed.

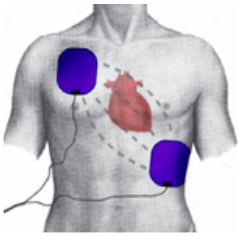

Figure 21. Illustration of electrical cardioversion (Walker Heart Institute/ Cardioversion, 2012, [Online image]. Available from: http://www.wregional.com).

Catheter Ablation

The catheter ablation is used to either heat up (Radiofrequency (RF) ablation) or freeze (cryoablation) the tissue causing the arrhythmia. The catheter ablation is performed through an electrophysiology (EP) study. Ablation means making small scar(s) in the heart tissue, so that it is unable to conduct electrical impulses. This is done using a long wire (catheter) into the heart through the femoral vein (groin) then moving the catheter tip towards the heart under the guidance of X-ray, see Figure 22.

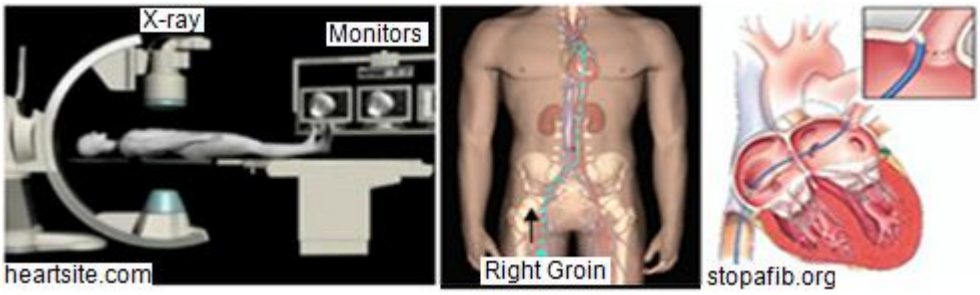

Figure 22. Left: example of an electrophysiology laboratory. Middle: the catheter is inserted into the femoral vein and advanced through the inferior vena cava, right atrium, then left atrium. Right: example of the catheter tip inside the left upper pulmonary vein.

With the catheters in place, recordings of the heart's electrical activity can be made from inside the heart known as Electrogram (EGM), see Figure 23. Signals from inside the heart are collected, and show changes in electrical potential, usually displayed over a period of time. In an EGM, the baseline corresponds to a value of zero. Each change of electrical potential represents atrial activation, and the distance between two neighbouring activations is defined as the cycle length (CL).

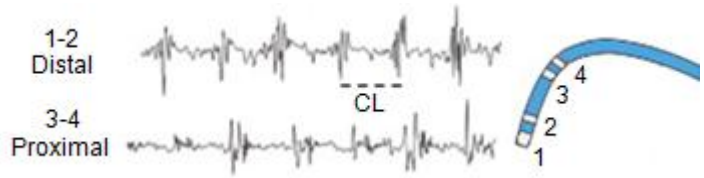

Figure 23. Left: example of signals between the distal and proximal bipoles from a catheter. Right: example of a catheter that is used for RF ablation (Takahashi, 2008).

There are two main recording modes used to generate the EGM, unipolar and bipolar. All EGMs are recorded using two electrodes. One is positive and one is negative, which are computed by subtracting the information at the negative from the positive electrode. In fact, a bipolar EGM is a derivative of two unipoles. A unipolar EGM uses the same process, but the negative electrode has a zero reference potential. This means that there is no electrical activities at the location of the negative pole, so unipolar EGM represents the view from one pole, see Figure 24. Once the physicians have identified the abnormal heart tissue, the catheter tip is positioned against the inner surface of the heart muscle close to the site of the origin of abnormal rhythm. At this point RF current (energy) is then passed into that area in order to burn the cells responsible for conducting abnormal rhythm, see Figure 25.

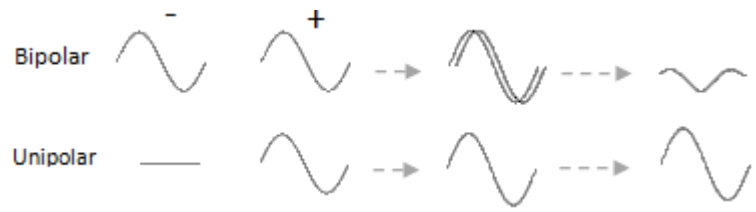

Figure 24. Examples of bipolar (top) and unipolar (bottom) signals, (The EP lab, 2012, [Online image]. Available from: http://www.theeplab.com).

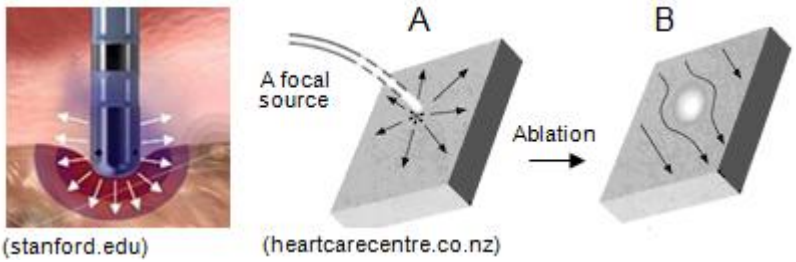

Figure 25. Left: the catheter tip sent the RF energy that destroys the abnormal tissues. Right: A, a focus (shown as star) is repeatedly firing and spreading to other cells. B, after ablation the tissue of the focus has been damaged and is no longer firing. Arrows show normal electrical propagation.

Cardiac ablation can be performed for rate control (destroy the AV node) or rhythm control (isolate the PVs). The ablation of the AV node destroys the AV node and block AV conduction. This has been an effective treatment for rate control but requires permanent pacemaker implantation (Ganz and Saperia, 2012). The ablation of the PVs ostium focuses on the elimination of triggers for AF via electrical isolation of the PVs. Sometimes it also includes additional lesions to be made in the body of the LA (e.g. roof and floor, see Figure 26) to modify arrhythmic substrate (Cox et al. 1991).

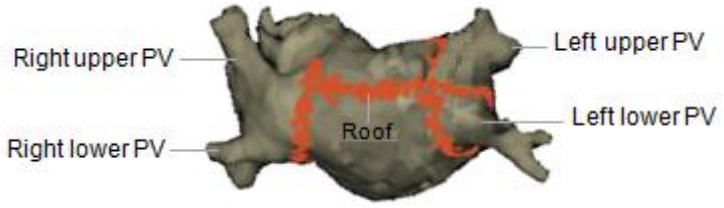

Figure 26. Illustration of PV isolation (orange lines) (Virtual medical centre, 2012, [Online image]. Available from: http://www.virtualmedicalcentre.com).

There is no recommend standard ablation procedure. More information on mapping, ablation lesions, and origins of AF is needed to improve AF treatment. Using catheters for mapping or ablation has some risks such as: bleeding, infection, damage to left atrial esophageal, damage to blood vessels and pain at the site where the ablation catheter was inserted.

The outcome of AF ablation differs depending on the AF type, and related heart disease. Practical difficulties in determining the outcome of AF therapy success rate depend on: the regularity and intensity of arrhythmia monitoring, whether patients on antiarrhythmic drugs during follow-up are categorised as successes or failure. Focusing on the RF ablation at 12 months of follow-up, it has been observed that the single procedure success of patients with persistent AF ranged from 22% to 45% (Calkins 2007; Fuster 2006). Another research study shows more than 80% of patients who undergo cardioversion for persistent AF after ablation, have recurrence (Chilukuri et al. 2010).

1.2. Engineering Background

The complexity of AF signals has been identified as targets for AF ablation. As a result, an understanding of the complexity of AF signals has been shown to be helpful in the detection and treatment of AF (Ng et al. 2010). Such signals contain information about the AF mechanism, which is hidden in its structure and may not be readily observed. This information has to be extracted so that the signal can be given meaningful interpretation. Therefore, signal processing techniques have become an essential tool for extracting clinically significant information from AF signals. These signal processing techniques are

used to understand the mechanism and possible sources of AF, resulting in guiding ablation or drug therapy in the treatment of AF.

This section reviews the signal processing techniques which have been used to analyse AF. The aim of this review was to introduce different methods concerning the understanding of AF, and to define the current 'state of the art' from which this project will advance. This section has been grouped in terms of body surface signal analysis (see section 1.2.1), intracardiac signal analysis (see section 1.2.2), and joint body surface and intracardiac signals analysis (see section 1.2.3). Finally, the methods that will be used in this PhD project to investigate AF characteristics are introduced (see section 1.2.4).

1.2.1. Review of Body Surface Signal Processing

The 12-lead ECG is the most common and readily available method to characterise cardiac activity non-invasively (Donnelly 2006; Trobec 2003). In body surface potential mapping, increased spatial sampling is used to allow more accurate detection of a cardiac abnormality (Finlay et al. 2005), and more accurate diagnosis of the cardiac pathologies (Bond et al. 2010). This has become a strong motivation for extracting cardiac activity from the body surface using more than 12 leads. In order to achieve this, the 12-lead ECG has been extended through the use of additional electrodes, a technique known as body surface potential mapping (BSPM). The BSPM uses 32 to 219 electrodes (leads) to record electrical activity over a large portion of the torso and back (Huebner 2010; Donnelly 2008; Finlay 2006; Hanninen 2001; Hoekema 1999a; Kornreich 1997). Unlike the 12-lead ECG technique, there is no standard representation or acquisition of the BSPM, however a lead system incorporating 64 leads is suffice for most applications (Hoekema et al. 1999b). AF could be

episodic, so it is possible to study AF when patients are in SR or when they are in AF. In the literature, the BSPM has been widely used to investigate the P-wave propagation across the body surface (Kozlikova 2011, 2007; Macfarlane 2010; Krandycheva 2006; Lian 2002; Medvegy 2002; Yamada 1999; Watanabe 1988). However, as patients studied in this PhD project were in AF, this section describes techniques for analysis when the patients are in AF.

Ihara suggested that the adaptation of the 12-lead ECG by putting one lead on the back produces a better view of AF (Ihara, 2007). Kornreich also explored using additional leads to the 12-lead ECG, and found that adding four leads to the 12-lead ECG (see Figure 27) improves diagnostic performance regardless of the subject or the disease group (Kornreich et al. 2008).

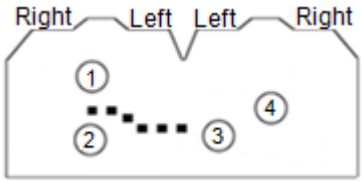

Figure 27. A schematic of the four additional leads to the 12-lead ECG (Kornreich et al. 2008). 3 limb leads have not been shown in the figure.

Figure 28 represents the steps involved in analysing the surface ECG signal when the patient is in AF, regardless of the number of electrodes that have been used.

Figure 28. A schematic representation of the steps involved in analysing the surface ECG when patient is in AF.

- Pre-processing includes filtering of baseline wander, muscle artifact, and mains interference
- Atrial activity (AA) estimation is achieved using QRST cancellation
- Parameter estimation includes estimating AF characteristics such as amplitude and frequency (rate).

Pre-processing

The methods of noise reduction have an important influence on the performance of the ECG signal processing. Baseline wander is a common artifact in the body surface signal caused by varying electrode contact during the recording. This could be due to patient movement, poor electrode contact with skin and breathing. The frequency range of baseline wander is usually less than 1 Hz (Karthikeyan et al. 2012). Good skin preparation can help to eliminate this type of artifact. However, removal of baseline wander is required in order to minimise changes in beat morphology which do not have cardiac origin. Different methods for removing the baseline wander have been presented such as; nonlinear filter (Jackek and Norbert 2005), time-varying digital filtering (Sörnmo, 1993), nonlinear filter bank (Leski and Henzel 2005), linear low-pass filter (Hargittai, 2008), cascade adaptive filtering (Laguna, 1992), selective filtering (Shusterman et al. 2000), and wavelet-based cascaded adaptive filter (Xu et al. 2007). An important concern in all of these methods is to remove the low-frequency components that are not related to the cardiac electrical activity. Figure 29 shows an ECG before and after filtering baseline wander.

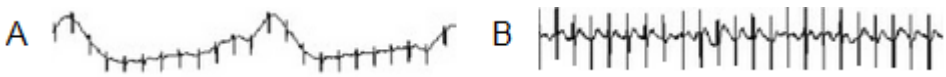

Figure 29. Illustration of an ECG with a baseline wander (A), and a clean ECG (B) (Computers in Biology and Medicine, 2012, [Online image]. Available from: http://www.computersinbiologyandmedicine.com).

Electromagnetic fields caused by a power line represent a noise source in the ECG. This artifact is characterised by 50 Hz sinusoidal interference, possibly accompanied by a number of harmonics (Husser et al. 2005). Removal of this interference is done using a 50 Hz Notch filter, since the spectral content

of atrial activity typically is below 25 Hz (Sandberg, 2007). Figure 30 shows an ECG with 50 Hz power line noise, before and after filtering.

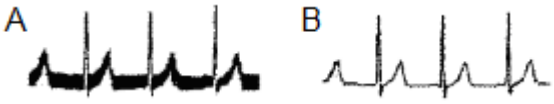

Figure 30. Illustration of an ECG with 50 Hz power line interference (A), and a clean ECG (B) (Levkon et al, 2005).

Muscle artifact with small amplitude and high frequency is another problem in ECG, since the spectral content of this artifact overlaps with QRS complex. Different filter systems have been provided to remove the muscle artifact (Mak 2010; Rahman 2009; Do-Un 2008; Kim 2006).

Atrial Activity Estimation

As AA has much smaller magnitude than ventricular activity (VA) in the surface ECG, the VA needs to be cancelled before the AA can be studied (Lemay et al. 2007). One of the most essential steps for this purpose is QRS (or beat) detection. Moreover, QRS detection could be used to identify AF as it distinguishes the ventricular rate and rhythm (Abacherli et al. 2009). QRS, followed by T-wave detection (QRST) is used in order to extract AA. Algorithms for the detection of QRST can significantly affect the signal analysis process, as they must be able to detect a variety of different morphologies and also ectopic beats. Many algorithms have been introduced such as: mathematical morphology (Trahanias 1993; Portet 2005), filter banks (Hamilton, 2002), adaptive filtering and wavelet transform (Kozakevicius, 2004), adaptive threshold QRS detector (Chiarugi et al. 2007a), first-derivative-based methods (often used in real-time analysis or for large datasets since they do not require manual segmentation of data, training of the algorithms) (Kohler et al. 2002),

zero-crossing (Arzeno et al. 2008), adaptive quantised threshold (Chouhan 2008; Elgendi 2009), and wavelet and artificial neural network (Abibullaev and Don Seo 2011). Figure 31 shows detected QRSTs of an ECG signal.

Figure 31. Illustration of a detected QRST of an ECG signal (Rooijakkers, 2012).

AA extraction or QRST cancellation is performed using various methods and algorithms such as; QRST morphology clustering cancellation (Di Marco 2011; Karimifard 2011), average beat subtraction (ABS) (Sörnmo 2009; Petrutiu 2006; Bollmann 2006a; Lemay 2007 and 2005; Xi 2003), spatiotemporal QRST cancellation (Klamor 2011; Stridh 2001), adaptive singular value (Alcaraz and Rieta 2008), independent components analysis (ICA) (Lemay et al. 2007), principal component analysis (PCA) (Langley 2006, 2000; Castells 2005a), maximum likelihood source separation (Castells et al. 2005b), blind source separation (BSS) (Rieta, 2004), and packet wavelet decomposition (Sanchez et al. 2002). Evaluations of QRST cancellation methods have confirmed that the cancellation methods are reliable for studying atrial fibrillatory wave characteristics (Vaya 2007; Lemay 2007; Langley 2006, 2002, 2000; Xi 2003). An evaluation by Langley showed that the extracted atrial signals from ICA, PCA and ABS algorithms exhibit very similar amplitude and frequency characteristics (Langley, 2002). Figure 32 shows the recording of lead V1 from a patient with AF and an appearance of the signal after subtraction of the QRST using ABS algorithm.

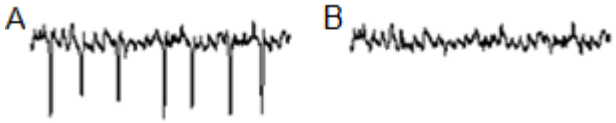

Figure 32. (A) Recording of lead V1 from a patient in AF and a rapid ventricular response. (B) Appearance of the signal after subtraction of the QRST using a template matching algorithm (Bollmann et al. 1998).

Parameter Estimation

Various parameters have been introduced to characterise AF in the time and frequency domains. The most common parameters based on surface ECG are amplitude, dominant frequency (DF), spectral concentration (SC) and organisation index. Methods to estimate these parameters are the focus of this section.

- **Amplitude**

It is believed that lead V1 has high amplitude F-waves due to the proximity of the lead to the RA (Petrutiu et al. 2006). Mostly regular AF cases known to have high-amplitude F-waves, while less regular AF cases have lower amplitude (Petrutiu et al. 2006). Measured AF amplitudes are used to make the distinction between coarse and fine AF (Langley et al. 2000). The AF amplitude is often described as fine (< 50 μV) or coarse (> 50 μV), which has been linked to specific heart conditions (Thurmann, 1965). Different studies of coarse versus fine AF, consider that either left atrial size or heart disease are responsible for the AF amplitude. These studies associate rheumatic heart disease with coarse F-waves and arteriosclerotic heart disease with fine F-waves (Morganroth et al. 1979). Xi showed that median peak to peak AF amplitude has intra-patient repeatability over 24 hours, whereas the inter-patient variability is high (Xi et al. 2004a). The relationships of AF amplitude were also investigated for different types of AF. It was found that there is no statistical

significance between AF amplitude and different types of AF, which include paroxysmal, persistent, and permanent. AF amplitude is also not different for patients taking anti-fibrillatory drugs when compared with those not taking anti-fibrillatory drugs, and AF amplitude is not age dependent (Petrutiu et al. 2006).

Xi described two methods to quantify F-wave amplitude. In the first method, the region of QRST complexes is excluded from analysis to avoid contribution of QRS residuals. Subsequently, the four individual F-waves with the largest peak-to-peak amplitude are selected. The average of these four amplitudes is selected as the representative peak-to-peak amplitude. The second method is by observation of the average value of the peak-to-peak F-wave amplitude for the entire duration of the recording (Xi et al. 2004b). The F-wave amplitude proved to be a successful predictor of AF recurrence after electrical cardioversion, with a diagnostic accuracy approximately 80% (Alcaraz and Rieta 2009a).

- **Spectral Analysis**

A periodic signal can be expressed as a sum of sine waves in the frequency domain. As a result, spectral analysis can be used to study AF with the goals of determining the location of dominant (fundamental) peak, and investigating the spectral shape (Corino et al. 2007).

i. Dominant Frequency

An AA signal typically exhibits a narrowband spectrum with a main frequency between 3–9 Hz (Castells 2005a; Bollmann 2000a; Holm 1998). The main peak in the frequency band determines the fibrillatory rate and is termed DF (Bollmann and Lombardi, 2006b). Previous studies have shown that DF is widely used as an indicator of atrial refractoriness (Chiarugi 2007b; Hayn 2007;

Nilsson 2006; Capucci 1995). AF DF has proved to be successful in monitoring AF treatment (Husser 2007; Raine 2004; Langley 2003) as well as in predicting spontaneous AF termination (Nilsson et al. 2006). Several studies support the idea that AF with a low DF is more likely to terminate spontaneously and responds better to treatment. When the fibrillation frequency is below 6 Hz the likelihood of successful pharmaceutical cardioversion is higher. These are important considerations when selecting candidates for cardioversion. Conversely, high AF DF is more often persistent and harder to manage (Nilsson 2006; Bollmann 2006a, 2000; Lazar 2004; Meurling 2001). Fibrillatory rate changes have been observed and showed that freedom from recurrent AF has been associated with the degree of fibrillatory rate reduction in lead V1 (Husser et al. 2006). Furthermore, several studies have shown that DF obtained from lead V1 is highly correlated with the fibrillatory rate of the RA (Petrutiu 2009; Hsu 2008; Husser 2007; Holm 1998). According to Langley, DF measurement reveals information regarding the atrial rhythm and AF stability non-invasively (Langley et al. 2000). Bollmann showed that the AF frequency decreases at night and increases in the morning. The above results should be taken into consideration in the management of AF. Also Sandberg showed that there is 0.15 ± 0.09 Hz circadian variation in the AF frequency. In previous studies (Meurling 2001; Langley 2000; Bollmann 2000b) the AF frequency was sparsely measured and consequently, the short-term variation could not be observed (Sandberg et al. 2010). A study of the fibrillatory rate in single paroxysmal AF episodes showed that the rate of long AF episodes increase over the first four minutes, while short episodes also showed an increase from the first to the second minute (Petrutiu et al. 2007).

From an electrophysiological point of view, the F-waves have time dependent properties. Therefore, time-frequency analysis can be used in order to investigate the variations in frequency over time to determine the atrial rate and AF characterisation (Petrutiu 2006; Stridh 2004). This method allows non-invasive monitoring of the fibrillatory rate and waveform of lead V1 on the ECG. The F-waves of surface ECG on lead V1 closely reflect right atrium activity (RAA) and, to a smaller degree, left atrium activity LAA (Husser et al. 2007). Vaya undertook a study to distinguish between the AF episodes that terminate immediately and those that sustain. He concluded that the combined analysis of time and frequency can be used to predict spontaneous termination of paroxysmal AF (Vaya and Rieta 2009). However, time-frequency analysis is more suitable when the outcome of AF treatment is under investigation as this method detects the changes in AF frequency (Corino et al. 2007).

ii. Spectral Concentration

SC is the atrial signal concentration of power around a main peak. This parameter can be used for different purposes, such as estimation of the quality of the AA extraction and the AF degree of organisation. Phlypo stated that higher SC is associated with more accurate AA estimation. SC decreases as the VA are not being cancelled properly (Phlypo et al. 2010). Moreover, lower SC is related with more spectral peaks in the AF frequency band, which may suggest disorganised AF. Higher SC is associated with a prominent spectral peak in the AF frequency band, which may suggest organised AF (Di Marco et al. 2012). However as all non-related AA components have spectral contents outside the AF frequency band (3–9 Hz), SC is suitable to estimate the AF degree of organisation (Castells et al. 2003).

iii. Organisation Index

AF organisation is defined as the degree of repetition in the AA (Everett 2001; Sih 1999). Investigation of AF organisation can potentially be used to provide information about the AF mechanism, as it has been demonstrated that the number of re-entries is related to AF organisation (Everett, 2001). AF organisation can be used to provide information about time variation in the onset and termination of AF. AF organisation is quantified by different methods such as studying TQ segments, non-linear metrics (e.g. sample entropy (SampEn), approximate entropy), and as previously mentioned, studying the SC (Alcaraz and Rieta 2010, 2009d; Nollo 2008; Nilsson 2006; Mainardi 2001; Hoekstra 1995). SampEn examines a time series and associates a positive number to the sequence, with low values corresponding to higher levels of regularity (Richman and Moorman 2002). However, a study has shown that the existence of QRST residual in the AA signal affects AF organisation estimation using non-linear methods. To improve upon on this, the fundamental waveform associated with the AA is obtained, and called main atrial wave (MAW). The MAW is obtained through selective filtering of the AA by tracking its DF. Alcaraz has demonstrated that AF organisation variation can be estimated from surface ECG through the application of SampEn to the MAW (Alcaraz and Rieta 2009c). His study has shown that the use of SampEn on the MAW predicts spontaneous termination of paroxysmal AF in 92% of the analysed episodes (Alcaraz and Rieta 2009b). The results of studying TQ segments suggest that a higher degree of spatial organisation is associated with a reduced variability of spatial organisation over time, and lower spectral variability associated with a more prominent spectral peak in the AF frequency band (Di Marco et al. 2012).

1.2.2. Review of Intracardiac Signal Processing

EP study is the cornerstone of AF ablation therapy (Baykaner et al. 2012). Processing and interpretation of the EGM recorded from inside the atria have played an important role in understanding the mechanisms of AF. However, as yet the extent to which the analysis of EGM can improve the efficacy of AF ablation therapy is still unknown. This section describes the steps involved in analysis of AF based on EGM (see Figure 33).

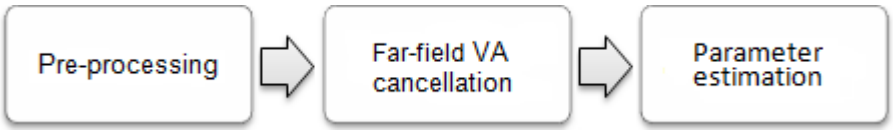

Figure 33. A schematic representation of the steps involved in analysing EGM.

- Pre-processing includes filtering of baseline wander, and mains interference
- Far-field VA cancellation, which is achieved by subtracting far-field QRS from EGM
- Parameter estimation, e.g. frequency (rate).

Pre-processing

Electrical activity recorded from inside the heart is passed through a series of electronic devices. This may cause artifacts from the circuits within the electronic sources during recording. Filters are used to remove artifacts while allowing frequencies of interest to pass. Choosing the filter is important and has a significant impact on the outcome of any analysis, and hence the conclusions which are drawn. The low-pass filter allows lower frequencies to pass and helps to remove high frequency environmental noise. Most common EGM pre-processing uses a band-pass filter with cut-offs at 40 to 250 Hz, followed by rectifying (using the absolute value of the output of the band-pass filter), and low pass filtering with a cut-off of 20 Hz (see Figure 34). This pre-processing extracts high-frequency components, and transforms a complex waveform of

the EGM into a series of atrial activations. This reduces the effect of varying EGM morphology and emphasizes the possible periodicity of the signal (Ng 2012, 2011, 2007; Richter 2011; Ravi 2009; Petrutiu 2009; Takahashi 2008; Lin 2006; Lazar 2004; Botteron 1996, 1995).

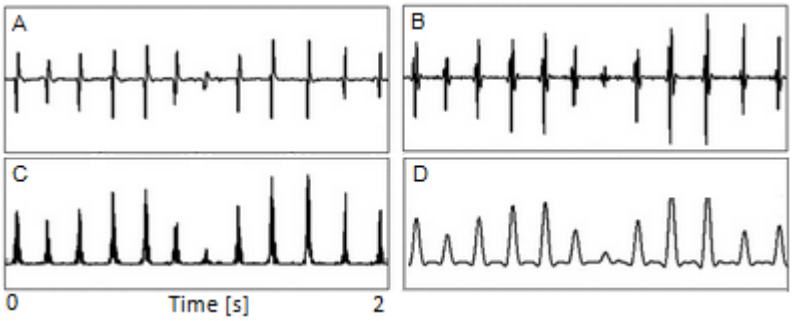

Figure 34. Illustrations of an EGM signal processing steps during atrial fibrillation. A: Unprocessed EGM, B: Band-pass filtering of 40 and 250 Hz, C: Rectifying, D: Low-pass filtering at 20 Hz (Ng et al. 2007).

Far-field Ventricular Activity Cancellation

Cancelling far-field VA on EGM allows detection of true atrial signals. Far-field VA was originally noted in recordings from CS, though it may be recorded from any part of the atrium. On bipolar atrial recordings far-field VA are significantly lower in amplitudes compare to unipolar atrial recordings (Griffin, 2012). However, Elvan's study of EGM before and after far-field VA subtraction shows there is no difference in DF derived from the bipolar and unipolar EGM (Elvan et al. 2009). The most common procedure for far-field VA subtraction is as follows: the surface ECG is used as a guide to identify the QRS, atrial signal windows synchronised with the detected QRS are averaged, and the templates are subtracted from the atrial signal at each ventricular activation time (Yoshida 2012; Faes 2002, 2001; Kandori 2002; Hoekstra 2000, 1997; Shkurovich 1998; Slocum 1985). In Salinet's study, QRST subtraction is based on the application of a band-pass filter between 8 and 20 Hz and low-pass filtering the rectified signal. The cut-off of frequency of the low-pass filter is

determined by the lowest RR interval of the ECG signals (354 beats per minute) and was chosen as 6 Hz. The peaks of the resulting signals were determined and areas corresponding to VA were replaced by flat interpolation, which is similar to the baseline (Salinet Jr et al. 2010). Jarman proposed an algorithm for far-field VA removal based on morphology. In this algorithm far-field QRS components of the unipolar non-contact EGM were subtracted using three steps: first, timing of far-field QRS was identified automatically from a reference site in the LA. The EGM from the LA site with clearest ventricular depolarisation were defined as a reference. Second, all of the identified ventricular components were overlaid to obtain a mean. Third, the mean ventricular complex was used to subtract the ventricular component of the EGM (Jarman et al. 2012). It should be noted that there are studies in which far-field VA subtraction has not been performed as it was not observed on the EGM (Petrutiu 2009; Sanders 2006; Biffi 2003).

Parameter Estimation

The evaluation of EGM parameters, such as fundamental frequency, provides a basis for selecting the appropriate AF treatment (Houben and Allessie 2006). Frequency analysis provides some explanation of the EGM by estimating both the fundamental frequency and the AF rhythm (Barquero-Perez et al. 2009). Frequency analysis was performed on the EGM recorded from PV, LA, CS, RA, and SVC. The highest DFs are mostly located at the arrhythmogenic PV ostium (Lin, 2006).

In a study presented by Sheldon, sites of complex fractionated atrial electrogram (CFAE) with a short mean CL (MCL) and sites with a high DF have been targeted for ablation in patients with persistent AF (Sheldon et al. 2009). A

characteristic frequency of CFAEs offers details of complexity of an EGM during AF; so it is capable for real-time application and can be a guide during catheter ablation (Nguyen et al. 2009). To investigate the atrial substrate characteristics near the SA node during SR, ongoing AF and before AF termination showed that the SA node activity during ongoing AF was similar to the rest of the RA and also DF around SA node area during AF termination was similar to during SR. This suggests that the sinus automaticity is preserved with local entrance block from the rest of the atrium (Tso et al. 2005). Advanced mapping techniques in AF showed that sufficient success rates can be achieved with left atrial ablation, in addition to complete PV isolation. Important techniques in this regard are the mapping of CFAE as well as identification of sites serving as sources of AF (Lickfett et al. 2008). Habel explained that DF and CFAE are temporally variable; consequently, sequential mapping can be misleading because of temporal variability (Habel et al. 2010). Since Haïssaguerre showed that ectopy from the PVs trigger AF, PV isolation has become central to most ablation approaches (Baykaner et al. 2012).

EGM AF organisation was defined by Faes as atrial activation morphology uniformity in time (Faes et al. 2002). Several methods for quantifying AF organisation estimated from inside the heart have been introduced including linear and non-linear analysis (Mainardi 2001; Sih 1999; Hoekstra 1995). Faes presented a method of evaluation AF organisation using regularity index. In his study the regularity index is defined by calculating the similar pairs of local activation waves in a window length of 90 ms. This enables the temporal AF organisation to be followed as well as identifying regions with different degrees of organisation. Assessment of the EGM regularity during AF

plays an important role in the treatment of AF, such as catheter ablation (Faes et al. 2002).

1.2.3. Review of Joint Body Surface and Intracardiac Signal Processing

There have been a few studies considering the joint body surface and intracardiac signals in AF. This helps to investigate whether intracardiac sites can be identified non-invasively, as well as allowing a non-invasive characterisation of AF. These should help AF intervention planning and therapy.

It has been thought that the ablation of high frequency sources is an effective therapy to restore SR. However, with this approach DF gradient need to be understood, which requires a study of the propagation of cardiac potential across the torso and back. Guillem studied 67-lead ECG recordings and EGM from both atria. She showed that spectral analysis of body surface recordings during AF allows a non-invasive identification of the atrium with the high frequency (Guillem et al. 2013). She used cardiac potential mapping method, which is not an approach followed in this study. Holm assessed the AF CL using the surface ECG and compared it with the intracardiac signal. They showed that AF CL correlates with the degree of atrial organisation. In general, shorter CL during AF was associated with a more organised AF. He also showed that the atrial CL in lead V1, ranging from 130 to 185 ms, represents the right atrium CL (Holm et al. 1998). A recent study showed that in AF, the correlation between the frequency of surface AA and atrial refractoriness, although significant, is not strong (Raitt et al. 2012). Several studies have quantified the frequency range of AF using the surface ECG. In these studies, ECG recordings obtained in patients during AF are compared to direct measurements from the RA and CS. AF DF on lead V1 and frequency measured in the RA and CS are significantly

correlated (Hsu 2008; Husser 2004; Shimizu 2003; Bollmann 1998). Ravi compared AF CL between the LA, RA, CS and 12-lead ECG. He estimated AF CL from the surface ECG in patients with persistent and paroxysmal AF prior to ablation. His study suggests that the mean of AF CL in leads V5, I and aVL can be used to estimate LA CL, leads aVF, II and III can be used to estimate CS CL, and V1, V2 and aVR can be used to estimate RA CL (Ravi et al. 2009). Sörnmo showed that the fibrillatory rate obtained from the surface ECG could be considered as an index to determine atrial fibrillatory cycle. He also suggested that the rate differences and variability between ECG and EGM increased with growing anatomical distances of the LA, RA, and PVs to lead V1 (Sörnmo et al. 2009).

1.3. Methods and Parameters Used in This PhD Study

In this study signal processing methods chosen to extract and study AF characteristics are based on the reviewed literature and are as follows:

I. The 12-lead ECG is the most common and readily available method to characterise cardiac activity non-invasively. In this study, AF was investigated in a more comprehensive way by using a 64-lead ECG. This could potentially discover body surface sites which might be particularly sensitive to atrial electrical activity, and it may spur the development of a greater understanding of the AF mechanism from the body surface.

II. AA estimation from the body surface and inside the heart was performed using the ABS method. The motivation for choosing this method was three-fold. Firstly, it allows a consistent method for signal processing of the body surface and intracardiac signals; Secondly, in this method all body surface sites can be studied individually whereas in other methods

(e.g. PCA) the body surface sites are combined; Thirdly, it has been shown that AA estimation using existing QRST cancellation methods exhibit similar results of the frequency characteristics.

III. AF amplitude (estimated from the body surface), DF and SC (estimated from the body surface and inside the heart) were chosen to be investigated. Amplitude was chosen to study how AF complexity is expressed on the body surface. SC was chosen to compare the body surface with intracardiac recordings. DF was chosen as it is the most common parameter used to study AF.

IV. New approaches were introduced for time synchronisation of the BSPM and EGM recordings, and to estimate amplitude of the AF signal from the BSPM recordings.

V. Although DF provides information about the main AF rate, other frequency components may be omitted or neglected. In this study a novel parameter was proposed and called Peak Type. This investigates any distinct frequency components on the body surface spectra and relates them to intracardiac DF to help determine if intracardiac DF agrees with body surface DF. If it does not, are there any other frequency components on the body surface sites that correspond to intracardiac DF.

VI. There is no evidence of AF investigation from the body surface and inside the heart in the time domain. In this study a novel method was proposed to relate AA from the body surface and inside the heart in time series with the following goals: firstly, to avoid QRST cancellation limitations such as VA residuals after cancellation, and secondly to study

AF in less processed signals which may present the true AF characteristics.

VII. A novel parameter was introduced and called intracardiac power. This investigates intracardiac DF power distribution on the body surface spectra. This is an important extension to the literature which helps to clarify where on the body surface intracardiac DF contributes as a dominant or non-dominant spectral peak.

1.4. Aim of Result Chapters in This PhD Study

The aim of this project was to investigate if the LA electrical activity could be observed preferentially in different sites on the body surface. This would be an asset to investigate and improve diagnosis of AF from the body surface. This aim was investigated exclusively in chapters 7 and 8, and to some extent in the end of chapters 3, 4, 5, and 6. However, prior to comparing the body surface and intracardiac recordings across subjects, following were essential to explore; each subject's data to justify outliers if there were any (chapter 3), if BMI had influence on the body surface recordings (chapter 4), if the body surface recordings were consistent over time (chapter 5), and over space (chapter 6).

Chapter 2. Methods

This chapter describes the recording equipment, patient recruitment, and recording protocols used in the study. The methods of data analysis, including signal processing and statistics are also discussed in this chapter. The body surface and intracardiac recording systems are explained in section 2.1 which introduces the components of these recording systems. Section 2.2 explains the data collection procedure and also provides background to the patients whose data is the focus of this work. The signal processing is explained in section 2.3, which includes body surface and intracardiac processing and estimation of different features. In section 2.4 different grouping of the body surface electrode sites are illustrated. Finally, statistical tests performed to interpret and understand the features are described in section 2.5.

2.1. Recording Equipment

Body surface potential mapping and electrophysiology recording systems were used to collect the data during this project. Familiarisation and a good understanding of the recording systems were essential prior to the start of data collection.

2.1.1. Body Surface Potential Mapping Recording System

BioSemi® (BioSemi, Amsterdam, Netherlands) ActiveTwo™ was used to record the cardiac electrical activity from the body surface. This equipment consists of sets of electrodes, an analogue to digital converter (A/D box), a USB receiver and a display device. A simple block diagram of the BSPM recording system is depicted in Figure 35, and each component is explained in the sections to follow.

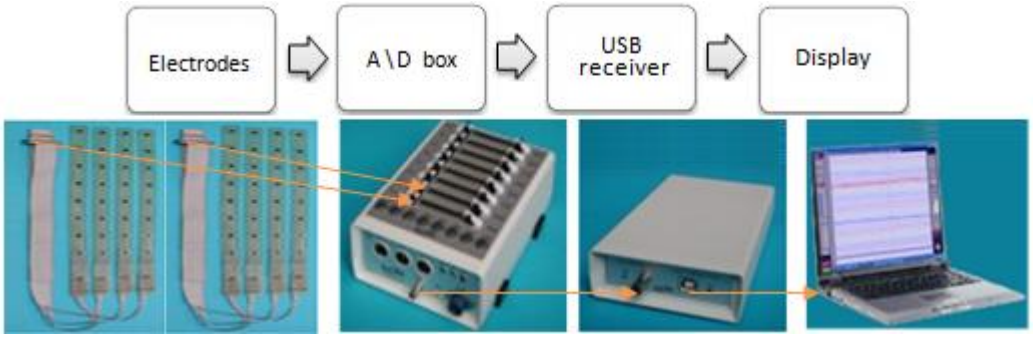

Figure 35. A schematic representation of the BSPM recording system components.

Electrodes: There are 3 bipolar electrodes that are used as limb leads, and 64 monopolar integrated pre-amplifier carbon electrodes (active electrodes) that are used as 64-lead BSPM. The active electrodes make the signal less sensitive to environmental noise and movement of the electrode cables. Carbon electrode discs and wires are invisible under X-ray machine. The 64-lead BSPM are arranged in 8 flexible rubber strips (length of 43 cm) with 8 electrodes on each strip (each 45 mm apart, centre distance). They are fixed in two sets of 4 strips, the electrodes in one set are numbered 1 to 32 (Set A), and the other set 33 to 64 (Set B).

A/D box: The electrode cables are fed into an analogue to digital convertor which digitises the signals with 24 bit resolution, 31nV digital resolution (least significant bit (LSB)) and sample rate of 2048 Hz. The digitised data is transmitted via an optical fibre data link to a USB receiver. A fibre optic link enhances the interference rejection and subject safety.

USB Receiver: The USB receiver converts the optical data coming from the A/D box to a USB output.

Data Acquisition Programe: LabVIEW software is used to display the signal on a digital screen. The collected signals are stored in BioSemi Data Format (BDF) on a standard personal laptop.

2.1.2. Intracardiac Recording System

LabSystem™ PRO EP recording system (Bard Electrophysiology, Lowell, MA, USA) was used to record the cardiac electrical activity from inside the heart. This contained a catheter, connection box, amplifier and a display device. A simple block diagram of instrumentation and component connections of the intracardiac recording system is depicted in Figure 36. An explanation of each component follows. Appendix A contains information about more sophisticated instrumentation and component connections.

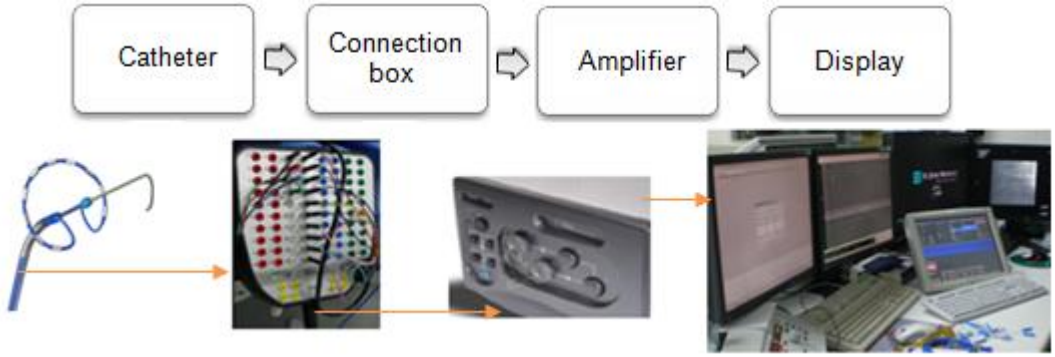

Figure 36. A schematic representation of the EGM recording system components.

Catheter: A range of catheters are used in the EP labs. Catheters differ based on the electrode spacing and the shape. Some types of catheters are used for mapping the electrical activity of the heart, and others are used for delivering ablation therapy. There are also some catheters that perform both mapping and ablation. Depending on the anatomical location within the heart that is being studied, the cardiologist will chose the appropriate type of catheter.

The types of mapping catheters that were used in this study are as follows:

- **PVAC:** A pulmonary vein ablation catheter (PVAC) (Ablation Frontiers, Carlsbad, CA, USA) was used to record EGM from the PVs. The PVAC® is a bipolar 10-electrode catheter with 3 mm long electrodes and 3 mm spacing between each electrode, see Figure 37 below.

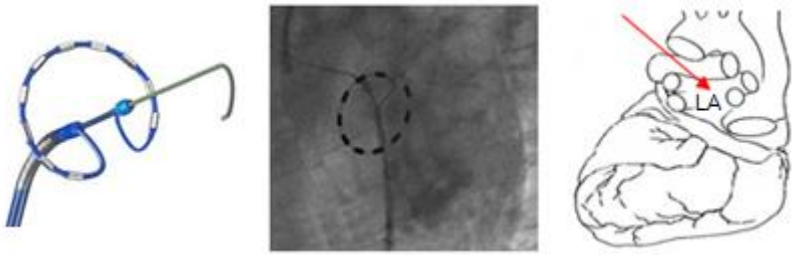

Figure 37. The PVAC catheter. Device view (Left), x-ray view (middle), and location in the heart (right).

- **CS:** A CS catheter (Bard Electrophysiology, Lowell, MA, USA) was used to record EGM from the CS. The CS® is a bipolar 10-electrode catheter with 2-5-2 mm spacing, see Figure 38 below.

Figure 38. The CS catheter. Device view (Left), x-ray view (middle), and location in the heart (right).

Amplifier: A CLEARSIGN Bard amplifier was used to amplify signals with 16-bit A/D converter and noise rejection filters. In order to find the frequency characteristic of the amplifier, which was not specified by the manufacturer, a test signal was performed in the EP lab. A 7 mV sine wave signal was generated by a signal generator (LEVELL R.C. Oscillator Type TG200DMP).

The generated signal was applied to the distal electrode pairs of a CS catheter. The catheter was connected to the amplifier via the connector box. The signal was displayed on the screen with sample rate of 1000 Hz. Figure 39 shows a block diagram of the component connections for this purpose.

Figure 39. A schematic representation of the connection route from the signal generator to display.

From the available software filter settings (band-pass filter cut-off frequencies 0.01- 400 Hz) two filter settings were selected for the experiment. (1) 30 - 200 Hz which was the standard setting used in the EP study, and (2) 0.01 - 400 Hz, which the frequency range of interest was well within this band. For characterising the frequency response of the amplifier, data was stored in American Standard Code for Information Interchange (ASCII) format, and loaded into Matlab. The gain was calculated and the frequency response curves were plotted, as shown in Figure 40. The results showed a flat frequency response curve when the 0.01 to 400 Hz filter setting was applied. This confirmed that the amplifier was sensitive to all frequencies in this range. It also suggested that the band-pass agreed with the filter cut-off frequency, as the amplifier passed the signals within the filter range. Moreover, the results showed a curved frequency response when the 30 to 200 Hz filter setting was used. This curved frequency response suggested that the band-pass agreed with the filter cut-off frequency as the amplifier passed the signals within the filter range and attenuated what was outside the defined range.

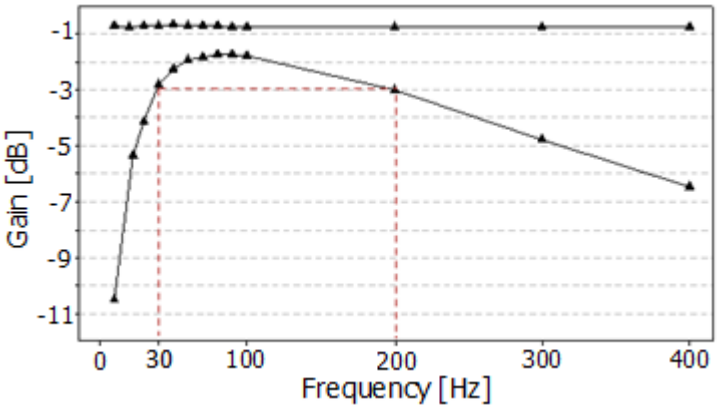

Figure 40. Amplifier frequency response plot. Top: 0.01 - 400 Hz filter setting. Bottom: 30 - 200 Hz filter setting. The red vertical dashed lines indicate the band-pass of the frequency response curve.

Data Acquisition Programe: LabSystem™ PRO V2-4a software was used to display the collected signals, as shown in Figure 41.

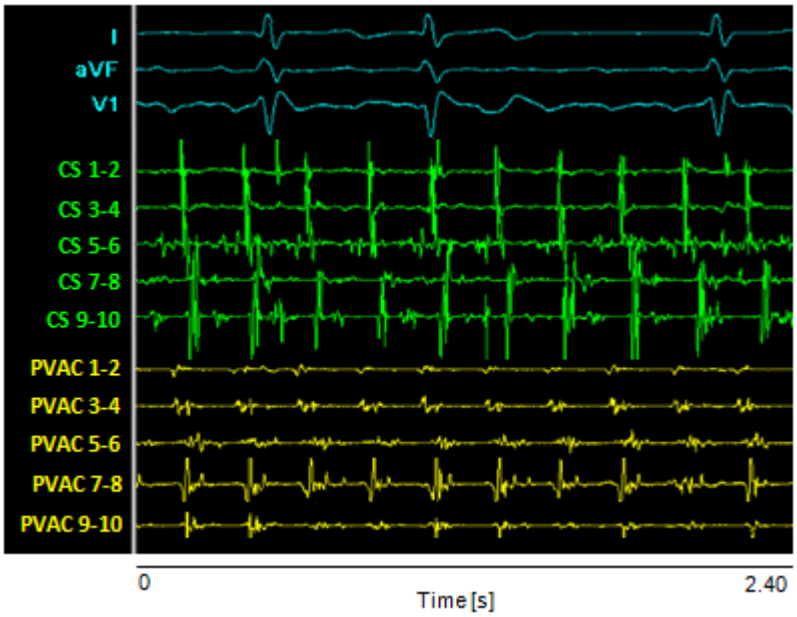

Figure 41. Illustration of the EGM recordings from 3 leads of the 12-lead ECG (blue), five CS sites (green), and five PVAC sites (yellow).

2.2. Patient Recruitment and Recording Protocols

To compare body surface and intracardiac recordings in AF patients, electrical activity from the heart was recorded simultaneously from the body surface and inside the heart. To obtain permission for recruiting patients and recording signals, letters of access and ethical approval were obtained.

2.2.1. Letter of Access for Research

This letter confirmed the right of access to conduct research through the Newcastle upon Tyne Hospitals NHS Foundation Trust. To obtain this access, a good understanding and strict adherence to the requirements of the NHS confidentiality code of practice and the Data Protection Act 1998 was demonstrated. This was done by undertaking good clinical practice (GCP) and Caldicott /data protection trainings.

2.2.2. Ethical Approval

The ethical approval form was completed and submitted to the Research Ethics Committee (REC), through the Integrated Research Application System (IRAS). For this purpose the project protocol, participant information sheet and participant consent form were prepared. The ethical approval form contained seventy six questions (e.g. summary of the study, methodology, identifying the potential risks and burdens for the participants, physical security arrangements for storage of personal data during the study). After submitting the completed form, an interview took place with the Sunderland Research Ethics Committee. The interview panel consisted of hospital consultants, nurses, healthcare professionals, statisticians, and lay people. The PhD student was interviewed by the panel, and the panel gave a favourable ethical opinion for three years (Ref: 10/H0904/55).

2.2.3. Patient Recruitment

Patients in AF coming to the Freeman Hospital for cardiac catheter ablation as part of their treatment were candidates for this research. To approach this group, initially a participant information sheet (see Appendix B) was sent to these patients. This information sheet was sent with their pre-

assessment appointment letter at least one week prior to their procedure being scheduled. The following were clearly explained on the information sheet: the purpose of the study, who is a suitable candidate, what will happen to patients who take part, any risk that personal information of the patients will be kept confidential, and who is organising the research. With the co-operation of the out-patient department nurses, these patients were seen by the PhD student after their pre-assessment appointment. If they were interested in the study and had questions, appropriate information was given and discussed. If they were willing to participate, they were seen on the day of their ablation procedure and informed consent was obtained.

2.2.4. Electrode Positioning

Prior to the ablation procedure, while patients were on the couch in the EP lab, the 67 electrodes (3 limb leads, and 64-lead BSPM) were attached to enable signals to be recorded from the body surface. This was done after skin preparation, such as shaving hair from electrode sites and wiping the skin surface to remove skin oil. Pre-defined anatomical references were identified for attaching the electrodes on the body surface. The anatomical references were important to keep the location of the electrodes consistent across all patients. However, it was essential to work around the cardiologist and technicians. As the data was being collected from patients during surgery, if necessary, the quality of signals for the cardiologist was prioritised over electrode placement. The electrode placement used in this study is shown in Figure 42. The Set A was used to record signals from anterior sites, and the Set B was used to record signals from posterior sites. The electrodes on Set A were placed approximately parallel with one another on the torso from the level of the top of

the sternum, down to the waist (anterior sites). The electrodes on Set B were placed on the back (posterior sites), in the corresponding locations as the anterior sites.

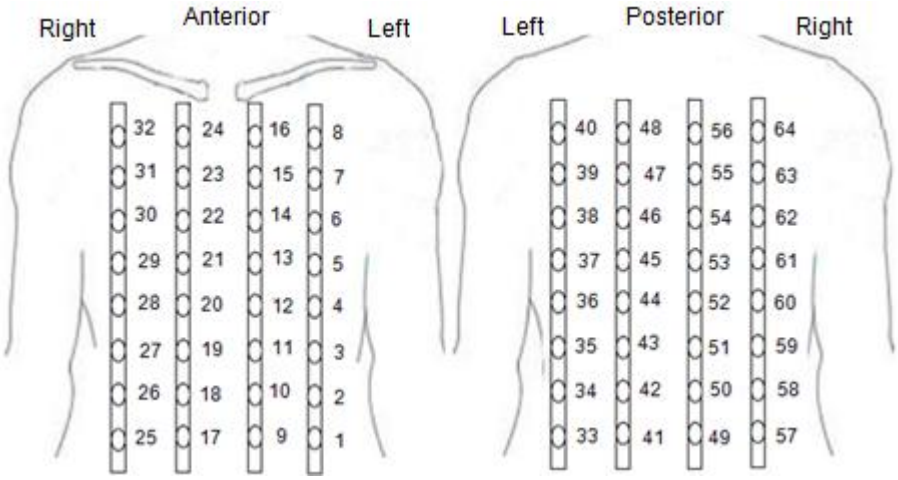

Figure 42. Electrode positioning on the body surface. One set with four flexible rubber strips numbered from 1 to 32 was used to record signals from anterior sites, and the other set numbered from 33 to 64 was used to record signals from posterior sites.

Distances between each vertical strip on the anterior and posterior were identified according to the other recording or mapping devices that were needed to be placed on the patients for the ablation procedure, e.g. electrode pads, see Figure 43.

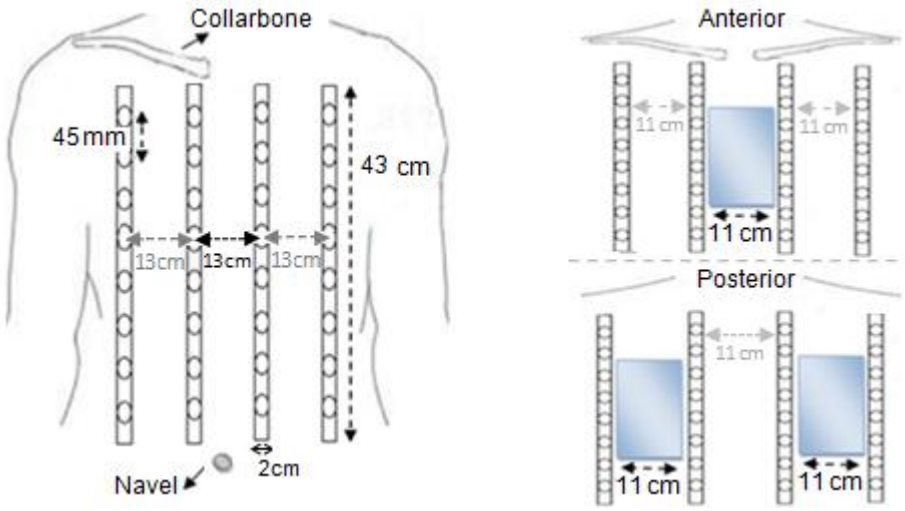

Figure 43. Spacing between vertical strips. Left: position of the anterior strips. Right: position of the electrode pads (blue) between the anterior and posterior strips.

For the BSPM recordings, site 22 was chosen for illustration and to compare between subjects. This site was chosen because: (1) it is closest to lead V1 on the 12-lead ECG which is often used for AF analysis (Petrutiu et al. 2006); (2) It usually has the largest AF signal amplitude between the 64 body surface sites (see chapter 6). Figure 44 shows the location of site 22 and lead V1 on the body surface.

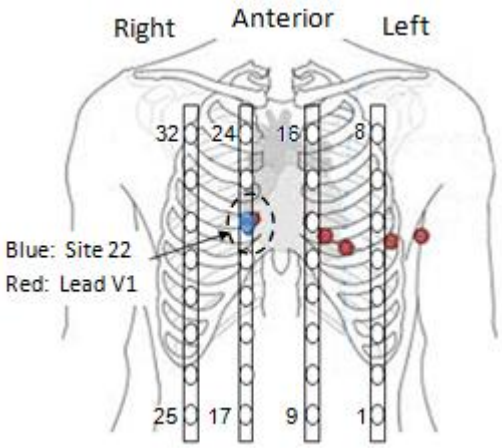

Figure 44. Illustration of location of site 22 (blue) and lead V1 (red).

For the intracardiac recordings, the signal recorded between electrode pairs 1 and 2 on the PVAC catheter was named PVAC1, between 3 and 4 was named PVAC2, between 5 and 6 was named PVAC3, between 7 and 8 was named PVAC4, and finally the signal between electrode pairs 9 and 10 was named PVAC5. In the same manner, signals recorded from the CS catheter were named CS1 to CS5. For the EGM recordings, sites CS4 and PVAC4 were chosen for illustration, in addition to comparing between subjects. These sites were chosen as they had good signal quality (kurtosis < 3) across all 20 subjects. Figure 45 shows the location of CS4 and PVAC4 on the catheters located inside the heart.

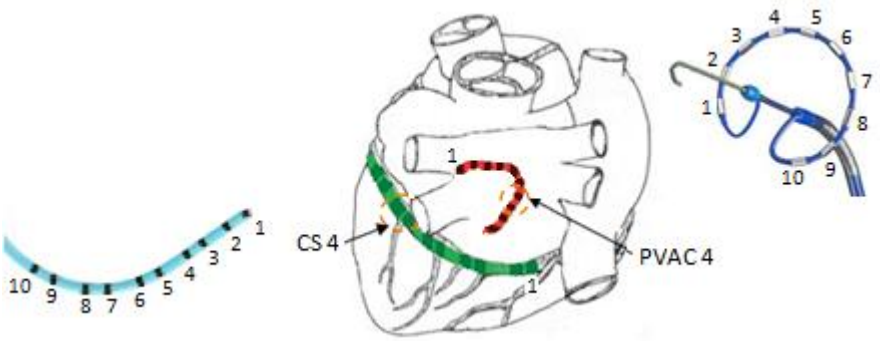

Figure 45. Illustration of locations of CS4 and PVAC4 inside the heart.

However, it is important to note that: (1) the location of the CS4 was not consistent across subjects, with small perturbations to the horizontal position in different patients. (2) The location of the PVAC4 was not consistent across subjects as it was in different PVs.

2.2.5. Description of Patients

Forty two patients were approached. Thirty five patients agreed to take part and were consented. Data was recorded from November 2010 to December 2011. In four patients, recorded data were not usable due to high levels of noise caused by excessive movement, breathing and x-ray machine noise. In six patients, recordings were not completed because they were in sinus rhythm as AF could not be induced. In five patients, recordings were not completed because they had some complication during the cardiac ablation and the electrodes had to be removed.

Data from twenty patients was analysed and the results are presented in this study. Table 1 summarises the patients recruited to this study for whom complete data was acquired.

Subject	Gender		Age	BMI	Type of AF		Previous Ablation	Number of ablation start to end of procedure	Heart disease	Ending the procedure			
	M	F			Par	Per				SR	AF	EC	F
1	√		55	26.3		√	1	6	None			√	
2	√		69	25.9	√		1	3	Atrial flutter			√	
3	√		61	24.0	√		None	3	None	√			
4	√		68	27.7	√		1	3	None		√		
5	√		72	28.1		√	None	5	None			√	
6		√	66	25.0		√	None	6	None	√			
7		√	61	38.5		√	None	4	None			√	
8	√		68	33.3	√		1	4	None	√			
9	√		56	24.3	√		None	4	None				√
10	√		56	26.3	√		1	3	None		√		
11	√		52	33.7		√	None	5	None			√	
12	√		40	26.2	√		1	3	Bradycardia	√			
13	√		64	28.4		√	None	4	Congestive failure			√	
14	√		61	26.3	√		1	5	None			√	
15	√		59	27.2	√		3	4	Pre-excitation syndrome			√	
16		√	71	39.0		√	None	5	Dyspnoea on exertion			√	
17	√		63	34.8	√		None	3	CABG*			√	
18	√		70	30.9	√		None	6	None			√	
19	√		47	27.9	√		None	2	None	√			
20	√		49	26.2	√		1	3	Atrial flutter			√	

*coronary artery bypass graft

Table 1. Description of subjects. Subject=patient's number. Gender: M=male, F=female. BMI=body mass index (kg/m^2). Type of AF: Par=paroxysmal, Per =persistent. Ending the procedure: at the end of the ablation procedure patient was in SR, or AF. If AF, patient finished in AF, or electrical cardioversion (EC) was performed, or Flecainide injected (F).

2.2.6. Recording Data

Two minute recordings were obtained simultaneously from the 64-lead body surface, five CS and five PVAC sites during catheter ablation procedure. The recordings were obtained before starting the procedure (baseline), before and after ablation of each PV, and after ending the procedure. In this study the baseline was analysed and the rest of the data is to be made available for future studies such as AF characteristics changes between ablation, which was beyond the aim of this work.

2.3. Signal Processing

The recorded signals contain information hidden in their structure, which was not readily observed when recording. This information had to be extracted in some way so that the signals could be given meaningful interpretation.

Therefore, signal processing was used for extracting clinically significant information hidden in the signals. The signal processing was performed using a laptop operated by Windows 7 Home Premium, 2.50 GHz processor 64-bit and i5-3210M CPU. All algorithms were developed in Matlab® (The MathWorks Inc., Natick, MA, USA) version 7.10.0. The following signal processing section is presented in four main groups:

- Time synchronisation between the body surface and intracardiac (section 2.3.1).
- Body surface processing (section 2.3.2): This includes format conversion, down sampling, WCT computation, and filtering, followed by AA estimation which was achieved via two methods: QRST cancellation, and isolating AF segments. Subsequently parameters of interest were estimated in two domains: Time (to estimate AF amplitude) and Frequency (to estimate DF and SC).
- Intracardiac processing (section 2.3.3): This includes format conversion, filtering, far-field ventricular activity cancellation, further filtering and rectification. The parameters of interest (DF and SC) were estimated in the same manner as used for the BSPM recordings.
- Body surface and intracardiac comparison (sections 2.3.4 to 2.3.8). This includes BSPM and EGM spectra morphology correlation, BSPM and EGM comparison in time domain, and estimation of two novel parameters, which are the intracardiac power distribution and the body surface peak type.

Figure 46 and Figure 47 show schematic representations of the BSPM and EGM processing, respectively.

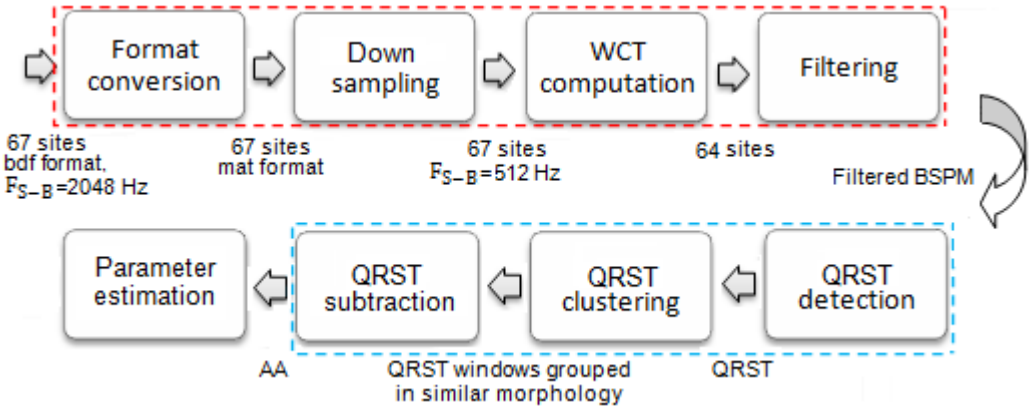

Figure 46. A schematic representation of BSPM processing. The 67 sites includes 3 limb leads and 64-lead BSPM. The red box denotes pre-processing and the blue box represents atrial activity estimation. F_{S-B} is the BSPM sampling frequency.

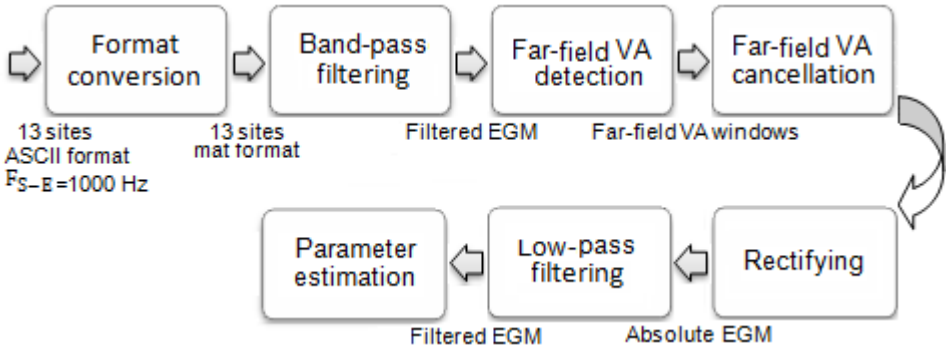

Figure 47. A schematic representation of EGM processing. The 13 sites includes 3 limb leads, 5 CS and 5 PVAC sites. F_{S-E} is the EGM sampling frequency.

2.3.1. Surface and Intracardiac Recording Time Alignment

Differences in the sample rate of the BSPM and EGM recordings were taken into account and the first beat of these recordings was synchronised manually. However, there was a time shift between the BSPM and EGM recordings over time, see Figure 48. To solve this problem, the EGM recordings were synchronised in time with BSPM recordings. For this purpose, lead I from the 12-lead ECG of the EP recording system (EP lead I), and lead I from the

BSPM recording system (ECG lead I) were used. Lead I was chosen as this signal was recorded independently on both the intracardiac and the body surface recording systems.

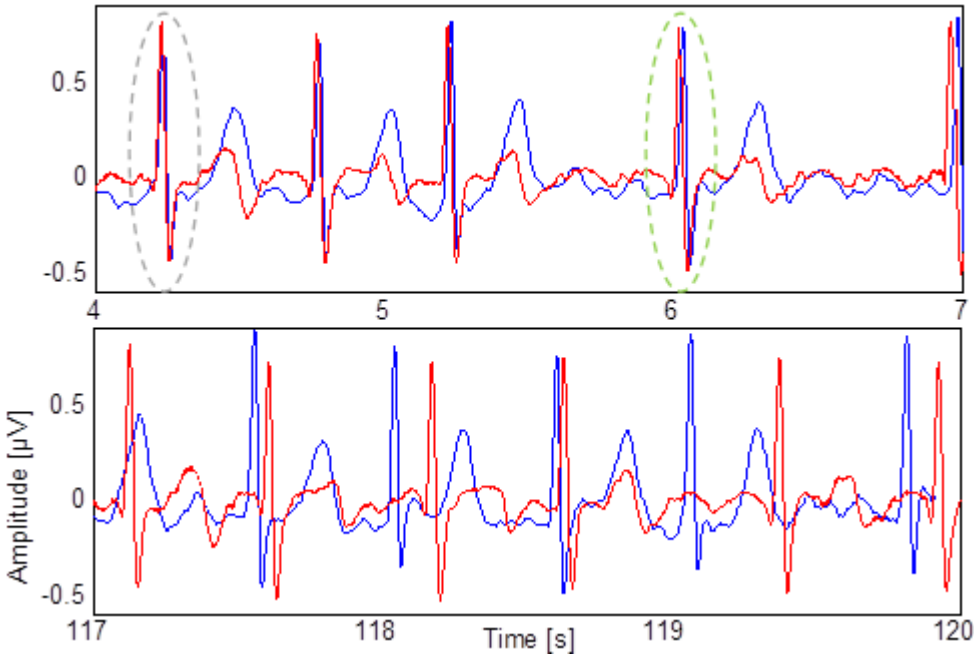

Figure 48. Illustration of the time shift between the EP lead I (red) and ECG lead I (blue) from subject 3. Top: the grey dashed circle show the first beat which is well synchronised, and the green dashed circle highlights a visible time shift in the 4th beat. Bottom: the last three seconds of the signals which are clearly desynchronised.

The time of the EGM signal (t_E) was modified using the following linear scaling:

$$t_E = t_B s + \delta t$$

Where t_B is the BSPM time, δt is the time difference between the two recordings, and s is some scaling parameter which adjusts for the differing clock speeds. Initially s was fixed at a pre-computed, empirically determined, value. Then optimal temporal shift in the EGM signal was searched for by looping over a wide range of values in δt. Within this loop the sum of squared differences between the normalised EGM and BSPM signals was computed, setting

$$\epsilon_{(\delta t)} = \sum_{i=1}^{n} (E_i - B_i)^2$$

Where E and B are the signals from the EGM and BSPM respectively, and n is the size of both time-series. The value of $\delta t = \delta t_0$, which minimises the sum of squares, ϵ (for the fixed value of s) was taken. The next step was to use the calculated value of δt to minimise ϵ as a function of δt and s. A reduced range in δt such that $\delta t_0 - 0.2 \leq \delta t \leq \delta t_0 + 0.2$ and $1.002 \leq s \leq 1.004$ was taken. Over these parameter values the following quantity was calculated

$$\epsilon_{(\delta t,s)} = \sum_{i=1}^{n} (E_i - B_i)^2$$

Again, the values of δt and s which minimised ϵ were searched through. Once these values were found, the time axis of the EGM signal was scaled with the chosen values of δt and s and further analysis proceeded with this modified signal. Figure 49 shows the synchronised BSPM and EGM signals.

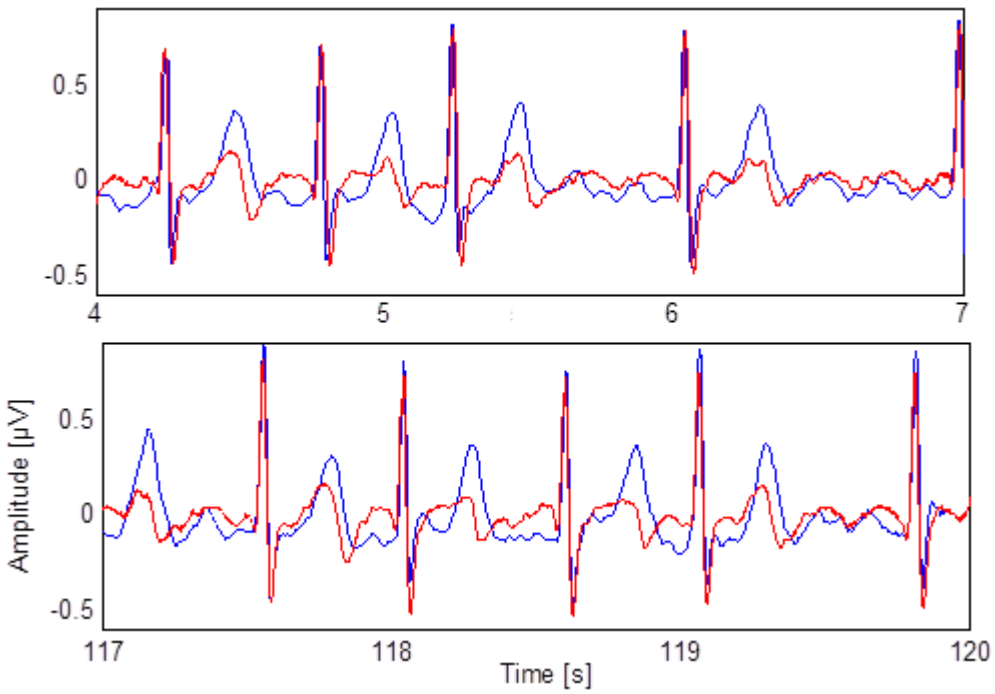

Figure 49. Illustration of the synchronised EP lead I (red) and ECG lead I (blue) for three seconds from the beginning and end of the two minute recordings (subject 3).

The BSPM and EGM time alignment was checked visually, and also through plotting the time points of the detected R-waves from both systems (see Figure 50). The results were satisfactory for all subjects.

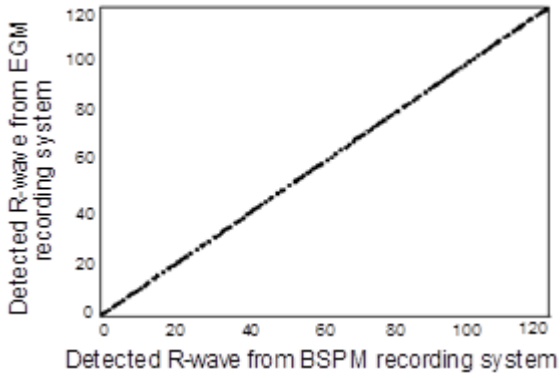

Figure 50. Illustration of time alignment accuracy between the BSPM and EGM recordings (subject 3).

2.3.2. Surface Recording Processing

Pre-Processing

The BSPM recordings in BDF format were loaded into Matlab and stored as .mat format. Sampling frequency (F_{S-B}) of the data was down sampled from 2048 Hz to 512 Hz, using the 'resample' function in Matlab. This reduced both the computational effort and more importantly, the memory requirements. AF exhibits DF 3 - 9 Hz components, which are far below $F_{s-B}/2$ (Nyquist Frequency), therefore the spectral content of AF was not altered by down sampling. The BSPM recordings were referenced to WCT by computing the average of the 3 limb leads and subtracting this from the 64 sites. The BSPM was filtered to clear the artifacts such as baseline wander, power line noise, patient movement noise, and any other possible noise. A second order, infinite impulse response (IIR), elliptical filter of low cut-off at 0.5 Hz and high cut-off at 100 Hz, for baseline wander removal and high frequency noise suppression was chosen. An elliptic filter was chosen as it provides the sharpest transition

between the pass-band and the stop-band. In addition, a Notch filter at 50 Hz was added to reduce electromagnetic (mains) interferences. Figure 51 shows the BSPM before and after filtering.

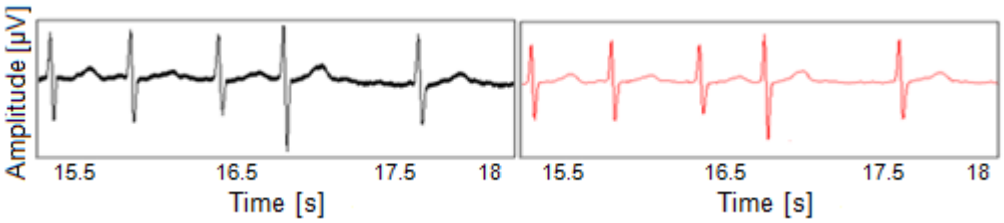

Figure 51. Illustration of the BSPM signal before (black) and after (red) filtering.

Atrial Activity Estimation

Atrial activity estimation was performed in two methods. QRST cancellation and isolation of the AF segments. Atrial activity estimated by QRST cancellation was used to investigate dominant frequency and spectral concentration variability between subjects, over time and over space. Atrial activity estimated by isolation of the AF segments was used to investigate AF amplitude variability between subjects, over time, over space, and comparing BSPM and EGM in time domain.

Method 1: QRST Cancellation

QRST Detection: This section explains the process by which the R-waves and the QRST windows (beats) were detected on the BSPM recordings. R-wave detection was performed on a single body surface site with a prominent upright T-wave. Subsequently these time points were used to detect the R-waves on all the BSPM sites. The entire procedure is outlined in Figure 52 and each step is explained later. The R-waves were clearly visible on the filtered BSPM, see Figure 53. A simple procedure to detect the temporal locations of these R-waves was to take the time derivative of the signal, y, which was defined as dy/dt. This gave a measure of the gradient of the signal, y, at a particular

instance of time, t. A threshold based on the 99.5 percentile of the positive gradient of the signal was defined.

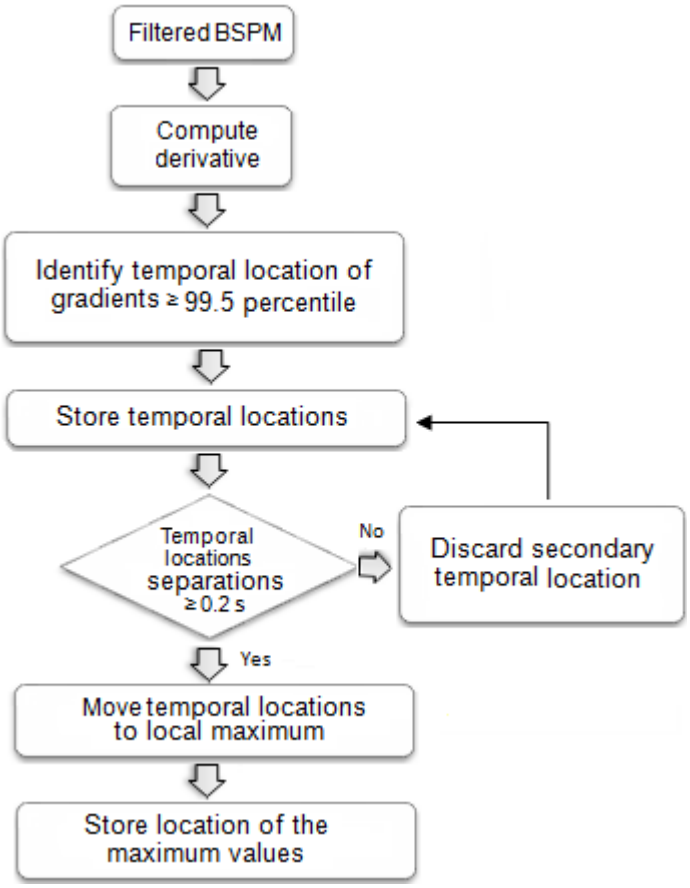

Figure 52. A schematic representation of R-wave detection algorithm.

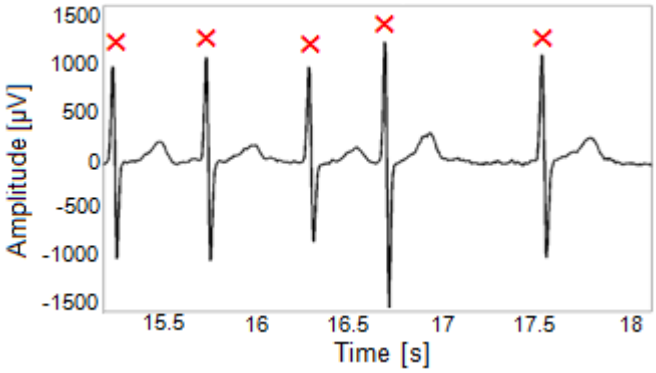

Figure 53. Illustration of five R-waves (the red crosses) on the filtered BSPM.

Since the R-waves in the signal were located where there was a rapid change in the sign of the signal (hence large gradients), location of the R-waves were readily identified, see Figure 54. From this, values of the positive gradients which mark the 99.5 percentile were computed, and the temporal locations of all

gradients were stored. When performing this analysis, the R-waves were checked manually and the threshold was modified if there were any missed R-waves or duplicate in detection. Importantly the separation between different R-waves was forced to be larger than 0.2 s.

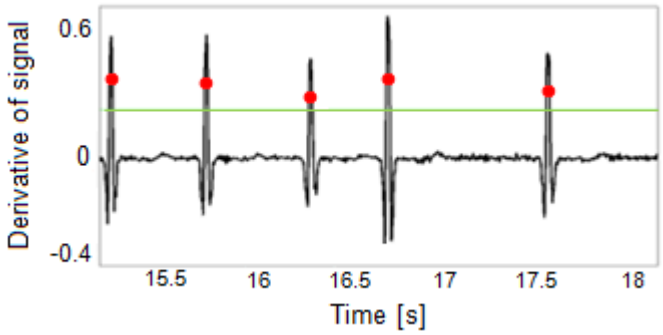

Figure 54. Illustration of five R-wave derivatives. The red dots are detected peaks and the green line is the threshold.

The detection of R-waves within milliseconds of each other arose due to fluctuations in the gradient of the signal at the location of the R-wave. If this check had not been performed then it could have incorrectly identified R-waves very close to each other. The second aspect of the algorithm was designed to account for the fact that the identified temporal locations were not true peaks of the R-waves. Indeed, maximal changes in the gradient were only located in the neighbourhood of the true peaks. To find the exact location of these peaks, the maximum value of the peaks within symmetric windows of 0.05 s on both sides of the identified temporal locations were searched through (see Figure 55). After identifying them, the temporal locations were moved to the maximum. The length of this window was chosen empirically to capture the whole QRS-wave.

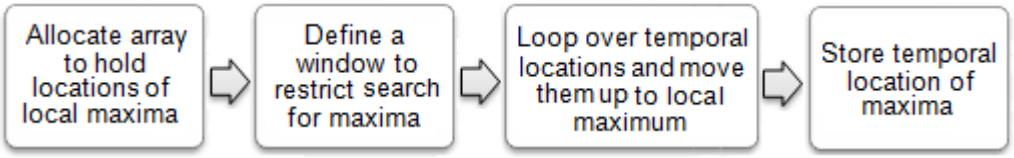

Figure 55. A schematic representation of floating detected peaks to local maximum.

After identifying the R-waves, a specific window associated with each R-wave was defined to capture the whole QRST-wave, and this was subsequently removed from the signal in a procedure defined later. In order to identify the QRST window, the start of the Q-wave and end of the T-wave were manually defined as $\mathrm{R}-\mathrm{t}_1$ and $\mathrm{R}+\mathrm{t}_2$, respectively. The window was delimited as t_1 to t_2 containing the QRST and optimised individually for each patient, see Figure 56. The window was sufficiently long to ensure it contained the full VA, from the start of the Q-wave to the end of the T-wave in all leads.

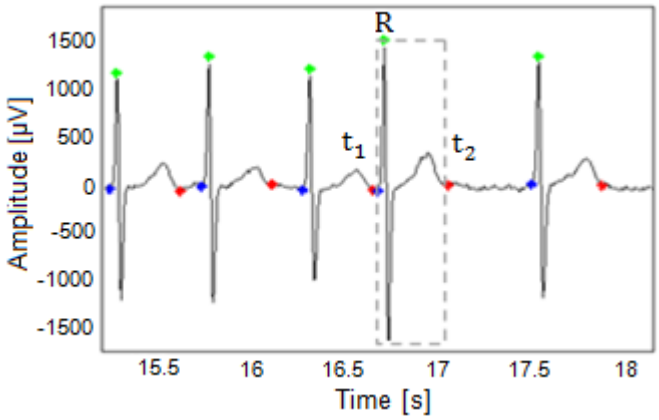

Figure 56. Illustration of a QRST-window. A window was specified associated with each R-wave (green dots) as $\mathrm{R}-\mathrm{t}_1$ and $\mathrm{R}+\mathrm{t}_2$.

QRST Morphology Clustering: Using the previous algorithm, the QRST-waves (beats) were identified, with the goal of removing them from the signal to 'extract' the AA for further analysis. However, removing these beats from the signal caused the loss of the entire AA within these time periods. It could also have potentially led to erroneous artifacts associated with repetitive periods of zero signals. A more robust approach was to subtract the beats from the signal using the ABS method. A limitation of this method was the residuals after subtraction. The ABS method relied on the assumption that the average beat represents each individual beat. However, beat morphology changes in time due to variations in the electrical axis of the heart and respiratory activity. The

approach taken in this study was to subtract the morphology of a 'typical' beat from the signal within each beat, known as beat morphology clustering. Figure 57 shows a schematic representation of this procedure.

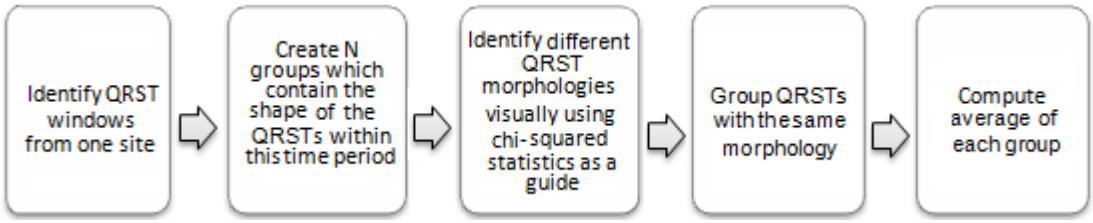

Figure 57. A schematic representation of beat morphology clustering procedure.

If there were N beats within the signal, then N QRST windows were identified. If the j^{th} of these windows to be denoted q_j, then the average window was computed as

$$\tilde{q} = \frac{1}{N}\sum_{j=1}^{N} q_j$$

However this was not a particularly satisfactory approach due to morphology changes and ectopic beats (see Figure 58). In this example, which was typical of the data, the majority of the beats had a similar morphology (coloured in black), and a small number of them had a very different morphology (coloured in blue). If the average of all the beats is computed, then the $\tilde{q}$ was expected to have a very similar shape to the majority of the beats. Subtracting this average from the beats with similar morphology would give very satisfactory results. Nevertheless it was clear that subtraction of this average from the beats with different morphology is not appropriate. Mathematically the majority of the beats were identifiable by the sum of square differences, defined as

$$\epsilon_j = \sum_{k=1}^{n} (q_j(k) - \tilde{q}(k))^2$$

where $q_j(k)$ represents the k^{th} member of the vector q_j. So ϵ_j is the sum of the j^{th} vector after subtracting the average and squaring.

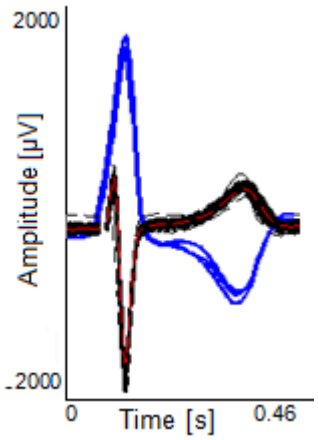

Figure 58.The beats within two minutes recordings from one BSPM site. The ectopic beats were coloured in blue to illustrate different morphologies.

Large values of X_j indicated that the morphology of that particular beat was very different to the average morphology, whereas low values indicated that the morphology of the beats were very similar to the average. The X_j was used as a guide and morphology clustering was performed manually (see Figure 59). Panel A shows the identified beats from one BSPM site. The red line shows the average according to all beats. Panel B shows the selected beats in a group on the right side of the vertical dashed line, and the beats to be selected into another group(s) on the left side of the vertical dashed line. Each bar corresponds to one beat. The arrow bar, underneath panel B, was moved to select the beats with the same morphology, with the aim of grouping them. By moving the arrow bar to the left, the vertical dashed line moved to the left and selected the bars on its right (green circle) in one group. The associated beat to each selected bar was coloured in blue on panel A. This was continued until all beats were grouped.

Using this technique the beats were grouped and their average morphology defined based on all the beats which fall within that group.

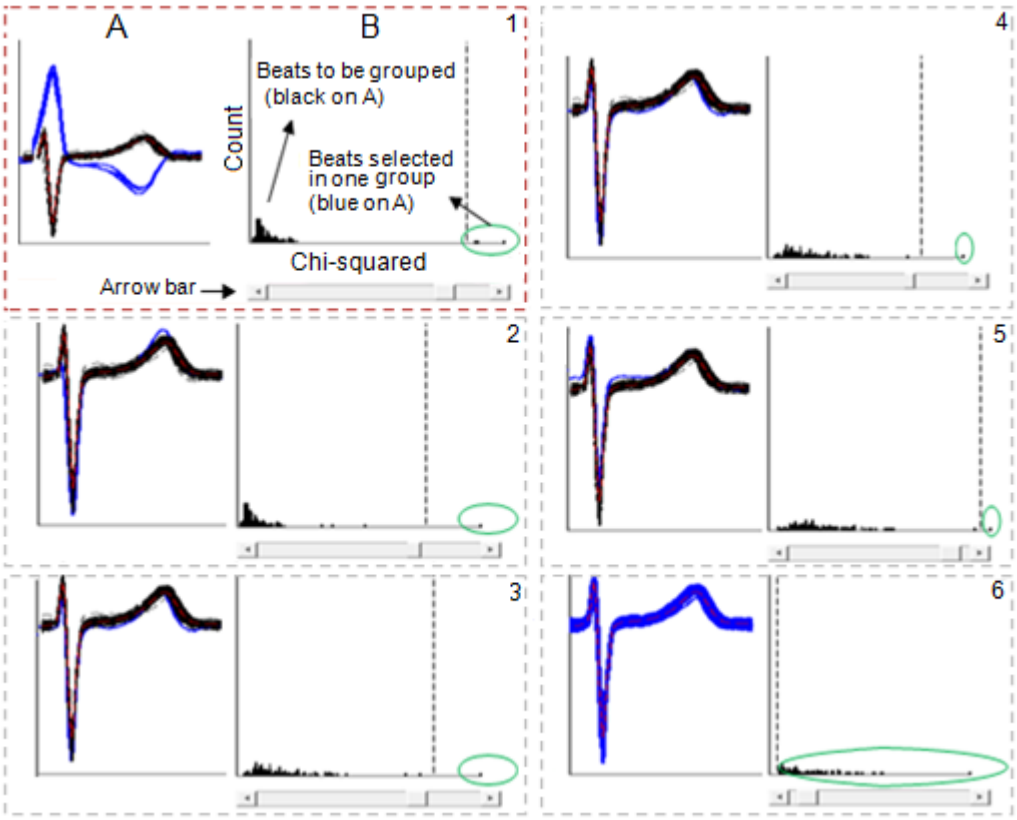

Figure 59. Morphology clustering of the beat inspection. 1 to 6 show different stages of the group selection.

QRST Subtraction: Having computed the average for each beat group, the average was subtracted from the associated group. Figure 60 shows the estimated AA after QRST cancellation.

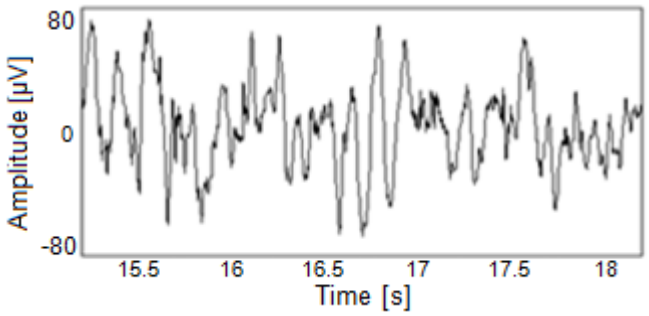

Figure 60. Illustration of the estimated atrial activity after QRST cancellation.

Method 2: Isolate AF Segments

AF can be observed without presence of VA, during the TQ segment of the ECG. This is the interval between the end of the T-wave and the start of the Q-wave of the next beat. These segments were extracted (explained later) and used to analyse the spatial and temporal variability of amplitude of AF signal. Figure 61 shows the TQ segment for one BSPM site, and Figure 62 shows the TQ segment for all BSPM sites, in one subject.

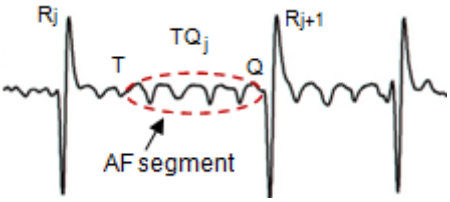

Figure 61. The j^{th} TQ segment within a two minute BSPM recording. TQ segments are the interval between the end of the T-wave and the start of the Q-wave of neighbouring beats, and contain F-waves.

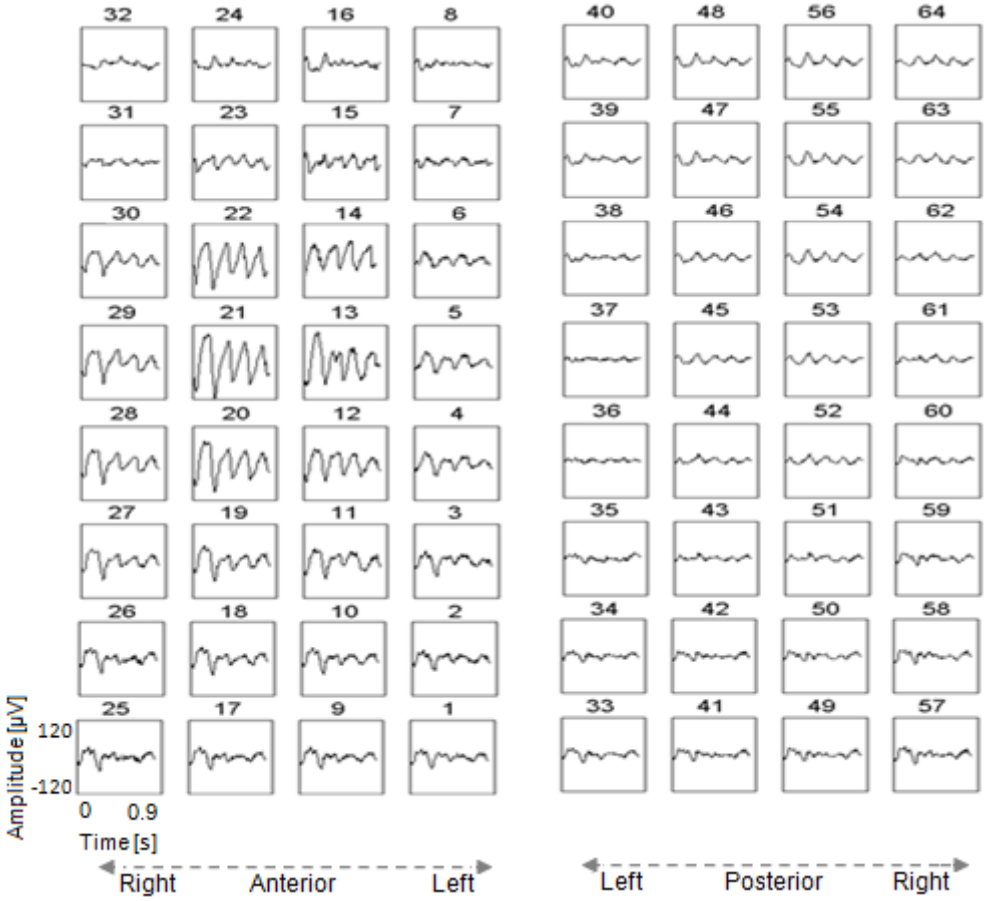

Figure 62. Spatial illustration of the j^{th} AF segment for each site (identified 1 to 64), subject 6.

Having identified the VA (previous section), TQ segments were automatically identified relative to the interval between the QRST windows containing only the AA and were referred to as ‘AF segments’.

Parameter Estimation

I. In the Time Domain

Amplitude: To estimate amplitude of the AF signal, the longest AF segment within the two minute BSPM recordings was selected (see section 2.3.2, isolate AF segments). Given the inherent noise in the AF segment, estimation of the amplitude was not a trivial process. AF signal amplitude was estimated by fitting a sinusoidal model to the AF segment. It was necessary to tune the model according to amplitude and frequency of the AF segment. An automatic algorithm was developed for this purpose. Figure 63 shows a schematic representation of the algorithm. Figure 64 shows an example of fitting the model to the AF segment in different stages for a noisy segment. Figure 65 shows some examples of the final step of fitting the sinusoidal model for the cases of both clean and noisy AF segments.

Peak to peak amplitude of the AF signal was estimated by fitting a sinusoidal model to each AF segment. Firstly, the AF segment was rescaled by subtracting the mean to stabilise the baseline, as shown below

$$\widehat{\mathrm{TQ_j(t)}} = \mathrm{TQ_j(t)} - \mathrm{mean}\left(\mathrm{TQ_j(t)}\right)$$

where t is time of the $\mathrm{TQ_j}$ signal. Secondly, a sine wave with amplitude of A was defined as

$$\mathrm{y_i(t)} = \mathrm{A sin}\left(2\pi \mathrm{f_i}\,(\mathrm{T_i} + \mathrm{k}\pi)\right),\ \mathrm{k} = [0,1]$$

in discrete intervals with F_r steps. The F_r is the frequency resolution equal to 0.125 Hz (parameter estimation in frequency domain). $k\pi$ was added to be able to translate the sine wave and match it with the shape of the signal. T_i is a period sufficient to capture a full waveform with a length proportional to the inverse of the sampling frequency $(1/f_i)$.

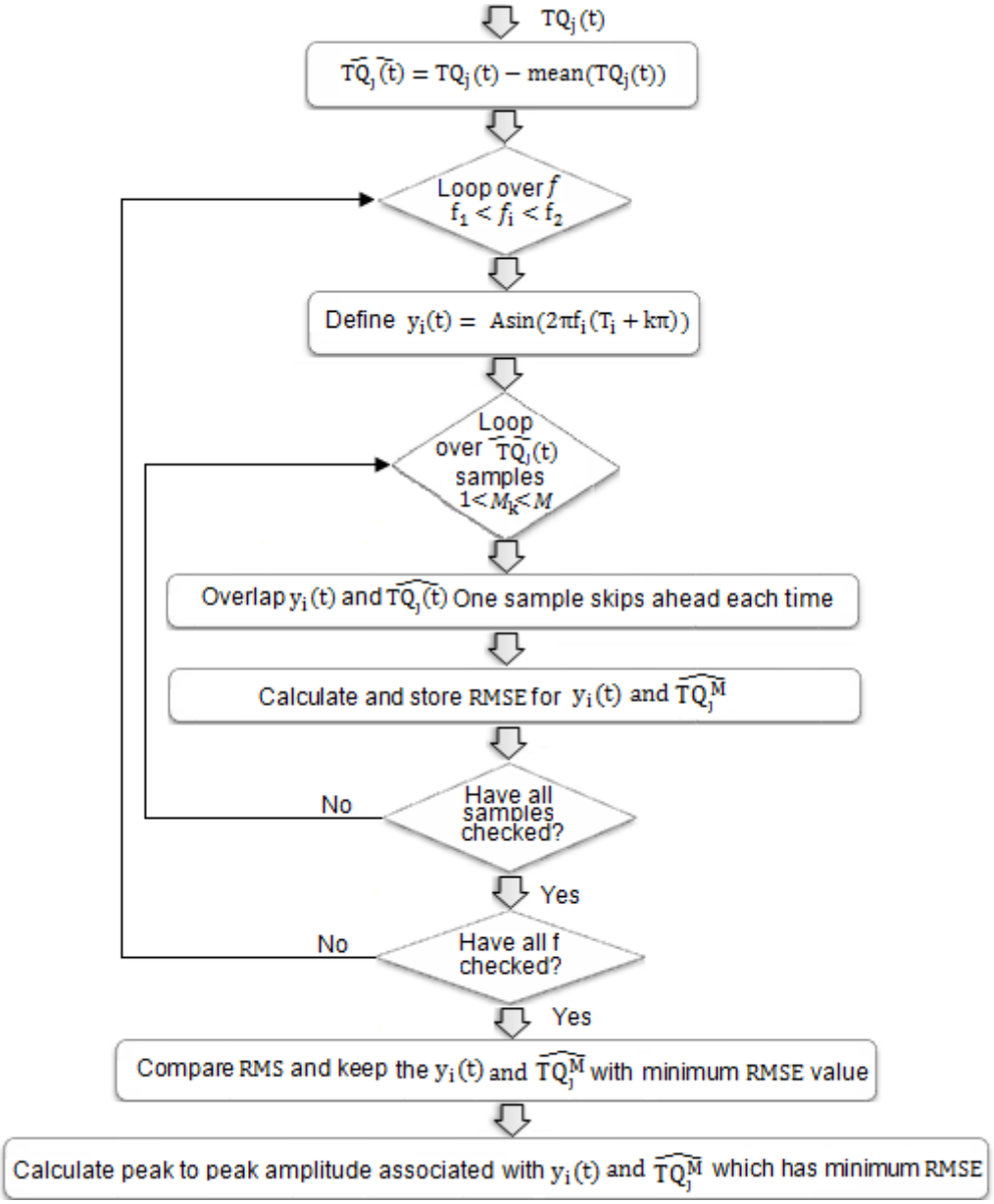

Figure 63. A schematic representation of AF amplitude estimation algorithm, by fitting a sinusoidal model.

The frequency range of f_i is 3 - 9 Hz. This range was chosen as it agrees with estimation of the typical AF DF in literature, and it fits with the estimation of

AF DF between subjects that were studied in this project (see chapter 3). Within each y_i , the amplitude was estimated as

$$A_i = (\max(\widehat{TQ_j(t)}) - \min(\widehat{TQ_j(t)}))/2$$

then $y_i(t)$ was overlapped with $\widehat{TQ_j(t)}$ from the first sample to the last sample moving one sample forward each time. So;

$$y_i^M = A\sin(2\pi f_i\,(T + k\pi))$$

where y_i^M is the model response, and M is number of samples within the $1/F_s$ intervals. The sinusoidal fit was estimated by subtracting y_i from $\widehat{TQ_j(t)}$ for each sample, with the squared residuals then averaged. To measure the discrepancy between this estimate and its true shape, the normalised root mean square error (RMSE) was computed and defined as

$$RMSE = \frac{\sqrt{\sum_{i=1}^{M}(y_i^M - \widehat{TQ_j})2\ /M}}{A}$$

The normalised sum takes into account amplitude variation and the number of points that were used to calculate the figure of merit, so it is an unbiased estimator of the quality of fit. The values of f_i were determined by seeking the combination of f_i and A_i which minimised RMSE. The pair (A_i, f_i) which does this was taken as the estimation of amplitude of the given AF segment, in a given body surface site. Mathematically it can be shown as

$$\{A_{optimal}, f_{optimal}\} = \text{argmin}\,\{\min\{RMSE\,(y_{ij}^M - \widehat{TQ_{ij}^M})\}\}$$

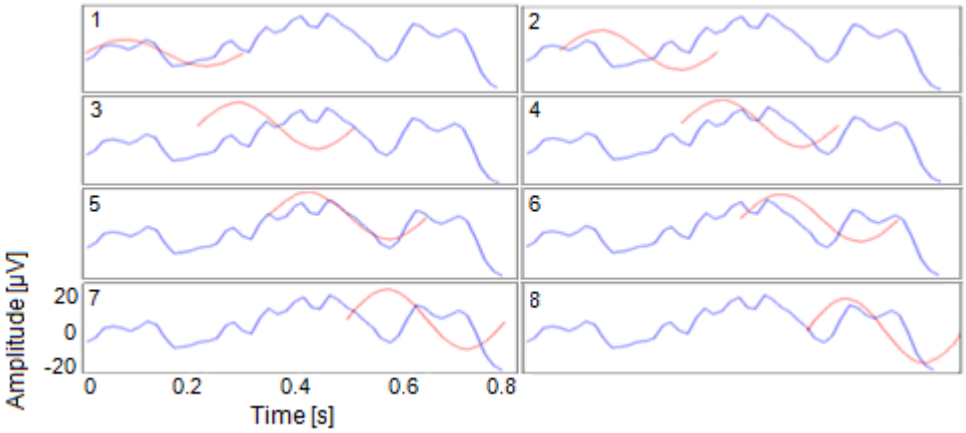

Figure 64. Illustration of AF signal amplitude estimations by the sinusoidal fit for a noisy AF segment. Eight panels show different steps of the fitting model to the segment from body surface site 45, subject 9. The blue signal is the AF segment. The red signal is the model. The model is overlapped with the AF segment from the first sample to the last sample moving one sample forward each time. The entire procedures for matching each sample are not shown. Eight steps that were more indicative were chosen to be shown.

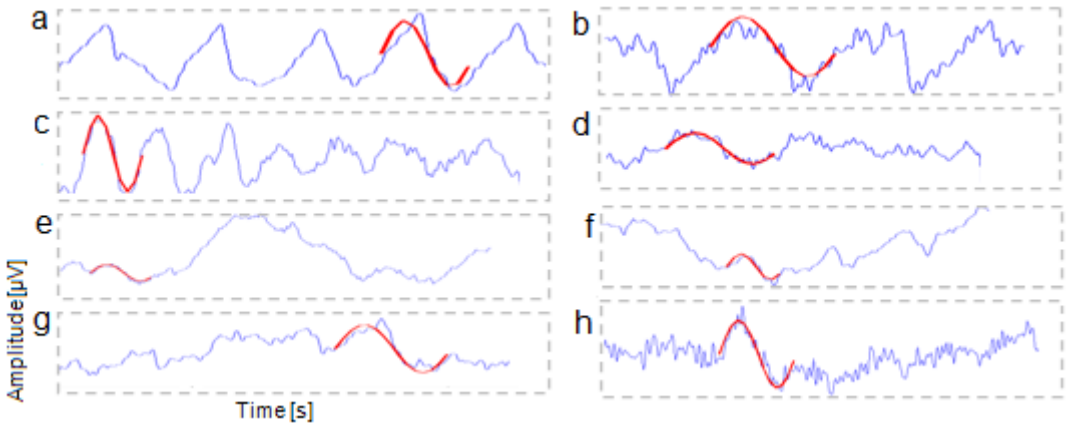

Figure 65. Illustration of AF signals amplitude estimation by the sinusoidal fit for the cases with clean (a) and noisy (b to h) AF segments. The blue signal shows the longest AF segment from different subjects at different body surface sites. The red signal shows the best sinusoidal fit. Peak to peak amplitude with the best sinusoidal fit was measured as AF amplitude.

Limitations of the estimation of the AF signal amplitude using AF segments are: (1) The j^{th} AF segment may not be the same length between subjects, thus observations may not be consistent; (2) the longest AF segments are collected from different times within the two minute recordings. Since AF is irregular, the AA within the two minutes may change, therefore observations for the same study group may be different if other segments were to be studied; (3) the model measures only one F-wave, which may not be representative of all.

II. In the Frequency Domain

To describe the periodicity of the AA, the frequency spectrum of the AA was computed, and DF and SC were estimated. The frequency spectrum describes how the power of the AA is distributed over different frequencies. This is known as power spectral density (PSD) and defined as the Fourier transform of the autocorrelation function of a continuous time process. Due to the inherent noise in the AA, the 'raw' PSD was not suitable. To reduce the spectrum variance, whilst keeping the estimation efficient, the Welch periodogram technique was used. This method sacrifices frequency resolution in exchange for noise reduction, and hence produces a smoother estimate of the PSD. Figure 66 shows a schematic representation of the steps that were taken to apply Welch's method to the data in this study.

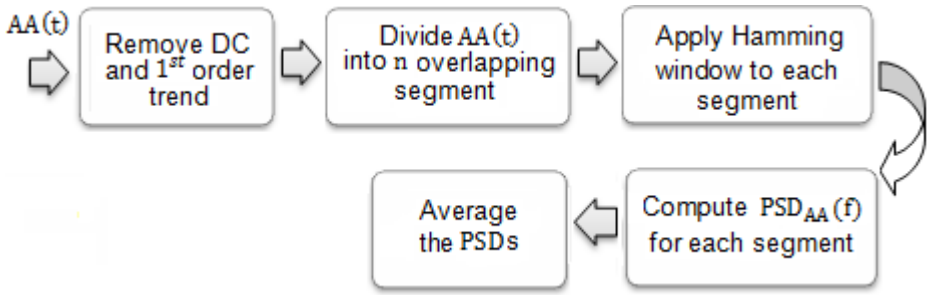

Figure 66. A schematic representation of Welch's method.

The DC and first order trend were removed from the $\mathrm{AA(t)}$, to meet the assumption that signals were stationary. The $\mathrm{AA(t)}$ was divided into n overlapping segments. The Hamming window function was applied to each segment and then they were overlapped. The window function is normally small or zero near its boundaries. As a result a significant portion of the signal is ignored in the analysis, which could be detrimental to the analysis. Overlapping the segments maximised the information that can be extracted from the signal and avoided this potential problem. Periodograms of the segments were

computed and averaged. In order to find the appropriate segmentation, different window and overlap durations were tested, and the trade-off between time and frequency resolution was experienced. A phenomenon encountered with using long window length was the large variance in the computed spectra. In this case, detection of the frequency components in the spectrum was highly sensitive to noise and the risk of false detection was high. In contrast, using a short window length led to inaccurate frequencies. In this case, detection of the frequency components in the spectrum was not exact as the frequencies were mainly obtained at one wide peak, see Figure 67.

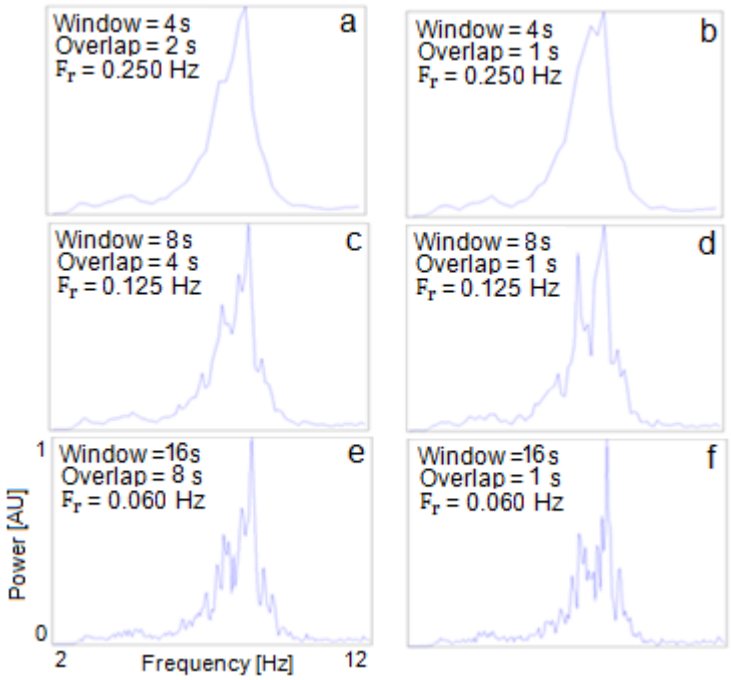

Figure 67. PSD estimation with different window duration and overlap to find appropriate segmentation (Subject 1, body surface site 22). The y-axis is normalised power. With long window length, variance of spectra was increased (e.g. f), and with short window length, frequencies were inexact (e.g. a). Panel d was used for analysis in this study as a compromise between extremes.

Finally, the $\mathrm{AA(t)}$ was divided into n overlapping segments, with each segment being 8 seconds long, with a 1 second overlap (sliding factor of 7 seconds). Each segment was windowed with a Hamming window, PSDs were computed for each segment, and then averaged. Given the ratio of sampling

frequency ($F_{s-B} = 512$ Hz) to length of the segments, frequency resolution (F_r) was 0.125 Hz. Figure 68 shows the PSD for all body surface sites in one subject.

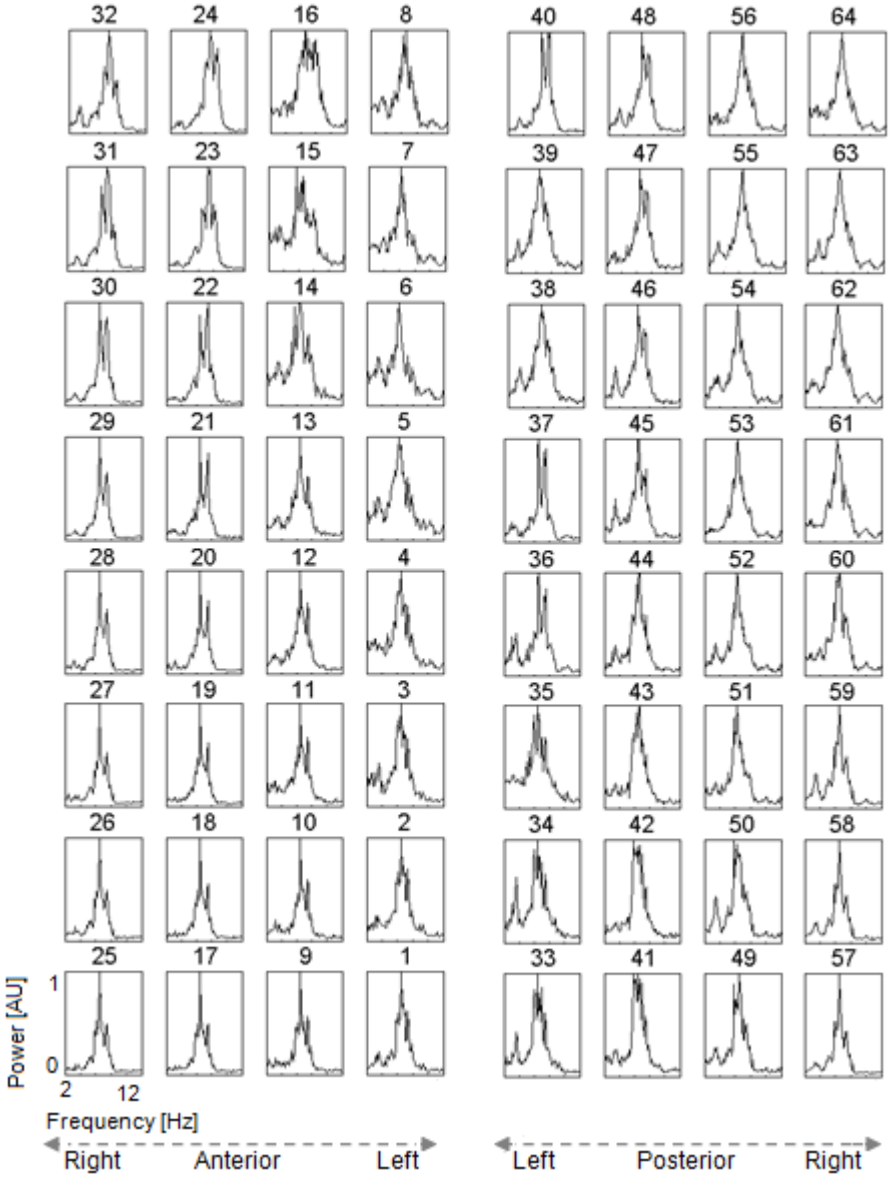

Figure 68. Spatial illustration of the PSD for each site (identified 1 to 64), subject 1.The y-axis is normalised power density to the maximum of each site.

Dominant Frequency: Given the $PSD_{AA}(f)$, DF was defined as the frequency f where:

$$DF = \arg\max\ (PSD_{AA}(f)), \quad f_1 \le f \le f_2$$

Here f_1 and f_2 define the frequency range of interest 3 to 9 Hz.

Spectral Concentration: Given the $\mathrm{PSD_{AA}(f)}$, SC was defined with similar approach to Castells, as

$$\mathrm{SC} = \frac{\int_{f_{min}}^{f_{max}} \mathrm{PSD(f).df}}{\int_{f_1}^{f_2} \mathrm{PSD(f).df}}$$

where $f_{max} = 1.17 \times DF$, $f_{min} = 0.82 \times DF$, $f_1 = 0$, and $f_2 = F_s/2$, F_s is sampling frequency (Castells et al. 2003). However, several changes were applied to the parameters defined by Castells: (1) It is likely that SC is affected by the effectiveness of the QRST suppression. To avoid this, f_1 was defined as the lowest value between 3 Hz and $DF - 1$ Hz. (2) If $f_2 = F_s/2$, it is likely that SC is affected by harmonics. To avoid this, f_2 was defined as the highest value between 9 Hz and $DF + 1$ Hz. (3) If $f_{max} = 1.17 \times DF$ and $f_{min} = 0.82 \times DF$, then the area under the curve between the f_{min} and f_{max} would be larger with higher DF. To define consistent window around DF, f_{min} and f_{max} were described as $DF - \Delta f$ and $DF + \Delta f$, respectively, where $\Delta f = 0.5$ Hz. This was chosen empirically to capture the whole frequency peak.

2.3.3. Intracardiac Recording Processing

The EGM recordings with sampling frequency (F_{S-E}) of 1000 Hz, stored in American Standard Code for Information Interchange (ASCII) format, were loaded into Matlab and stored in .mat format. A second order, IIR, Butterworth filter at low cut-off 40 Hz and high cut-off 250 Hz was used to remove baseline shift and high-frequency noise (see Figure 69). In order to identify and cancel far-field VA, the R-waves were detected on lead I from the 12-lead ECG of the EP recording system by means of a proprietary threshold-based automated detector (see section 2.3.2, QRST detection). The detected points (far-field VA) from all recordings were inspected visually to remove any missed or false

detections. A window with duration of 0.12 s (±0.06 s either side of the R-waves) was defined and called the VA-window, and marked on the EGM sites (see Figure 70). A template was constructed from averaging the VA-windows and subtracted from each VA-window for each EGM site.

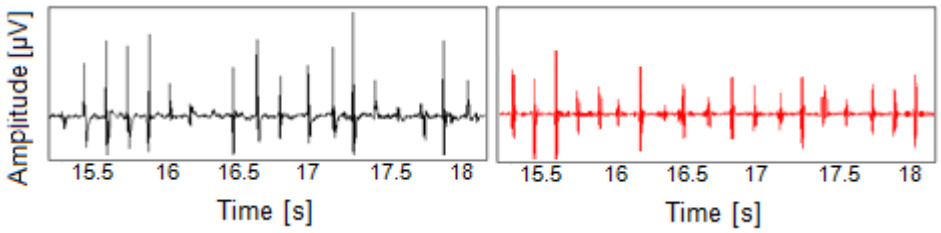

Figure 69. Illustration of the EGM signal before (black) and after (red) band-pass filtering.

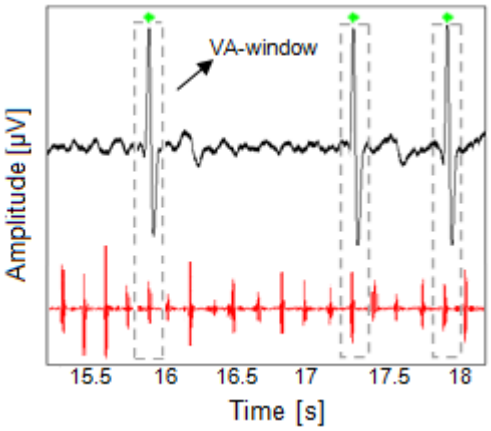

Figure 70. Illustration of identifying far-field VA on the EGM signal.

Afterwards, the EGM was rectified using the 'abs' function in Matlab. The signal was further low-pass filtered at low cut-off 20 Hz, see Figure 71. The EGM parameters (DF and SC) were estimated in the same manner as BSPM recordings.

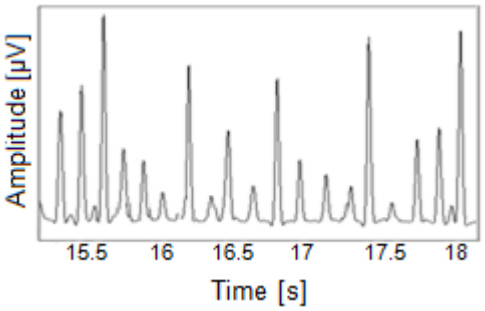

Figure 71. Illustration of the EGM signal after processing.

Figure 72 and Figure 73 show EGM signals, for one subject at all sites in the time and frequency domains, respectively.

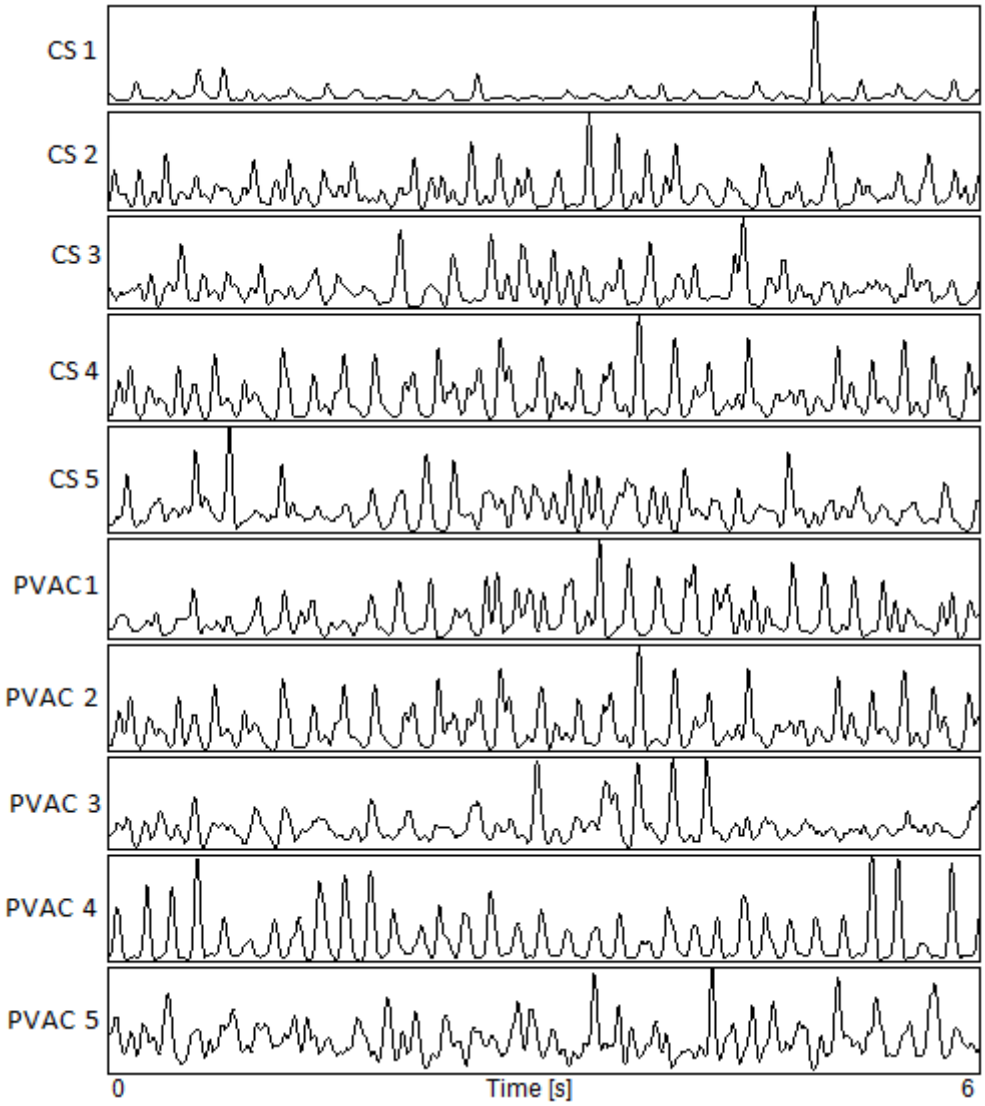

Figure 72. The EGM signals from subject 11. The y-axis is amplitude which was normalised to the maximum of each site.

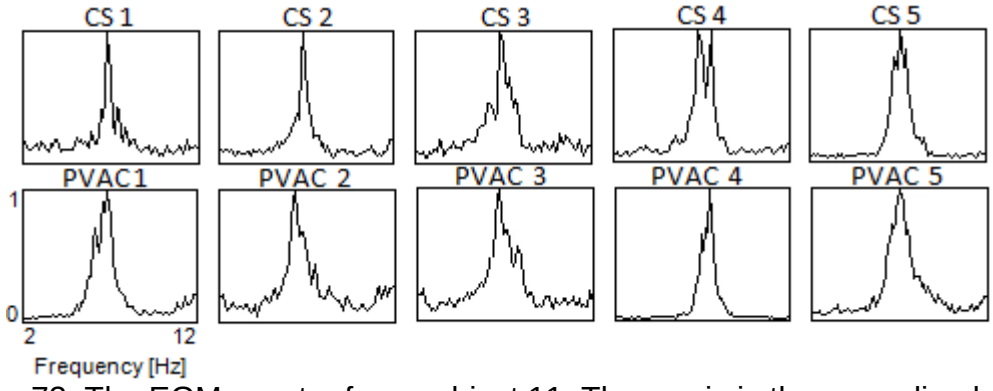

Figure 73. The EGM spectra from subject 11. The y-axis is the normalised power density to the maximum power of each site.

2.3.4. Morphology Correlation

In order to study correlation between the BSPM and EGM spectra the PSDs were normalised to the maximum power of each site and then the Pearson correlation coefficient was computed. Figure 74 and Figure 75 show three representative cases.

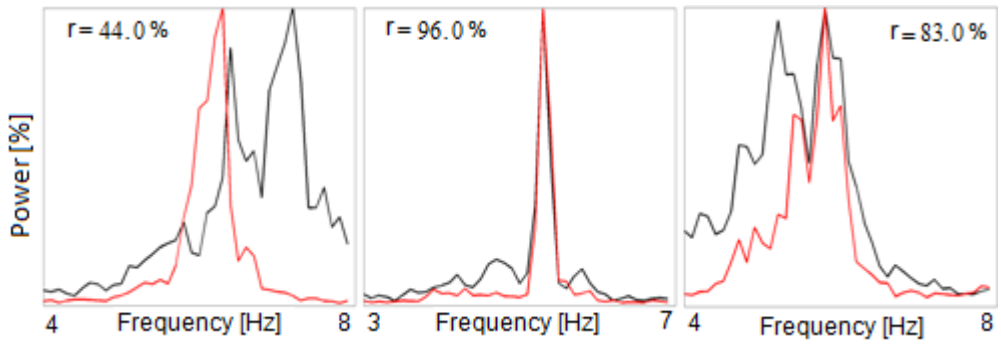

Figure 74. The PSDs with different correlations between BSPM site 22 (black) and CS4 (red). Left to right the PSDs are from subjects 1, 8 and 13.

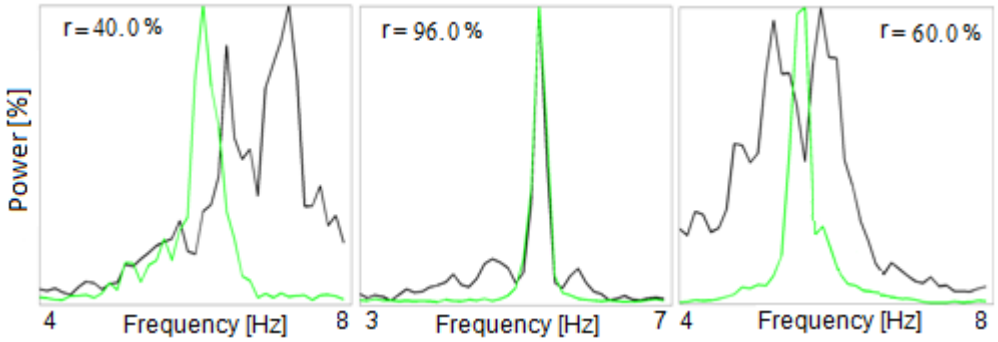

Figure 75. The PSDs with different correlations between BSPM site 22 (black) and PVAC4 (green). Left to right the PSDs are from subjects 1, 8 and 13.

The result of this study will be shown in chapter 7.2.

2.3.5. Innovative Method: Estimation of Intracardiac Dominant Frequency Power Distribution on the Body Surface Spectra

The dominant peak of the BSPM and EGM spectrum may not be the same. Of interest was if the BSPM spectra had large power associated with EGM DF. A method was developed to determine in which BSPM sites EGM DF power associated with BSPM spectrum is highest. DF estimated from the EGM

was marked on the BSPM PSD to measure EGM DF power distribution on the BSPM spectrum. Figure 76 shows a schematic representation of this procedure.

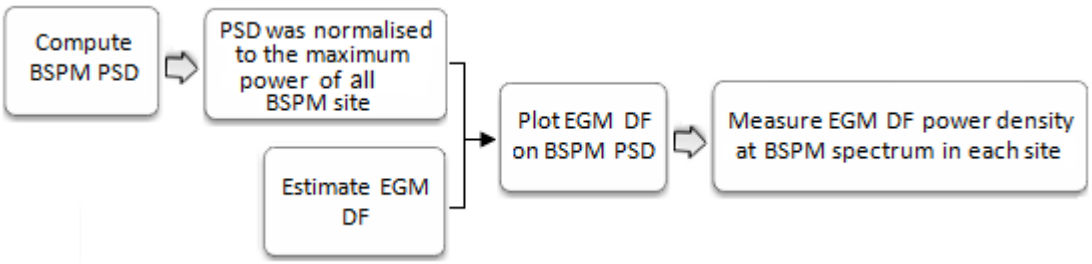

Figure 76. A schematic representation of determining EGM DF power distribution associated with BSPM DF.

If f_{EGM} is DF of a given EGM site and the power spectral density of a BSPM site is given by PSD_{BSPM}, then the power of f_{EGM} on PSD_{BSPM} denoted, P, computed as

$$P = PSD_{BSPM}(f_{EGM}) \times 100 \quad \%$$

Note that each PSD_{BSPM} (computed at each BSPM site) was normalised to the maximum power of all the sites. Hence the unit of P is a percentage, and defines the percentage of the PSD_{BSPM} power associated with f_{EGM}.

Figure 77 gives a visual definition of this quantity for four representative cases of the f_{EGM}. The result of this study will be shown in section 8.1.

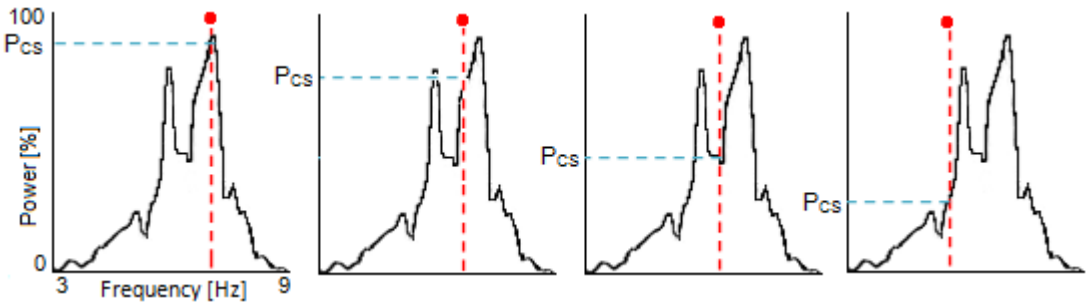

Figure 77. Illustration of a BSPM PSD from subject 1, site 22 and f_{EGM} power for four representative cases. In these examples the red dots indicate locations of CS DF on a given BSPM spectrum, and the P_{CS} indicates CS DF power distribution.

2.3.6. Innovative Method: Classifying Body Surface Frequency Components According to Intracardiac Dominant Frequency

Typically there are several peaks in the BSPM spectrum ($\mathrm{PSD_{BSPM}}$). The frequency and power density of these peaks may differ across the BSPM sites. Therefore, analysing only DF omits some information in the spectrum. To avoid this, a method was developed to determine which BSPM sites exhibit a peak (not necessarily the dominant one) at the AF frequency estimated from EGM recordings. In this approach, DF estimated from the EGM ($\mathrm{f_{EGM}}$) was contrasted with the $\mathrm{PSD_{BSPM}}$ to identify if $\mathrm{f_{EGM}}$ corresponds to any peak of the $\mathrm{PSD_{BSPM}}$. Figure 78 shows a schematic representation of this procedure.

The $\mathrm{f_{EGM}}$ was estimated for each EGM site and the $\mathrm{PSD_{BSPM}}$ for each BSPM site was computed and normalised to the site with maximum power. Frequency components that appeared as distinct peaks were then detected in the $\mathrm{PSD_{BSPM}}$. This was done in the following manner: a distinct peak was said to occur if amplitude of the $\mathrm{PSD_{BSPM}}$ was larger than the preceding or following value, along the frequency axis, i.e.

$$\mathrm{PSD_{BSPM}}(\mathrm{f_i}) > \max\left(\mathrm{PSD_{BSPM}}(\mathrm{f_{i-1}}),\ \mathrm{PSD_{BSPM}}(\mathrm{f_{i+1}})\right),$$

where $\mathrm{f_i}$ is the value of the i^{th} discrete frequency. The frequencies at which this occurs were denoted $\hat{\mathrm{f}}_{\mathrm{BSPM}}$, and had an associated spectral power $\widehat{\mathrm{P}}_{\mathrm{BSPM}}$. This procedure was repeated for all BSPM sites and the method could be used efficiently by pre-computing all the PSDs. By performing this identification of peaks in the $\mathrm{PSD_{BSPM}}$, some small peaks were identified which may just be due to noise in the signal. Hence a threshold was set; any $\widehat{\mathrm{P}}_{\mathrm{BSPM}}$ less than 20% of the maximum of $\mathrm{PSD_{BSPM}}$ were discarded.

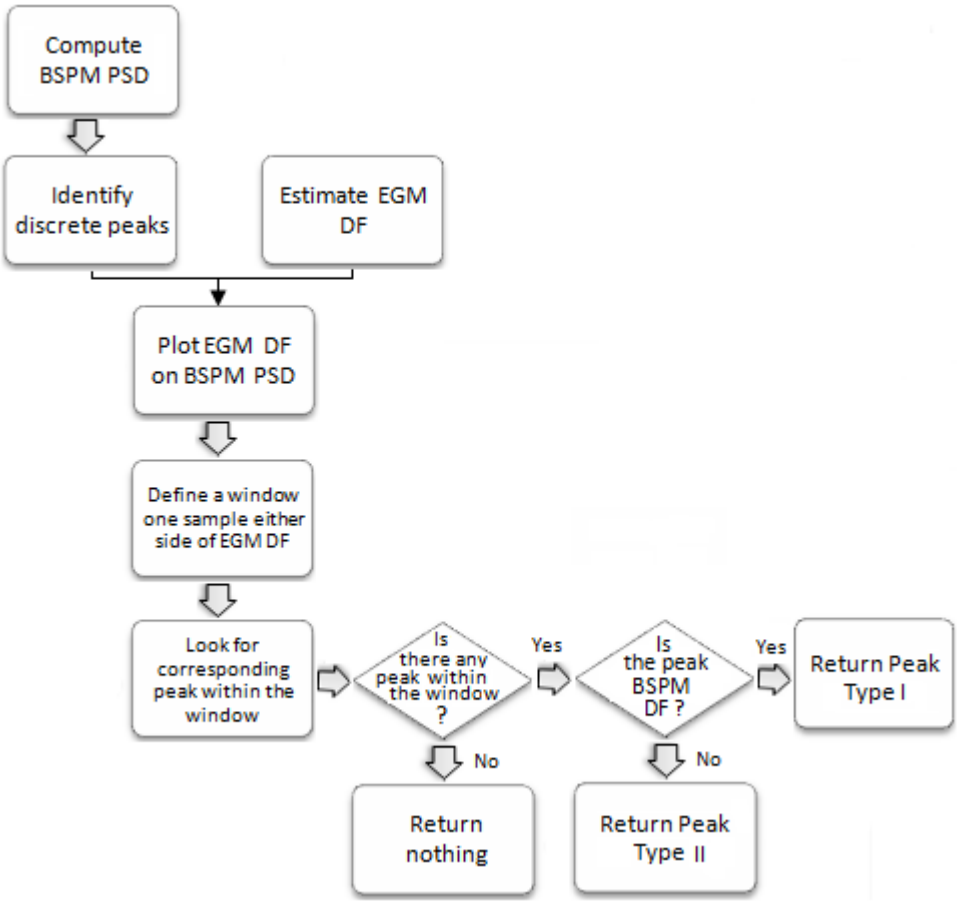

Figure 78. A schematic representation of determining EGM DF to corresponding peaks on the BSPM PSD.

The f_{EGM} may not perfectly align with a value of $\hat{f}_{BSPM}$ and a small amount of deviation from the values was allowed. A window of width 0.25 Hz (one sample either side of the f_{EGM}) was defined (i.e. for the i^{th} DF the window is $\hat{f}_{EGM}(i) \pm 0.125$), then any peaks of $\widehat{P}_{BSPM}$ within this window were identified. A further classification of the peaks was then made as follows; the maximal peak of the PSD_{BSPM} was identified as BSPM DF. If there was a dominant-peak within 0.25 Hz of f_{EGM} then the peak was classified as a Type I (see Figure 79, A). If there was a non-dominant peak within 0.25 Hz of f_{EGM} then that the peak was classified as Type II (see Figure 79, B). Afterwards the number of each peak type was counted at each BSPM site across all subjects. This was then used to

investigate if there are any BSPM sites where the peaks are classified as Type I in the majority of subjects. The result of this study will be shown in section 8.2.

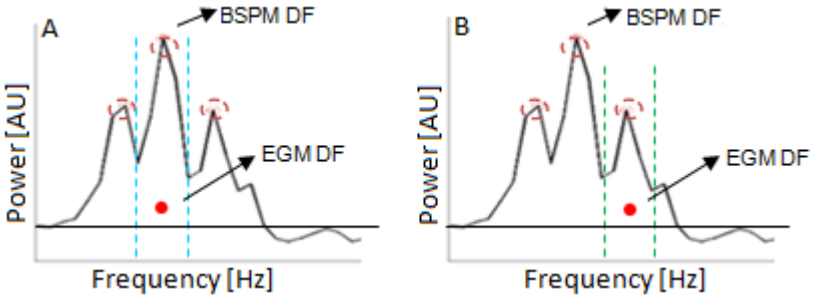

Figure 79. Illustration of a BSPM PSD and its corresponding peaks to EGM DF (subject 18, site 22). The distinct frequency peaks were identified as red circles. The horizontal black line indicates the threshold.

2.3.7. Innovative Method: Time Domain Analysis to Identify Intracardiac Activations on the Body Surface

This section explains the method used to investigate if there is any relationship in the time series between the body surface and intracardiac recordings. In other words, are intracardiac activations preferentially detectable at different body surface sites? In this analysis, the longest AF segment was selected from the BSPM recordings (Figure 80, step 1). The corresponding segments, in the same time interval, on the CS and PVAC recordings were selected (Figure 80, step 2). CS and PVAC activations were detected on the segments (Figure 80, step 3). The time points of the CS and PVAC activations were marked on the AF segment on the BSPM recordings (Figure 80, step 4). After that, a window around the EGM activations on the BSPM AA was defined, sufficiently wide to cover the activation phase shifts, shown in Figure 81. The windows were averaged and the EGM activations were marked on the average, see Figure 82. Figure 83 shows all these steps together. The aim of the averaging was to check consistency of the CS and PVAC activations on the BSPM. In other words, if the AA waveforms are triggered by EGM activations

then the average will possess a large amplitude, with similar shape to that of each AA waveform. To quantify the relationship between AA and EGM activations, it was attempted to detect the atrial activations from the BSPM and EGM separately, calculate the MCL for each measurment source, then correlation the BSPM and EGM MCL. The result of this study will be shown in section 8.3.

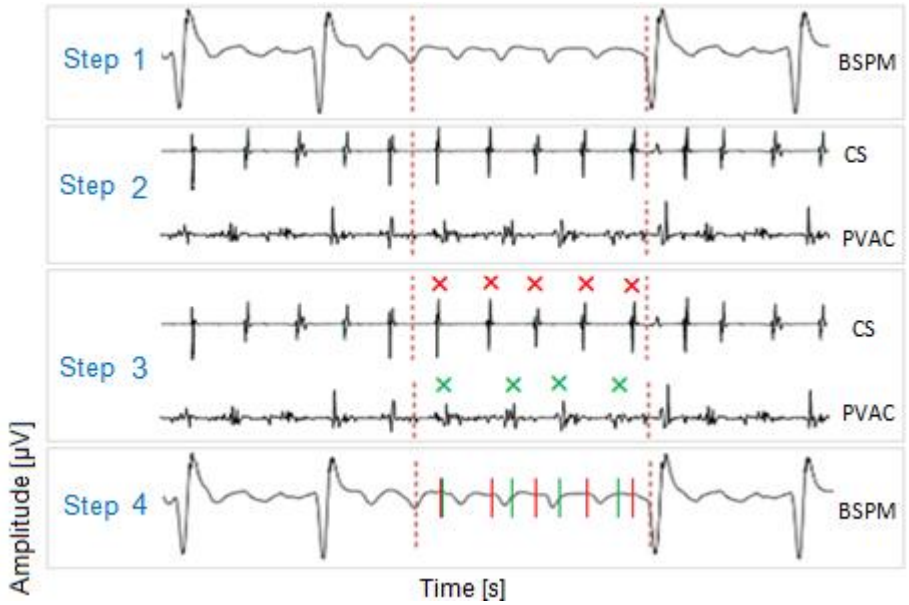

Figure 80. Illustration of detecting EGM activations on the BSPM signal. Step 1: the AF segment was selected on BSPM site 22. Step 2: the corresponding segment (in time) was selected on CS4 and PVAC4 (interval between red dashed lines). Step 3: CS (red crosses) and PVAC (green crosses) activations were detected. Step 4: the CS and PVAC activations were marked on the BSPM data (red and green lines).

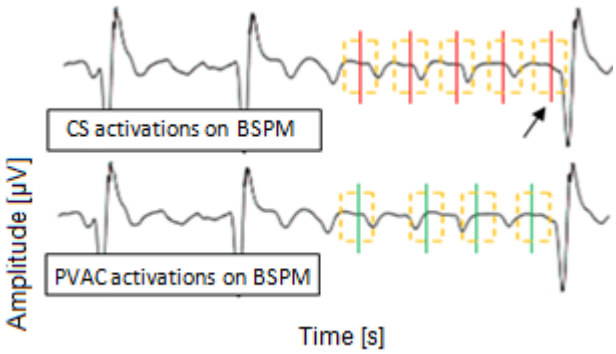

Figure 81. Illustration of windowing (orange dashed squares) the EGM activations (red and green lines) on the BSPM signal. The activations whose window includes the part of the T-wave or Q-wave have been discarded from averaging. An example of this case is shown by the black arrow.

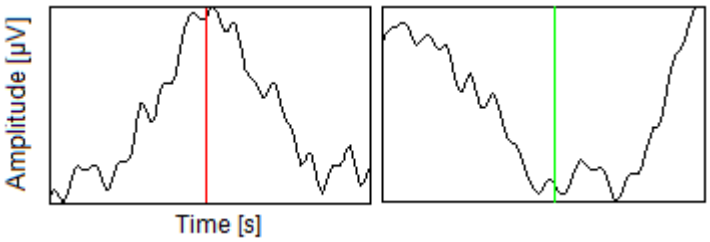

Figure 82. Illustration of a normalised generated beat from the BSPM by the EGM activations. The red and green lines indicate CS and PVAC activations, respectively (for illustration purpose only, it is not constructed from Figure 81).

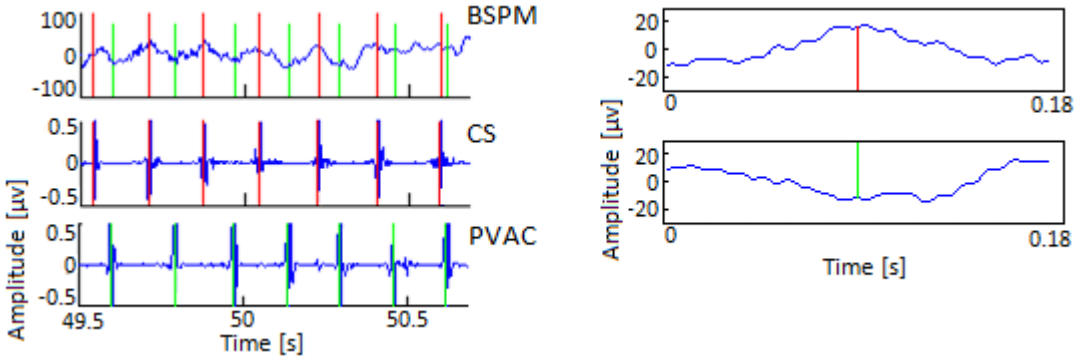

Figure 83. Example of detected EGM activations and the averaged window from the second longest AF segment at site 1 (subject 1).

2.4. Data Analysis Design

In this section, the different statistical arrangements (each chosen to extract different information from the data) are outlined. The majority of the analysis was performed on three distinct arrangements: the AF characteristic differences between subjects (see chapter 3), the AF characteristic changes over time (see chapter 5), and the AF characteristic changes over space (see chapter 6). Depending on the aim of each study, a table for statistical analysis was constructed and denoted ‘Design’. The Design indicates size of the statistical table, and has different numbers of rows and columns as necessary. If 'A' is to be denoted for a parameter of interest then;

- Two dimensional statistical Design:

  Design = number of sites × number of subjects, or Design = number of subjects × number of sites, was mainly used for constructing plots (e.g.

Box and Whisker plot), testing distribution for normality, and non-parametric tests (e.g. the Friedman test) to study the AF characteristics between subjects and spatial variability, see Figure 84.

- Three dimensional statistical Design:

  Design = (number of subjects × number of sites) × 3, was mainly used for parametric tests (e.g. factorial analysis of variance (ANOVA)) when there were two fixed factors (e.g. subjects and sites), see Figure 85.

- Four dimensional statistical Design:

  Design = (number of subjects × number of repetitions × number of sites) × 4, was mainly used for ANOVA when there were three fixed factors (e.g. subjects and sites over time), see Figure 86.

Site \ Subject	1	⋯	20
1	$A_{1\text{-}1}$	⋯	$A_{20\text{-}1}$
⋮	⋮	⋮	⋮
N	$A_{1\text{-}N}$	⋯	$A_{20\text{-}N}$

Figure 84. Example of Design = 64 × 20 or Design = 5 × 20, were used for the BSPM and EGM non-parametric test, respectively.

Subject	Repetition	A
1	1	$A_{1\text{-}1}$
	⋮	⋮
	N	$A_{1\text{-}N}$
⋮	⋮	⋮
20	1	$A_{20\text{-}1}$
	⋮	⋮
	N	$A_{20\text{-}N}$

Figure 85. Example of Design = (20 × 64) × 3 or Design = (20×5) × 3, were used for the BSPM and EGM parametric test, respectively.

Subject	Repetition	Site	A
1	1	1	$A_{1\text{-}1\text{-}1}$
		⋮	⋮
		N	$A_{1\text{-}1\text{-}N}$
	⋮	⋮	⋮
	n	1	$A_{1\text{-}n\text{-}1}$
		⋮	⋮
		N	$A_{1\text{-}n\text{-}N}$
⋮	⋮	⋮	⋮
20	1	1	$A_{20\text{-}1\text{-}1}$
		⋮	⋮
		N	$A_{20\text{-}1\text{-}N}$
	⋮	⋮	⋮
	n	1	$A_{20\text{-}n\text{-}1}$
		⋮	⋮
		N	$A_{20\text{-}n\text{-}N}$

Figure 86. Example of Design = (20 × 4 × 64) × 4 or Design = (20 × 4 × 5) × 4, were used for the BSPM and EGM parametric test of temporal variability, respectively.

2.4.1. Between Subject Analysis

To investigate differences in the AF characteristics between subjects, the parameter of interest was analysed across the sites for each subject (Design = number of sites × number of subjects). A Box and Whisker plot was constructed, and normality of data distribution in each subject was tested. To test for a significant difference in the data a non-parametric test (Design= number of sites × number of subjects) or a parametric test (Design= (number of subjects × number of sites) × 3) was used according to the normality test result.

2.4.2. Temporal Variability Method Description

Signal Processing: Temporal variability of AF amplitude, DF and SC were investigated for all subjects. For AF amplitude, the five longest AF segments were selected and amplitude of the AF signal was estimated for each segment. For AF DF and SC, the temporal variability was investigated with two related approaches. Firstly, the two minute BSPM and EGM recordings were divided into four consecutive, non-overlapping segments (T1 to T4), each 30 seconds

long. Secondly, the two minute BSPM and EGM recordings were divided into two consecutive, non-overlapping segments (T1 and T2), each 60 seconds long. In both approaches, PSD and then DF and SC were estimated for each segment.

Statistical Tests: Using the median value across the sites in each subject, a Box and Whisker plot was constructed for each segment (Design= number of subjects × number of segments). The data distribution was tested across the sites in each segment (Design= (number of subjects × number of sites) × number of segments). A parametric test (Design= (number of subjects × number of segments × number of sites) × 4), or a non-parametric test (Design= (number of subjects × number of sites) × number of segments) was used according to the normality test result, to test for a significant difference in the parameter of interest between the segments.

2.4.3. Definition of Electrode Groups Used to Describe Spatial Variability

To investigate spatial variability, the parameter of interest was analysed from two minute recordings between the sites. A Box and Whisker plot was constructed (Design= number of subjects × number of sites), and data distribution was checked across subjects in each site. A parametric test (Design= (number of subjects × number of sites) × 3), or a non-parametric test (Design= number of subjects × number of sites) was used according to the result of the data distribution test.

For additional investigation of the spatial variability estimated from the body surface recordings, the 64 sites were grouped into anterior and posterior, left and right, vertical electrode lines, and horizontal electrode lines. The aim of

grouping the body surface sites was to facilitate a reduction in the number of sites to be studied each time. These classifications are explained as follows:

Anterior and Posterior Sites: the 64 body surface sites were grouped into anterior (sites 1 to 32) and posterior (sites 33 to 64), see Figure 87. The median values of the parameter of interest across the anterior and the posterior sites were calculated (Design= number of subjects × 2).

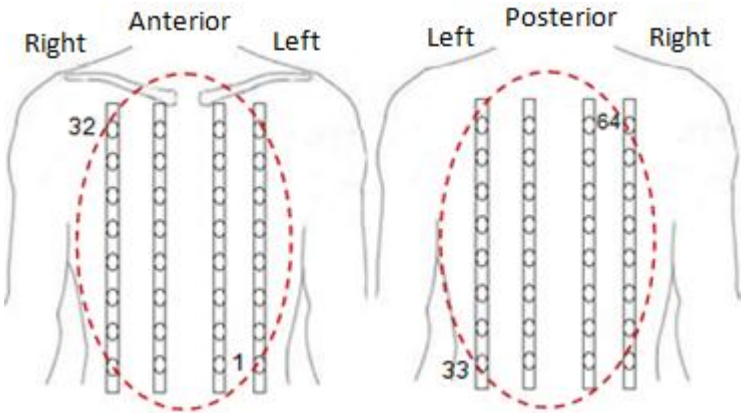

Figure 87. Illustration of the anterior (sites 1 to 32) and posterior (sites 33 to 64) electrode arrangements.

Left and Right Sites: the 64 body surface sites were grouped into left and right with two approaches. Initially, sites on the left anterior and posterior (sites 1 to 16 and sites 33 to 48) were denoted Left, and sites on the right anterior and posterior (sites 17 to 32 and sites 49 to 64) were denoted Right, see Figure 88. The median values of parameter of interest across Left and Right were calculated (Design = number of subjects × 2). The 64 body surface sites were then grouped into four further classes, anterior left (sites 1 to 16), anterior right (sites 17 to 32), posterior left (sites 33 to 48), and posterior right (sites 49 to 64), see Figure 89. The median values of the parameter of interest across each class were calculated (Design = number of subjects × 4).

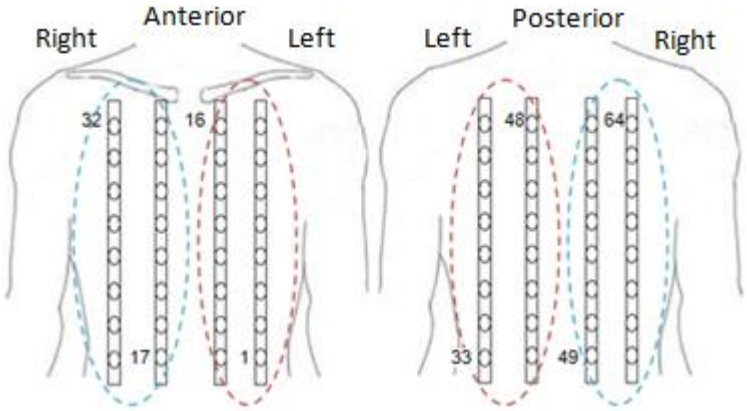

Figure 88. Illustration of the left and right electrode arrangements, first approach. The left body surface is shown in red. The right body surface is shown in blue.

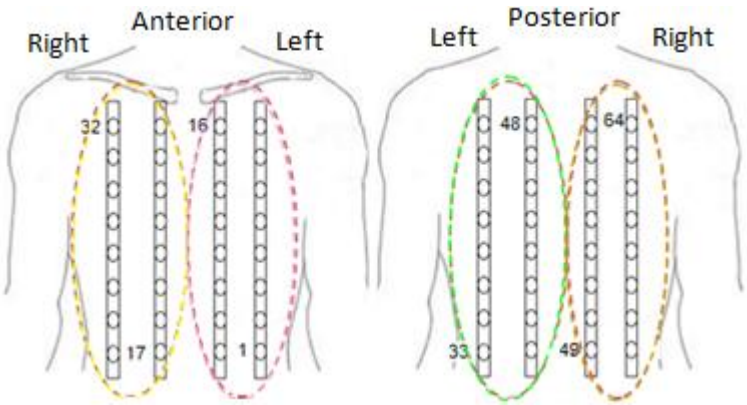

Figure 89. Illustration of the left and right electrode arrangements, second approach. The anterior left, anterior right, posterior left, and posterior right are shown in different colours.

Vertical Electrode Lines: the 64 body surface sites were also grouped into eight vertical lines (8 electrode strips, 8 electrodes on each strip, e.g. sites 1 to 8 vertical line one, 9 to 16 vertical line two, etc), see Figure 90. The median values of the parameter of interest across each vertical line were calculated (Design = number of subjects × 8). The vertical lines were named according to their anatomical location on the body surface as follows: on the anterior side, four vertical lines from left to right were named anterior lateral left (ALL), anterior central left (ACL), anterior central right (ACR), and anterior lateral right (ALR). On the posterior side, four vertical lines from left to right were named

posterior lateral left (PLL), posterior central left (PCL), posterior central right (PCR), and posterior lateral right (PLR).

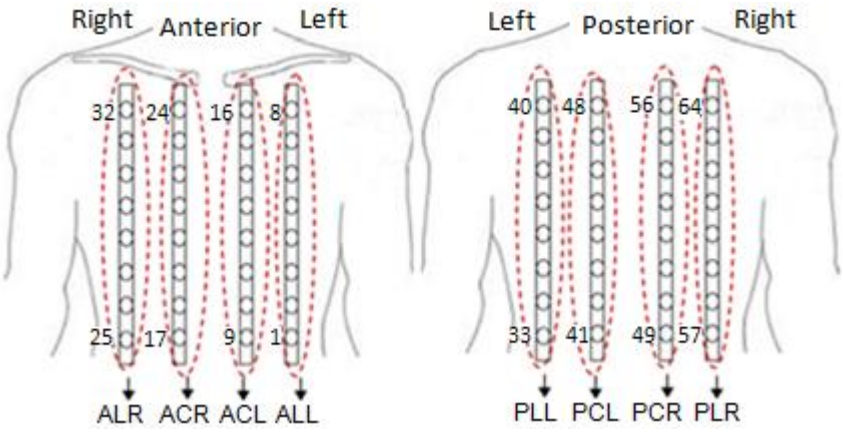

Figure 90. Illustration of the vertical electrode lines arrangement.

Horizontal Electrode Lines: the 64 body surface sites were also grouped into sixteen horizontal lines, (sites 1, 9, 17, 25 called line one, sites 2, 10, 18, 26 called line two, etc), see Figure 91. The median values of the parameter of interest across each line was calculated (Design = number of subjects×16).

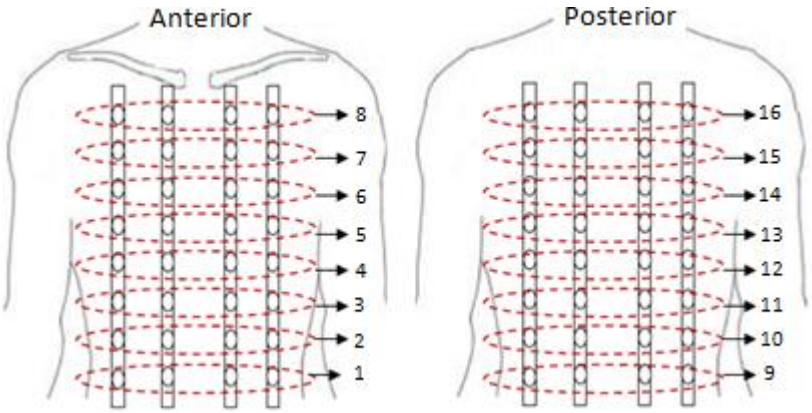

Figure 91. Illustration of the horizontal electrode lines arrangement.

2.5. Statistical Analysis

To describe and interpret the AF characteristics obtained through the measurements, statistical analysis was performed. To choose an appropriate statistical test, the question posed was "is the data independent?". As a rule of thumb, results on the same individual are not independent. The data in this

study was collected from one source (the heart) at different locations (body surface and inside the heart) at the same time in each subject, so the data is not independent. Consequently, the statistical tests for related samples were used.

As appropriate, different plots were used to summarise the data. In this study Box and Whisker, Bland-Altman, and scatter plots were most commonly used for the analysis. These are described later in this section.

To describe the shape and spread of the data, statistical distribution was analysed. Knowing the distribution of the data was important as it determined whether parametric or non-parametric statistical tests were appropriate. Since the sample sizes of the data used for the analysis in some designs were small (e.g. between intracardiac sites was 10), the distribution was checked in two ways: numerically using the Kolmogorov–Smirnov test, and graphically using visual inspection of a histogram. The null hypothesis (H_0) was that the data follow a specified distribution.

Paired t-test (for paired comparison of two groups) or ANOVA for repeated measures (for the comparison of more than two groups) was used when data was normally distributed. Wilcoxon signed-rank (for paired comparison of two groups) or Friedman test for related samples (for the comparison of more than two groups) was used when data was not normally distributed. H_0 was set as there is no difference between the variable being compared. In the entire statistical tests that have been used in this study, the hypothesis was rejected if p-value was less than the fixed significance level (α) of 0.05.

In multiple comparisons, the type I error (or false positive, when the null hypothesis is rejected although it is true) was controlled using Bonferroni correction.

Box and Whisker Plot

Here the data was described through a five-number summary: the smallest observation (min), lower quartile or 25^{th} percentile (Q1), median or 50^{th} percentile (Q2), upper quartile or 75^{th} percentile (Q3), and largest observation (max). The Box and Whisker plot was used to visualise the centre, spread, and overall range of the data distribution. The whiskers extended from Q1 to the smallest non-outlier, and from Q3 to the largest non-outlier in the data set (see Figure 92). Outliers were considered as values larger than Q3 by at least 1.5 times the inter-quartile range (IQR), or smaller than Q1 by at least 1.5 times the IQR. The range is the spread of all data, the distance between the smallest and largest values, including any outliers.

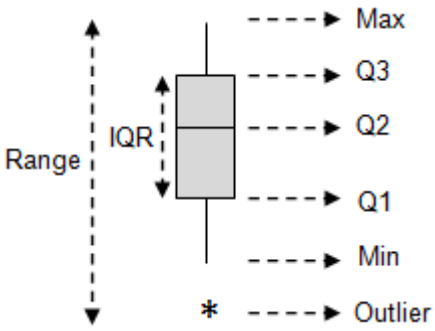

Figure 92. Illustration of a Box and Whisker plot.

Bland-Altman Plot

To compare AF characteristic estimated from the body surface and inside the heart, a Bland-Altman plot was used. The aim was to verify whether AF characteristic estimated from these measurement methods were similar or not. AF characteristic estimated from inside the heart were used as reference

value. Limits of agreement (LOA) and bias were used to describe whether there is an agreement between these two measurement methods (see Figure 93):

- Limits of agreement (LOA) are limits that 95 % of the points fall either side of the bias. There are upper and lower LOA which show the minimum and maximum error between the two measurements. LOAs are calculated as bias ± 1.96 of standard deviation (SD). LOA describes the range for 95% of comparison points.

- Bias is the mean difference between the two methods of measurement (ideal bias is zero).

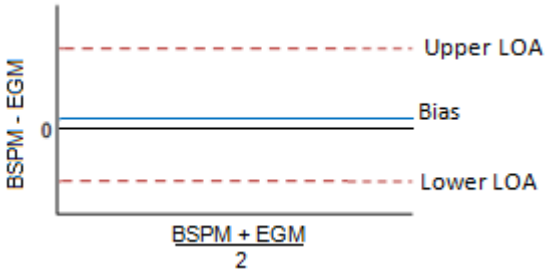

Figure 93. Illustration of a Bland-Altman plot.

Scatter Plot for Regression Analysis

Linear regression analysis was used to investigate how independent variables related to dependent variables. This shows the effect of the independent variable on the dependent variable. Mathematically if there is a single independent variable the following model fits,

$$Y_i = \beta_0 + \beta_1 X_i + \varepsilon_i$$

β_1 quantifies the relationship between the independent variable X and the dependent variable Y (see Figure 94). β_0 and β_1 represent the Y-intercept and the slope of the relationship, respectively. The ε represents normally distributed noise. The null hypothesis is that there is no significant difference between the

slope of the fitted line and zero. This is quantified by p-value. Coefficient of determination (R^2) is the square of the correlation between the dependent and independent variable, which shows how each independent variable correlates with dependent variable. The R^2 can be used to assess the strength of the correlation. Effectively, it quantifies the spread of the points along the line.

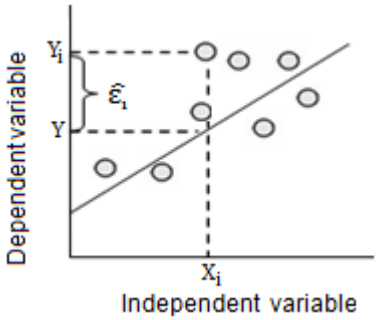

Figure 94. Illustration of a linear regression plot.

In this study plots were constructed using Minitab® 16.1.0 (Minitab, PA, USA), and IBM® SPSS® Statistics version 19 (SPSS Inc, IL, USA) was used for statistical tests.

Chapter 3. Differences in Atrial Fibrillation Characteristics Between Subjects

As described in chapter 1, AF history is known to affect AF characteristics. Since subjects who have been recruited for this study had different AF histories, this chapter quantifies the AF characteristics in each subject to have overview of each subject's data and justify outliers. For this purpose, differences in AF characteristics estimated from the body surface (amplitude, DF and SC) and inside the heart (DF and SC) were investigated between subjects. DF and SC were also compared between the body surface and intracardiac recordings.

3.1. Amplitude

I. AF Amplitude Estimated from the Body Surface

Figure 95 shows the longest AF segment within the two minute recordings (see section 2.3.2 for the methodology of isolating AF segments) selected from body surface site 22 for each subject and Figure 96 shows the AF segments' durations. Peak to peak amplitude of this segment was measured for each site for each subject and shown in Figure 97 in the Box and Whisker plot. A colour map of amplitude on a global scale across all subjects is shown in Figure 98, and Figure 99 shows the individual scale for each subject. The Friedman test showed that subjects exhibited significant differences in amplitude ($p<0.001$), (Design=64×20, see section 2.4).

The median amplitude measured across the 64 sites ranged from 19.2 μV (subject 18) to 90.0 μV (subject 3) with median and IQR of 35.9 (21.0 – 57.3) μV across all subjects.

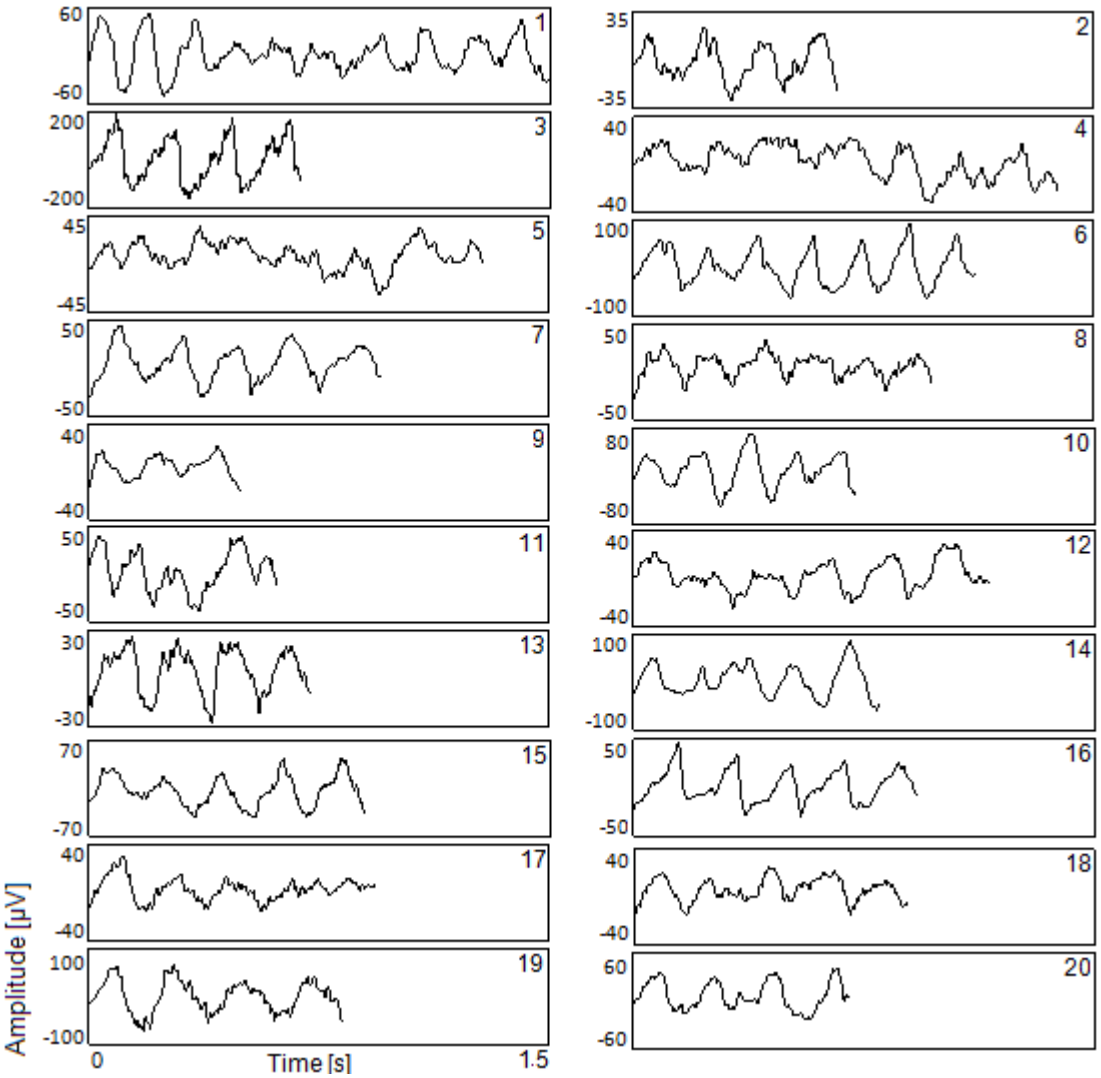

Figure 95. Illustration of the longest AF segment for each subject (identified 1 to 20) from body surface site 22.

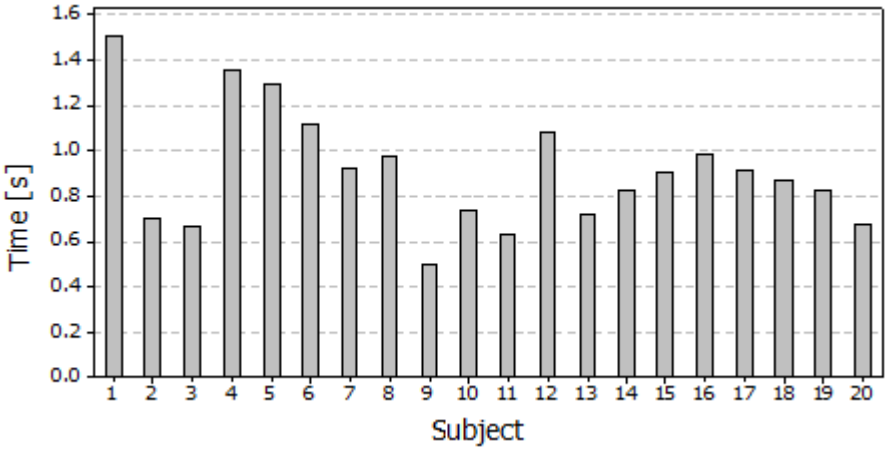

Figure 96. Duration of the longest AF segment for each subject.

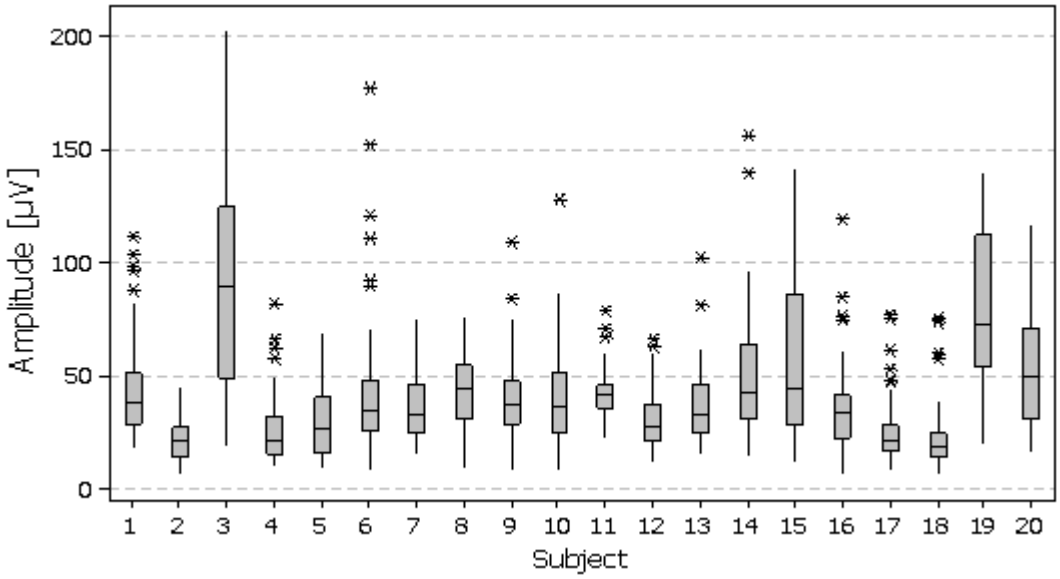

Figure 97. AF amplitude across the body surface sites for each subject. Each bar is constructed from 64 values.

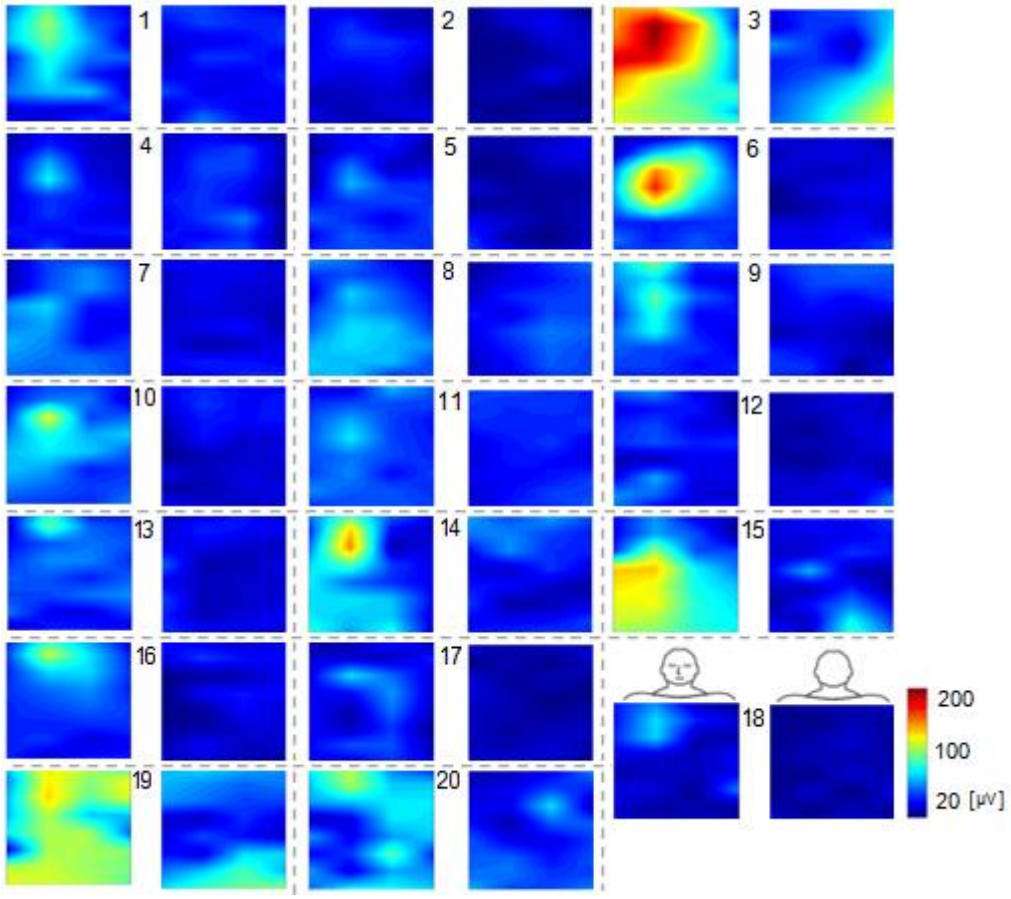

Figure 98. Spatial colour map of AF amplitude for each subject (identified 1 to 20) global scale.

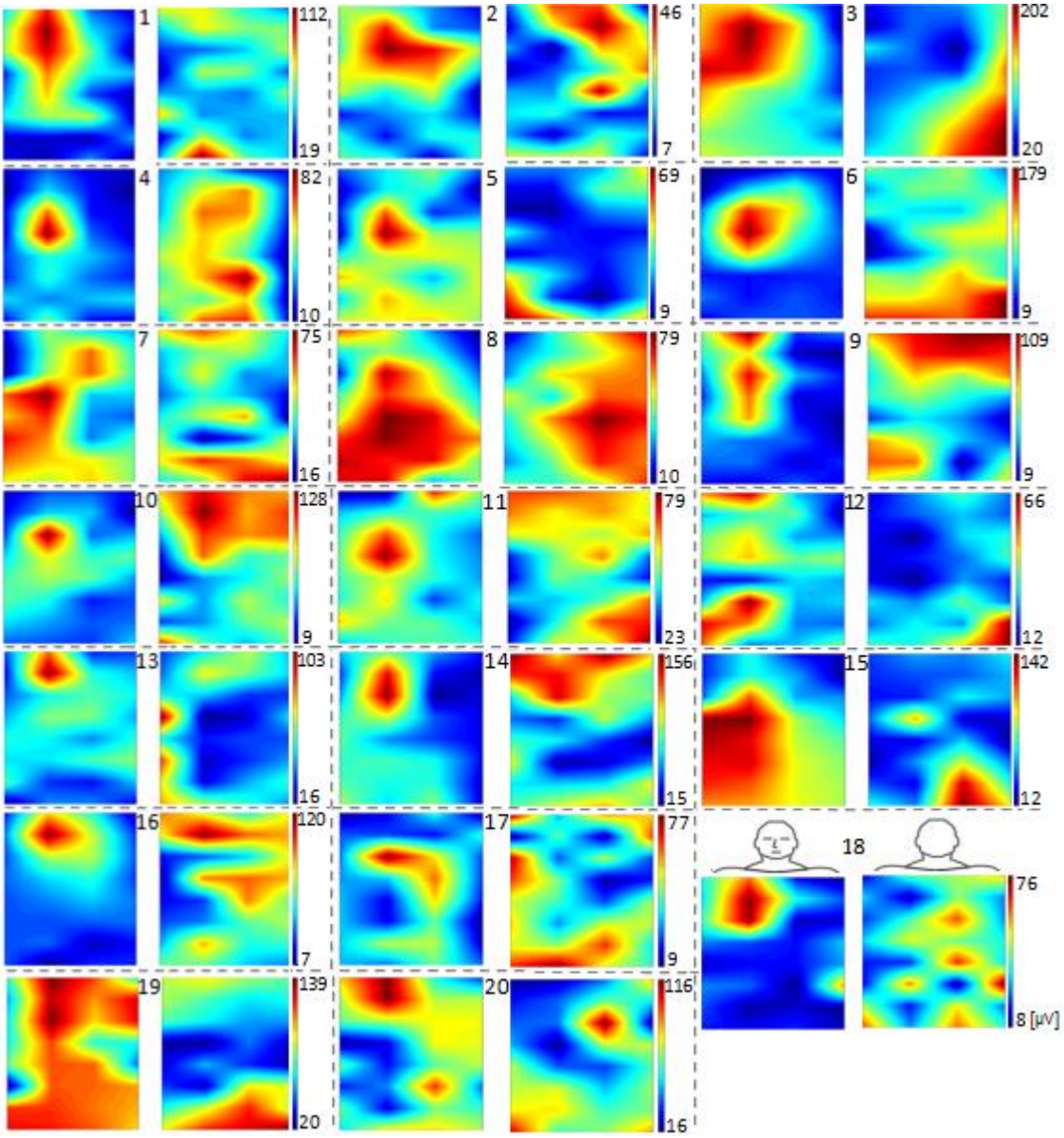

Figure 99. Spatial colour map of AF amplitude for each subject (identified 1 to 20) individual scale.

According to the literature, mostly organised AF cases are known to have high-amplitude F-waves, while less organised AF cases have lower amplitude (Petrutiu et al. 2006). However, in this study cases with well organised AF (e.g. subjects 7 and 8) had small amplitude, and cases with disorganised AF had larger amplitude (e.g. subjects 11 and 19).

In some subjects there were relatively small differences in amplitude across the sites, whereas in other subjects there were relatively large

differences. For example, the amplitude range (maximum – minimum) in subject 2 was 39.0 μV and in subject 6 was 168.0 μV.

Interestingly there was a consistent pattern of high amplitude on the anterior upper right body surface sites, close to site 22, in all subjects. Although there were some posterior sites with high amplitude in each subject the sites were not consistent between subjects. The amplitude difference between subjects could be related to certain factors such as: complexity of AF, subject's BMI and AF history which includes the type of AF and the number of previous ablations. To investigate these factors, the complexity of AF and the effect of BMI on AF amplitude were investigated, and these results are shown in section 3.3 and chapter 4.

A limitation of this analysis was that AF amplitude was estimated from a single AF segment within the two minute BSPM recordings. As the AF segments may fluctuate over time, it is possible that the AF amplitude could be different for the same study group if other AF segments were studied. This concern was investigated in chapter 5 by studying temporal variability of AF amplitude.

II. AF Amplitude Estimated from Inside the Heart

Several factors may influence measurements of the intracardiac signal amplitude, e.g. catheter contact with the heart tissue, thickness of the atrial muscle, pressure to the catheter applied by the cardiologist, and previous scars. As a result, amplitude of the local atrial electrogram may not be indicative of AF amplitude estimated from the body surface. For this reason, amplitude of the intracardiac recordings was not studied in the thesis.

3.2. Dominant Frequency

I. Dominant Frequency Estimated from the Body Surface

PSD and then DF were estimated from the two minutes of the BSPM AA for each site in each subject. Figure 100 shows the PSD from body surface site 22 for each subject. The Box and Whisker plot of DF across the body surface sites for each subject is shown in Figure 101. The colour map of DF across the body surface sites is shown later in Figure 106.

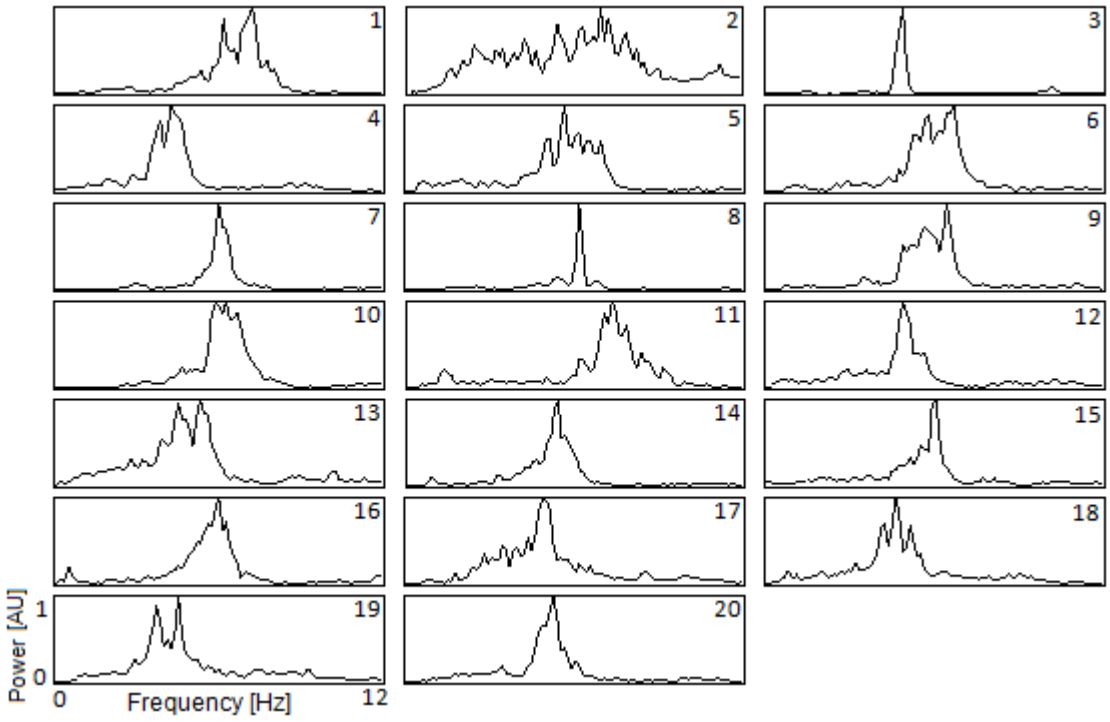

Figure 100. Illustration of the PSD for each subject (identified 1 to 20) from body surface site 22. The y-axis denotes normalised power density to the maximum of each subject.

The Friedman test showed that subjects exhibited significant differences in DF ($p<0.001$). The median DF measured across the 64 sites ranged from 4.1 Hz (subject 12) to 7.5 Hz (subject 11) with median and IQR of 5.9 (5.1– 6.2) Hz across all subjects. DF estimated from the body surface was significantly different between subjects. Moreover, in some subjects there were relatively small differences in DF across the sites, whilst in others there were relatively

large differences across the sites (e.g. DF range in subjects 3 and 8 were 0.0 Hz, and in subject 10 was 3.3 Hz).

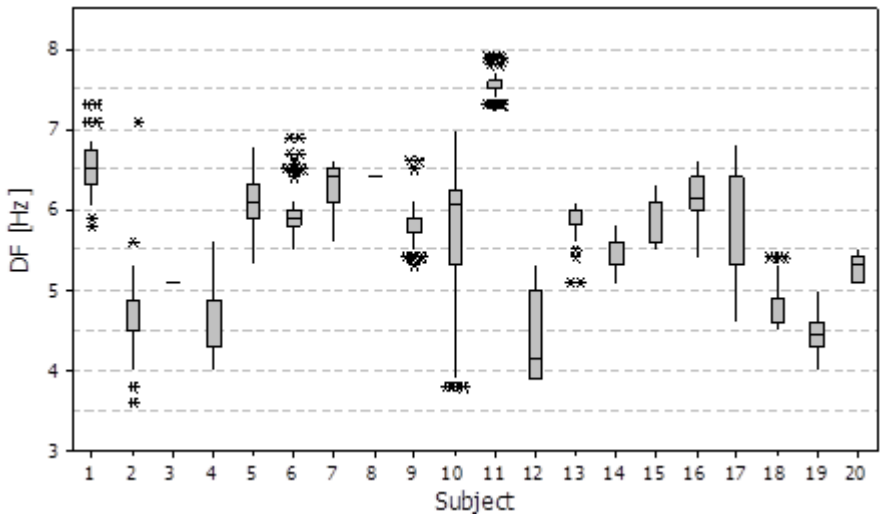

Figure 101. DF across the body surface sites for each subject. Each bar is constructed from 64 values.

The DF difference between subjects could be related to the same factors as mentioned in the previous section (complexity of AF, type of AF and the number of previous ablations). To investigate the DF difference further, complexity of AF and effect of BMI on DF were investigated and the results are shown in section 3.3 and chapter 4, respectively.

II. Dominant Frequency Estimated from Inside the Heart

PSD and then DF were measured from the two minute EGM recordings for each site in each subject. Figure 102 and Figure 103 show the PSD from CS4 and PVAC4 for each subject, respectively. The Box and Whisker plots of DF across the five CS and five PVAC sites are shown in Figure 104. DF was not normally distributed across all the EGM sites in most of subjects (Design=10×20). The Friedman test showed that subjects exhibited significant differences in DF ($p<0.001$) estimated from either CS sites or PVAC sites (Design=5×20). The median DF, measured across the five CS sites ranged

from 4.3 Hz (subject 9) to 7.1 Hz (subjects 5 and 7) with median and IQR of 5.9 (5.1– 6.4) Hz across all subjects. The median DF, measured across the five PVAC sites, ranged from 4.3 Hz (subject 18) to 7.1 Hz (subject 7) with median and IQR of 5.6 (5.1– 6.0) Hz across all subjects.

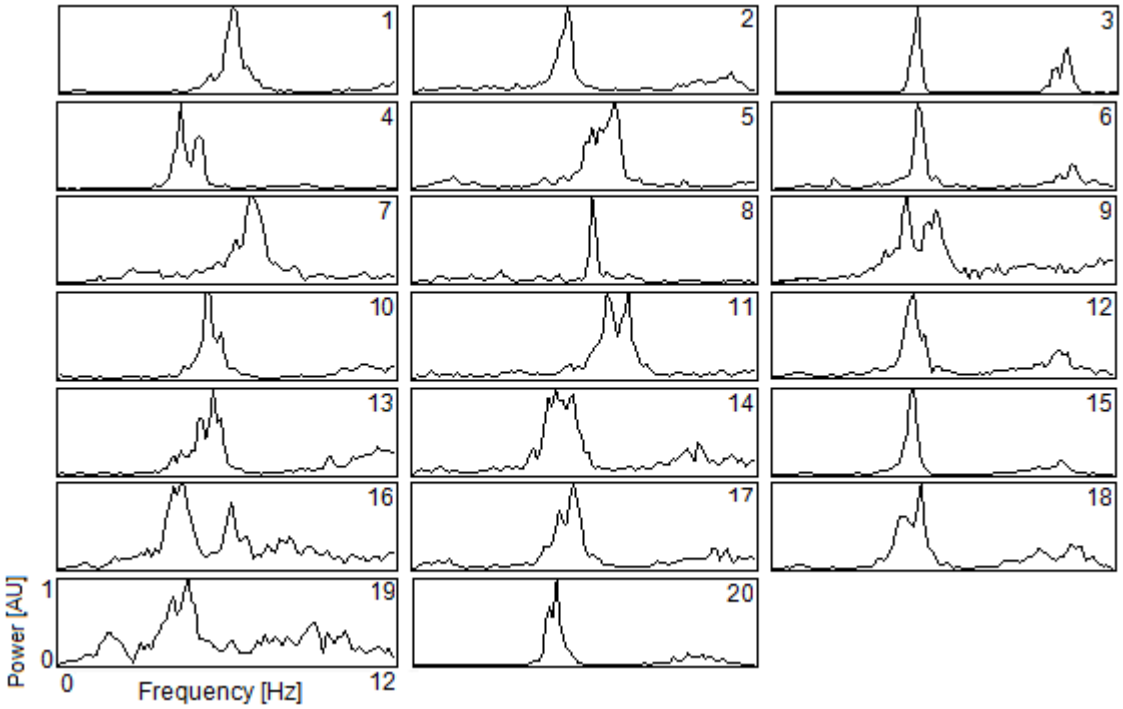

Figure 102. The PSD for each subject (identified 1 to 20) from CS site 4.

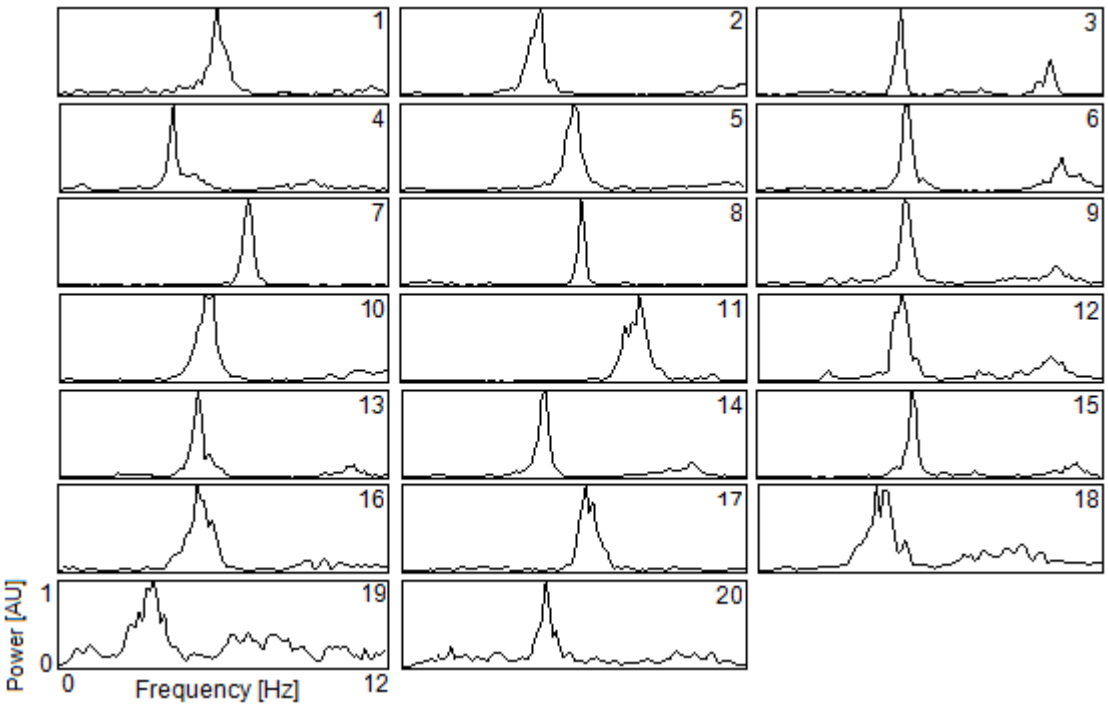

Figure 103. The PSD for each subject (identified 1 to 20) from PVAC site 4.

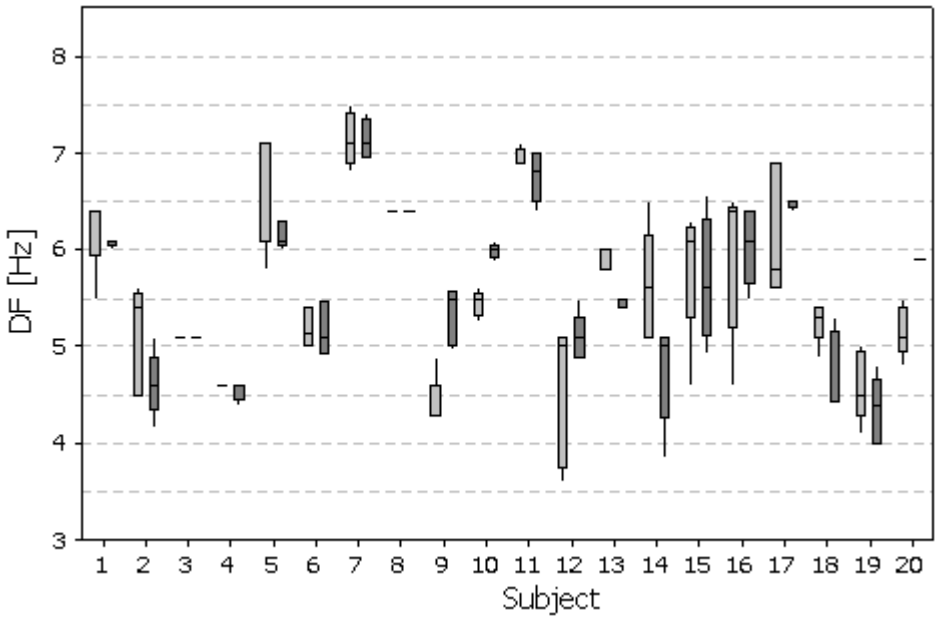

Figure 104. DF across CS (light grey) and PVAC (dark grey) for each subject. Each bar is constructed from 5 values.

The results showed that in some subjects there were relatively small differences in DF across both CS and PVAC sites (e.g. in subject 7, CS DF range = 0.7 Hz and PVAC DF range = 0.5 Hz), whereas in others there were relatively large differences in DF across both CS and PVAC sites (e.g. in subject 15, CS DF range = 1.7 Hz and PVAC DF range = 2.0 Hz). However in some subjects the differences in DF across the CS sites was relatively small, but across the PVAC sites was not, or vice versa (e.g. in subject 12, CS DF range = 1.5 Hz and PVAC DF range = 0.6 Hz).

Consistency in DF between the CS and PVAC sites may suggest less complexity of the AF (see section 3.3). However, differences may suggest that the CS and the PVAC electrodes captured atrial activations from different AF sources as they were located in different AF re-entrant pathways.

III. Comparison of Dominant Frequency Estimated from the Body Surface and Inside the Heart in Individual Subjects

It was evident from the previous section that some subjects had a single narrow dominant peak, and some subjects had broad multiple peaks in their frequency spectra computed from both body surface and intracardiac recordings. However, some subjects had a single dominant peak in the intracardiac frequency spectrum but multiple peaks in the body surface frequency spectrum (e.g. subject 1).

To facilitate the comparison, the data from Figure 101 and Figure 104 have been combined into Figure 105.

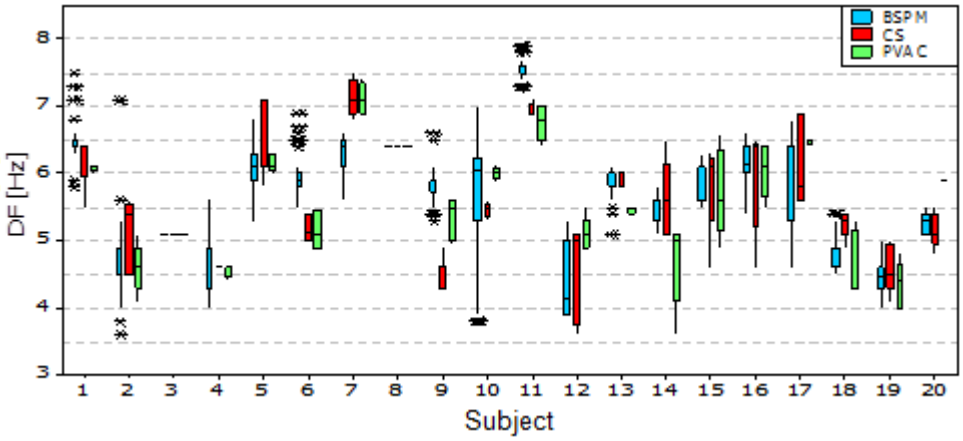

Figure 105. DF across BSPM, CS and PVAC sites for each subject. This figure is constructed using the data from Figure 101 and Figure 104 plotted together.

This figure showed that DF between the BSPM, CS and PVAC across all sites in some subjects were in perfect agreement (e.g. subjects 3 and 8), in some subjects were in good agreement but not necessarily with the same range of values (e.g. subject 19), and other subjects had poor agreement in DF (e.g. subject 11). To further facilitate the comparison of body surface and intracardiac DF, Figure 106 shows DF of the BSPM, CS and PVAC plotted in colour for each subject.

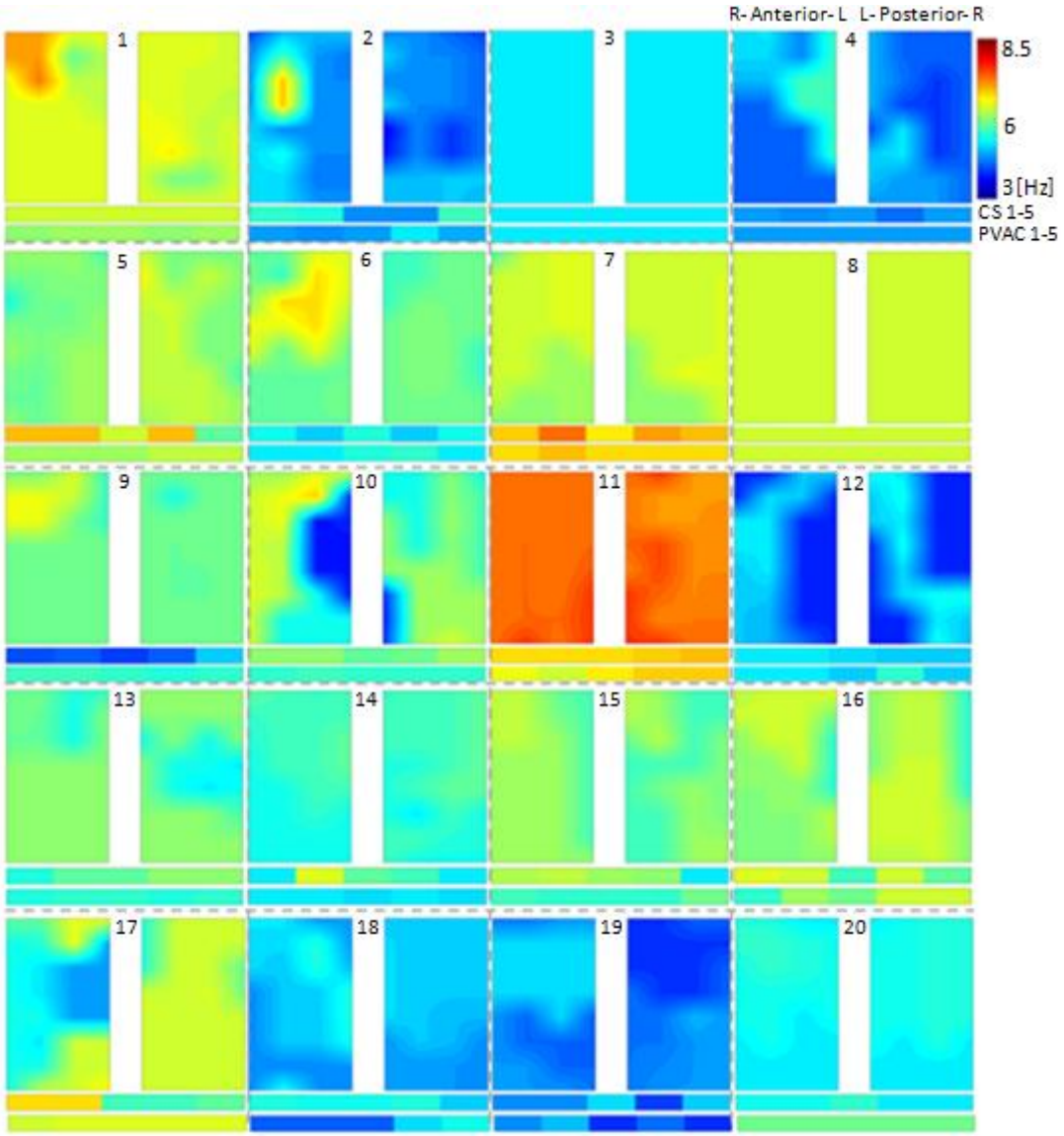

Figure 106. Spatial colour maps of DF for each subject (identified as 1 to 20). The vertical panels indicate BSPM anterior (left) and posterior (right). The horizontal panels indicate EGM from five CS sites (top: CS1 to CS5 from left to right) and five PVAC sites (bottom: PVAC1 to PVAC 5 from left to right).

Figure 106 did not reveal any consistent pattern in DF between subjects meaning there were no specific body surface sites that capture the same DF as the EGM sites in all subjects.

Good agreement in DF between the body surface and intracardiac recordings may indicate well organised AF (see section 1.1.3, AF complexity) with a single pathway as all the sites from different measurements capture one frequency. However, poor agreement may indicate less organised AF with more

than one pathway as the sites from different measurements capture different frequencies. Each component may represent a re-entrant pathway within the atria. This illustrates the limitation of using only DF as a measure of AF, since it fails to capture the full information contained in the frequency spectrum.

The linear regression analysis and scatter plots between the median DF estimated from the BSPM and both the CS and PVAC are shown in Table 2 and Figure 107.

	Median DF [Hz]			
Source	**p-value**	$\mathbf{R^2}$ **[%]**	$\boldsymbol{\beta_0}$	$\boldsymbol{\beta_1}$
BSPM & CS	<0.001	54.3	1.2	0.8
BSPM & PVAC	<0.001	70.1	0.5	0.9

Table 2. Linear relationship between the median BSPM and EGM DF for 20 subjects.

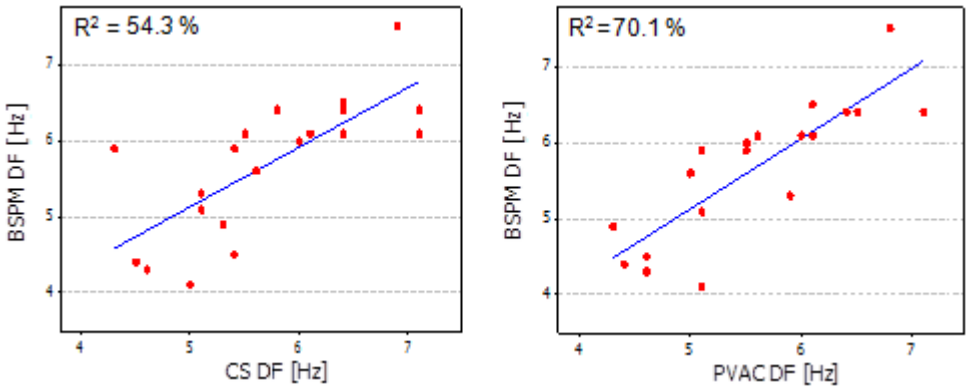

Figure 107. Linear relationship of the median DF estimated from the body surface and inside the heart.

The strong positive linear relationship between body surface and intracardiac DF may suggest that AF DF could be consistently estimated from body surface sites. However, DF estimated from the body surface showed closer agreement with DF estimated from the PVAC recordings rather than from CS.

Similarly, this analysis was repeated between DF estimated from BSPM site 22 with both CS4 and PVAC4 (see Table 3 and Figure 108).

	DF [Hz]			
Source	**p-value**	**R^2 [%]**	**β_0**	**β_1**
BSPM site 22 & CS4	0.042	21.0	3.8	0.4
BSPM site 22 & PVAC4	0.026	24.6	3.2	0.5

Table 3. Linear relationship between BSPM site 22 and EGM DF for 20 subjects.

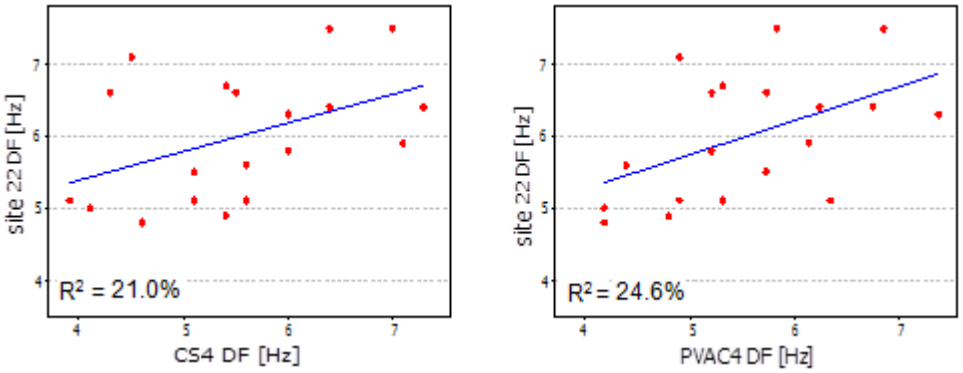

Figure 108. Linear relationship of DF estimated from the body surface site 22 and inside the heart.

The weak positive linear relationship between body surface site 22 and intracardiac DF may suggest that additional electrodes to the 12-lead ECG give more accurate estimation of DF from the body surface.

3.3. Spectral Concentration

I. Body Surface Spectral Concentration

SC was estimated from the PSD computed over the two minute BSPM AA for each site in each subject. The Box and Whisker plot of SC across the body surface sites for each subject is shown in Figure 109. The results of the Friedman test showed that subjects exhibited significant differences in SC ($p<0.001$).

The median SC, measured across the 64 sites, ranged from 19.0 % (subject 13) to 60.5 % (subject 3) with median and IQR of 27.8 (31.0 – 43.8) % across all subjects.

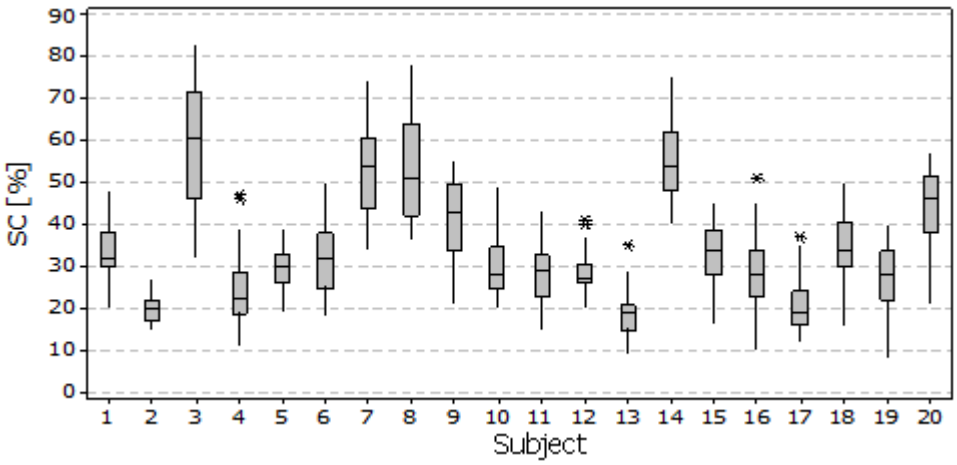

Figure 109. SC across the body surface sites for each subject. Each bar is constructed from 64 values.

SC significant difference between subjects suggested that subjects had different degrees of AF complexity. This was expected as subjects had different AF histories. To investigate whether these results agreed with the AF degree of complexity estimated from the intracardiac recordings, SC was estimated from inside the heart as explained below and later compared to SC from the body surface.

II. Inside the Heart Spectral Concentration

SC was measured from the two minute EGM recordings in the same manner as the BSPM for each site in each subject. The Box and Whisker plot of SC across the five CS and five PVAC sites is shown in Figure 110. The Friedman test showed that subjects exhibited significant differences in SC ($p<0.05$) estimated from either CS or PVAC sites.

The median SC, measured across the five CS sites, ranged from 21.1 % (subject 9) to 86.0 % (subjects 3) with median and IQR of 47.5 (39.5 – 56.8) % across all subjects. The median SC, measured across the five PVAC sites, ranged from 36.3% (subject 18) to 90.0% (subject 3) with median and IQR of 63.0 (53.3 – 70.0) % across all subjects.

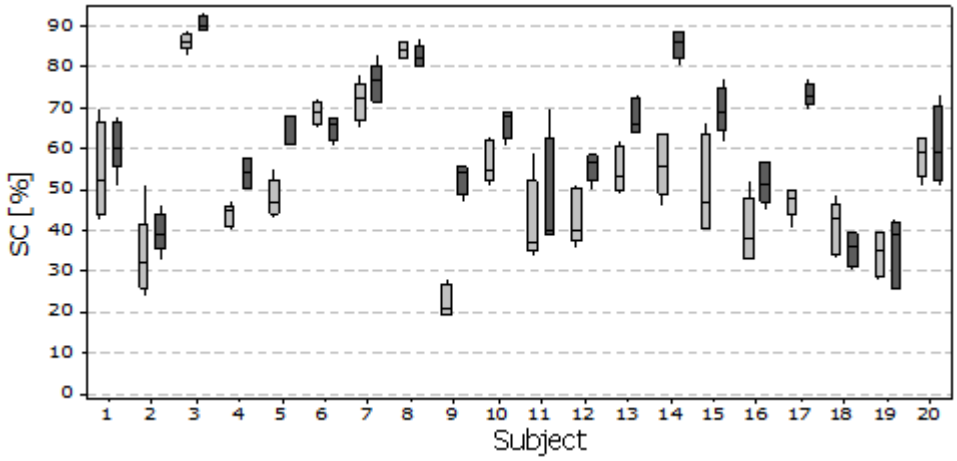

Figure 110. SC across CS (light grey) and PVAC (dark grey) for each subject. Each bar is constructed from 5 values.

The results showed that SC estimated from inside the heart was significantly different between subjects. Eighty percent of subjects[1] had larger median SC in PVAC than in CS. This may suggest that there was far-field atrial activity from the RA or other AF pathways on the CS. In other words, the PVAC sites may capture more localised frequencies from the LA, while the CS sites capture AF frequencies from different sources (e.g. the LA and RA). Further evidence of this is apparent in Figure 102 and Figure 103, as the PVAC frequency spectra had a single dominant peak in most subjects compared to the CS which had multiple peaks in those subjects (e.g. subjects 4, 5, 9, and 14). Differences in SC between the CS and PVAC sites were investigated statistically in chapter 6 by studying spatial variability.

III. Comparison of the SC Estimated from Body Surface and Inside the Heart in Individual Subjects

To facilitate the comparison of body surface and intracardiac SC, Figure 111 combines the data from Figure 109 and Figure 110.

[1] Subjects 1, 2, 3, 4, 5, 7, 9, 10, 11, 12, 13, 14, 15, 16, 17, and 19.

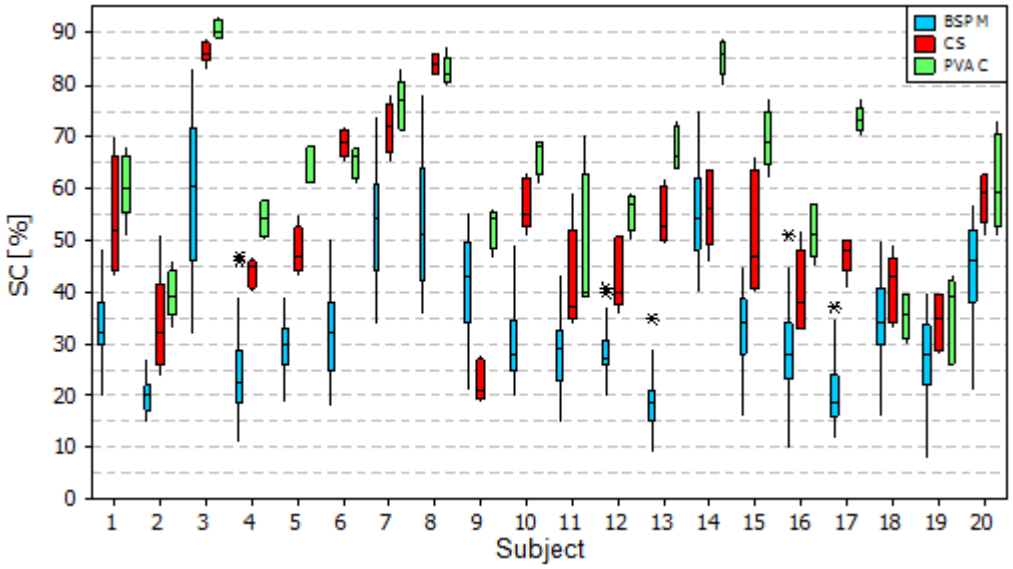

Figure 111. SC across the BSPM, CS and PVAC sites for each subject. This figure is constructed by jointly plotting the data from Figure 109 and Figure 110.

Figure 111 showed that all subjects had larger SC in PVAC than BSPM, and ninety-five percent of subjects[2] had larger SC in CS than BSPM.

Figure 112 shows SC of the BSPM, CS and PVAC plotted in colour for each subject. This figure did not show any consistent pattern in SC between subjects. This may suggest that there was no specific body surface site that consistently represent AF organisation in all subjects.

The linear regression analysis and scatter plots between the median SC estimated from the BSPM and both the CS and PVAC are shown in Table 4 and Figure 113.

[2] Subjects 1, 2, 3, 4, 5, 6, 7, 8, 10, 11, 12, 13, 14, 15, 16, 17, 18, 19 and 20.

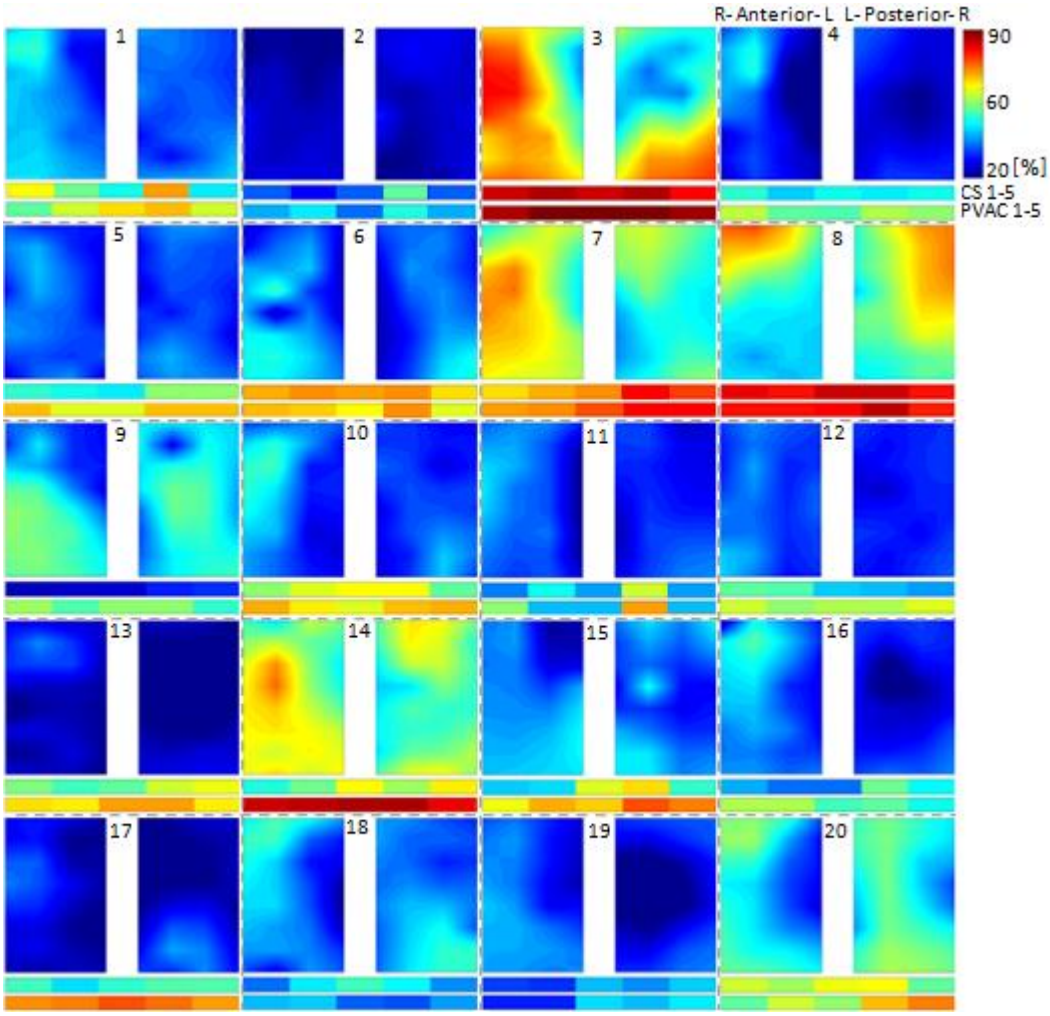

Figure 112. Spatial colour map of SC for each subject (identified 1 to 20). The vertical panels indicate BSPM anterior (left) and posterior (right). The horizontal panels indicate EGM SC from five CS sites (top: CS1 to CS5 from left to right) and five PVAC sites (bottom: PVAC1 to PVAC 5 from left to right).

	Median SC [%]			
Source	**p-value**	**R^2 [%]**	**β_0**	**β_1**
BSPM & CS	0.004	38.4	11.0	0.5
BSPM & PVAC	0.006	35.0	5.6	0.5

Table 4. Linear relationship between the median BSPM and EGM SC for 20 subjects.

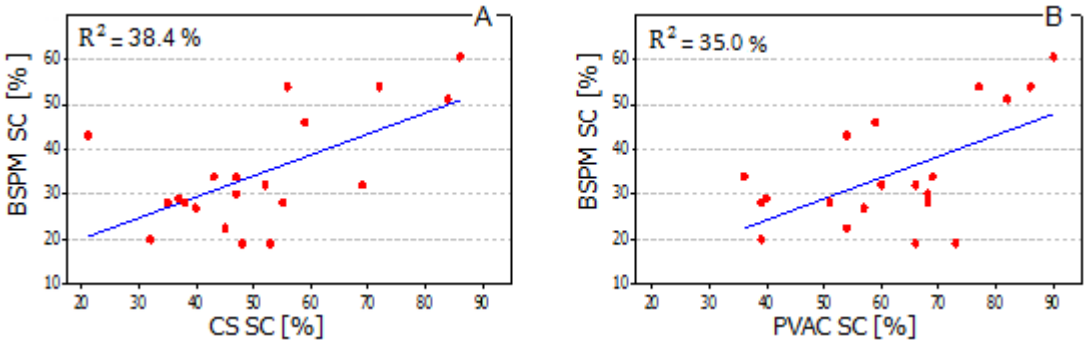

Figure 113. Linear relationship of the median SC estimated from body surface and inside the heart.

Figure 113 showed a positive linear relationship between BSPM and EGM SC. However, the strength of the relationship was weak and SC values were not normally distributed around the linear fit. To investigate whether the three subjects (3, 7 and 8) on the right side of the linear fit in Panel A, and the four subjects (3, 7, 8, and 14) on the right side of the linear fit in Panel B were influential to show the positive relationship or not, these subjects were discarded and analysis was repeated. The results showed no linear relationship between SC estimated from the body surface and inside the heart ($p>0.05$, $R^2<$ 0.2 %). Subjects 3 and 8 are in well organised AF and subjects 7 and 14 are more organised compared to the other subjects. This suggests that the body surface was unlikely to indicate AF complexity estimated from inside the heart in less organised AF cases.

Similarly, this analysis was repeated between SC estimated from BSPM site 22 with both CS4 and PVAC4 (see Table 5 and Figure 114).

		SC [%]		
Source	**p-value**	**R^2 [%]**	**β_0**	**β_1**
BSPM site 22 & CS4	0.002	42.4	13.3	0.6
BSPM site 22 & PVAC4	0.003	39.8	8.6	0.6

Table 5. Linear relationship between BSPM site 22 and EGM SC for 20 subjects.

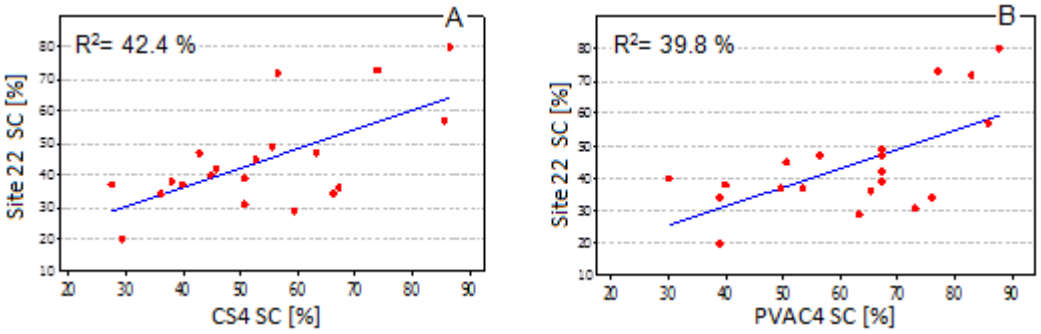

Figure 114. Linear relationship of SC estimated from the body surface site 22 and inside the heart.

The positive linear relationship between body surface site 22 and intracardiac SC may suggest that the body surface site with large amplitude was more likely to represent a degree of AF organisation estimated from inside the heart. The median SC may have been affected by noise at the posterior body surface sites due to low amplitude at these sites.

3.4. Relationship Between Atrial Fibrillation Characteristics

The AF characteristics estimated from the body surface and inside the heart for each subject were shown earlier in this chapter. Investigation of relationship between these characteristics estimated either from the body surface or inside the heart may motivate the development of a better understanding of the AF mechanism. For this purpose, the relationships between the AF characteristics estimated from body surface and from inside the heart form the focus of this section.

To investigate further the relationship between the AF characteristics estimated from the body surface, the linear regression analysis was performed with median values computed across the 64 sites in each subject between amplitude with DF, amplitude with SC, and SC with DF, see Table 6.

Source: Estimate from BSPM	p-value	R^2 [%]	β_0	β_1
Amplitude & DF	0.741	0.6	5.9	0.0
Amplitude & SC	0.013	30.1	18.8	0.4
SC & DF	0.648	1.6	5.4	0.0

Table 6. Linear relationship between the atrial fibrillation characteristics estimated from the body surface.

To investigate relationship between AF characteristics estimated from inside the heart, the linear regression analysis was performed with median values computed across the five CS and five PVAC sites in each subject between SC with DF (see Table 7).

Source: Estimate from EGM	p-value	R^2 [%]	β_0	β_1
CS SC & CS DF	0.247	7.7	5.0	0.0
PVAC SC & PVAC DF	0.131	12.0	4.5	0.0
CS SC & PVAC SC	<0.001	59.3	24.3	0.7
CS DF & PVAC DF	<0.001	57.6	1.5	0.7

Table 7. Linear relationship between the atrial fibrillation characteristics estimated from inside the heart.

According to the results, there was no linear relationship between signal amplitude and DF estimated from the body, nor between DF and SC estimated from the body surface and inside the heart. However, there was a weak positive linear relationship between amplitude and SC estimated from the body surface. This may suggest that SC computed from the AF signal with large amplitude was less affected by noise. As a result, components of the frequencies in the AF band were less undulated.

Chapter Summary

In this chapter AF characteristics (amplitude, DF and SC estimated from the BSPM recordings, and also DF and SC estimated from the EGM recordings) were analysed between subjects. AF amplitude estimated from the body surface ranged from 19.0 to 90.0 μV. AF DF estimated from the body surface ranged from 3.5 to 8 Hz which agreed with DF estimated from inside the heart. AF SC ranged from 19.0% to 60.5% estimated from the body surface, and from 21.0% to 90.0% estimated from inside the heart.

There was a significant difference in AF characteristics between subjects. These differences could be related to factors such as complexity of AF, BMI, and AF history.

In some subjects there were relatively small differences in AF characteristics across the body surface and intracardiac sites and in others

relatively large differences. Subjects in well organised AF exhibited good agreement of the AF characteristics between the BSPM, CS and PVAC recordings. However, subjects in less organised AF exhibited poor agreement of the AF characteristics between the BSPM, CS and PVAC or else between the CS and PVAC recordings. The AF characteristic differences in each subject may suggest that different sites captured atrial activations from different AF sources as they were located in different AF re-entrant pathways.

There was a positive strong linear relationship between the median DF estimated from the body surface and intracardiac recordings across the sites. However, this relationship decreased between single body surface site (site 22, closest to lead V1) and intracardiac recordings. This suggested more accurate estimation of AF DF using additional electrodes to lead V1. Furthermore, there was a positive but weak linear relationship between the median SC estimated from the body surface and intracardiac recordings across the sites. However, this relationship increased between single body surface site (site 22, with the largest amplitude) and intracardiac recordings. This suggested that there were other factors that may affect estimation of SC from the body surface sites such as noise and BMI.

It can be concluded that in subjects with organised AF, the AF characteristics estimated from the body surface sites can be used as a measure of AF. However, in subjects with complex AF, the AF characteristics estimated from the body surface sites may not be in good agreement with the measurements from inside the heart.

Chapter 4. Effect of Body Mass Index on Atrial Fibrillation Characteristics

There are no known studies of effect of BMI on the AF characteristics in the literature. As the aim of this PhD study was to investigate how AF characteristics were expressed on the body surface, it was important to know if any physiological factors affect AF characteristics estimated from the body surface. The effect of BMI on the AF characteristics were investigated in this chapter using linear regression analysis between BMI with the AF characteristics estimated from anterior site 22, posterior site 49, and the median across 64 sites.

- Site 22 was chosen as it had the largest AF signal amplitude on the anterior site (see chapter 6). In addition, as discussed earlier, site 22 was closest to lead V1 on the 12-lead ECG, the commonly used lead for AF analysis.

- Site 49 was chosen as it had the largest AF signal amplitude on the posterior site (see chapter 6). Moreover, it had strong morphology correlation with PVAC (see chapter 7).

- The median across 64 body surface sites was also investigated as there was large variability of the AF characteristics between body surface sites (see chapter 6). It was thought that one body surface site might not be indicative of the actual value of the AF characteristics across the whole body surface.

This chapter also investigates whether there is a relationship between subject's BMI and the differences of the AF characteristics estimated from the body surface and inside the heart.

4.1. Amplitude and BMI

The linear regression analysis between amplitude estimated from the longest AF segment (see chapter 2, parameter estimation, amplitude) showed a negative correlation (R^2= 20.2 %, p=0.043) between site 22 and BMI, see Figure 115. There was also no correlation between site 49 and BMI, or between the median across the sites and BMI (R^2 ≤10.0 %, p>0.05), see Table 8. Figures are shown in Appendix C.

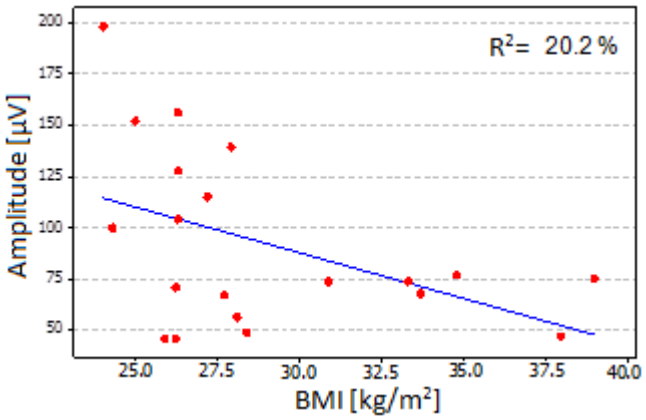

Figure 115. Linear relationship between BMI and AF amplitude from body surface site 22.

The results suggested that BMI may explain 20.2 % of the variance in amplitude estimated from the anterior body surface sites. The negative relationship suggested that amplitude decreased with an increase in BMI. However, as the R^2 value was small it may suggest that other factors affect amplitude as well, for example the type of AF. No relationship between amplitude estimated from site 49 and BMI may suggest that the effect of BMI may not be perceived on the posterior sites. This could be the reason for not

having any linear relationship between the median amplitude across the body surface sites as well. Calculating the median value possibly blurs the effect of BMI, as large BMI appears to have more effect on the anterior body surface sites.

4.2. Dominant Frequency and BMI

The linear regression analysis showed no correlation (R^2< 12.2 %, p>0.05) between DF estimated from sites 22 and 49 with BMI (see Appendix C). However, it showed a positive correlation (R^2= 20.0 %, p=0.046) between BMI and the median DF across the sites as shown in Figure 116 and Table 8.

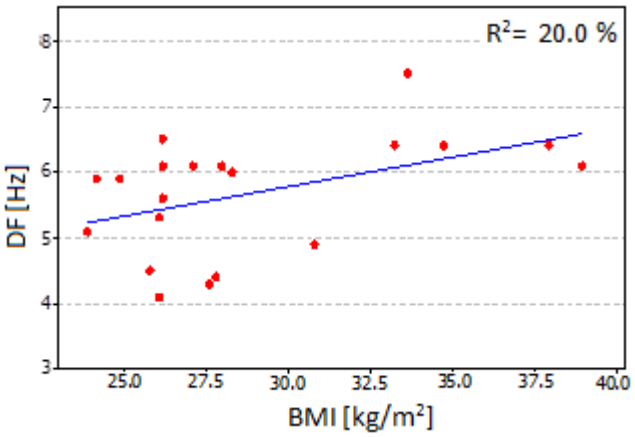

Figure 116. Linear relationship between BMI and the median DF across the BSPM sites.

The results may suggest that BMI explains 20.0 % of the variance in DF estimated from the body surface sites. In addition, the linear regression analysis was used between BMI and the estimated error in DF (see Figure 117 and Figure 118). The estimated error was introduced to study DF differences between the body surface and inside the heart. Using EGM DF as a reference, the estimated error was calculated by subtracting CS4 and PVAC4 DF from BSPM DF site 22. This would indicate if body surface DF had been under or overestimated in relation to BMI.

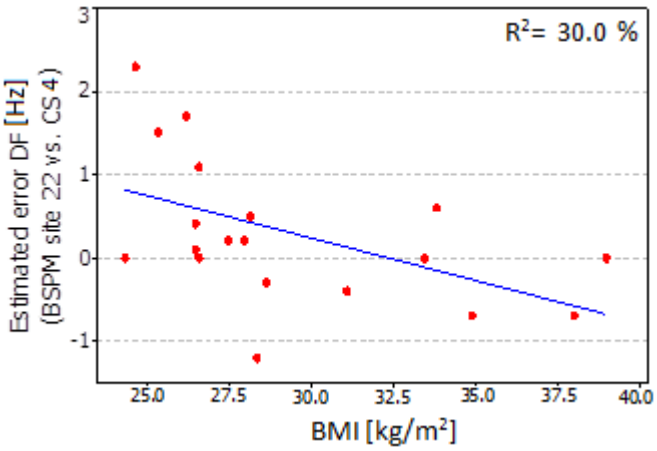

Figure 117. Linear relationship between BMI vs. estimated error DF (BSPM site 22 vs. CS4) for 20 subjects. There are 19 points visible as subjects 1 and 10 had overlapping values.

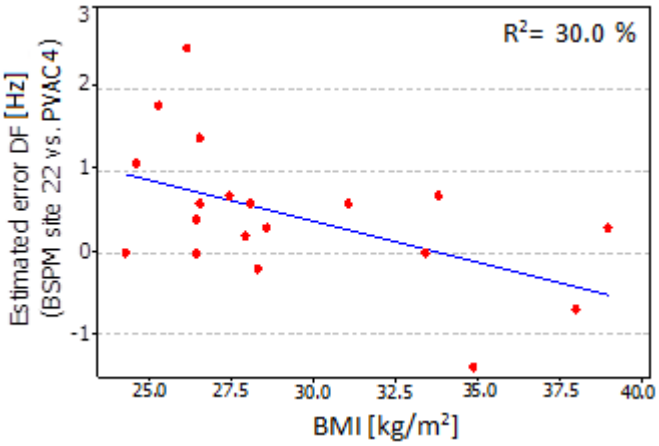

Figure 118. Linear relationship between BMI vs. estimated error DF (BSPM site 22 vs. PVAC4) for 20 subjects. There are 19 points visible as subjects 1 and 10 had overlapping values.

The results showed a negative correlation (p=0.022 BSPM site 22 vs. CS, and p=0.019 BSPM site 22 vs. PVAC), with R^2 =30.0 %. This suggested that the BMI may explain 30.0 % of the variance in DF estimated from the anterior body surface sites compared to DF estimated from inside the heart.

To examine if the relationship between BMI and BSPM DF, as well as BMI and DF estimated error were not because of artifacts, CS and PVAC DF versus BMI were plotted (see Figure 120).

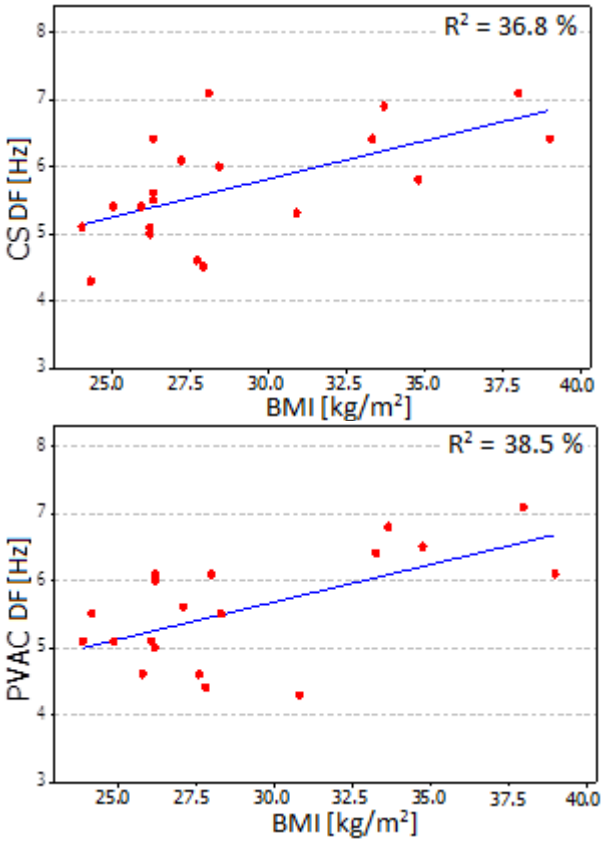

Figure 119. Linear relationship between BMI and the median DF across the CS sites (top) and PVAC sites (bottom).

The results suggest that subjects with larger BMI had AF with larger DF. Similarly, this analysis was repeated for site 49 and the median across all the sites. These results showed no significant correlation between the BMI and the estimated error DF for both analysis ($p>0.05$, $R^2 \leq 2.0$ %). A positive linear relationship between the median DF and BMI, as well as a negative linear relationship between the estimated error DF and BMI may suggest that with increasing BMI, the body surface recordings underestimate DF. However, the estimated error DF was 0.0 Hz in four subjects (3, 8, 14 and 16) from BSPM site 22 vs. CS, and in three subjects (3, 8, and 12) from BSPM site 22 vs. PVAC. This suggested that there was no difference between BSPM and EGM DF in these subjects. Two of these subjects (3 and 8) had consistent DF across all BSPM, CS and PVAC sites and they were in well organised AF (see section 1.1.3, description of AF complexity). The other subjects: 14 (Male, overweight,

paroxysmal AF), 12 (Male, overweight, paroxysmal AF), and 16 (Female, very obese, persistent AF) were overweight but DF from site 22 and EGM DF were the same. This suggested that BMI could not predict the DF difference between the body surface and inside the heart.

4.3. Spectral Concentration and BMI

The relationship between BMI and SC was also studied in the same manner as DF. The results showed no significant correlation between BMI with SC from site 22, site 49, and the median across the sites (p>0.05) with $R^2 < 4.0$ % (see Appendix C). In addition there was no significant correlation between BMI and the estimated error SC (p>0.05) with $R^2 < 7.0\%$, see Table 8. Hence, BMI was unlikely to have influenced estimation of SC from the body surface sites.

Source	p-value	R^2 [%]	β_0	β_1
BMI & Amplitude site 22	0.043	20.2	220.5	-4.4
BMI & Amplitude site 49	0.238	10.0	69.6	-1.1
BMI & Median Amplitude	0.175	7.3	99.5	-2.0
BMI & DF site 22	0.758	5.3	5.7	0.1
BMI & DF site 49	0.069	12.1	1.1	0.1
BMI & Median DF	0.046	20.0	3.1	0.1
BMI & ΔDF (site 22 vs. CS)	0.022	30.0	3.2	-0.1
BMI & ΔDF (site 22 vs. PVAC)	0.019	30.0	3.3	-0.1
BMI & ΔDF (site 49 vs. CS)	0.950	2.0	1.1	0.1
BMI & ΔDF (site 49 vs. PVAC)	0.751	1.0	1.1	0.1
BMI & ΔDF (median vs. CS)	0.850	1.0	1.1	0.1
BMI & ΔDF (median vs. PVAC)	0.765	1.1	1.1	0.1
BMI & SC site 22	0.650	1.2	33.5	0.4
BMI & SC site 49	0.613	1.0	51.9	-0.4
BMI & Median SC	0.835	2.0	19.5	-0.1
BMI & ΔSC (site 22 vs. CS)	0.950	2.0	1.1	0.1
BMI & ΔSC (site 22 vs. PVAC)	0.761	6.3	1.1	0.1
BMI & ΔSC (site 49 vs. CS)	0.850	2.0	1.3	0.1
BMI & ΔSC (site 49 vs. PVAC)	0.781	3.6	1.6	0.1
BMI & ΔSC (median vs. CS)	0.780	2.0	1.1	0.1
BMI & ΔSC (median vs. PVAC)	0.776	3.0	1.2	0.1

Table 8. Linear relationship between the atrial fibrillation characteristics and BMI.

Chapter Summary

In this chapter the effect of BMI on the AF characteristics estimated from the body surface recordings was investigated. The weak linear relationship between the AF characteristics and BMI may suggest that BMI had a small effect (less than 30.0%) on AF characteristics estimated from the body surface. Moreover, other factors may affect the AF characteristics estimated from the body surface, for example type of AF and noise. This could not be further investigated as the number of subjects with each type of AF was not statistically powerful enough to indicate this.

The limitation of this study was that the BMI was not normally distributed. Fourteen subjects had BMI less than 30 $\mathrm{kg/m^2}$ and six subjects had BMI greater than 30 $\mathrm{kg/m^2}$, so this could have biased the results.

Chapter 5. Temporal Variability of Atrial Fibrillation Characteristics

In this chapter the AF characteristics repeatability over the two minute recordings were investigated. The aim was to study the consistency of the AF characteristics over the duration of the recordings. This can indicate stability of the AF rhythm and determine whether these characteristics vary over time or are constant during stable clinical conditions. Moreover, the linear relationship between temporal variability estimated from the body surface and intracardiac recordings were studied for DF and SC.

5.1. Amplitude Temporal Variability

To investigate how AF amplitude changes over time, amplitude of the five longest AF segments, TQ1 to TQ5, was measured within the two minute BSPM recordings at each site for each subject. The median amplitude across the body surface sites and duration for each segment are shown in Figure 120.

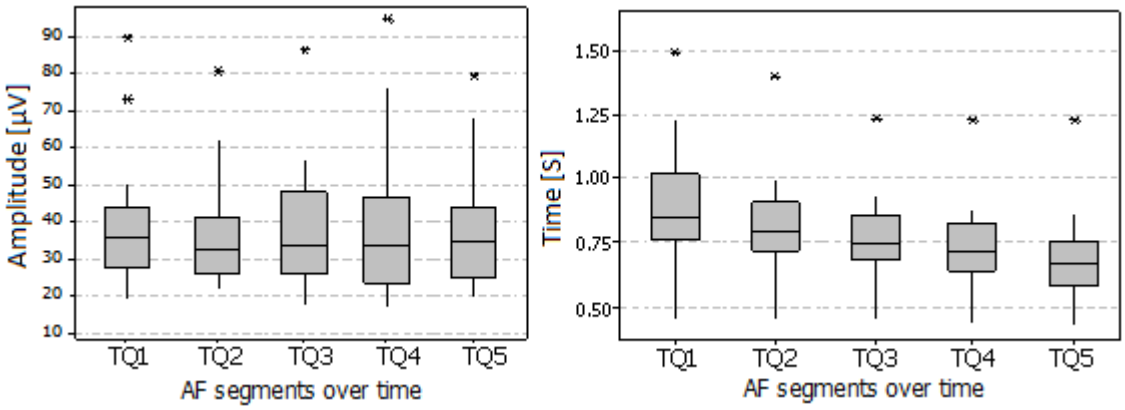

Figure 120. The median amplitude (left) and its duration (right) for each AF segment. Each bar is constructed from 20 values.

An example of the signals from the five longest AF segments for one subject is shown in Figure 121.

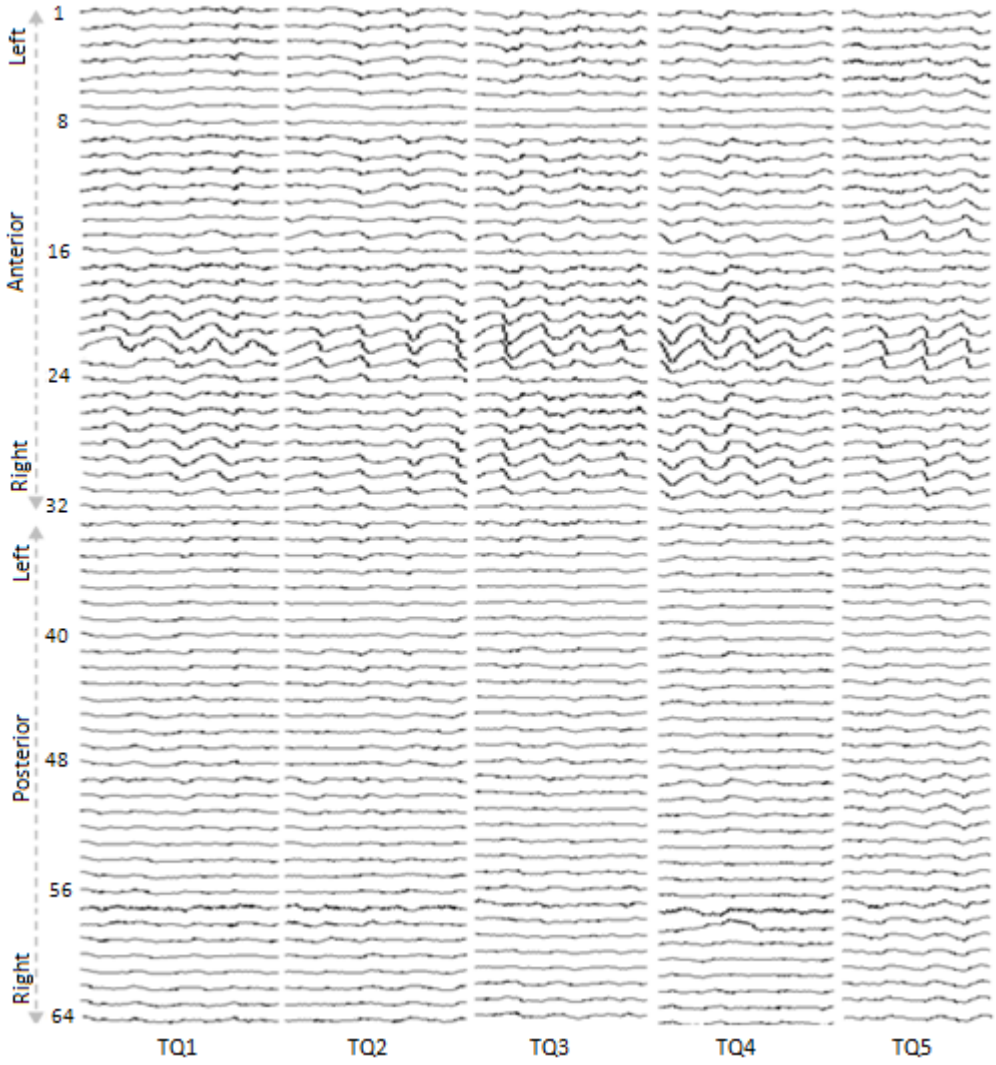

Figure 121. AF signal from five longest AF segments, within two minutes, for 64 body surface sites, subject 20. For each AF segment: the x-axis is time [s] and the y-axis is amplitude [μV] with all signals plotted in the same amplitude range.

The Friedman test showed that the segments did not exhibit significant differences ($p>0.05$) in amplitude (Design= 20×5, see section 2.4). The median amplitude between the segments ranged from 33.0 μV (TQ2) to 36.0 μV (TQ1).

AF amplitude temporal variability was quantified by the IQR of amplitude across the five AF segments in each subject to investigate if amplitude was more stable over time in subjects with larger amplitude. The linear regression analysis was performed between the median AF amplitude and its temporal variability as shown in Figure 122.

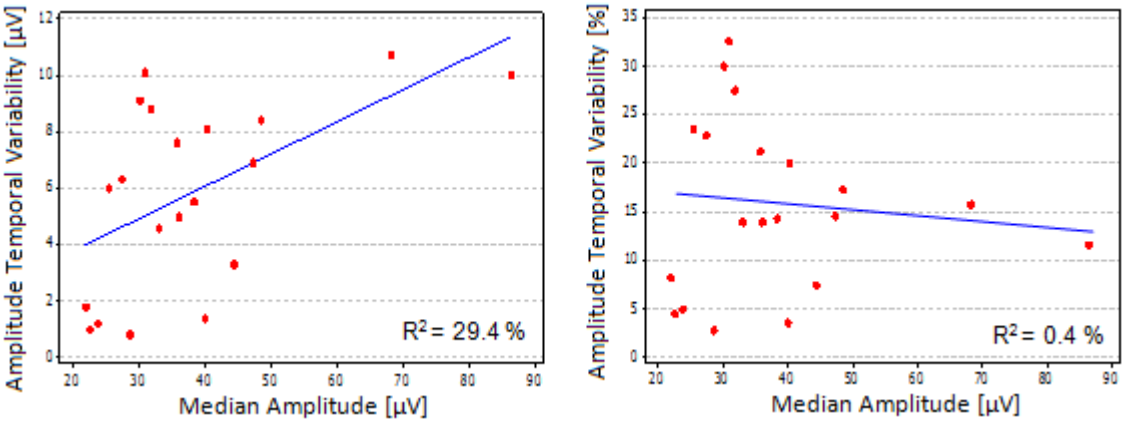

Figure 122. Linear relationship between the median and inter-quartile range of amplitude estimated from the body surface (20 subjects). Amplitude temporal variability in µV (left) and percentage of the actual amplitude (right).

The results showed a positive but weak linear relationship between the median and temporal variability of AF amplitude (p=0.014, R^2= 29.4 %) shown in Figure 122, left panel. However, there was no relationship between the median and temporal variation of the actual AF amplitude in percentage (p=0.789, R^2= 0.4 %) shown in Figure 122, right panel. The results suggested that subjects with large amplitude were unlikely to possess more stable amplitude over time. For example subject 3 with the largest median amplitude (86.5 µV) had 11.6% temporal variability, subject 19 with the median amplitude of 68.2 µV had 15.7% temporal variability, and subject 4 with the median amplitude of 28.7 µV had 2.8% temporal variability. Moreover, subjects with small amplitude temporal variability (e.g. in subjects 2, 4, and 18 where temporal variability was less than 2 µV) were not necessarily in organised AF. Consequently, temporal variability was unlikely to indicate stability of the AF rhythm.

The limitations of this analysis were: (1) the AF segments were collected at different times within the two minute recordings for each subject; (2) the

duration of the segments was different between subjects, so observations for the same study group could be different if other segments were to be studied.

5.2. Dominant Frequency Temporal Variability

I. Temporal Variability of Body Surface Dominant Frequency

To investigate whether AF DF changes over time, DF was estimated at each site for each subject in three ways: (1) over two minute BSPM recordings (T_{120}); (2) for two consecutive, non-overlapping segments, each 60 seconds long ($T_{1\text{-}60}$ and $T_{2\text{-}60}$); (3) for four consecutive, non-overlapping segments, each 30 seconds long ($T_{1\text{-}30,}$ $T_{2\text{-}30,}$ $T_{3\text{-}30,}$ and $T_{4\text{-}30}$). Median DF across the body surface sites for each subject in each segment was calculated and is shown in Figure 123.

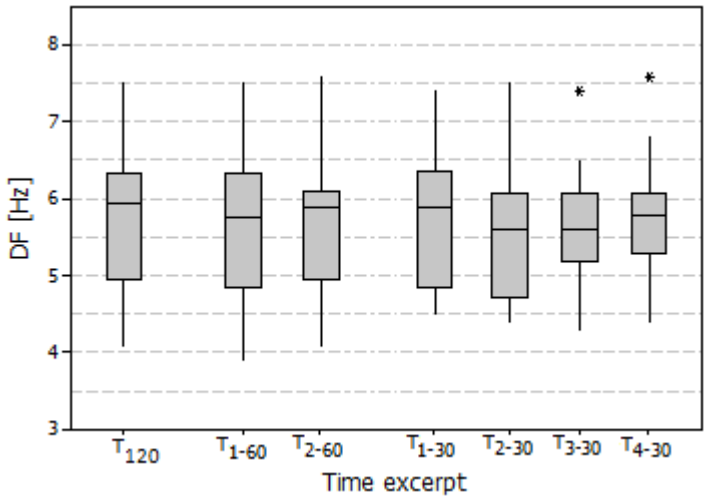

Figure 123. The median DF for each segment. Each bar is constructed from 20 values calculated as the median across the body surface sites for each subject.

The Friedman test showed that DF did not exhibit significant differences ($p>0.05$) between either 60 seconds (Design= 20×2) or 30 seconds (Design= 20×4). Furthermore, paired comparison using the Wilcoxon signed-rank test between DF estimated from the two minutes and the other time segments showed no significant differences ($p>0.05$).

The median DF calculated for the two segments ranged from 5.8 Hz (T_{1-60}) to 5.9 Hz (T_{2-60}), and for the four segments ranged from 5.6 Hz (T_{2-30}) to 5.9 Hz (T_{1-30}). Table 9 shows the median DF difference between each 60 second segment and each 30 second segment.

BSPM Median DF [Hz]	
Source	**Difference**
T_{1-60} and T_{1-30}	-0.1
T_{1-60} and T_{2-30}	0.1
T_{1-60} and T_{3-30}	0.1
T_{1-60} and T_{4-30}	-0.1
T_{2-60} and T_{1-30}	0.0
T_{2-60} and T_{2-30}	0.3
T_{2-60} and T_{3-30}	0.3
T_{2-60} and T_{4-30}	0.1

Table 9. The BSPM median DF variability between each 60 second segment and each 30 second segment.

DF temporal variability was quantified by the IQR of DF across the segments in each subject to investigate if DF was more stable over time in subjects with smaller DF. The linear regression analysis between the median DF and its temporal variability showed no significant correlation ($p>0.05$ with $R^2< 0.4$ %). This suggested that the subjects with small median DF were unlikely to possess more stable DF over time.

II. Temporal Variability of Inside the Heart Dominant Frequency

DF temporal variability of intracardiac measurements was also investigated in the same manner as described for the BSPM recordings. The median DF across the five CS and five PVAC sites for each segment is shown in Figure 124.

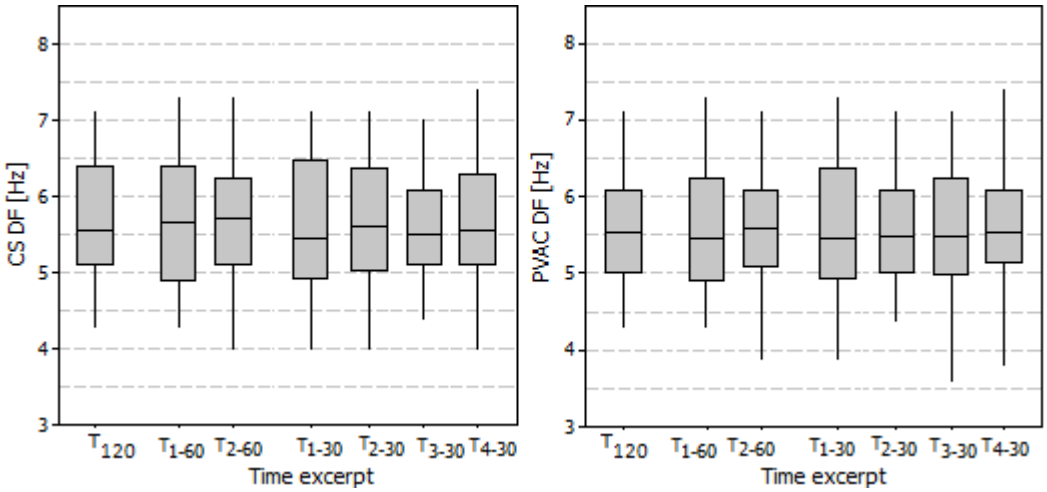

Figure 124. The median DF for each segment. Each bar is constructed from 20 values, calculated as the median DF across the five CS sites (left) and five PVAC sites (right) for each subject.

The Friedman test indicated that DF was not significantly different between the segments for both CS and PVAC ($p>0.05$). Moreover, paired comparison using the Wilcoxon signed-rank test between DF estimated from the two minute and other time segments indicated that there was no significant difference over time ($p>0.05$). The CS median DF calculated for the two segments ranged from 5.6 Hz ($T_{1\text{-}60}$) to 5.7 Hz ($T_{2\text{-}60}$), and for the four segments ranged from 5.4 Hz ($T_{1\text{-}30}$ and $T_{2\text{-}30}$) to 5.5 Hz ($T_{3\text{-}30}$ and $T_{4\text{-}30}$). The PVAC median DF calculated for the two segments ranged from 5.5 Hz ($T_{1\text{-}60}$) to 5.6 Hz ($T_{2\text{-}60}$), and for the four segments ranged from 5.4 Hz ($T_{1\text{-}30}$) to 5.6 Hz ($T_{4\text{-}30}$). Table 10 shows the median DF difference between each 60 second segment and each 30 second segment. Intracardiac DF temporal variability was also quantified by the IQR of DF across the segments in each subject. The linear regression analysis between the median DF and its temporal variability showed no significant correlation ($p>0.05$, $R^2< 0.4$ %). This agreed with the BSPM results which suggested that subjects with small median DF were unlikely to possess more stable DF over time.

Median DF [Hz]		
Source	Difference	
	CS	PVAC
$T_{1\text{-}60}$ and $T_{1\text{-}30}$	0.2	0.0
$T_{1\text{-}60}$ and $T_{2\text{-}30}$	0.0	-0.1
$T_{1\text{-}60}$ and $T_{3\text{-}30}$	0.1	-0.1
$T_{1\text{-}60}$ and $T_{4\text{-}30}$	0.1	-0.1
$T_{2\text{-}60}$ and $T_{1\text{-}30}$	0.3	0.2
$T_{2\text{-}60}$ and $T_{2\text{-}30}$	0.1	0.1
$T_{2\text{-}60}$ and $T_{3\text{-}30}$	0.2	0.1
$T_{2\text{-}60}$ and $T_{4\text{-}30}$	0.1	0.1

Table 10. The EGM median DF variability between each 60 second segment and each 30 second segment.

III. Differences of the Dominant Frequency Variance over Different Time Periods

To investigate DF variance over time, DF difference (ΔDF) was calculated between the longer segments ($T_{1\text{-}60}$ and $T_{2\text{-}60}$), and shorter segments ($T_{1\text{-}30}$, $T_{2\text{-}30}$, $T_{3\text{-}30}$, and $T_{4\text{-}30}$). Then variance of the ΔDF were compared between the longer and shorter segments in each measurement source (BSPM and EGM), using the Levene's test (non-parametric F-test), as shown in Figure 125.

The ΔDF between the longer segments was calculated by subtracting the $T_{2\text{-}60}$ DF from the $T_{1\text{-}60}$ DF. The ΔDF between the shorter segments was calculated as follows:

- Minimum and maximum DF were identified between the four segments,
- The segments with the minimum and maximum DF were collected for each subject to calculate the ΔDF from them. It resulted a table (Design = 20×2) containing subjects at each raw, and the collected segments at each column with the maximum or minimum DF. Note: maximum or minimum DF may come from different segments (either $T_{1\text{-}30}$, $T_{2\text{-}30}$, $T_{3\text{-}30}$, or $T_{4\text{-}30}$) for different subjects,

- The second column's DF (either maximum or minimum) was subtracted from the first column 's DF. This way helped to avoid missing the sign of the ΔDF.

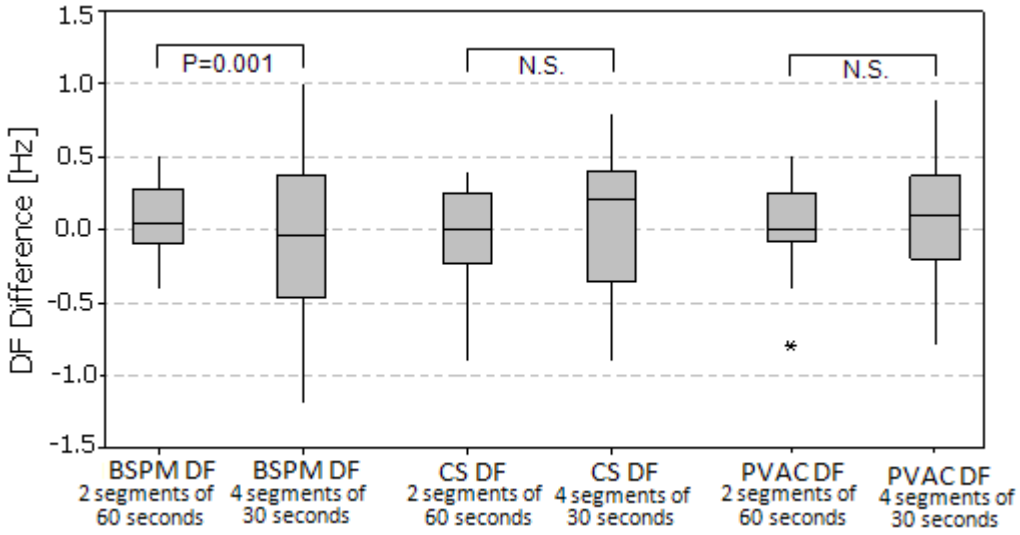

Figure 125. Paired changes of DF between 60 second and between 30 second segments for BSPM, CS and PVAC recordings. Each bar is constructed from 20 values calculated as the DF difference between the segments for each subject. The statistical p-value indicates a difference in variance using the Levene's test.

There was a significant difference in the DF difference variances estimated from the 60 seconds and 30 seconds duration of the BSPM recordings (p=0.001). However, there was no significant difference in the DF difference variances estimated from the 60 seconds and 30 seconds duration of the EGM recordings (p>0.05).

These results showed that the body surface DF estimated from the longer duration had smaller variance compared to the shorter duration. The variance of BSPM DF for the 60 seconds was 0.1 Hz^2, and for the 30 seconds was 0.3 Hz^2. The two minute recording is likely to have smaller variability compared to the 60 seconds recordings.

IV. Comparison of the Dominant Frequency Temporal Variability Estimated from Body Surface and Inside the Heart

In this section differences between BSPM and EGM of the paired changes was investigated (see Figure 125). Paired comparison of the DF differences between segments was performed between BSPM and EGM using the Wilcoxon signed-rank test. There was no significant difference between DF differences estimated from the body surface and inside the heart ($p>0.05$).

The relationship of the DF temporal variability estimated from the BSPM and EGM recordings was investigated using linear regression analysis between paired of the BSPM ΔDF (calculated as $T_{1\text{-}60} - T_{2\text{-}60}$) and EGM ΔDF (calculated as $T_{1\text{-}60} - T_{2\text{-}60}$ for both CS and PVAC), and also between paired of the BSPM ΔDF (calculated as $T_{3\text{-}30} - T_{1\text{-}30}$) and EGM ΔDF (calculated as $T_{1\text{-}30} - T_{2\text{-}30}$ for CS and $T_{1\text{-}30} - T_{4\text{-}30}$ for PVAC). There was no correlation between the DF temporal changes estimated from the BSPM and EGM ($p>0.05$, $R^2< 3.0\%$). This suggested that the DF temporal variability estimated from the body surface may be affected by other factors or sources of AF, as it may capture several re-entrant pathways (with possible variations in frequency) circulating round the atria, taking different paths or directional switches in time. It is important to bear in mind that these differences were not statistically significant.

5.3. Spectral Concentration Temporal Variability

I. Temporal Variability of Body Surface Spectral Concentration

To investigate whether AF SC changed over the two minute BSPM recordings, SC was estimated in the same approach as DF. Median SC across the body surface sites in each subject for each segment is shown in Figure 126.

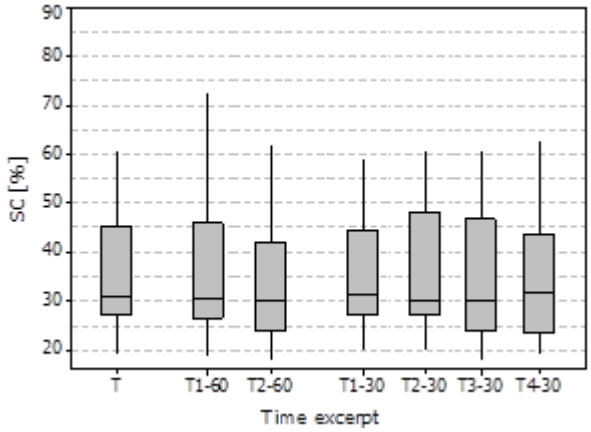

Figure 126. The median SC for each segment. Each bar is constructed from 20 values calculated as the median across the body surface sites for each subject.

The Friedman test showed that SC did not exhibit significant differences between either 60 second or 30 second ($p>0.05$). Paired comparison using the Wilcoxon signed-rank test between SC estimated from the two minutes and the other time segments showed no significant differences over time ($p>0.05$).

The median SC calculated for the two segments ranged from 30.5 % ($T2\text{-}_{60}$) to 31.2 % ($T_{1\text{-}60}$), and for the four segments ranged from 30.0 % ($T_{2\text{-}30}$) to 32.0 % ($T_{4\text{-}30}$). The median SC variability between each 60 second segment and each 30 second segment are shown in Table 11.

SC temporal variability was quantified by the IQR of SC across the segments in each subject to investigate if SC was more stable over time in subjects with larger SC. The linear regression analysis between the median SC and its temporal variability showed no significant correlation ($p>0.05$, $R^2< 0.9$ %). This suggested that subjects with large median SC were unlikely to possess more stable SC over time.

BSPM Median SC [%]	
Source	**Difference**
$T_{1\text{-}60}$ and $T_{1\text{-}30}$	-1.0
$T_{1\text{-}60}$ and $T_{2\text{-}30}$	0.5
$T_{1\text{-}60}$ and $T_{3\text{-}30}$	0.5
$T_{1\text{-}60}$ and $T_{4\text{-}30}$	-1.5
$T_{2\text{-}60}$ and $T_{1\text{-}30}$	-1.3
$T_{2\text{-}60}$ and $T_{2\text{-}30}$	0.3
$T_{2\text{-}60}$ and $T_{3\text{-}30}$	0.3
$T_{2\text{-}60}$ and $T_{4\text{-}30}$	-1.8

Table 11. The BSPM median SC variability between each 60 second segment and each 30 second segment.

II. Temporal Variability of Inside the Heart Spectral Concentration

The SC temporal variability was also investigated from inside the heart in the same manner as described earlier. The median SC for each subject calculated across the five CS and five PVAC sites for each segment is shown in Figure 127. The Friedman test showed that SC did not exhibit significant differences ($p>0.05$) between either 60 second or 30 second. The median SC calculated for the two segments ranged from 44.6 % ($T_{2\text{-}60}$) to 47.5 % ($T_{1\text{-}60}$) for CS, and ranged from 48.9 % ($T_{2\text{-}60}$) to 51.2 % ($T_{1\text{-}60}$) for PVAC. The median SC calculated for four segments ranged from 47.5 % ($T_{1\text{-}30}$ and $T_{3\text{-}30}$) to 51.0 % ($T_{4\text{-}30}$) for both CS and PVAC recordings. The median SC variability between each 60 second segment and each 30 second segment are shown in Table 12.

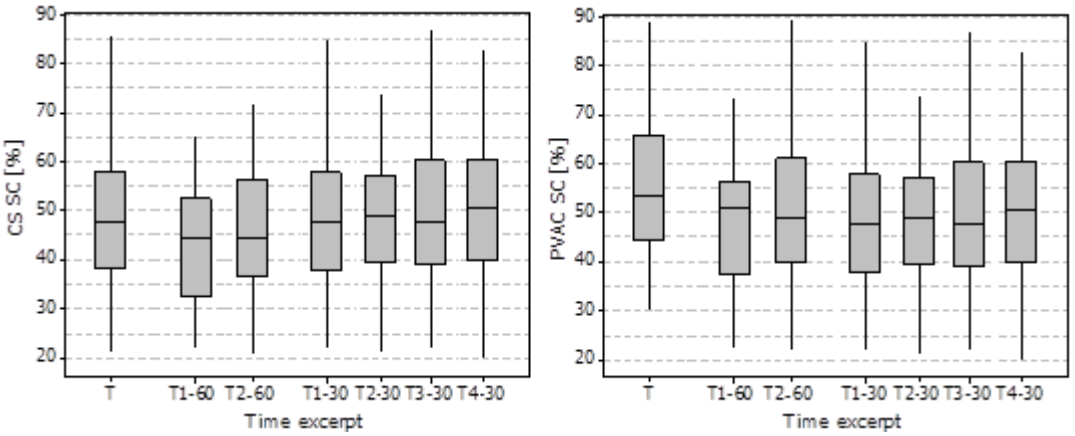

Figure 127. The median SC for each segment. Each bar is constructed from 20 values, calculated as the median SC across the five CS sites (left) and five PVAC sites (right) for each subject.

Median SC [%]		
Source	Difference	
	CS	PVAC
$T_{1\text{-}60}$ and $T_{1\text{-}30}$	-3.4	3.2
$T_{1\text{-}60}$ and $T_{2\text{-}30}$	-4.4	2.2
$T_{1\text{-}60}$ and $T_{3\text{-}30}$	-3.4	3.2
$T_{1\text{-}60}$ and $T_{4\text{-}30}$	-5.9	0.6
$T_{2\text{-}60}$ and $T_{1\text{-}30}$	-3.4	0.9
$T_{2\text{-}60}$ and $T_{2\text{-}30}$	-4.4	-0.1
$T_{2\text{-}60}$ and $T_{3\text{-}30}$	-3.4	0.9
$T_{2\text{-}60}$ and $T_{4\text{-}30}$	-5.9	-1.7

Table 12. The EGM median SC variability between each 60 second segment and each 30 second segment.

Paired comparison using the Wilcoxon signed-rank test was performed between SC estimated from the two minute and the other time segments. The results showed that SC estimated from the EGM did not change significantly between the two minute with first and second minute, or between the two minute with each 30 second ($p>0.05$). Intracardiac SC temporal variability was quantified by the IQR across the segments in each subject. The linear regression analysis between the median SC and its temporal variability showed no significant correlation ($p>0.05$, $R^2< 2.0$ %). This agreed with the BSPM results which suggested that subjects with larger SC were unlikely to possess more stable SC over time. Moreover, stability over time was less likely to indicate the degree of AF organisation. In other words, subjects with stable SC temporal variability over time were not necessarily in organised AF. It is important to bear in mind that these differences were not statistically significant.

III. Differences of the Spectral Concentration Variance over Different Time Periods

To investigate SC variance between the two segments of 60 second and four segments of 30 second for BSPM and EGM, Figure 128 was constructed. SC differences were calculated in the same manner as DF.

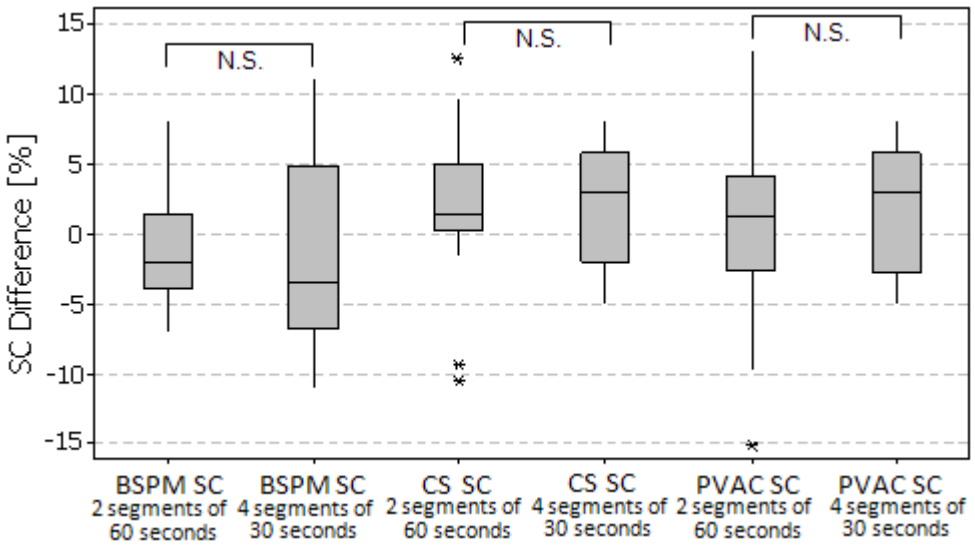

Figure 128. Paired changes of SC between 60 second and between 30 second segments for BSPM, CS and PVAC recordings. Each bar is constructed from 20 values calculated as the SC difference between the segments for each subject. The statistics indicates no significant difference in variance using Levene's test.

Figure 128 shows the SC differences between the two segments of 60 seconds duration, and SC differences between the four segments of 30 seconds duration estimated from the BSPM, CS and PVAC recordings. The variances of the SC differences were compared between the two segments and four segments in each measurement source using the Levene's test. There was no significant difference of the SC difference variances estimated from the 60 seconds and 30 seconds duration in both the BSPM and EGM recordings ($p>0.05$).

These results showed that body surface and intracardiac SC estimated from the longer duration had smaller variance compared to the shorter duration; bear in mind that the variance was not statistically significant. Consequently, the two minute recording was reliable for the analysis of AF SC.

IV. Comparison of the Spectral Concentration Temporal Variability Estimated from Body Surface and Inside the Heart

In this section differences between BSPM and EGM of the paired changes (see Figure 128) was investigated. Paired comparison of the SC differences between segments was performed between BSPM and EGM using the Wilcoxon signed-rank test. There was no significant difference between SC differences estimated from the body surface and inside the heart ($p>0.05$).

The relationship of the SC temporal variability estimated from the BSPM and EGM was investigated using linear regression analysis between paired of the BSPM ΔSC (calculated as $T_{1\text{-}60} - T_{2\text{-}60}$) and EGM ΔSC (calculated as $T_{1\text{-}60} - T_{2\text{-}60}$ for both CS and PVAC), and also between paired of the BSPM ΔSC (calculated as $T_{2\text{-}30} - T_{4\text{-}30}$) and EGM ΔSC (calculated as $T_{1\text{-}30} - T_{4\text{-}30}$ for both CS and PVAC). There was no correlation between the BSPM and EGM SC temporal variability ($p>0.05$, $R^2< 16.2\%$). This suggested that the BSPM SC temporal variability may be affected by other factors or sources of AF, as it may capture several re-entrant pathways circulating round the atria. It is important to bear in mind that these differences were not statistically significant.

Chapter Summary

In this chapter the repeatability of AF amplitude estimated from the body surface recordings was assessed over the two minutes by studying the five longest AF segments. The repeatability of DF and SC estimated from the body surface and inside the heart were also assessed by dividing the two minute recordings into two segments of 60 seconds and four segments of 30 seconds duration. The AF characteristics estimated from the body surface and inside

the heart were repeatable over the duration of the recordings. There was no evidence that subjects with large AF amplitude and high SC had more stable amplitude over the two minute recordings. There was no evidence that subjects with small DF had more stable DF over the two minute recordings. Moreover, the temporal variation of DF was small (0.1 Hz) compared to between subject variability (3.4 Hz, see chapter 3), which suggested that the two minute recording variation was acceptable for AF analysis.

Chapter 6. Spatial Variability of Atrial Fibrillation Characteristics

This chapter investigates spatial variability of the AF characteristics estimated from the body surface and inside the heart. The aim was to explore how AF characteristics were expressed across the body surface and along the catheters sites. This could potentially discover body surface sites which might be particularly sensitive to the left atrial activity, and it may spur the development of a greater understanding of the AF mechanism from the body surface. Moreover, the linear relationship between each body surface site and selected intracardiac sites were investigated across all subjects.

6.1. Spatial Variability of Body Surface Amplitude

To investigate AF amplitude spatial variability, peak to peak amplitude was estimated from the longest AF segment within the two minute recordings for each body surface site in each subject. Figure 129 illustrates the amplitude range for each site across subjects.

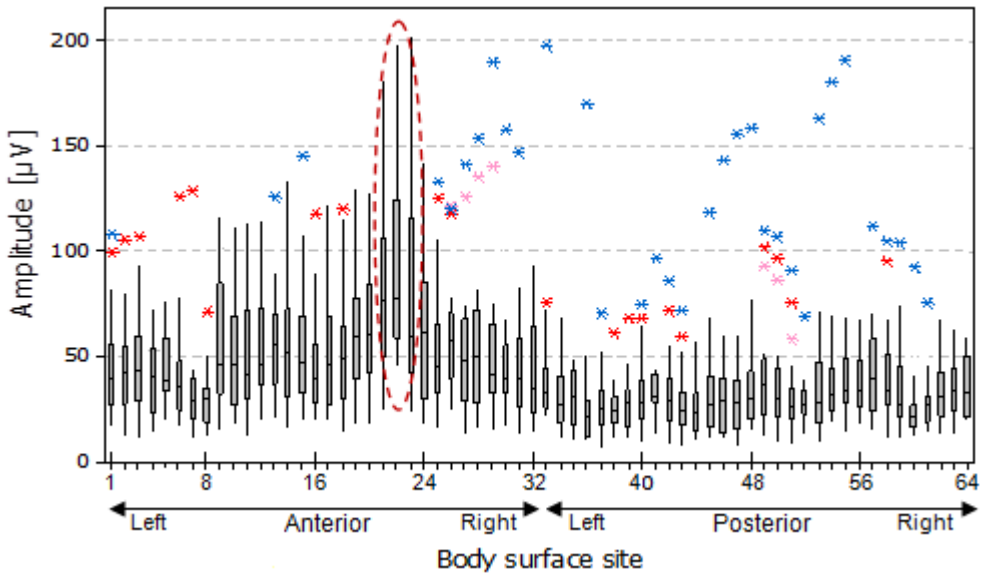

Figure 129. AF amplitude for each body surface site. Each bar is constructed from 20 values from each subject. Outliers from subject 3 (blue), subject 15 (pink), and subject 19 (red) are also displayed. The largest AF amplitude could be seen on the anterior central right, close to site 22 (dash red marked).

To visualise the differences in amplitude between the body surface sites, Figure 130 shows a colour map of the median amplitude across subjects.

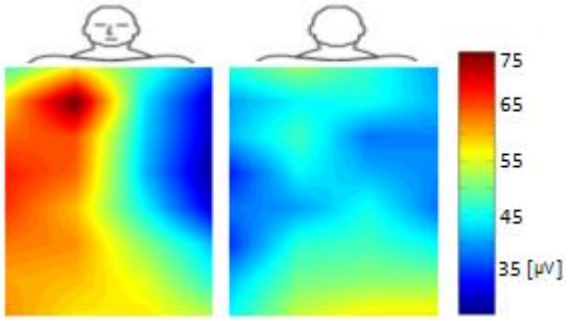

Figure 130. Spatial colour map of the median amplitude across subjects (values are from the horizontal lines in each bar in Figure 129).

The Friedman test showed that AF amplitude exhibited significant differences ($p<0.001$) between the sites (Design=20×64, see section 2.4).

The median amplitude measured across subjects ranged from 21.8 μV (site 60) to 77.4 μV (site 22), with median and IQR of 34.4 (29.2 – 44.9) μV across all the sites.

To investigate more precisely where on the body surface the amplitude differences occurred, the body surface sites were grouped according to their anatomical location into four groups: anterior and posterior, left and right, vertical lines and horizontal lines (see chapter 2 for definition of electrode groups).

Spatial Variability of Amplitude at the Anterior and Posterior Sites: Paired comparison using the Wilcoxon signed-rank test showed that amplitude was significantly different between the anterior and posterior sites ($p<0.001$), Design= 20×2, see Figure 131.

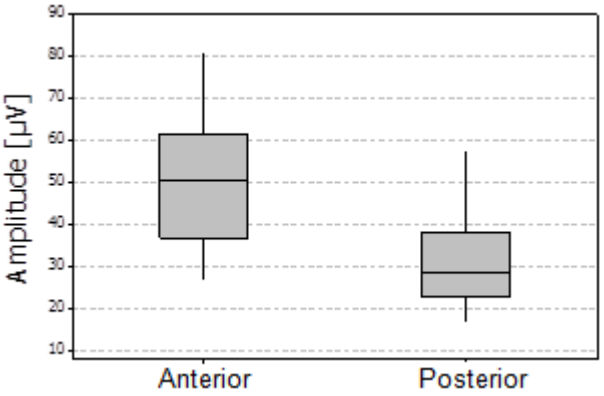

Figure 131. AF amplitude of the anterior and posterior body surface sites. Each bar is constructed from 20 values calculated as the median across the anterior and posterior sites in each subject.

Spatial Variability of Amplitude at the Left and Right Sites: (I) Paired comparison using the Wilcoxon signed-rank test showed that amplitude was significantly different between the left and right sites (p=0.001), Design= 20×2. (II) Paired comparison using the Wilcoxon signed-rank test showed significant differences in amplitude between the possible pairs except between the posterior left and posterior right (p=0.001), see Figure 132.

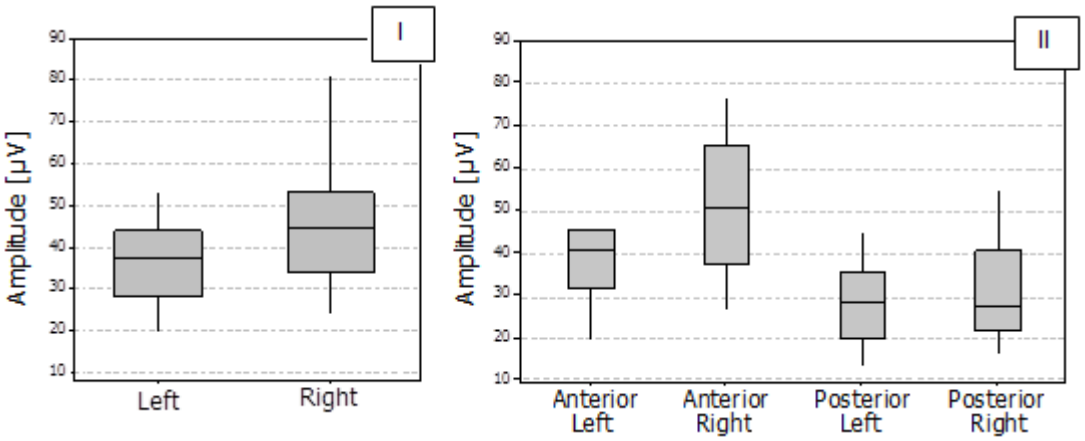

Figure 132. AF amplitude for the left and right body surface sites. Each bar is constructed from 20 values calculated as the median across the left and right sites in each subject.

Spatial Variability of Amplitude at the Vertical Electrode Lines: The Friedman test showed that amplitude exhibited significant differences between the vertical lines (p<0.001), Design= 20×8, see Figure 133. Paired comparison

using the Wilcoxon signed-rank showed significant differences between all possible pairs except ACL & ALR, PLL & PCL, and PCR & PLR (see Appendix D, Table 18).

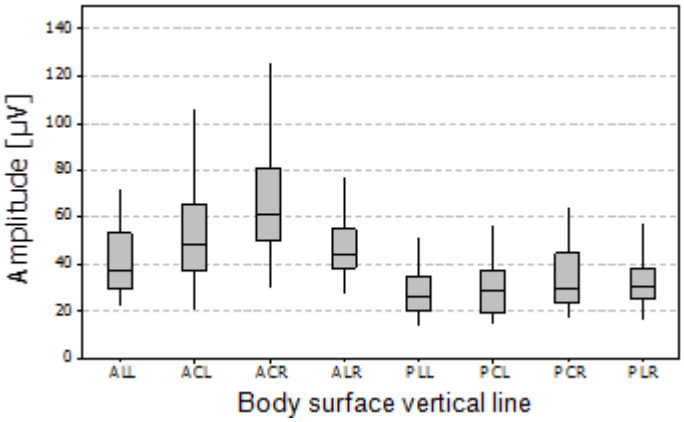

Figure 133. AF amplitude for the vertical lines on body surface sites. Each bar is constructed from 20 values calculated as the median across the vertical electrodes in each strip for each subject.

Spatial Variability of Amplitude at the Horizontal Electrode Lines: The Friedman test showed that AF amplitude exhibited significant differences between the horizontal lines ($p<0.001$), Design= 20×16, see Figure 134. Paired comparison using the Wilcoxon signed-rank showed significant differences between the possible pairs except between some anterior lower body surface and some posterior lower body surface sites (see Appendix D, Table 19).

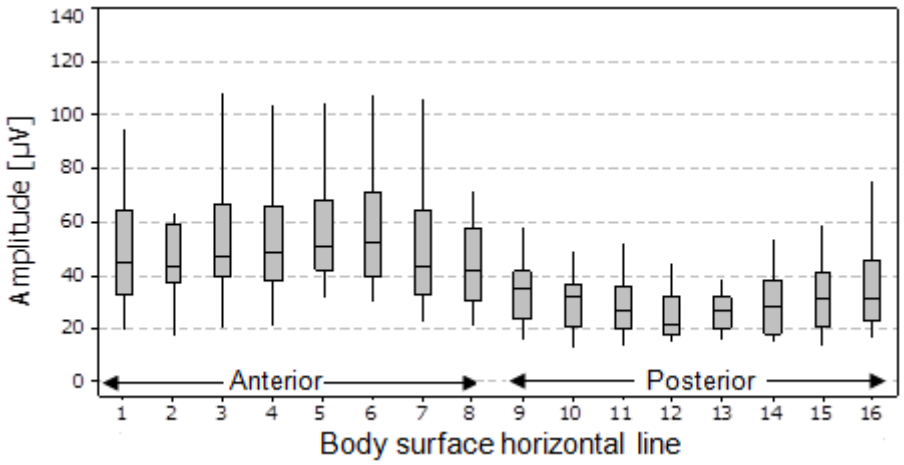

Figure 134. AF amplitude for the horizontal lines on body surface sites. Each bar is constructed from 20 amplitude values calculated as the median across the horizontal electrodes in each line for each subject.

According to the results, AF amplitude was significantly larger on the body surface sites close to the anterior upper central right. This may suggest that these sites represent AF better than other body surface sites (in terms of the amplitude). According to the literature in the 12-lead ECG, lead V1 is used for AF analysis due to its proximal location to the RA. The anterior upper central right sites are close to lead V1, therefore they may capture AA from the RA. To investigate whether these sites also capture AA from the LA, DF estimated from the anterior upper central right sites was compared with DF estimated from inside the heart (see section 6.2, part III).

6.2. Spatial Variability of Dominant Frequency

I. Spatial Variability of Dominant Frequency at the Body Surface

To investigate AF DF spatial variability, DF was estimated over the two minute BSPM recordings in each subject for each site. Figure 135 illustrates DF for each site across subjects, and Figure 136 shows a colour map of the median DF across subjects. The Friedman test showed that AF DF exhibited significant differences between the sites (p=0.025), Design=20×64.

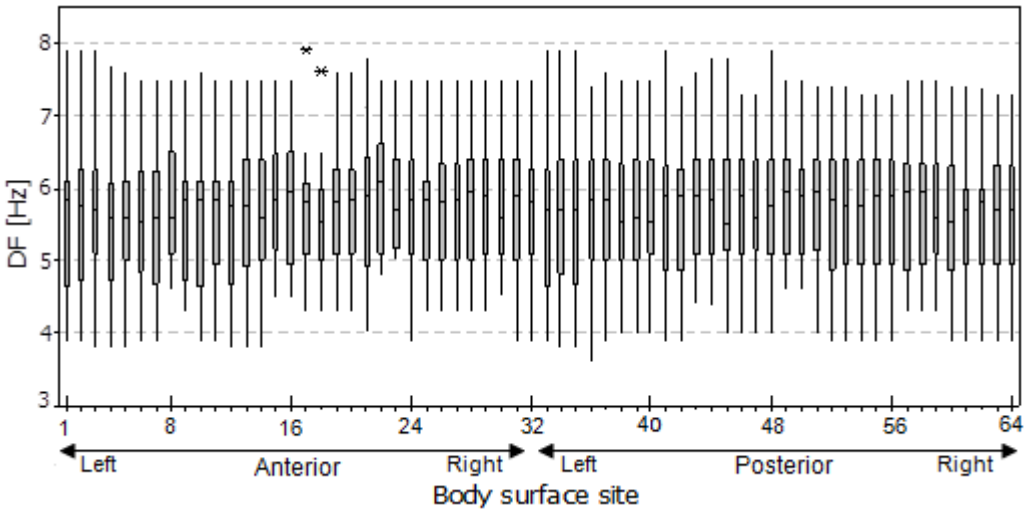

Figure 135. DF for each body surface site. Each bar is constructed from 20 values from each subject. Outliers belong to subjects 11 and 18.

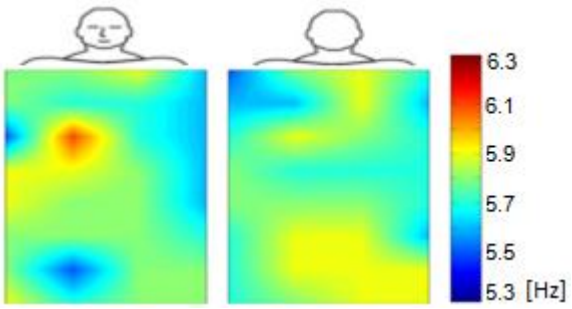

Figure 136. Spatial colour map of the median DF across subjects (values are from the horizontal lines in each bar in Figure 135).

The median DF, measured across subjects ranged from 5.5 Hz (site 45) to 6.1 Hz (site 22), with median and IQR of 5.6 (5.3 – 6.0) Hz across all the sites.

To investigate where on the body surface the DF differences occurred, DF changes was studied between the anterior and posterior, left and right, vertical lines and horizontal lines.

Spatial Variability of DF at the Anterior and Posterior Sites: Paired comparison using the Wilcoxon signed-rank test showed that DF was not significantly different between the anterior and posterior sites ($p>0.05$), Design= 20×2, see Figure 137.

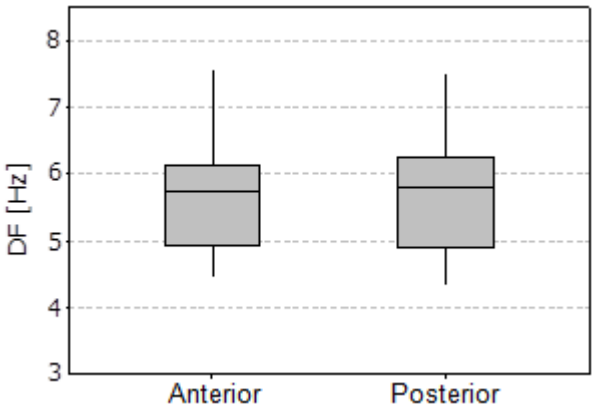

Figure 137. DF for the anterior and posterior body surface sites. Each bar is constructed from 20 values calculated as the median across the anterior and posterior sites in each subject.

Spatial Variability of DF at the Left and Right Sites: (I) Paired comparison using the Wilcoxon signed-rank test showed no significant differences between the left and right sites ($p>0.05$), Design= 20×2. (II) The factorial ANOVA test showed that DF was not significantly different between the left and right anterior and the left and right posterior sites ($p>0.05$), Design = (20×4) ×3, see Figure 138.

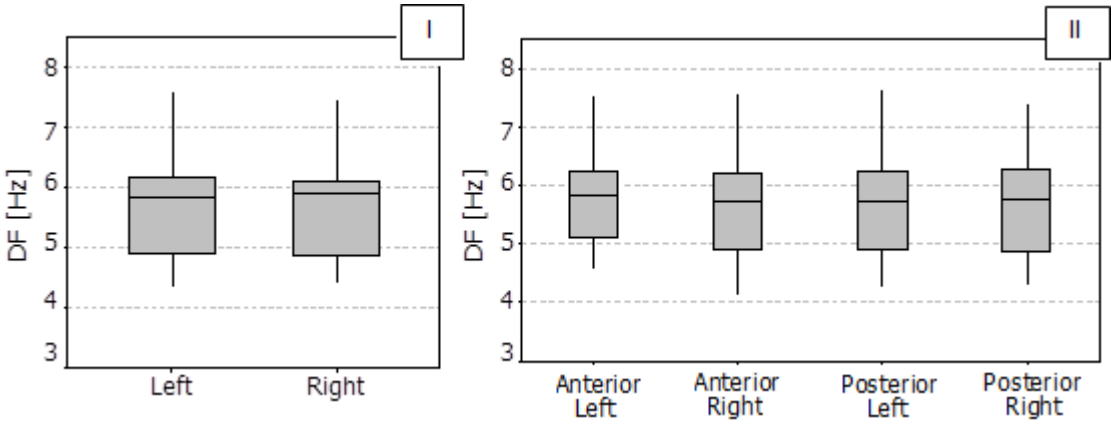

Figure 138. DF for the left and right body surface sites. Each bar is constructed from 20 DF values calculated as the median across the left and right sites in each subject.

Spatial Variability of DF at the Vertical Electrode Lines: The Friedman test showed that AF DF did not exhibit significant differences between the vertical lines ($p>0.05$), Design = 20×8, see Figure 139.

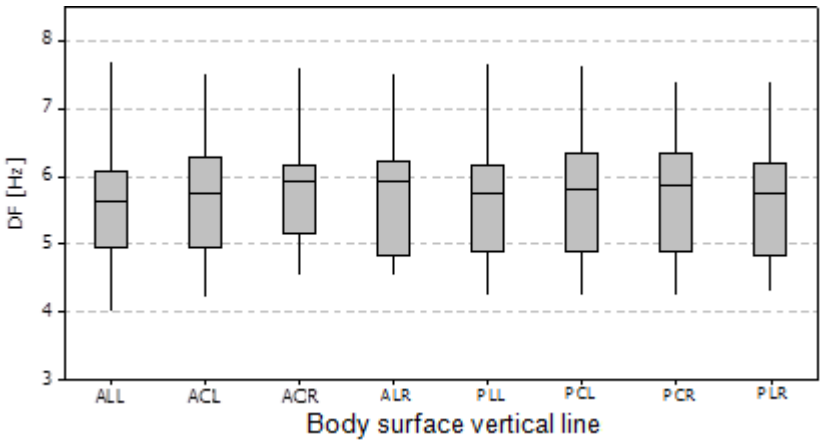

Figure 139. DF for the vertical lines on body surface. Each bar is constructed from 20 values calculated as the median across the vertical electrodes in each strip for each subject.

Spatial Variability of DF at the Horizontal Electrode Lines: The Friedman test showed that DF exhibited significant differences between the horizontal lines (p=0.020), Design= 20×16, see Figure 140. Paired comparison of all possible pairs using the Wilcoxon signed-rank test showed significant differences between the anterior central sites and anterior upper sites (p=0.035), and between the anterior upper sites and posterior central sites (p=0.032).

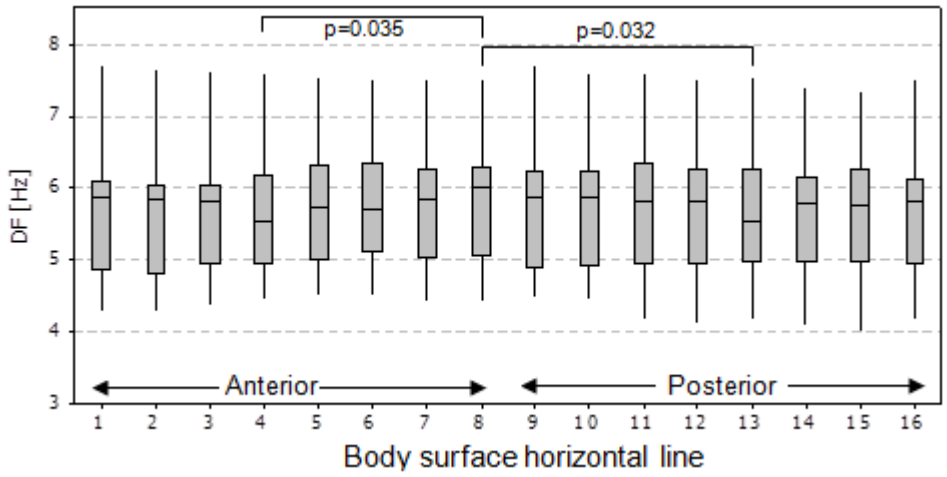

Figure 140. DF for the horizontal lines on body surface sites. Each bar is constructed from 20 values calculated as the median across the horizontal electrodes in each line for each subject.

According to the results, DF changed significantly across the body surface sites, more precisely between the anterior upper sites with the anterior and posterior central sites with DF difference of 0.5 Hz.

II. Spatial Variability of Dominant Frequency at the Intracardiac Sites

To investigate changes in DF along catheter sites, DF was estimated with the same methodology as applied to the BSPM recordings for each EGM site in each subject. Figure 141 illustrates DF for each site across subjects. The factorial ANOVA showed that DF exhibited significant differences between ten EGM sites (p=0.040) including five CS and five PVAC, Design = (20×10)×3.

However, DF did not exhibit significant differences between either CS or PVAC ($p>0.05$), Design = (20×5) ×3.

The median DF (measured across subjects) between the CS sites ranged from 5.4 Hz (CS5) to 5.7 Hz (CS2), and between the PVAC sites ranged from 5.5 Hz (PVAC3) to 5.8 Hz (PVAC5).

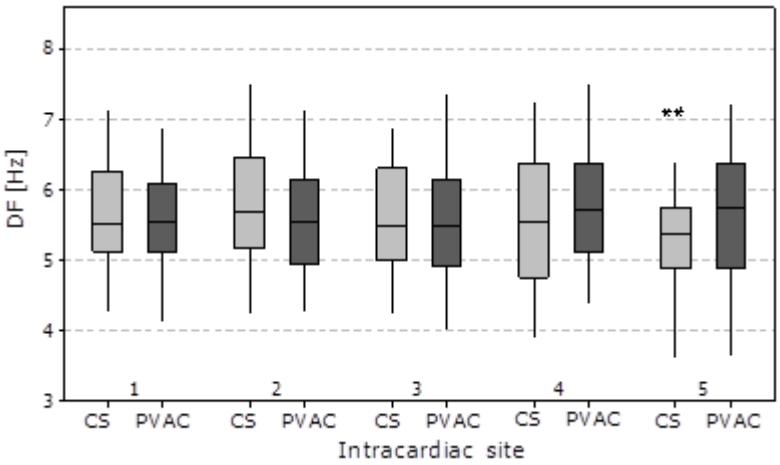

Figure 141. DF for the CS (light grey) and PVAC (dark grey) sites. Each bar is constructed from 20 values for each subject. The outliers belong to subjects 7 and 11.

There was no significant difference in DF estimated from any of the electrodes of the same catheter, either CS or PVAC. However, there was a significant difference in DF between the CS and PVAC catheters. The DF difference (smallest CS DF vs. largest PVAC DF) was 0.4 Hz. The difference in DF between CS and PVAC catheters may suggest that the CS captured different frequencies from different far-field sources.

III. Comparison of Body Surface and Intracardiac Dominant Frequency for Each Site

In this section, linear correlation analysis was performed between each body surface site and the selected intracardiac sites CS4 and PVAC4 (see section 2.2.4). The aim was to investigate whether BSPM DF spatial variability

could determine which body surface site represent the CS recordings, and which body surface represent the PVAC recordings. Figure 142 shows a colour map of the correlation coefficient between BSPM and EGM DF at each body surface site.

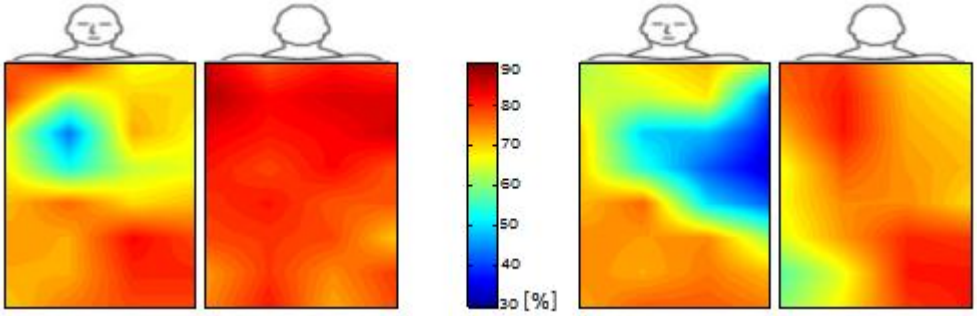

Figure 142. Spatial colour maps of the correlation coefficient between BSPM and CS DF (left), and between BSPM and PVAC DF (right).

The results showed that DF at anterior and posterior upper right sites had the strongest linear relationship with CS DF. Also, DF at posterior upper left and lower right sites had the strongest linear relationship with PVAC DF. This analysis potentially suggested that the body surface sites close to the anterior upper central right were a good representation of CS DF, or more likely the RA DF. Moreover, the body surface sites close to the posterior upper left and lower right were a good representation of the LA DF.

6.3. Spatial Variability of Spectral Concentration

I. Spatial Variability of Spectral Concentration at the Body Surface

To investigate SC spatial variability, SC was estimated in each subject for each body surface site. Figure 143 illustrates SC for each site across subjects. Figure 144 shows a colour map of the median SC across subjects. The Friedman test showed that SC exhibited significant differences between the sites ($p<0.001$), Design = 20×64.

The median SC measured across subjects ranged from 22.0 % (site 5) to 44.5 % (site 23) with median and IQR of 31.0 (28.5 – 36.0) % across all sites.

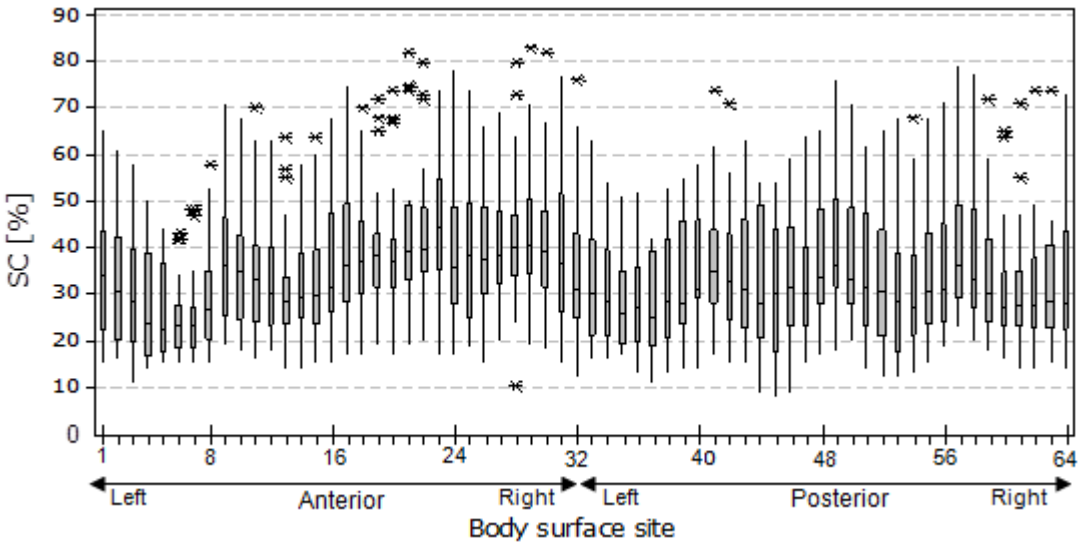

Figure 143. SC for each body surface site. Each bar is constructed from 20 values from each subject. Outliers belong to subjects 3, 7, 8 and 14.

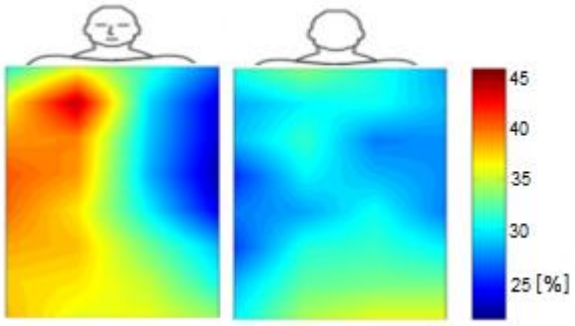

Figure 144. Spatial colour map of the median SC (values are from the horizontal lines in each bar in Figure 143).

The body surface sites were grouped into anterior and posterior, left and right, vertical lines and horizontal lines, and SC changes were analysed between each group.

Spatial Variability of SC at the Anterior and Posterior Sites: Paired comparison using the Wilcoxon signed-rank test showed that SC was not significantly different between the anterior and posterior sites ($p>0.05$), Design= 20×2, see Figure 145.

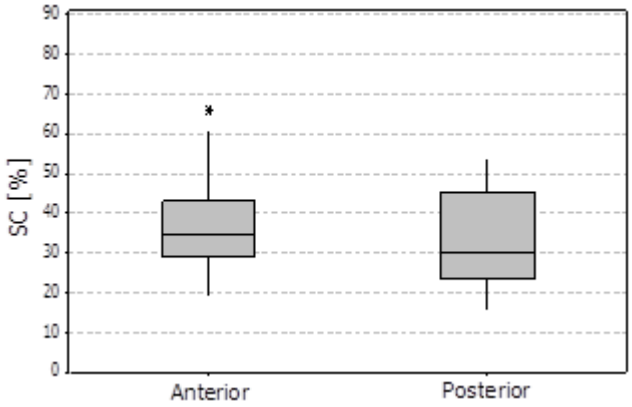

Figure 145. SC for the anterior and posterior body surface sites. Each bar is constructed from 20 values calculated as the median across the anterior and posterior sites in each subject.

Spatial Variability of SC at the Left and Right Sites: (I) Paired comparison using the Wilcoxon signed-rank test showed that SC was significantly different between the left and right sites (p=0.008), Design= 20×2. (II) Paired comparison using the Wilcoxon signed-rank test between all possible pairs showed that SC was significantly different between the anterior right with anterior left (p<0.001), posterior left (p<0.001) and posterior right (p=0.001) as shown in Figure 146 (see Appendix D, Table 20).

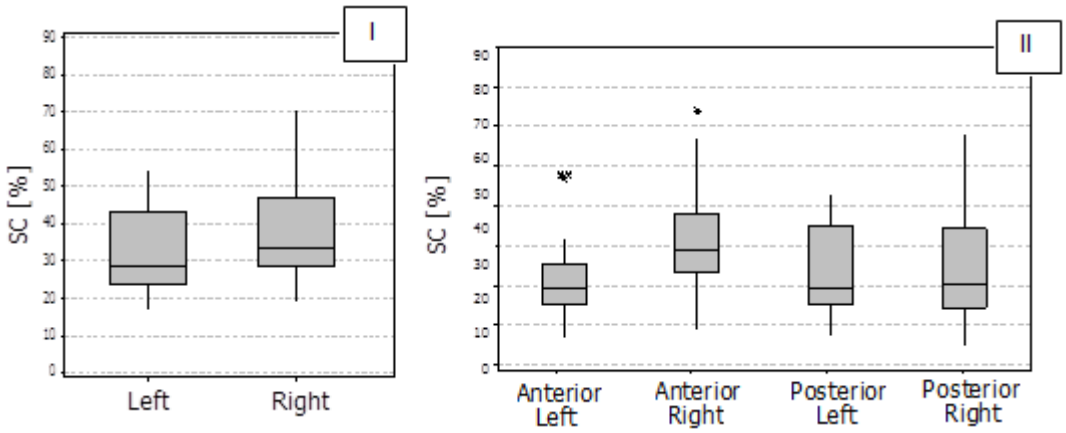

Figure 146. SC for the left and right body surface sites. Each bar is constructed from 20 values calculated as the median across the left and right sites in each subject.

Spatial Variability of SC at the Vertical Electrode Lines: The Friedman test showed that SC exhibited significant differences between the vertical lines ($p<0.001$), Design = 20×8, as shown in Figure 147 (see Appendix D, Table 21).

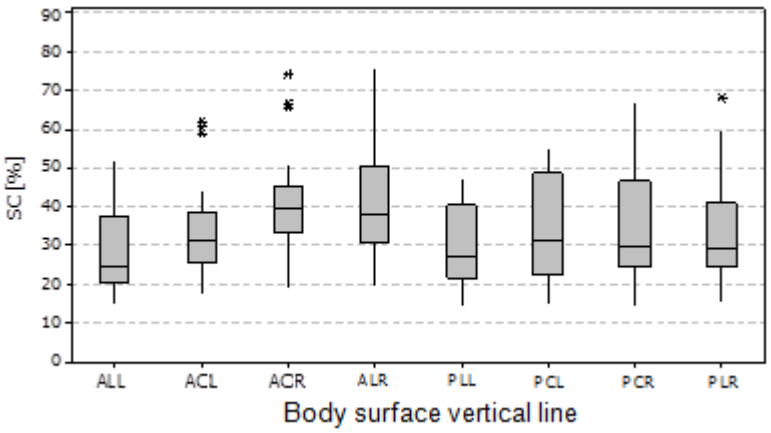

Figure 147. SC for the vertical lines on body surface sites. Each bar is constructed from 20 values calculated as the median across the vertical electrodes in each strip for each subject.

Spatial Variability of SC at the Horizontal Electrode Lines: The Freidman test showed that SC did not exhibit significant differences between the horizontal lines ($p>0.05$), Design= 20×16, see Figure 148.

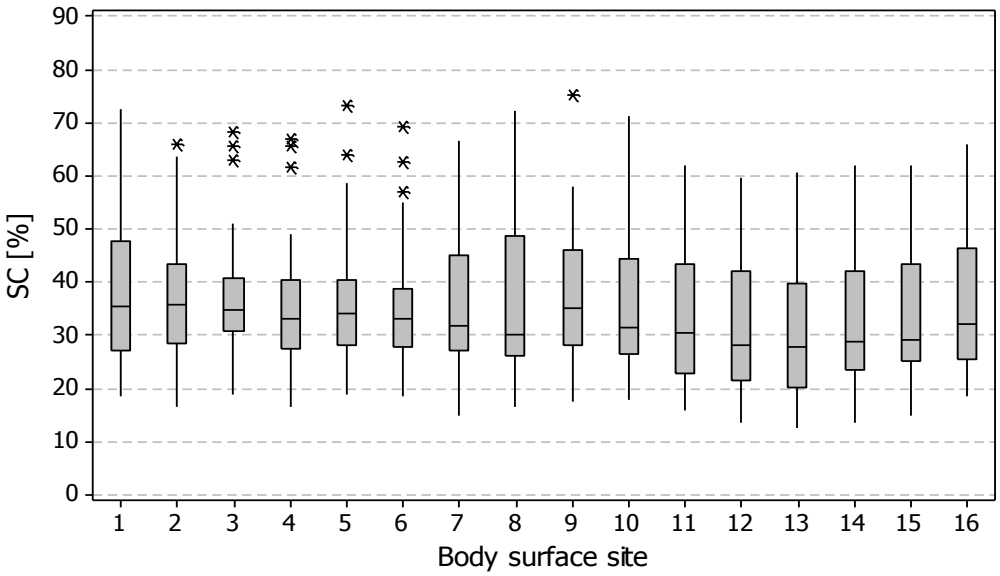

Figure 148. SC for the horizontal lines on body surface sites. Each bar is constructed from 20 values calculated as the median across the horizontal electrodes in each line for each subject.

The results showed that SC changed significantly across the 64 body surface sites, between the left and right, and also between the vertical lines. This could suggest: (1) body surface sites captured AA from different AF sources with different frequencies. (2) Some of the body surface sites have low SC due to noise.

II. Spatial Variability of Spectral Concentration at the Intracardiac Sites

To investigate changes in SC along the catheter sites, SC for each EGM site in each subject was estimated with the same method as used for the BSPM recordings. Figure 149 illustrates SC for each site across subjects. The factorial ANOVA showed that AF SC exhibited significant differences between ten EGM sites ($p<0.001$), Design = (20×10) ×3. However, it did not exhibit significant differences between either CS or PVAC sites ($p>0.05$), design = (20×5) ×3.

The median SC across subjects ranged from 47.0% (CS2) to 51.0% (CS4) for CS, and 60.5% (PVAC2) to 68.5 % (PVAC5) for PVAC.

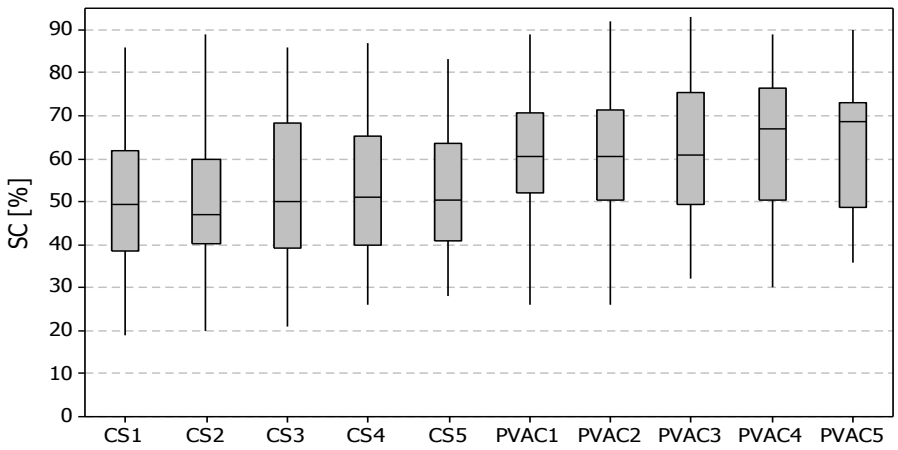

Figure 149. SC for each intracardiac site. Each bar is constructed from 20 values for each subject.

SC consistency along the sites in each catheter, either CS or PVAC, may suggest that each catheter might capture more localised frequency. However,

SC significant differences between CS and PVAC catheters, with CS SC being smaller than PVAC SC, may suggest that there were far-field atrial activities from RA or other AF pathways on the CS recordings.

III. Comparison of Body Surface and Intracardiac Spectral Concentration for Each Site

The linear correlation analysis was performed to investigate whether there were any body surface sites that corresponded to AF complexity estimated from CS or PVAC. Figure 150 shows a colour map of the linear relationship between BSPM and EGM SC at each body surface site.

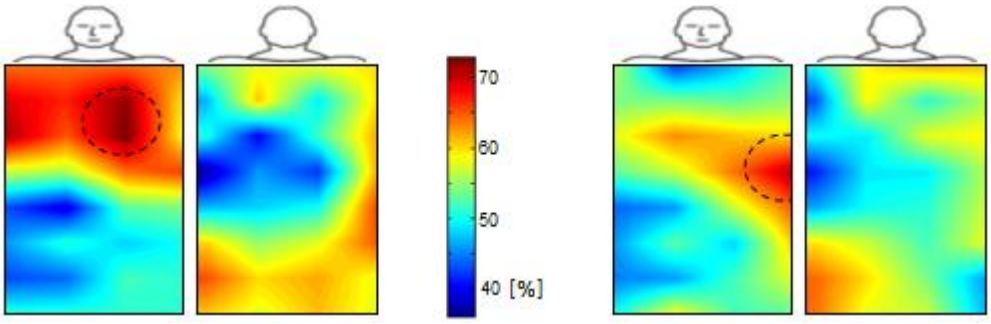

Figure 150. Spatial colour maps of the correlation coefficients between BSPM and CS SC (left), and between BSPM and PVAC SC (right). The BSPM sites with strongest linear relationship with EGM SC are marked with dashed circles.

The results showed that SC at anterior upper left sites had the strongest linear relationship with CS. Also, SC at anterior central lateral left had the strongest linear relationship with PVAC. This analysis potentially suggested that the body surface sites close to the anterior upper left might be a good representation of AF organisation estimated from the CS.

Chapter Summary

In this chapter the spatial variability of the AF characteristics between the body surface and intracardiac sites were investigated. AF characteristics (amplitude, DF, and SC) changed significantly across the body surface sites. However, DF and SC did not change significantly from any of the sites of the same catheter, either CS or PVAC.

There was a consistent pattern of high AF characteristics on the anterior upper central right body surface sites in all subjects. These sites also had the largest correlation coefficients of DF compared between the body surface and CS. This may suggest that the body surface sites close to the anterior upper central right were the best representatives of DF estimated from the CS recordings. Furthermore, the body surface sites close to the posterior upper central left and the posterior lower right had the largest correlation coefficients of DF compared between the body surface and PVAC that may suggest that these sites were the best representatives of DF estimated from the PVAC recordings.

The body surface sites close to the anterior central lateral left gave the best representation of SC estimated from the PVAC recordings. Moreover, the body surface sites close to the anterior upper central left gave the best representation of SC estimated from the CS recordings. This may suggest that the anterior central lateral left sites were the best representatives of AF organisation estimated from the PVAC recordings, and the anterior upper central left sites were the best representatives of AF organisation estimated from the CS recordings. Since the anterior upper central right body surface

sites had the highest AF characteristics and strongest relationship with CS DF, it suggested that these sites may be capturing AA from the RA.

Chapter 7. Relationship Between Frequencies Derived from Individual and Groups of Body Surface Sites and Those Derived from Intracardiac Sites

To investigate agreement of the body surface and intracardiac spectra, the body surface and intracardiac recordings were compared in the frequency domain using five different approaches. Intracardiac spectra from CS4 and PVAC4 were overlapped with body surface spectra at each site for each subject. The relationships between the spectral peaks were manually checked (see section 7.1). The same approach was performed automatically using the morphology correlation analysis of the body surface and intracardiac spectra (see section 7.2). Body surface DF agreement estimated from groups of sites (the anterior and posterior, and also the vertical electrode lines) were examined with the median DF across the CS and PVAC sites using Bland-Altman plot (see section 7.3). Paired comparison of DF was performed between each body surface site with each intracardiac site (see section 7.4). DF estimated from body surface with the largest SC was also compared with CS4 and PVAC4 (see section 7.5).

7.1. Visual Comparison of Body Surface and Intracardiac Spectra

To visually investigate the relationship between BSPM and EGM spectra, the spectra from the CS4 and PVAC4 were plotted on top of each body surface site. Figure 151 and Figure 152 show the BSPM spectra from subject 3 overlaid with the CS4 and PVAC4 spectrum, respectively. Figure 153 and Figure 154 show the BSPM spectra for subject 1 overlaid with the CS4 and PVAC4 spectrum, respectively.

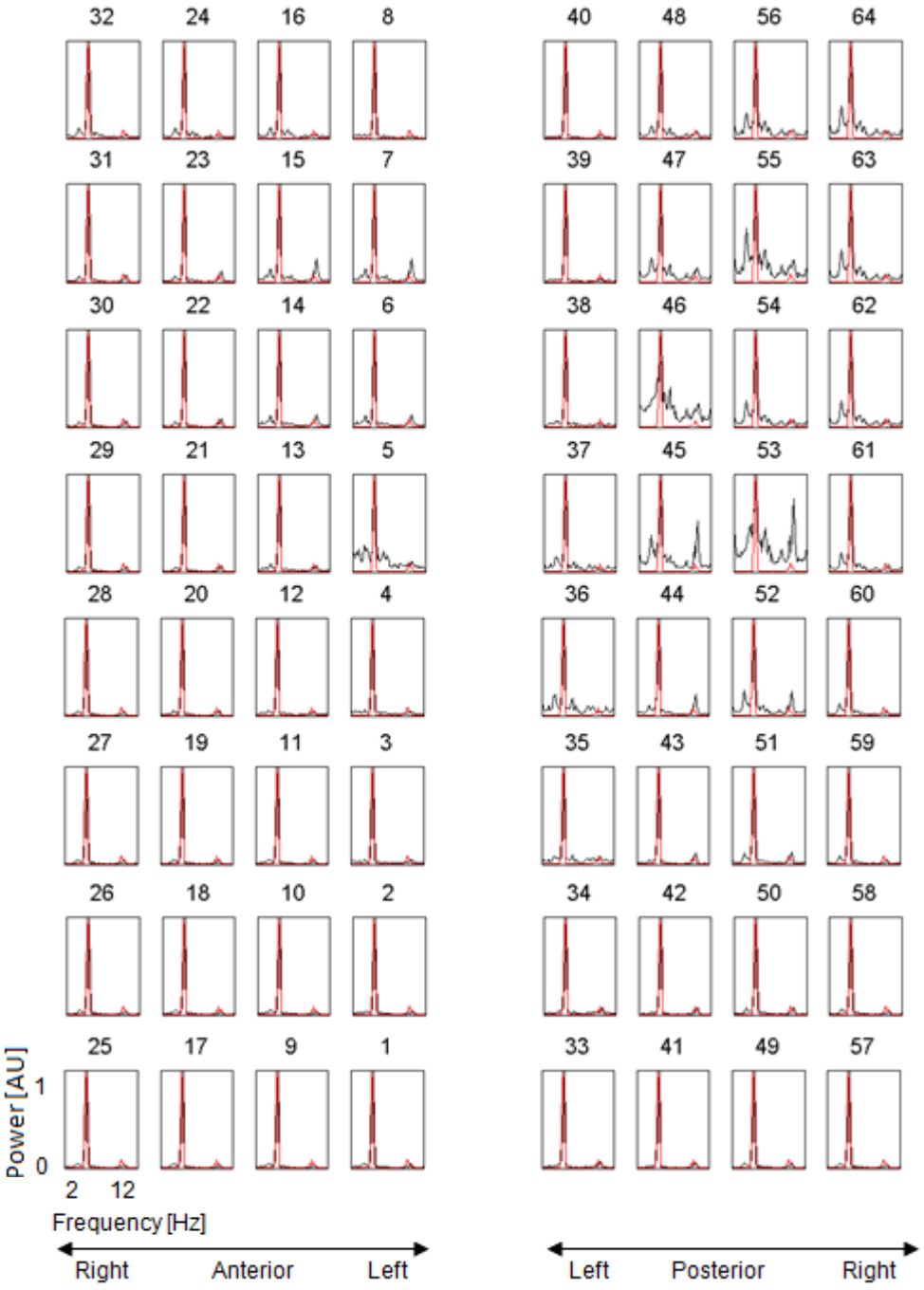

Figure 151. Spatial illustration of the spectra estimated from each body surface site (identified 1 to 64) in black, and CS4 in red for subject 3 with single peak spectra (highly organised AF). For each PSD, the x-axis is frequency 2 - 12 Hz and the y-axis denotes normalised power density to the maximum of each site.

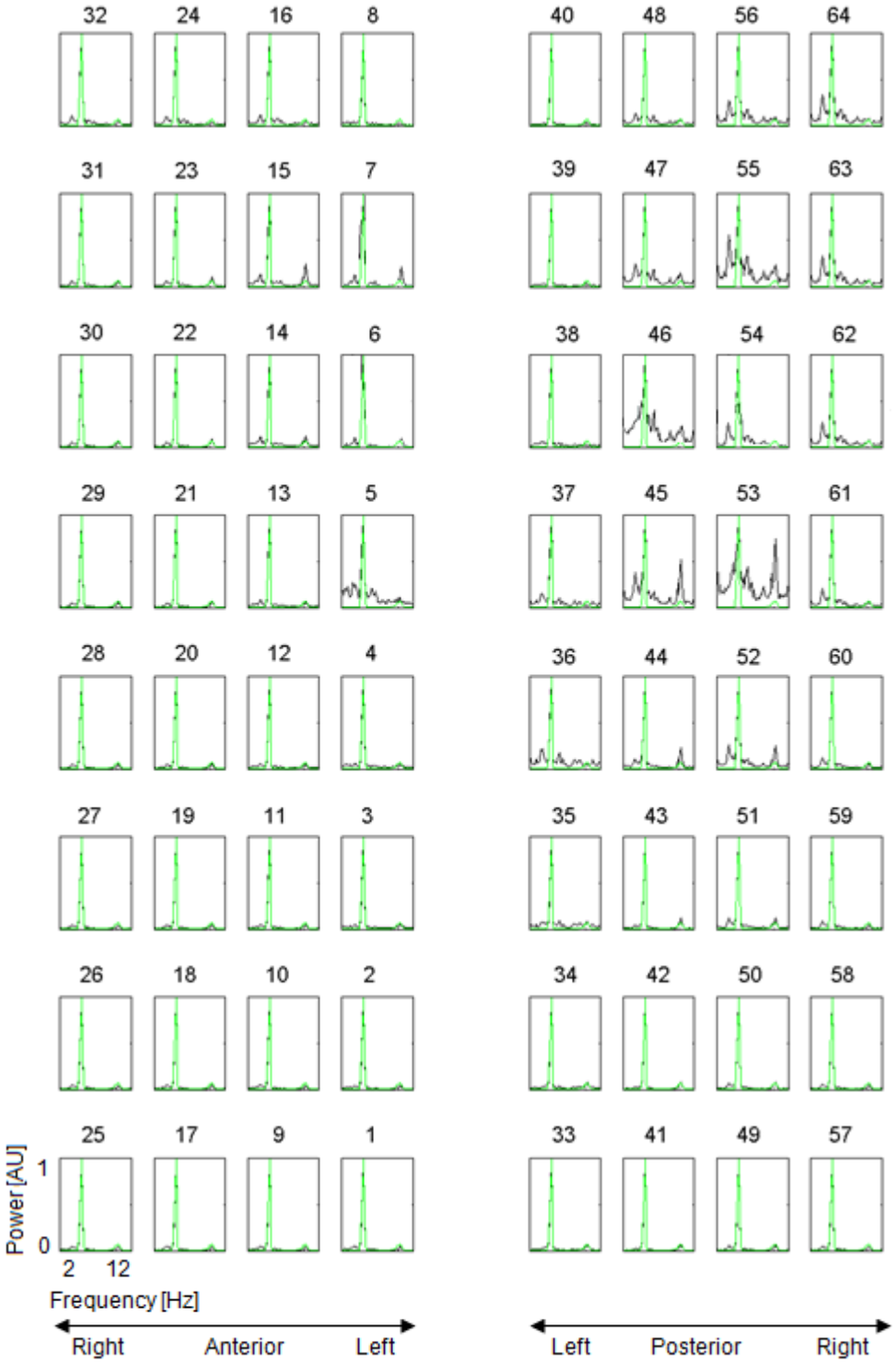

Figure 152. Spatial illustration of the spectra estimated from each body surface site (identified 1 to 64) in black, and PVAC4 in green for subject 3 with single peak spectra (highly organised AF). For each PSD, the x-axis is frequency 2 - 12 Hz and the y-axis denotes normalised power density to the maximum of each site.

Figure 153. Spatial illustration of the spectra estimated from each body surface site (identified 1 to 64) in black, and CS4 in red for subject 1 with multiple peaks (less organised AF). For each PSD, the x-axis is frequency 2 - 12 Hz and the y-axis denotes normalised power density to the maximum of each site.

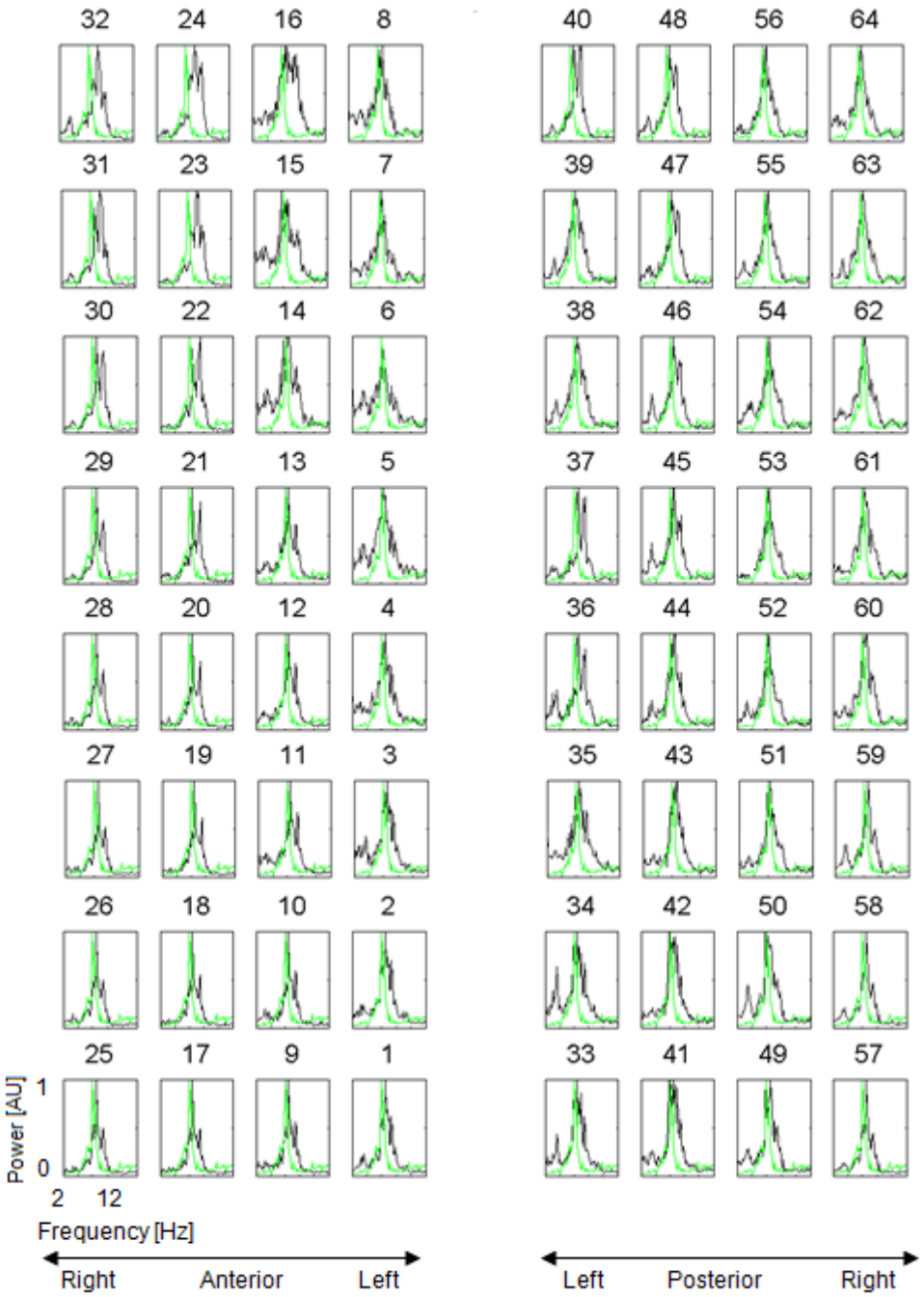

Figure 154. Spatial illustration of the spectra estimated from each body surface site (identified 1 to 64) in black, and PVAC4 in green for subject 1 with multiple peaks (less organised AF). For each PSD, the x-axis is frequency 2 - 12 Hz and the y-axis denotes normalised power density to the maximum of each site.

According to the results (Figure 151 and Figure 152), in some subjects where the spectra had a single peak, good agreement between EGM and BSPM was apparent in the entire spectra. The presence of a single frequency component with the same dominant peak in the BSPM and EGM was thought to

be the result of a simple organised AF rhythm with one frequency re-entry pathway, so all EGM and BSPM sites captured one frequency.

Conversely, according to the results of Figure 153 and Figure 154, in some subjects the BSPM spectra had multiple peaks, which these peaks may or may not be agree with the EGM dominant peak. The presence of additional frequency components suggests less organised AF with multiple re-entrant pathways circulating round the atria, taking different paths, with possible variations in frequency, or directional switches in time. Consequently, the BSPM sites may reflect all or some of the frequency components presented on the EGM spectra.

The BSPM and EGM spectra were visually checked for all sites in all subjects. There was no BSPM site that showed only the EGM dominant peak consistently among 20 subjects. There was no BSPM site that did not have corresponding spectral peak to the EGM dominant peak consistently among 20 subjects.

Overall the results showed agreement between the body surface and intracardiac spectral peaks, but may or may not be the dominant peaks. This results illustrated the limitation of using only DF as a measure for comparing the body surface and intracardiac recordings, since it failed to capture the full details of the underlying frequency spectrum in less organised AF cases. Moreover, in clinical practice, in well organised AF cases measurements of DF represents the electrical activity of the inside the heart. However, in complex AF cases it may not represent the inside the heart events.

7.2. Morphology Correlation of Body Surface and Intracardiac Spectra

To quantify similarities in the morphology between the BSPM and EGM spectra, linear correlation was computed between normalised PSDs of each BSPM site with EGM (CS4 and PVAC4) in AF band of 3 - 8.5 Hz. The median correlation coefficient, r, was calculated across subjects for each BSPM site (BSPM vs. CS4 and BSPM vs. PVAC4). A spatial colour map of the median r is shown in Figure 155.

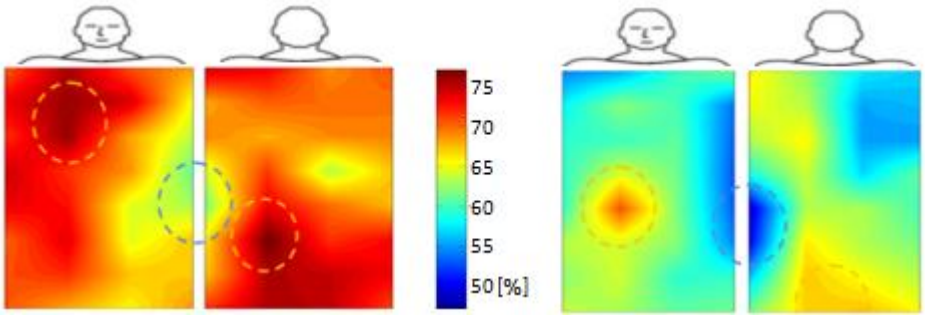

Figure 155. Spatial colour maps of the median correlation coefficients. The BSPM and CS (left), and BSPM and PVAC (right). Regions with largest correlation are shown with red dashed circles. Regions with lowest correlation are shown with blue dashed circles.

The results showed stronger correlation between the body surface and CS spectra rather than PVAC. The largest correlation was between the anterior body surface site 22 and the posterior body surface site 43 with the CS. Moreover, the largest correlation between the anterior body surface and PVAC was at site 20, and between the posterior body surface and PVAC was at site 49. The smallest correlation between the anterior and posterior body surface for both CS and PVAC were at sites 5 and 36, respectively. The median and IQR of the DF difference between four body surface sites (sites 20, 22, 43 and 49) which had the largest correlation with intracardiac recordings are given in Table 16 across all subjects.

To investigate whether there was a significant difference between the anterior and posterior body surface sites with the largest and smallest correlation coefficient values, linear regression analysis was performed. The results showed that the anterior and posterior sites indicating the largest and smallest r were significantly different, see Figure 156.

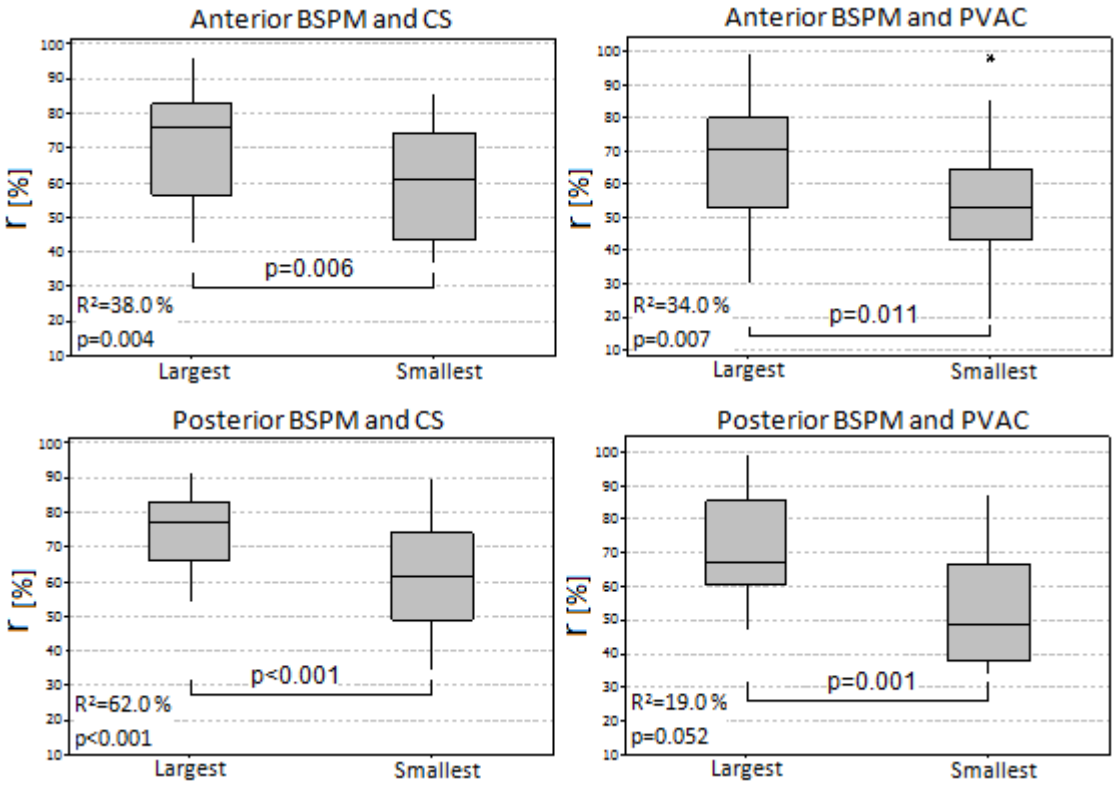

Figure 156. The correlation coefficients between the largest and smallest anterior body surface sites with CS and PVAC (top), and between the largest and smallest posterior body surface sites with CS and PVAC (bottom).

This analysis suggested that body surface sites close to the anterior upper central right and posterior lower central had the strongest morphology correlation with intracardiac recordings.

7.3. Dominant Frequency Agreement Using Bland-Altman Plot

To investigate how well body surface and intracardiac DF measurements agreed, the Bland-Altman plot was constructed. The median DF was computed across the anterior and posterior sites, and across the CS and PVAC sites.

Then the CS and PVAC median DF were compared with the anterior and posterior median DF (see Figure 157). The Bland-Altman results are shown in Table 13.

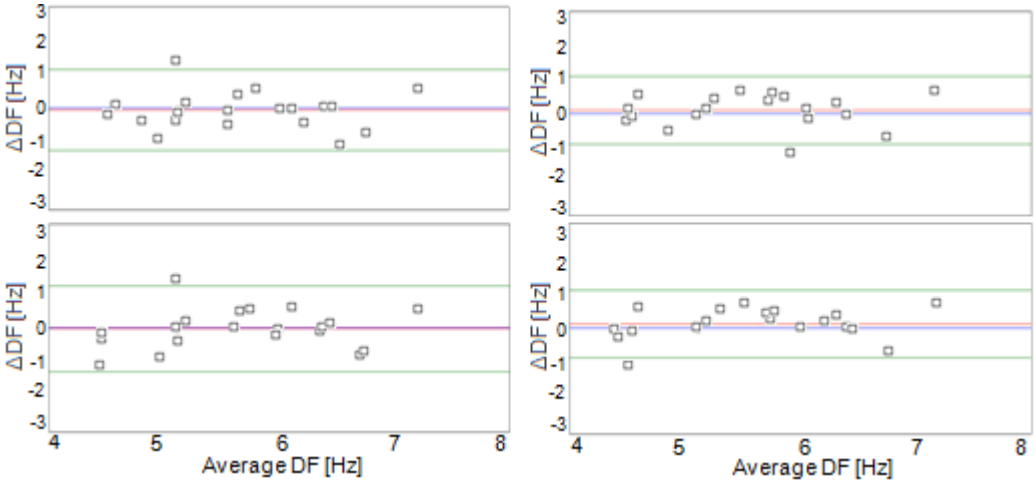

Figure 157. Bland-Altman plots of BSPM and EGM DF. Top left: anterior body surface and CS. Top right: anterior body surface and PVAC. Bottom left: posterior body surface and CS. Bottom right: posterior body surface and PVAC. Black squares indicate 20 subjects.

Source	DF [Hz]		
	Bias	LOA	P_{Trend}
Anterior vs. CS	-0.1	1.1	0.8
Posterior vs. CS	0.0	1.2	0.1
Anterior vs. PVAC	0.1	1.0	0.6
Posterior vs. PVAC	0.1	1.0	0.4

Table 13. Bland-Altman results of the anterior and posterior body surface sites and intracardiac DF for 20 subjects.

The results showed that the differences did not increase or decrease by increasing or decreasing the average (P_{Trend}>0.05, the fitted line between the two measurements has zero slope). There was no bias if DF estimated from the body surface was used to predict EGM DF, indicating that the two methods were systematically producing the same results. Moreover, there was no increasing of the scatter around the bias line by increasing the average, which suggested the variability of the measurements were consistent. However, the LOA was about 1.0 Hz, meaning that the difference between measurements

lied within 2.0 Hz (± LOA) approximately 95% of the time. Overall the results showed small bias, not narrow LOA, and no relation between the average and difference DF. These suggested that DF estimated from the anterior and posterior sites were not in perfect agreement with DF estimated from the CS and PVAC recordings. However, the average discrepancy between methods was very small (between -0.1 and 0.1). To investigate whether analysing precise regions of the body surface reduced the LOA, BSPM DF in eight vertical lines were studied with DF estimated from the CS and PVAC recordings. The median DF was computed across each vertical line and then compared with CS and PVAC at each of the lines (see Figure 158, Figure 159, and Table 14). The results were similar to the previous analysis. DF estimated from the body surface and inside the heart agreed with the small average discrepancy between the methods. The median and IQR of the DF difference between the body surface regions compared with EGM recordings (shown in Table 13 and Table 14) are given in Table 16 across all subjects.

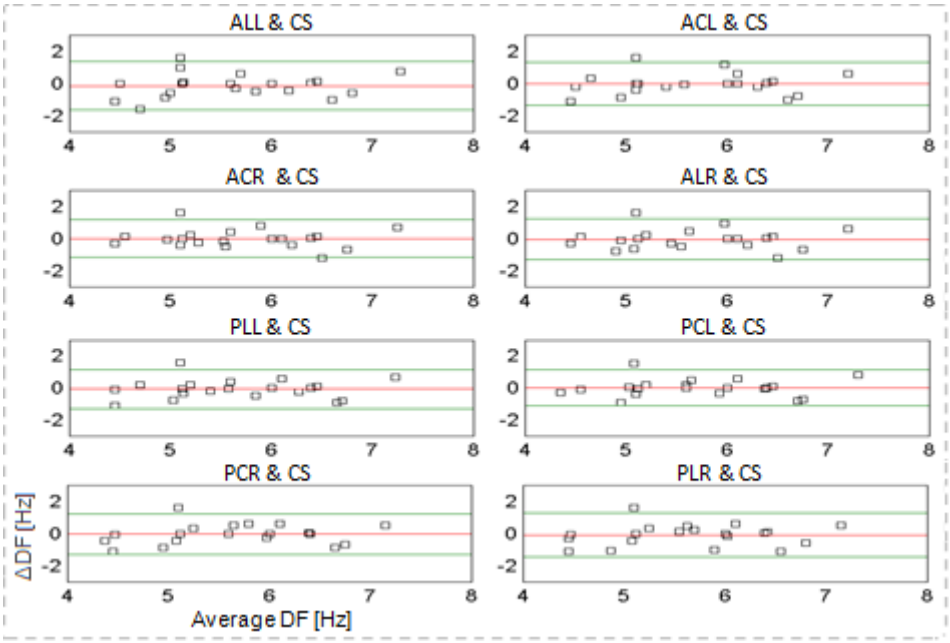

Figure 158. Bland-Altman plots of body surface vertical lines and CS DF. Black squares indicate 20 subjects.

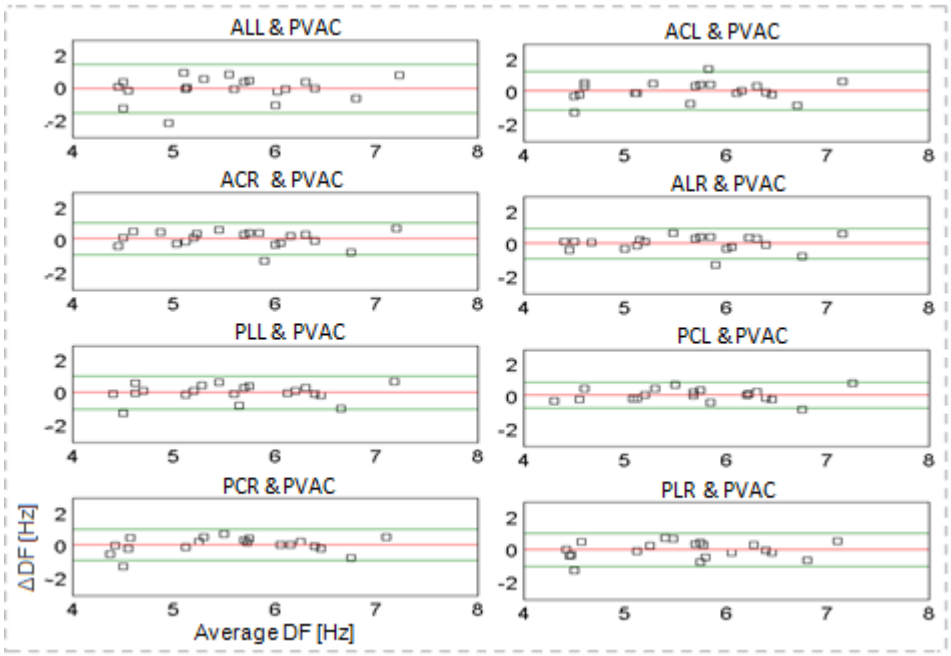

Figure 159. Bland-Altman plots of body surface vertical lines and PVAC DF. Black squares indicate 20 subjects.

Source	DF [Hz]		
	Bias	LOA	P_{Trend}
BSPM strip ALL vs. CS	-0.1	1.5	0.5
BSPM strip ACL vs. CS	0.0	1.3	0.4
BSPM strip ACR vs. CS	0.0	1.2	0.6
BSPM strip ALR vs. CS	0.0	1.3	0.7
BSPM strip PLL vs. CS	0.1	1.2	0.7
BSPM strip PCL vs. CS	0.0	1.1	0.6
BSPM strip PCR vs. CS	0.0	1.3	0.5
BSPM strip PLR vs. CS	-0.1	1.3	0.4
BSPM strip ALL vs. PVAC	0.0	1.5	0.4
BSPM strip ACL vs. PVAC	0.1	1.2	0.3
BSPM strip ACR vs. PVAC	0.1	1.0	0.4
BSPM strip ALR vs. PVAC	0.1	0.9	0.4
BSPM strip PLL vs. PVAC	0.1	1.1	0.3
BSPM strip PCL vs. PVAC	0.1	0.8	0.3
BSPM strip PCR vs. PVAC	0.1	1.0	0.2
BSPM strip PLR vs. PVAC	0.0	1.0	0.1

Table 14. Bland-Altman results of the vertical lines of body surface sites and intracardiac DF for 20 subjects.

7.4. Dominant Frequency Paired Comparison

DF estimated from the body surface and inside the heart were investigated using paired comparisons between each site of these sources. For example, DF from each BSPM site was paired with DF from each EGM site for all subjects. A Kolmogorov-Smirnov test was used to check the distribution for each pair. According to the result of the normality test, paired comparison using the Wilcoxon signed-rank test or the paired t-test was used to examine significant differences. The Bonferroni correction test was used to adjust the significant level. The results showed that there was no significant difference between any of the BSPM and EGM sites. To investigate if there were any body surface site that had the same DF as the intracardiac sites, the DF difference between the BSPM and EGM for each site were investigated by subtracting each EGM site from each BSPM site in each subject (e.g. $\Delta DF_{(BSPM\ 1\ vs.\ CS1)}$ = BSPM site 1 - CS1, $\Delta DF_{(BSPM\ 2\ vs.\ CS1)}$ = BSPM site 2 - CS1, ..., $\Delta DF_{(BSPM\ 64\ vs.\ CS1)}$ = BSPM site 64 - CS1, for subject 1). Two examples of the ΔDF are shown in Figure 160 (BSPM vs. CS4) and Figure 161 (BSPM vs. PVAC4) across 20 subjects. Figure 162 shows spatial colour maps of the median ΔDF for CS and PVAC.

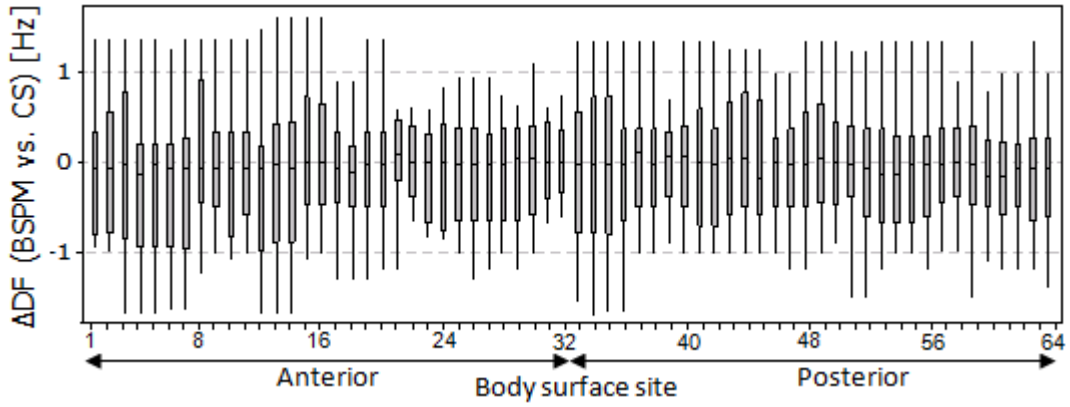

Figure 160. Illustration of the ΔDF for BSPM vs. CS4. Each bar is constructed from 20 values.

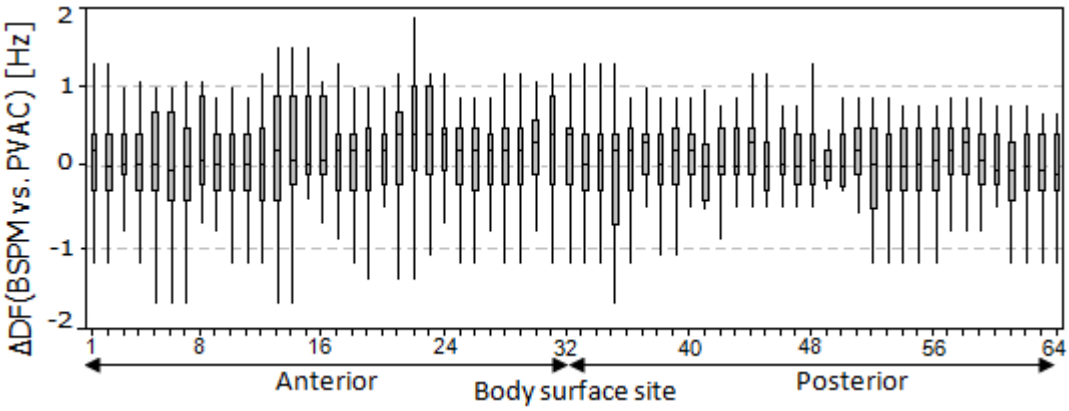

Figure 161. Illustration of the ΔDF for BSPM vs. PVAC4. Each bar is constructed from 20 values.

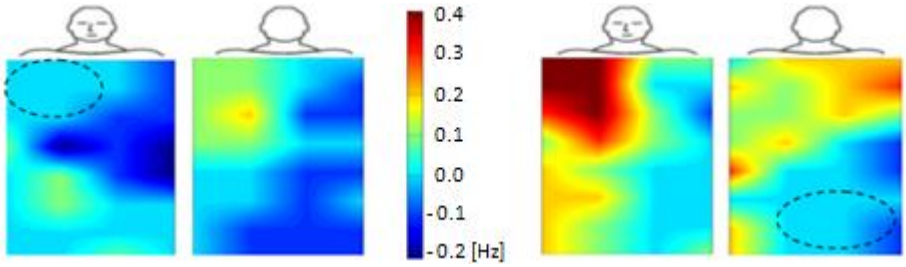

Figure 162. Spatial colour maps of the median ΔDF. BSPM vs. CS4 (left), and BSPM vs. PVAC4 (right) across subjects. The dashed circles indicate the smallest median ΔDF, representing the BSPM sites in good agreement with EGM DF.

According to the normality test result, the one-sample Wilcoxon signed-rank test or one-sample t-test was used to test for significant differences (Design = 64×1). The Bonferroni correction test was used to adjust the significant level.

The results showed that there was no significant difference in DF between the BSPM and EGM sites. The median ΔDF of BSPM vs. CS4 was zero in sites 16, 22, 23, 24, 31, 32, and 58 (see Figure 163). The median ΔDF of BSPM vs. PVAC4 was zero in sites 2, 7, 41, 42, 43, 45, 47, 49, 50, 53, 54, and 62. This showed that on these sites BSPM and EGM DF were the same.

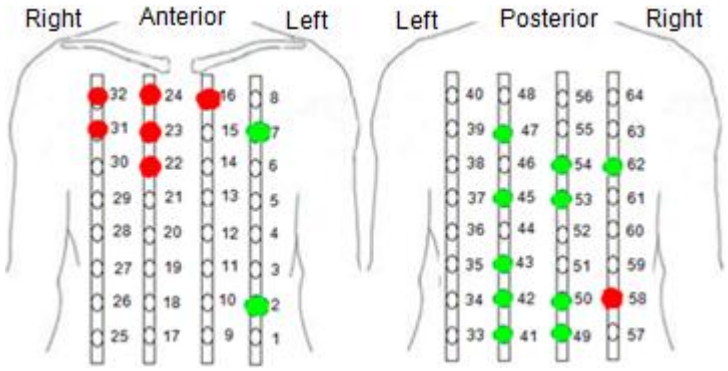

Figure 163. Illustration of the body surface sites where their median DF were the same as CS4 (red) and PVAC4 (green).

Although it is common in the literature to use lead V1 of a 12-lead ECG to analyse the AF, these results suggested that the anterior upper central right sites (which are closest to lead V1) may overestimate PVAC DF. It is important to bear in mind that these differences were not statistically significant. The median and IQR of the DF difference between two body surface sites (sites 22 and 49) which had zero DF difference with intracardiac recordings are given in Table 16 across all subjects.

7.5. Dominant Frequency Comparison Based on Body Surface Site with the Largest Spectral Concentration

Body surface sites with the largest SC can have less influence of noise, and therefore these sites may give better estimation of DF compared to other body surface sites. This section investigated whether body surface sites with the largest SC were in good agreement with AF DF estimated from inside the heart. For this purpose, DF difference was calculated by subtracting EGM DF estimated from selected sites (CS4 and PVAC4) from the body surface site with the largest SC, see Table 15.

Subject	BSPM site	SC [%]	ΔDF [Hz]	
			BSPM vs. CS	BSPM vs. PVAC
1	23	48.2	-0.9	-1.3
2	23	27.0	-1.1	-0.5
3	22	83.4	0.0	0.0
4	22	47.6	-0.1	-0.4
5	22	39.4	1.3	0.4
6	21	50.5	-1.2	-1.0
7	21	74.7	0.9	0.5
8	25	78.9	0.0	0.0
9	27	55.3	-1.6	-0.5
10	22	49.1	-1.1	-0.8
11	29	43.5	-0.5	-0.5
12	25	41.0	-1.0	0.6
13	23	35.7	0.3	-0.4
14	21	75.5	0.0	-1.0
15	23	45.3	-0.3	1.3
16	23	51.6	0.1	0.1
17	23	37.2	-0.6	0.3
18	24	50.9	-0.4	-0.8
19	28	40.0	-1.1	-0.9
20	22	57.5	-0.4	0.4
Median (IQR)	-	48.7(15.1)	-0.4(-1.0)	-0.4(-1.1)

Table 15. The DF differences between the body surface (from the sites with the largest SC), and intracardiac recordings.

According to the results, DF in subjects 3, 8, and 14 were in good agreement between the BSPM and EGM recordings. However, subjects 3 and 8 were well organised AF and DF in these subjects was the same in all sites (BSPM and EGM). These results suggested that DF estimated from the body surface sites with the largest SC were not in good agreement (zero difference) with DF estimated from inside the heart. Consequently, the body surface sites with the largest SC were not necessarily good representation of AF DF, and may have been related to a different intracardiac site. Table 16 shows the DF differences between the body surface sites in close agreement with the intracardiac recordings (according to the results of the this chapter) with CS4 and PVAC4 sites.

Source	ΔDF [Hz]
	Median (IQR)
BSPM site 22 vs. CS	0.0 (1.2)
BSPM site 43 vs. CS	0.0 (0.7)
BSPM site 20 vs. PVAC	0.0 (0.6)
BSPM site 49 vs. PVAC	0.0 (0.8)
BSPM anterior vs. CS	0.0 (0.1)
BSPM posterior vs. CS	0.0 (0.7)
BSPM anterior vs. PVAC	0.0 (0.9)
BSPM posterior vs. PVAC	0.0 (0.5)
BSPM strip ALL vs. CS	0.0 (0.6)
BSPM strip ACL vs. CS	0.0 (0.4)
BSPM strip ACR vs. CS	0.1 (0.8)
BSPM strip ALR vs. CS	0.1 (0.8)
BSPM strip PLL vs. CS	0.0 (0.4)
BSPM strip PCL vs. CS	0.0 (0.3)
BSPM strip PCR vs. CS	0.0 (0.4)
BSPM strip PLR vs. CS	0.0 (0.5)
BSPM strip ALL vs. PVAC	-0.1 (1.1)
BSPM strip ACL vs. PVAC	-0.1 (1.1)
BSPM strip ACR vs. PVAC	0.0 (0.8)
BSPM strip ALR vs. PVAC	-0.1 (1.0)
BSPM strip PLL vs. PVAC	0.0 (0.9)
BSPM strip PCL vs. PVAC	0.0 (0.7)
BSPM strip PCR vs. PVAC	0.0 (0.7)
BSPM strip PLR vs. PVAC	-0.1 (0.8)
BSPM site with the largest SC vs. CS	-0.4(-1.0)
BSPM site with the largest SC vs. PVAC	-0.4(-1.1)

Table 16. The median and IQR of the DF differences between the selected body surface and intracardiac sites for 20 subjects. The body surface sites were selected according to the results of this chapter.

This table suggested that the median DF across the anterior body surface sites had the smallest difference with the CS DF, and the median DF across the posterior body surface sites had the smallest difference with PVAC DF among 20 subjects.

Chapter Summary

In this chapter the body surface and intracardiac spectra were compared using different methods. The visual comparison showed an agreement between the BSPM and EGM spectral peaks at all BSPM sites, but these peaks may or may not be the dominant one. The morphology correlation analysis showed that body surface site 22 (close to anterior upper central right) and site 43 (close to posterior lower central left) had the largest morphology correlation between the BSPM and CS spectra. Also, body surface site 20 (close to anterior central right) and site 49 (close to posterior lower central right) had the largest morphology correlation between the BSPM and PVAC spectra. The Bland-Altman plot showed that the DF estimated from the body surface and inside the heart agreed with the small (close to zero) average discrepancy and the large LOA (about 2 Hz) between the methods. The dominant frequency paired comparison showed that the median ΔDF (BSPM vs. CS4) was zero in sites close to anterior upper right and posterior lower lateral right. Also, the median ΔDF (BSPM vs. PVAC4) was zero at sites located on the vertical electrode lines close to anterior lateral left, posterior central left, posterior central right, and posterior lateral right.

Joining the results from the morphology correlation and DF paired comparison showed that body surface site 22 (close to anterior upper central right), and site 49 (close to posterior lower central right) had the largest morphology correlation and the smallest DF difference with CS4 and PVAC4, respectively. Overall these results suggested that the body surface site 22 was a good representative of the CS recordings, and site 49 was a good representative of the LA recordings.

Chapter 8. Innovative Methods for Examining the Relationship Between Body Surface and Intracardiac Signals

This chapter introduces two novel AF characteristics for comparing the body surface and intracardiac recordings in the frequency domain. These novel AF characteristics were called EGM power distribution (see section 8.1) and Type of the BSPM spectral peak (see section 8.2). The aim of introducing these methods was to examine the entire spectra in the frequency range of interest at each body surface site based on intracardiac DF.

Also in this chapter, results of another new approach were described for the BSPM and EGM comparison in the time domain. The aim was to identify if there was a distinct F-wave on the AF segment corresponding to EGM atrial activity.

8.1. Estimation of Intracardiac Dominant Frequency Power Distribution on the Body Surface Spectra

This section investigated which body surface site expresed EGM DF with the highest power, P, (see section 2.3.5), and if there was any pattern for the EGM power distribution across the body surface. To do this, EGM DF power distribution was measured for the CS4 and PVAC4 DF on each body surface site. An example is shown in Figure 164.

The Box and Whisker plots of P_{CS} and P_{PVAC} were constructed for each BSPM site as shown in Figure 165. Figure 166 shows the spatial colour map of the median P_{CS} and P_{PVAC}.

Spatial colour maps of P_{CS} and P_{PVAC} were also constructed for each subject, as shown in Figure 167 and Figure 168.

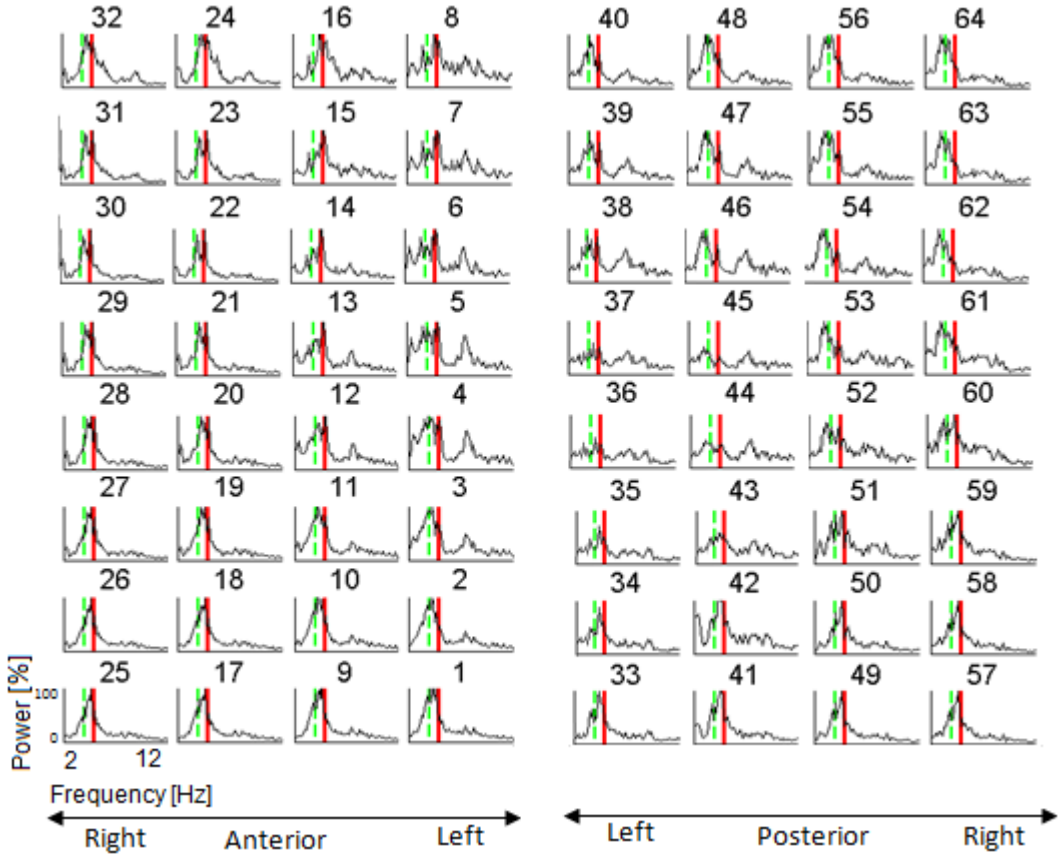

Figure 164. The BSPM PSD for each body surface (identified 1 to 64), subject 19. The red line indicates CS DF, and the dashed green line indicates PVAC DF. The y-axis represents the normalised power to maximum of all BSPM sites.

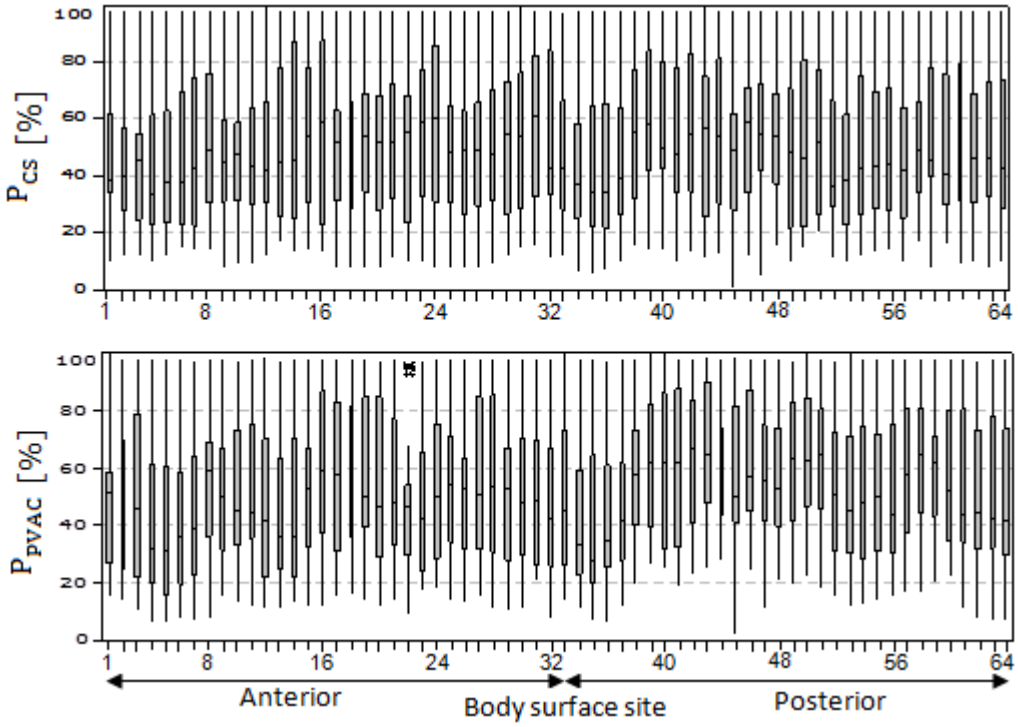

Figure 165. Top: P_{CS} , and bottom: P_{PVAC} across subjects for each body surface site. Each bar is constructed from 20 values. Outliers are associated with subjects 3, 8 and 12.

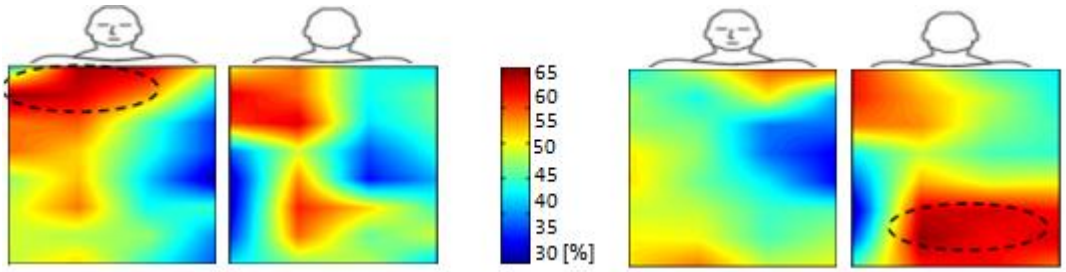

Figure 166. Spatial colour maps of the median P_{CS} (left) and P_{PVAC} (right) across subjects (horizontal lines in each bar from Figure 165). The dashed circles indicate the largest EGM DF power distribution on the body surface sites.

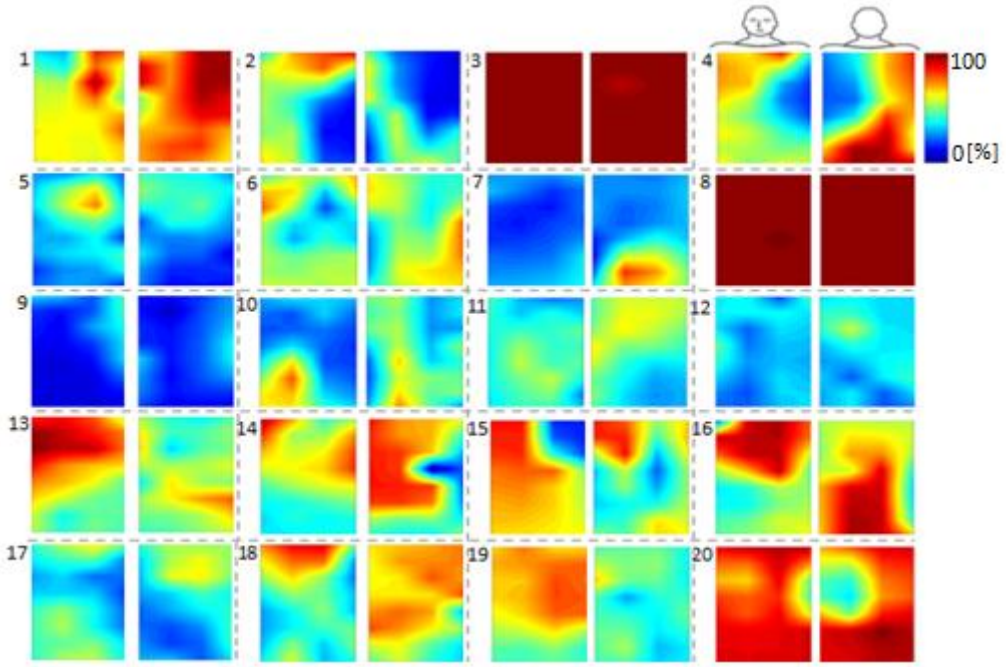

Figure 167. Spatial colour map of P_{CS} for each subject (identified 1 to 20).

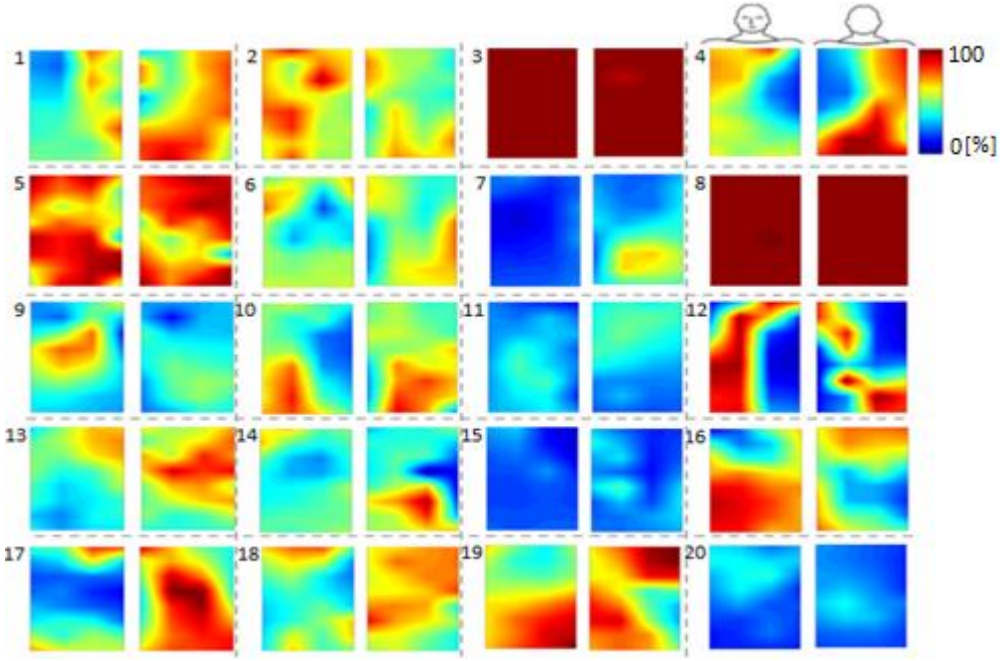

Figure 168. Spatial colour map of P_{PVAC} for each subject (identified 1 to 20).

Visual inspection of EGM DF power distribution on BSPM spectra (see Figure 167 and Figure 168) suggested a natural grouping of subjects in terms of EGM power distribution;

1. High P_{CS} and P_{PVAC} on all BSPM sites (subjects 3 and 8, the continuous red maps), indicated good agreement between BSPM, CS and PVAC DF. These subjects have homogeneous power distribution across body surface sites while the majority of subjects exhibit spatial variation in power distribution.
2. Power distribution was the same for CS and PVAC, e.g. subjects 4, 6, 7, 10, 11, and 18.
3. Low P_{CS} indicated poor agreement between BSPM and CS DF, e.g. subjects 5, 6, 7, 9, 11 12 and 17.
4. Low P_{PVAC} indicated the observed poor agreement between BSPM and PVAC DF, e.g. subjects 7, 11, 15, and 20.

In group 1, the distribution in P was the same across all BSPM and EGM sites, suggesting that this group may indicate well organised AF. In group 2, the P distribution was the same for both CS and PVAC across all body surface sites although EGM DF did not necessarily agree with BSPM DF. This group may indicate cases where the AF was less organised possibly as a result of multiple re-entrant AF pathways. It was also observed that EGM DF agreed with some of the BSPM sites in DF but not with others. This suggested that the EGM sites were not able to capture some re-entrant pathways since they were not located in parts of the LA and CS which placed on the re-entrant pathways that some BSPM sites could capture. An alternative explanation was that the re-entrant pathways cancel each other out from the view of some of the BSPM sites. In groups 3 and 4, EGM DF did not agree with BSPM DF. This group indicated very disorganised AF cases suggesting BSPM sites were not able to capture some CS or PVAC re-entrant pathways.

The results showed that in most of the subjects P_{CS} was larger on the anterior upper right body surface sites. This may suggest that these sites were more likely to express CS DF in comparison to other surface sites. The results also showed that P_{PVAC} was larger on the lower posterior body surface sites. This may suggest that these sites were more likely to express PVAC DF in comparison to other surface sites.

The paired t-test was used to test if there was a significant difference between the upper and lower sites in P_{CS} and P_{PVAC} , also between the P_{CS} and P_{PVAC} for all possible pairs. The results showed a significant difference ($p<0.001$) between the upper and lower sites for P_{CS} and P_{PVAC} , and also between the lower body surface sites for P_{CS} and P_{PVAC} (see Figure 169).

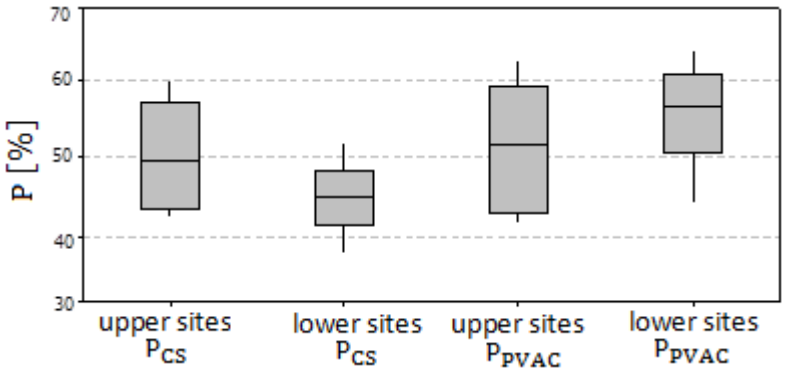

Figure 169. EGM power distribution of the upper and lower body surface sites. Each bar is constructed from 8 values.

Overall these results suggested that AF had an individual behaviour. In some subjects there were some BSPM sites that completely expressed EGM DF with high value of the power, and other BSPM sites did not. In an attempt to explain these differences, subjects were grouped according to the AF type, BMI and the number of previous ablations. However, none of the attempted groupings showed any consistent distribution, and so the underlying cause of these differences in BSPM remains unknown.

8.2. Classifying Body Surface Frequency Components According to Intracardiac Dominant Frequency

This analysis is motivated by some important questions: Are there any body surface sites where spectral peak is classified as Type I (dominant peak which correspond to EGM DF) ? (see section 2.3.6). If so, are these sites consistent across subjects? If not, are these body surface sites have any spectral peaks are classified as Type II (non- dominant peak which correspond to EGM DF) ? To answer these questions this section investigated whether there were any distinct frequency peaks on the BSPM spectra which corresponded to EGM DF. The type of BSPM peaks for each site were identified for selected EGM sites (CS4 and PVAC4). An example of the peak types of the BSPM spectra (according to EGM DF) is shown in Figure 170.

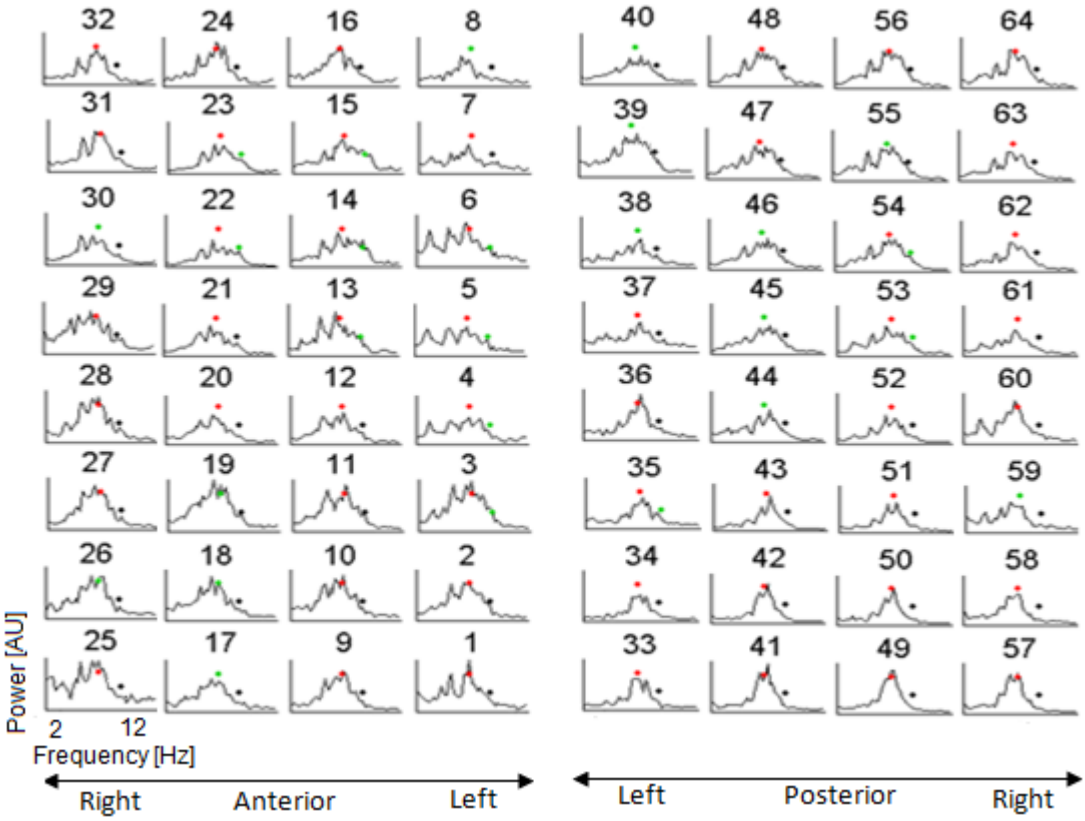

Figure 170. Spatial illustration of a typical BSPM spectra and its corresponding peaks to EGM DF. The body surface sites were identified 1 to 64, for subject 5. EGM DF were plotted as dots (bottom CS4 and top PVAC4) and coloured in red if they were Type I BSPM spectra, coloured in green if they were Type II, and coloured in black if there was no associated peak in BSPM spectra to them.

Bar plot of peaks Type I and II according to CS DF was constructed across subjects for each body surface site as shown in Figure 171. This illustrated which body surface site had peak Type I in the majority of subjects (as shown by the highest red bar), and which body surface site had peak Type II in the majority of subjects (highest green bar).

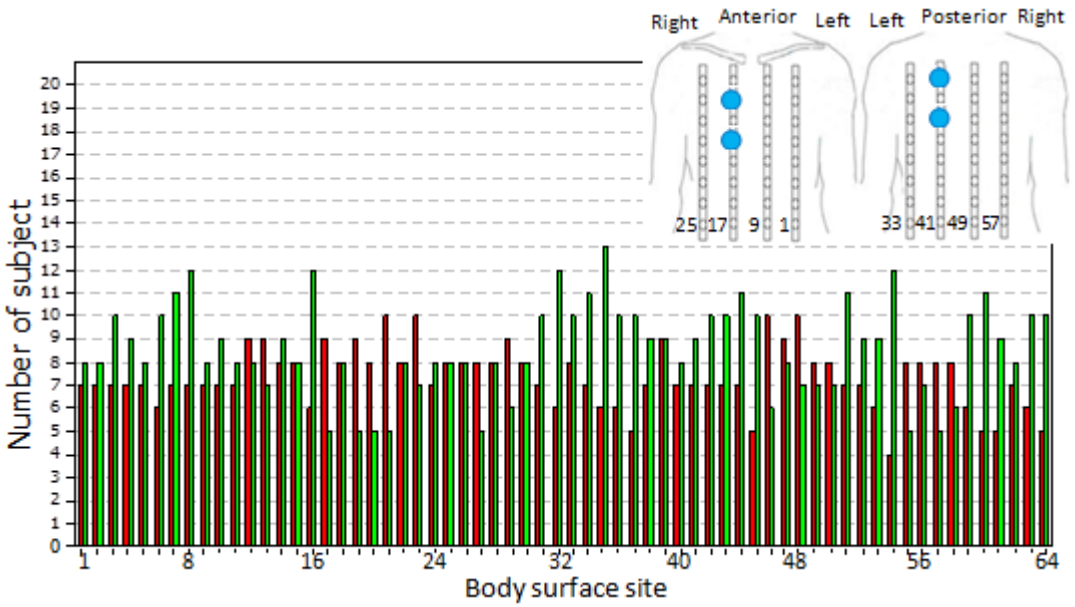

Figure 171. BSPM peak type according to CS DF. At each body surface site, number of subjects with Type I peak shown in the red bar and Type II peak shown in the green bar. On BSPM sites 21, 23, 46 and 48 (blue circles) more subjects capture CS DF (Type I, red bar). On BSPM site 54, fewer subjects capture CS DF.

The results showed that sites 21, 23, 46 and 48 captured CS DF in the dominant peak of the BSPM spectra in fifty percent of subjects. Moreover, sites 8, 16, 32, 35, and 54 captured CS DF in the non-dominant peak of the BSPM spectra in sixty percent of subjects. This may suggest that these sites were a good representation of DF estimated from the atria. The reason is, the CS has a four chambers view of the heart, and far-field VA had been cancelled on the CS recordings, so the results of the CS measurements are more likely to represent the atria.

Bar plot of the peaks type I and II was constructed across subjects for each body surface site according to PVAC DF, as shown in Figure 172. This illustrated which body surface site had peak Type I or II in the majority of subjects.

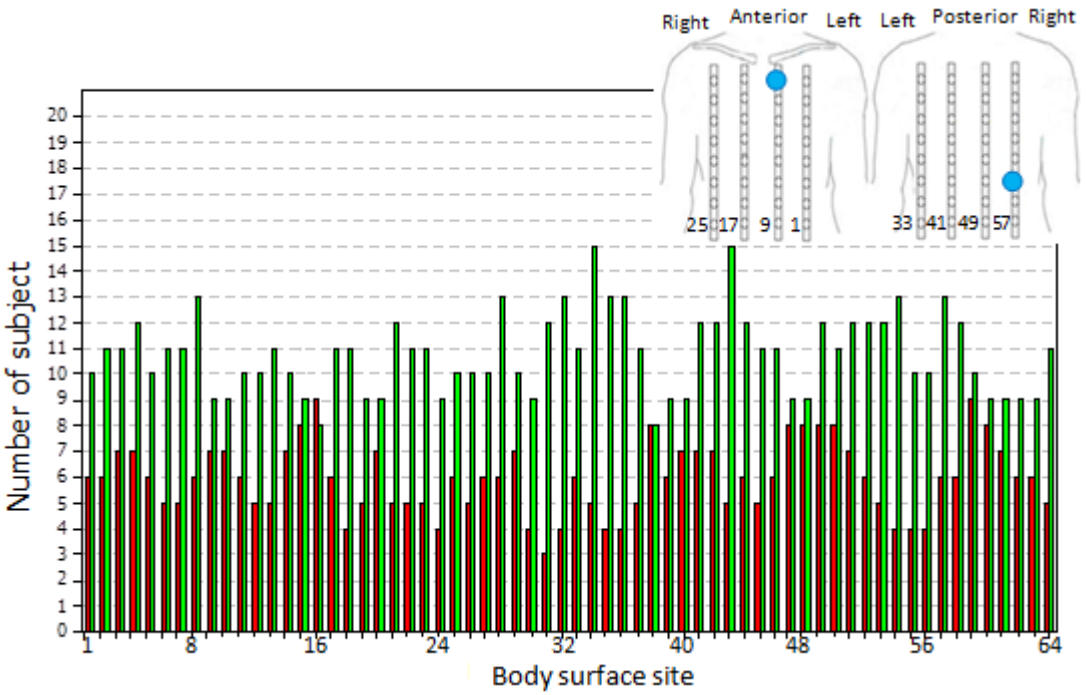

Figure 172. BSPM peak type according to PVAC DF. At each body surface site, number of subjects with Type I peak shown in the red bar and Type II peak shown in the green bar. On BSPM sites 16 and 59 (blue circles) more subjects capture PVAC DF (Type I, red bar). On BSPM site 31, fewer subjects capture PVAC DF.

The results showed that sites 16 and 59 captured PVAC DF in the dominant peak of the BSPM spectra in forty-five percent of subjects (nine subjects). Moreover, sites 34 and 43 captured PVAC DF in the non-dominant peak of the BSPM spectra in seventy-five percent of subjects (fifteen subjects).

Summing up the number of subjects with dominant and non-dominant peak at each body surface site (red and green bars in Figure 171 and Figure 172), showed that CS and PVAC DF was apparent on all of the BSPM sites in at least sixty-five percent of subjects as shown in Figure 173.

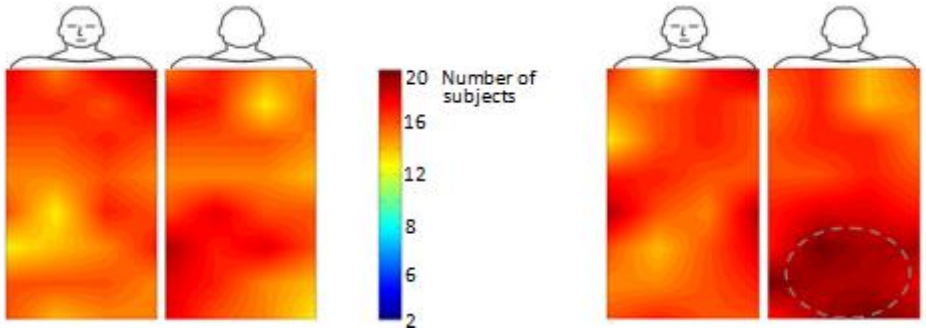

Figure 173. Body surface sites with Type I and Type II peaks according to CS DF (left) and PVAC DF (right). The grey dashed circle shows that in the posterior lower body surface sites all 20 subjects captured PVAC DF as a dominant peak on the body surface spectra.

The significant differences across the BSPM sites between Type I peak from CS and PVAC, between Type II peak from CS and PVAC, between CS Type I and II peaks, and finally between PVAC Type I and II peaks was investigated by paired comparison using the Wilcoxon signed-rank test. The results (see Table 17) showed that the BSPM sites that indicated peak type I were significantly different to the sites that indicated peak type II for both CS and PVAC. Moreover, the BSPM sites that represented CS DF were significantly different when compared to the BSPM sites that represented PVAC DF.

Number of Subjects	
Source	p-value
Type I , CS and PVAC	<0.001
Type II , CS and PVAC	<0.001
CS , Type I and II	0.004
PVAC, Type I and II	<0.001

Number of Subjects	
Source	Median (Q1-Q3)
CS Type I	7 (6-8)
CS Type II	8 (7-10)
PVAC Type I	6 (5-7)
PVAC Type II	12 (9-13)

Table 17. The Wilcoxon signed-rank test results for type of body surface spectral peak according to either CS or PVAC DF.

The results suggested that all body surface sites detected EGM DF, such that in some sites it agreed with BSPM dominant peak and in some sites it agreed with BSPM non-dominant peak. No BSPM site was found that did not

have a corresponding (dominant or non-dominant) peak to EGM DF across all subjects. Sixty-five percent of subjects captured a corresponding peak to EGM DF on the entire BSPM site. For CS a dominant peak was more observed than a non-dominant peak. Conversely, for PVAC a non-dominant peak was more observed than a dominant peak. There were no consistent BSPM sites that EGM DF captured differentially. AF EGM DF was likely to be seen as a dominant or non-dominant frequency peak on any of the body surface sites.

8.3. Time Domain Analysis to Identify Intracardiac Activations on the Body Surface

This section investigated if there were any relationships, evident in the time series, between the AA from the body surface and activations from the intracardiac recordings. In other words, can electrical activity from intracardiac recordings be seen as distinct F-waves on AF segments of the body surface recordings? For this purpose, the CS and PVAC activations were detected and marked onto each body surface recordings (see section 2.3.4). Figure 174 shows examples of the CS and PVAC activation time points on the anterior and posterior BSPM sites in one subject.

To investigate the consistency of EGM activations on the body surface sites, EGM activation time points were marked on the AF segment and a window around these EGM activations on the BSPM AA was defined. The AA within these windows were averaged and marked on the EGM activations of the average waveform. Figure 175 shows an example of the generated activations across the body surface based on the CS and PVAC activation time points.

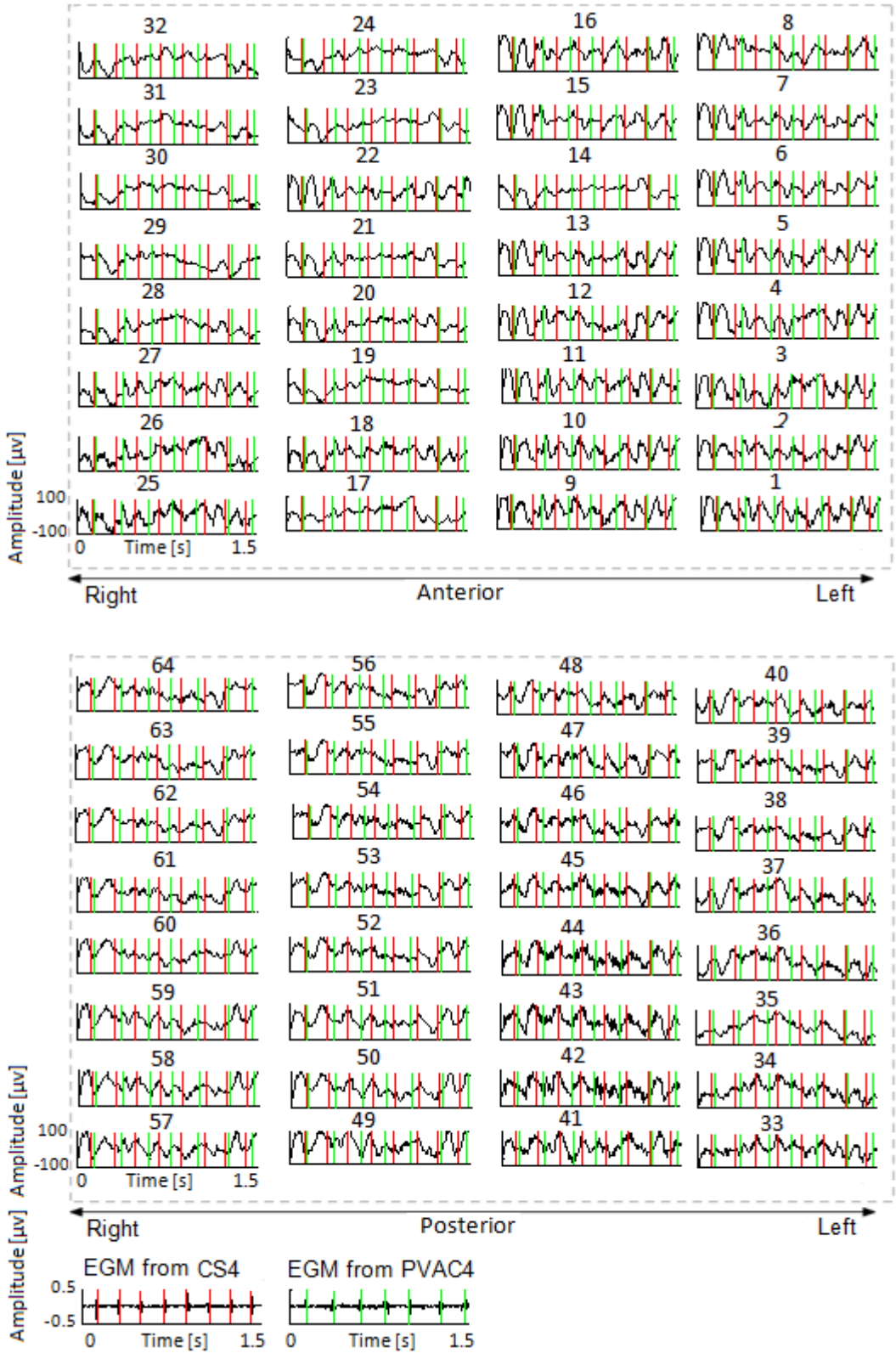

Figure 174. Spatial illustration of EGM activations time points on anterior (top) posterior (bottom) BSPM sites, subject 1. The CS4 and PVAC4 activations were mapped on BSPM signals, displayed as the red and green lines, respectively, on each site.

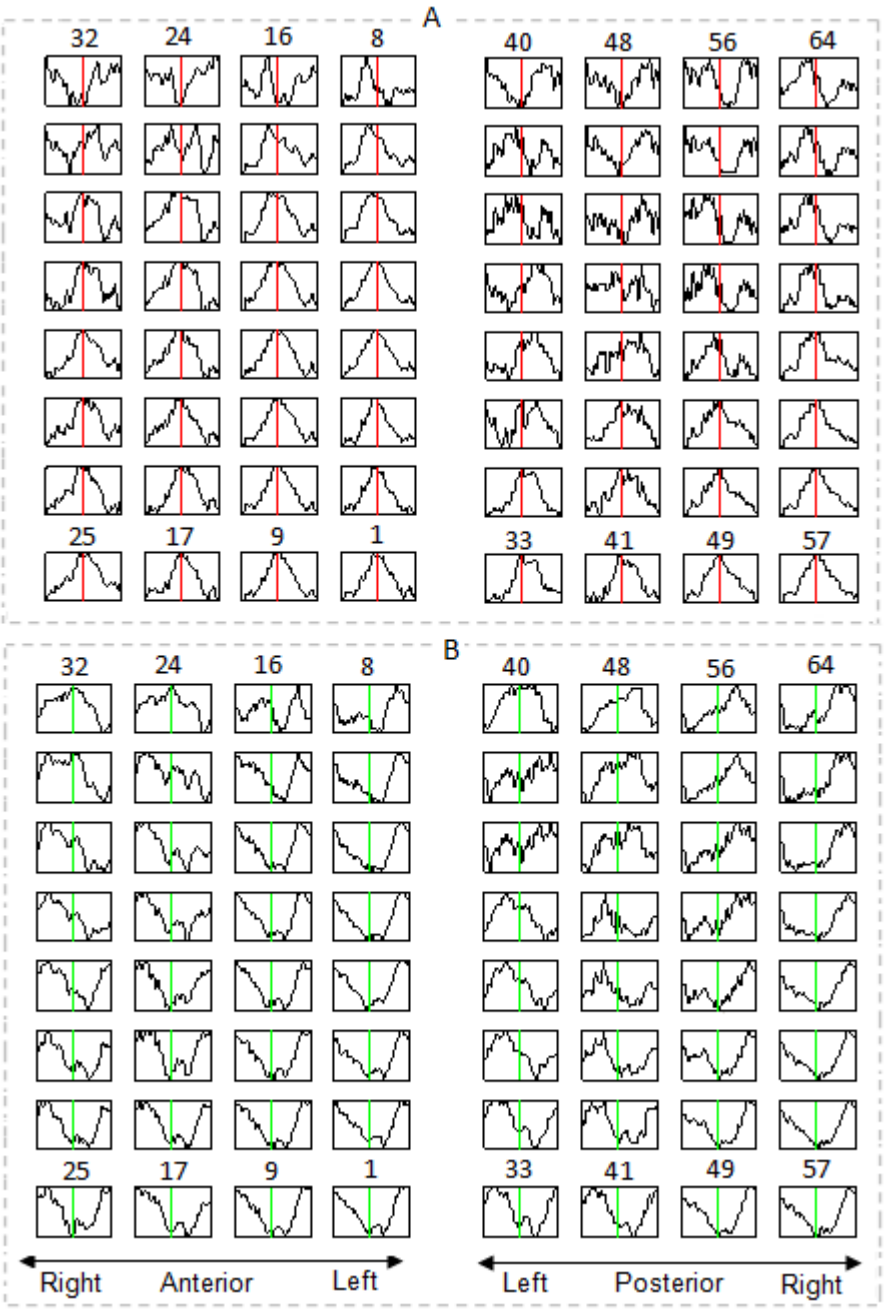

Figure 175. Spatial illustration of the average BSPM AA according to CS (A) and PVAC (B) activations for each site, subject 1. In each site the x-axis represents time with duration of 0.12 s, and the y-axis denotes normalised amplitude to the maximum of each site.

Visual inspection of all 20 subjects showed that in six subjects (1, 6, 7, 10, 19, and 20) the CS activations corresponded closer to the peak of AA on the lower body surface sites. However, the PVAC activations corresponded more with the trough of AA on these sites. In contrast, the CS activations corresponded closer to the trough and the PVAC activations corresponded

more with the peak of AA on the upper BSPM sites. On the body surface anterior central right sites the CS and PVAC activation time points moved between the peak and trough on a positive and negative gradient, respectively. Moreover, the generated BSPM average beat based on the EGM activations showed morphology of the AA on the majority of sites. This may suggest that the EGM activations were consistent on each body surface site. If this was not the case, the average would be flat or not have any clear morphology. Conversely, in three subjects (3, 8 and 9) the CS and PVAC activations were almost aligned with each other as well as with the peak of the AA on the body surface. In eleven subjects the EGM activations were more varied between the peak and trough in different body surface sites. Moving the location of the EGM time points on the body surface activations from lower to upper sites was more likely due to propagation of the AA which was a result of the temporal changes in the voltage distribution throughout the F-wave cycle or mechanism of the AF.

To quantify the results, correlation analysis between the body surface and intracardiac MCL were attempted as follows: the BSPM, CS and PVAC activations were detected separately from the longest AF segment. The mean of the time differences between the activations were calculated for each source. The idea was to identify if the MCL of any of the body surface sites had a large correlation with the CS and PVAC MCL. However, this study could not be completed as detection of the atrial activations on some of the body surface sites were impossible due to low amplitude and noise. Unfortunately this could not be tracked with the available study group. A greater number of subjects with the same AF history would be needed to draw firm conclusions.

Chapter Summary

The body surface sites close to the anterior upper right sites had larger P_{CS}, and the body surface sites close to the posterior lower right sites had larger P_{PVAC}. This suggested that at these sites EGM DF was closer to the BSPM DF which resulted higher power of EGM DF on the BSPM spectra. Moreover, all body surface sites detected EGM DF, such that in some sites it agreed with BSPM dominant peak and in some sites it agreed with BSPM non-dominant peak. There was no body surface site that did not have a corresponding (dominant or non-dominant) peak to EGM DF across all subjects. Moreover, there was no body surface site that did not have a corresponding (dominant or non-dominant) peak to either CS or PVACDF.

Chapter 9. Conclusion

9.1. Main Findings

In this thesis, the objectives that were outlined at each chapter have all been accomplished. This chapter summarises the main scientific contributions of these analysis.

Objective: Quantifying the AF characteristics in each subject allowing between subject comparisons.

Response: In this study, AF amplitude estimated from the body surface in 20 subjects ranged from 19.0 to 90.0 μV. AF DF estimated from the body surface ranged from 3.5 to 8 Hz between subjects which agreed with the DF estimated from inside the heart. AF SC between subjects ranged from 19.0% to 60.5% estimated from the body surface, and ranged from 21.0% to 90.0% estimated from inside the heart. It can be concluded that DF estimated from the body surface recordings represent main AF rate. However, SC estimated from the body surface recordings is unlikely to estimate AF degree of organisation. Subjects in organised AF had larger AF amplitude, lower DF and greater SC compared to subjects in complex AF. There was a consistent pattern of high AF characteristics on the anterior upper right body surface sites in all subjects. It can be concluded that these sites were best representative of AF characteristics on the body surface. Moreover, BMI explained approximately 20.0% of amplitude and DF variability estimated from the body surface compared to measurements from inside the heart.

Objective: Study of temporal and spatial variability of the AF characteristics.

Response: The AF characteristics estimated from the body surface and inside the heart were consistent over the two minute recordings.

The AF characteristic differences across the body surface in less organised AF suggested that body surface sites may capture atrial activations from different AF re-entrant pathways.

Objective: Comparing the AF characteristics estimated from the body surface and inside the heart.

Response: There was evidence of more accurate estimation of the AF characteristics using additional electrodes to lead V1 in the 12-lead ECG. The AF characteristics were apparent on all 64 body surface sites. However, the anterior upper central body surface sites were more likely to express AF from the CS recordings, and the posterior lower central body surface sites were more likely to express AF from the PVAC recordings. Overall the results suggested that the body surface site 22 was the best representative of the RA, and site 49 was the best representative of the LA.

9.2. Guide for Future Work

The following should be considered in future studies: subjects to be studied with the same AF histories and similar range of physiological factors, have more recording sites in the left atrium, include recording sites in the right atrium, and stay consistent in anatomical location across subjects. These would help to compare intracardiac signals with body surface recordings more accurately.

9.3. Clinical Application

Covering the anterior and posterior sides of the torso and calculating the median across them would provide more precise estimation of the AF characteristics. This may not be practical due to additional cost, the extra time taken and the need for additional training of the cardiac technicians. Some additional electrodes to the 12-lead ECG on the posterior lower body surface may facilitate estimation of the AF characteristics from the left atrium.

Appendix A

Illustration of More Sophisticated Intracardiac Recording Systems

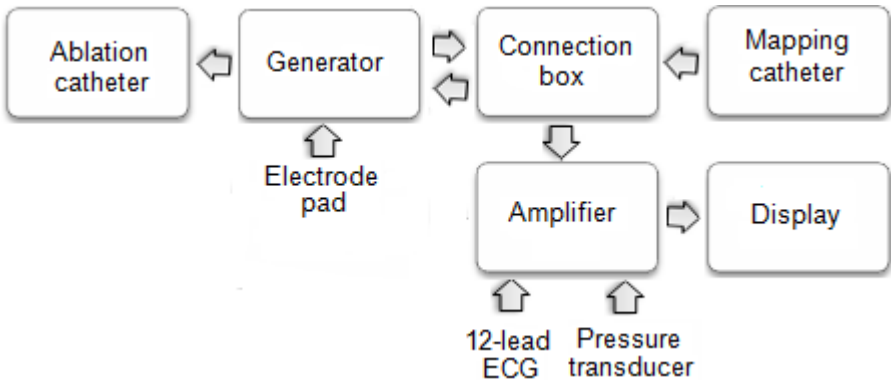

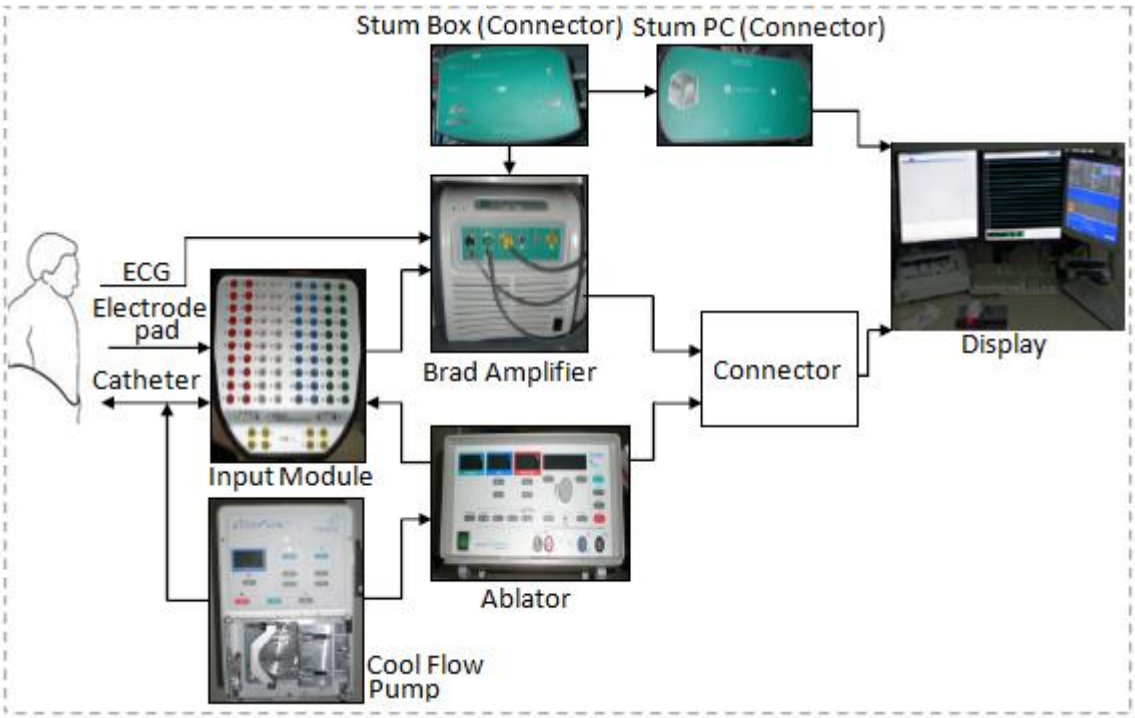

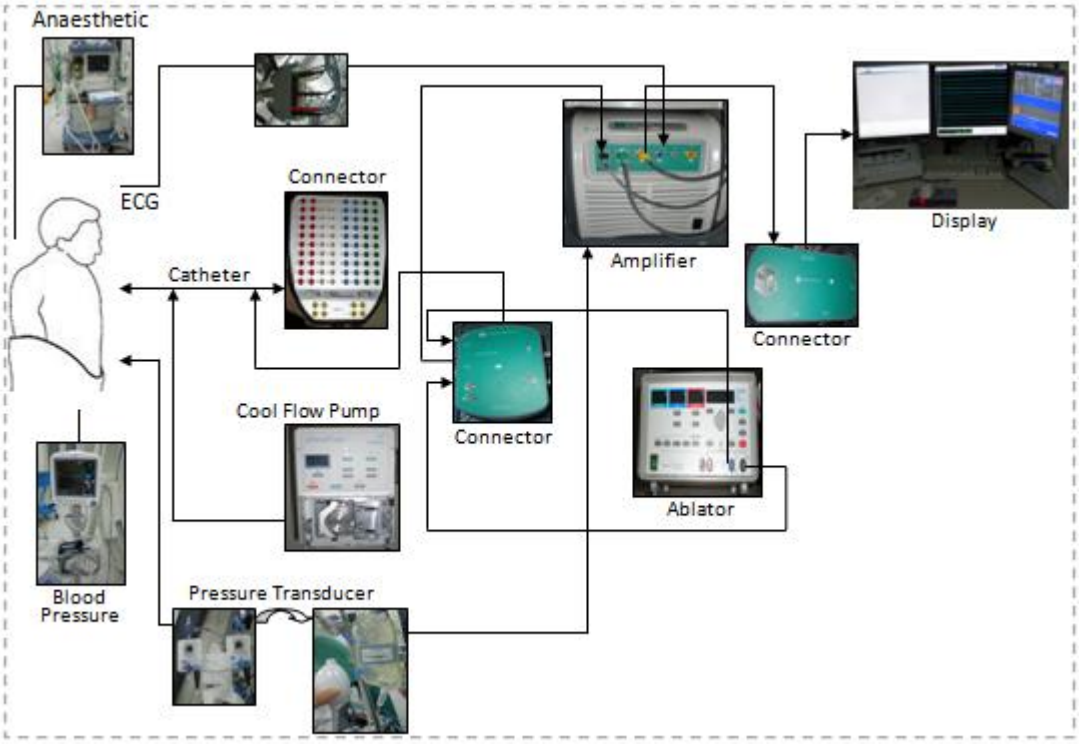

Catheter, amplifier, and display have been explained in Chapter 2. Generator, electrode pads, and pressure transducer are explained below.

Generator: The GENius™ multi-channel RF generator, generates RF energy that is delivered to the heart by the PVAC catheter with the following specifications: A thermocouple (for temperature measurement), maximum temperature limit 100°C, RF output frequency 450-550 kHz, impedance range 40-250 ohm, and power 100 watt. Typically values for the energy vary between 15 and 40 watt. In temperature control, basically a target temperature is set, when the temperature reaches this target and then become consistent power is subsequently varied to maintain the temperature. For ablation purposes, energy is delivered from one electrode to another (two poles). The number of times energy is pulsed between the electrodes is also set. In fact the number of pulses in relation to the selected electrodes (energy delivery between two poles) gives the ablation. There are different ratios available from 1:1 to 4:1. The choice of ratio is dependent on the thickness of tissue and the depth of the

required lesion. 1:1 is typically used for a 7 mm burn, whereas 4:1 is 3 mm burn in depth. A small footprint allows placement in nearly any location.

Electrode Pads: Electrode pads, dispersive electrode, patient plate, grounding pad or return electrode has a large and wide surface area, promotes low current density, which in turn can be safely directed out of the patient's body during the EP procedure to prevent burn. It prevents patient burns if the surgical instruments become accidentally energized during the procedure. The electrode pad also is designed to offset the noise.

Pressure Transducer: A pressure transducer is used for direct blood pressure measuring. It converts the mechanical pressure to an electrical signal that is displayed on a monitor. It includes a domed portion which is connected to a line interposed in a patient's blood supply system (e.g. vein). A sterile solution serves to interface the patient's blood system and the pressuring measuring apparatus. The Wheatstone bridge is a measuring instrument and is used to measure an unknown electrical resistance by balancing two legs of a bridge circuit, one leg of which includes the unknown component.

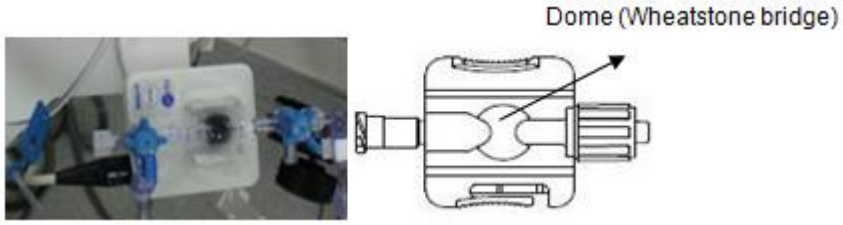

Its operation is similar to the original potentiometer. A tube attached at the end of the catheter is connected to the pressure transducer hose, which is joined to pressure bag. The pressure bag is placed with saline and inflates to 200-300 mmHg to ensure adequate pressure exists above the patient’s systolic measurement. Pressure in the heart pushes down the fluid on the tube and it goes all the way down to the end of the tube and deflects the black dome, and

that goes upon on screen. This setup allows 1–3 ml per hour of flush solution to be delivered through the catheter to maintain patency, minimize clot formation, and prevent backflow of blood from the catheter as it sits in the pulmonary artery. The low-compliance tubing from the flush system is in turn connected to a pressure transducer a device that translates one form of energy into another. As the catheter moves through the heart chambers, pulsating waves created by changes in the systolic and diastolic pressures within the heart are transmitted from the catheter tip through the low-compliance tubing to the diaphragm of this transducer. These pulsations induce motion on the diaphragm and are converted to low-voltage electric signals that are transmitted via the cables to the bedside monitor. A time-temperature curve is plotted which represents the time it takes for the blood to change from a warmer baseline temperature to a cooler temperature after the injection and then back to the baseline temperature as the blood circulates.

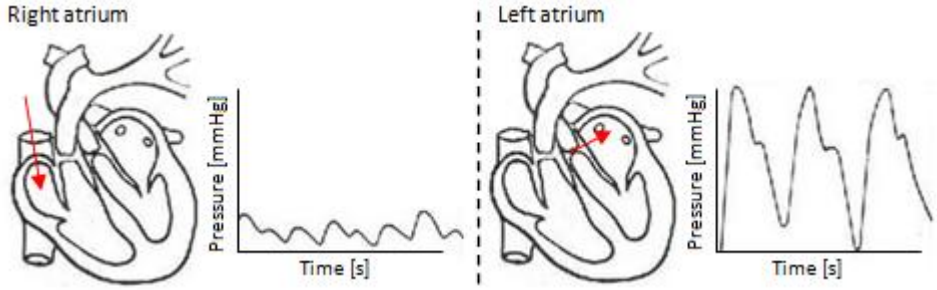

At the monitor, these signals are amplified, filtered, and displayed as pressure waveforms and numerical pressure readings. These waveforms change as the catheter progresses through the heart during insertion, letting clinicians know exactly where in the heart the catheter is. It's important to continuously monitor these waveforms to ensure that the catheter does not slip into other chambers, example below. A chest radiograph is always used to verify the placement.

Appendix B

Participant Information Sheet

Relationship Between Intracardiac and Body Surface Potentials
November 2010

An invitation to take part in a pilot research study
You are being invited to take part in a pilot research study. Before you decide it is important for you to understand why the research is being done and what it will involve. Please take time to read the following information carefully and discuss it with others if you wish. Ask us if there is anything that is not clear or if you would like more information. Take time to decide whether or not you wish to take part.

What is the purpose of the study?
The electrocardiogram (12-lead ECG) is a simple measurement for detecting heart abnormal heart rhythms from body surface. We believe there is important information contained in the ECG which is currently not used. In order to test this we need to record electrocardiograms with more than 12 leads in patients with abnormal heart rhythms.

Why have I been chosen?
Patients with abnormal heart rhythms will be asked to take part in this study. So you may have been asked to take part because you have an abnormal heart rhythm.

Do I have to take part?
It is up to you to decide whether or not to take part. If you do decide to take part you will be given this information sheet to keep and be asked to sign a consent form. If you decide to take part you are still free to withdraw at any time and without giving a reason. Your decision to withdraw at any time or not to take part, will not affect the standard of care that you receive.

What will happen to me if I take part?
You will be having your routine electrophysiological (EP) study to manage your irregular heart rhythm.

Prior to entering the theatre you will have 32 electrodes attached to your chest and 32 electrodes attached to your back as shown in the picture. Attaching the electrodes will take less than 10 minutes. Once you are on the theatre table and ready for the EP study, a 5 minute ECG recording will be taken.

The clinician will then perform their standard procedure of the EP study, and ECG recording will be taken at several intervals throughout the EP study. This does not interrupt or effect EP study.

At the end of the procedure a final 5 minute ECG recording will be taken before you go to the recovery area where the electrodes will then be removed.
Another 5 minute ECG recording will be taken before you discharge from hospital and it can be done at any time which is convenient for you.


Is there any risk in taking part?
There is no risk from ECG electrodes although there might be slight discomfort from having electrodes attached on the body. If you request we can remove the electrodes at any time.

Will my taking part in this study be kept confidential?
Your participation will be kept confidential and your ECG data will be anonymised and allocated a study number. Your personal details will not be seen by anyone.

What will happen to the results of the research study?
We hope to publish the results of this research in science, medical and medical engineering journals, at conferences, and through press releases. No personal data is published.

Who is organising and funding the research?
This is a PhD research study undertaken by Marjan Bojarnejad. It is being organised by the lead researcher Dr Philip Langley, the director of Medical Physics Department Professor Allan Murray, and Dr John Bourke Cardiologist at Freeman Hospital. It is funded party by the Engineering and Physical Sciences Research Council (EPSRC) and partly by Medical Faculty of Newcastle University.

Contact for further information,
If you have any questions or would like further information please contact:

Miss Marjan Bojarnejad
Medical Physics Department
Freeman Hospital
Newcastle upon Tyne
NE7 7DN
Tel. 0191 2336161 ext 26727
Marjan.bojarnejad@nuth.nhs.uk

Appendix C

Effect of BMI on the Atrial Fibrillation Characteristics Figures

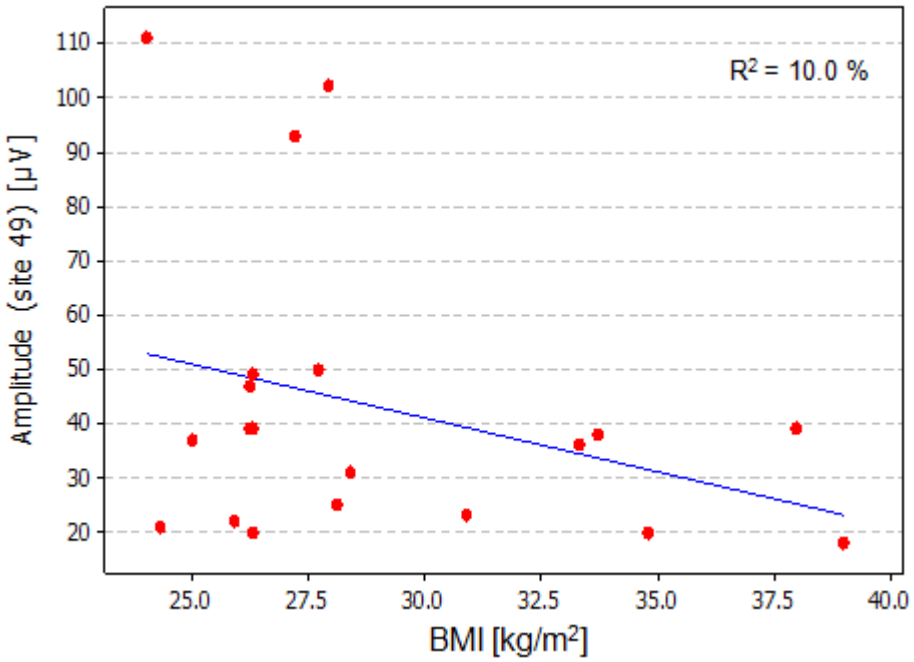

Figure C-1: Linear relationship between BMI and AF amplitude estimated from site 49.

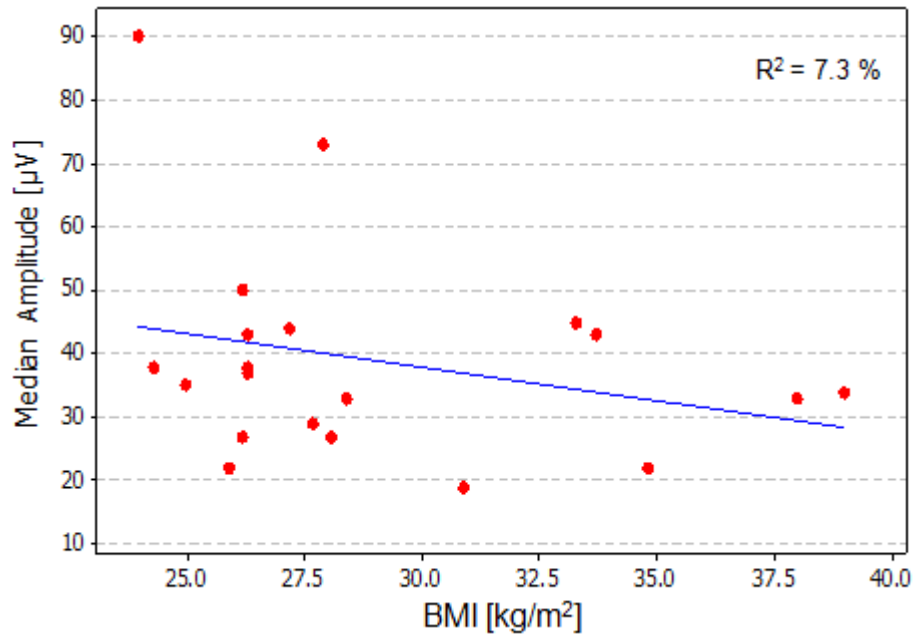

Figure C-2: Linear relationship between BMI and the median AF amplitude estimated across the body surface sites.

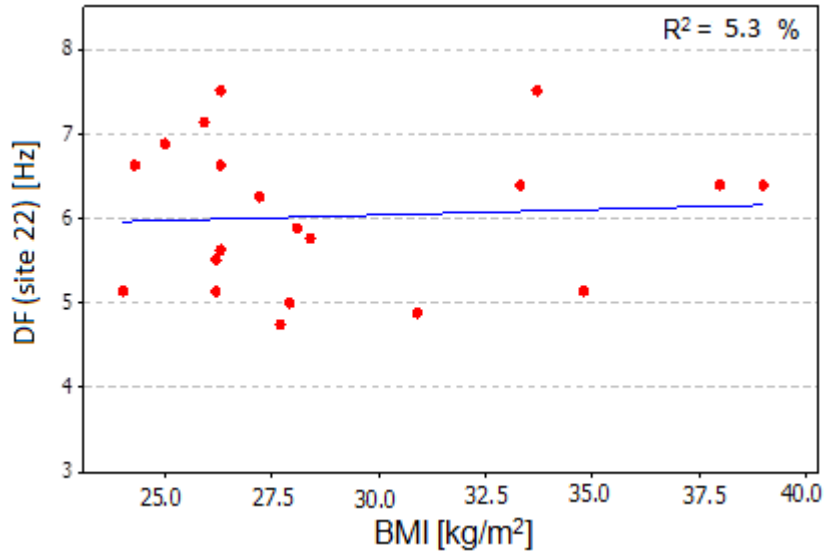

Figure C-3: Linear relationship between BMI and AF DF estimated from site 22.

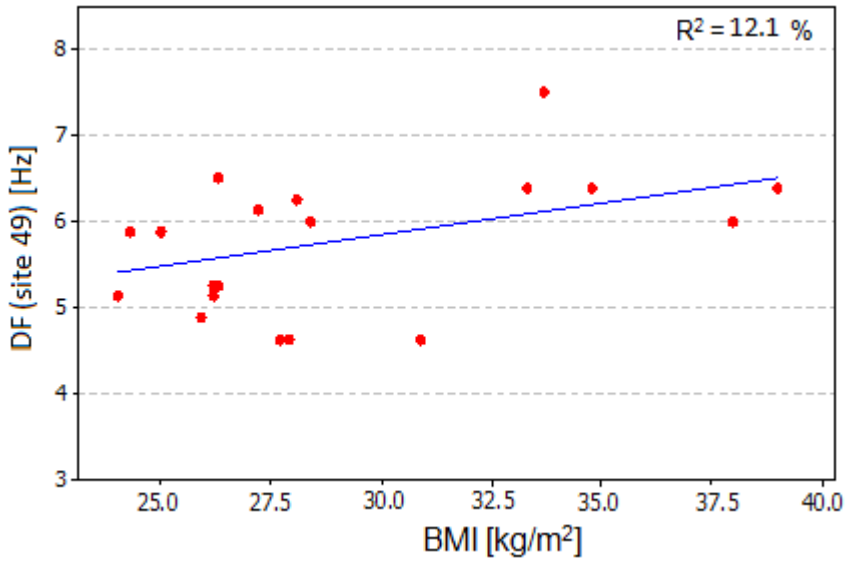

Figure C-4: Linear relationship between BMI and AF DF estimated from site 49.

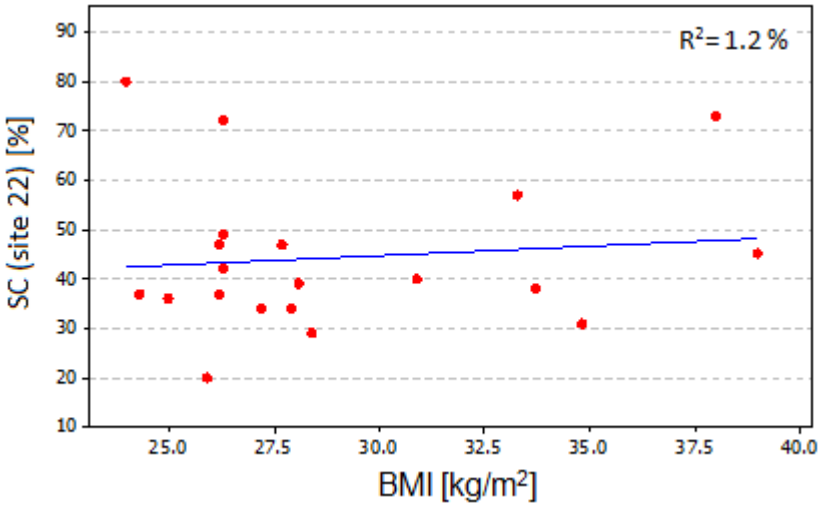

Figure C-5: Linear relationship between BMI and AF SC estimated from site 22.

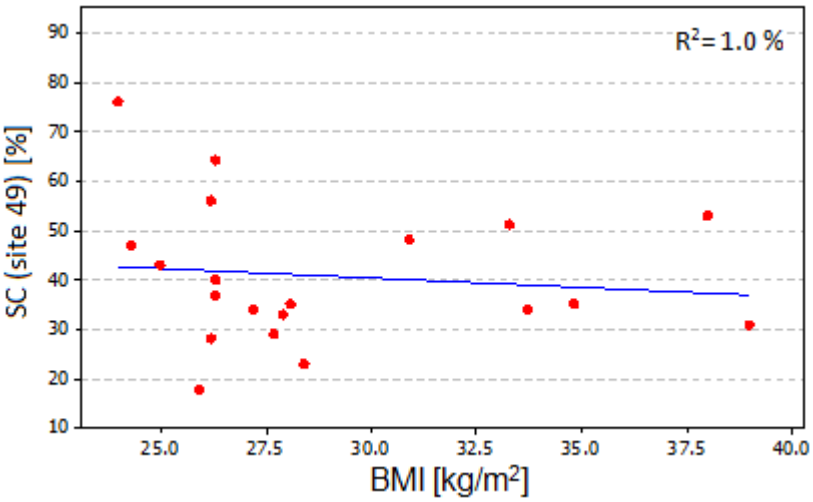

Figure C-6: Linear relationship between BMI and AF SC estimated from site 49.

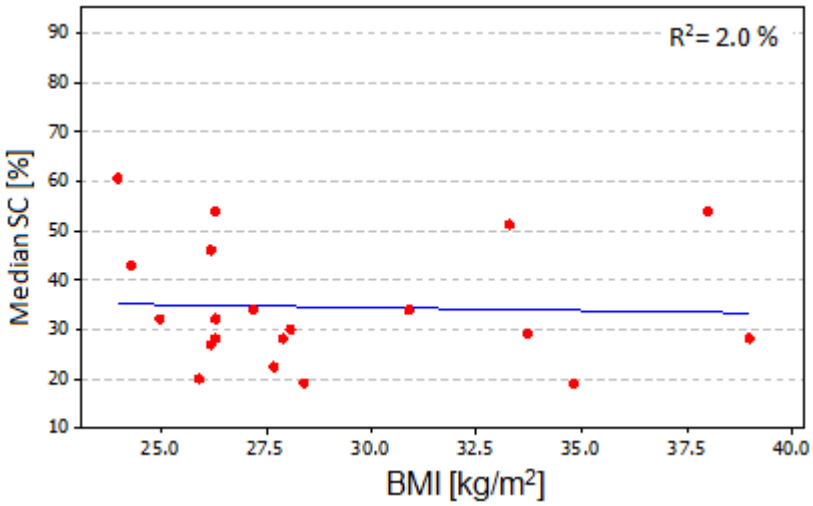

Figure C-7: Linear relationship between BMI and the median SC estimated across the body surface sites.

Appendix D

Spatial Variability of the Atrial Fibrillation Characteristics Tables

AF Amplitude [μV]			
Sources	**p-value**	**Sources**	**p-value**
A_LL and A_CL	0.004	**A_CR and P_LL**	<0.001
A_LL and A_CR	<0.001	**A_CR and P_CL**	<0.001
A_LL and A_LR	0.044	**A_CR and P_CR**	<0.001
A_LL and P_LL	<0.001	**A_CR and P_LR**	<0.001
A_LL and P_CL	0.001	**A_LR and P_LL**	<0.001
A_LL and P_CR	0.019	**A_LR and P_CL**	<0.001
A_LL and P_LR	0.017	**A_LR and P_CR**	<0.001
A_CL and A_CR	0.001	**A_LR and P_LR**	<0.001
A_CL and A_LR	0.881	**P_LL and P_CL**	0.117
A_CL and P_LL	<0.001	**P_LL and P_CR**	0.017
A_CL and P_CL	<0.001	**P_LL and P_LR**	0.023
A_CL and P_CR	<0.001	**P_CL and P_CR**	0.015
A_CL and P_LR	<0.001	**P_CL and P_LR**	0.052
A_CR and A_LR	<0.001	**P_CR and P_LR**	0.881

Table 18. AF amplitude paired comparison between the vertical lines.

AF Amplitude [μV]					
Sources	**p-value**	**Sources**	**p-value**	**Sources**	**p-value**
1 and 2	<0.001	**3 and 15**	0.001	**7 and 13**	0.427
1 and 3	<0.001	**3 and 16**	<0.001	**7 and 14**	<0.001
1 and 4	0.001	**4 and 5**	0.244	**7 and 15**	0.002
1 and 5	0.002	**4 and 6**	0.001	**7 and 16**	0.438
1 and 6	0.642	**4 and 7**	<0.001	**8 and 9**	0.187
1 and 7	0.044	**4 and 8**	<0.001	**8 and 10**	0.163
1 and 8	0.698	**4 and 9**	0.001	**8 and 11**	0.365
1 and 9	0.234	**4 and 10**	<0.001	**8 and 12**	0.001
1 and 10	0.301	**4 and 11**	<0.001	**8 and 13**	0.079
1 and 11	0.796	**4 and 12**	0.079	**8 and 14**	0.179
1 and 12	0.002	**4 and 13**	0.001	**8 and 15**	0.088
1 and 13	0.023	**4 and 14**	<0.001	**8 and 16**	0.039
1 and 14	0.163	**4 and 15**	<0.001	**9 and 10**	0.959
1 and 15	0.301	**4 and 16**	0.003	**9 and 11**	0.088
1 And 16	0.002	**5 and 6**	0.005	**9 and 12**	0.003
2 and 3	<0.001	**5 and 7**	0.001	**9 and 13**	0.277
2 and 4	0.017	**5 and 8**	0.001	**9 and 14**	0.001
2 and 5	0.013	**5 and 9**	0.004	**9 and 15**	0.063
2 and 6	<0.001	**5 and 10**	0.003	**9 and 16**	0.014
2 and 7	<0.001	**5 and 11**	0.001	**10 and 11**	0.438
2 and 8	<0.001	**5 and 12**	0.211	**10 and 12**	0.017
2 and 9	0.001	**5 and 13**	0.007	**10 and 13**	0.66
2 and 10	<0.001	**5 and 14**	<0.001	**10 and 14**	0.013
2 and 11	<0.001	**5 and 15**	<0.001	**10 and 15**	0.023
2 and 12	0.002	**5 and 16**	0.109	**10 and 16**	0.121
2 and 13	<0.001	**6 and 7**	0.717	**11 and 12**	0.001
2 and 14	<0.001	**6 and 8**	0.365	**11 and 13**	0.088
2 and 15	<0.001	**6 and 9**	0.535	**11 and 14**	0.056
2 and 16	<0.001	**6 and 10**	0.698	**11 and 15**	0.134
3 and 4	<0.001	**6 and 11**	0.535	**11 and 16**	0.039
3 and 5	<0.001	**6 and 12**	0.004	**12 and 13**	0.01
3 and 6	<0.001	**6 and 13**	0.605	**12 and 14**	<0.001
3 and 7	<0.001	**6 and 14**	0.179	**12 and 15**	0.001
3 and 8	<0.001	**6 and 15**	0.056	**12 and 16**	0.163
3 and 9	<0.001	**6 and 16**	0.196	**13 and 14**	0.011
3 and 10	<0.001	**7 and 8**	0.002	**13 and 15**	0.026
3 and 11	0.001	**7 and 9**	0.329	**13 and 16**	0.352
3 and 12	<0.001	**7 and 10**	0.301	**14 and 15**	0.301
3 and 13	<0.001	**7 and 11**	0.021	**14 and 16**	0.002
3 and 14	0.001	**7 and 12**	0.004	**15 and 16**	0.015

Table 19. AF amplitude paired comparison between the horizontal lines.

AF SC [%]			
Source			p-value
Left_Anterior	and	Right_Anterior	0.001
Right_Anterior	and	Left_Posterior	0.972
Right_Anterior	and	Right_Posterior	0.942
Left_Anterior	and	Left_Posterior	0.002
Left_Anterior	and	Right_Posterior	0.009
Left_Posterior	and	Right_Posterior	0.739

Table 20. AF SC paired comparison between the left and right sites.

AF SC [%]			
Sources	p-value	Sources	p-value
A_LL and A_CL	0.003	A_CR and A_LR	0.655
A_LL and A_CR	<0.001	A_CR and P_CL	0.008
A_LL and A_LR	<0.001	A_CR and P_CR	0.017
A_LL and P_LL	0.258	A_CR and P_LR	0.004
A_LL and P_CL	0.008	A_LR and P_LL	0.001
A_LL and P_CR	0.013	A_LR and P_CL	0.006
A_LL and P_LR	0.020	A_LR and P_LR	0.005
A_CL and A_CR	<0.001	P_LL and P_CR	0.028
A_CL and A_LR	<0.001	P_LL and P_CL	0.033
A_CL and P_LL	0.057	P_LL and P_LR	0.058
A_CL and P_CL	1.000	P_LR and P_CR	0.020
A_CL and P_CR	0.763	P_LR and P_LR	0.564
A_CL and P_LR	0.492	P_CL and P_LR	0.617
A_CR and P_LL	0.001	P_CR and P_LR	0.157

Table 21. AF SC paired comparison between the vertical lines.

References

Abacherli R., Leber R., Lemay L., Kappenberger L., (2009). Development of a toolbox for electrocardiogram-based interpretation of atrial fibrillation. Journal of Electrocardiology; 42: 517–521.

Abibullaev B., and Don Seo H., (2011). A new QRS detection method using wavelets and artificial neural networks. Journal of Medical Systems; 35(4): 683-691.

Alcaraz R. and Rieta J.J. (2009a). Time and frequency recurrence analysis of persistent atrial fibrillation after electrical cardioversion. Physiol Meas; 30(5):479-489.

Alcaraz R. and Rieta J.J. (2010). A review on sample entropy applications for the non-invasive analysis of atrial fibrillation electrocardiograms. Biomedical Signal Processing and Control; 5(1): 1–14.

Alcaraz R., and Rieta J.J. (2009d). Sample entropy of the main atrial wave predicts spontaneous termination of paroxysmal atrial fibrillation Med. Eng. Phys; 31:917–922.

Alcaraz R., and Rieta J., (2009b). Surface ECG organization analysis to predict paroxysmal atrial fibrillation termination. Comput Biol Med; 39(8):697-706.

Alcaraz R., and Rieta J., (2009c). Non-invasive organization variation assessment in the onset and termination of paroxysmal atrial fibrillation. computer methods and programs in biomedicine; 9 (3):148–154.

Alcaraz R., and Rieta J.J., (2008). Adaptive singular value cancelation of ventricular activity in single-lead atrial fibrillation electrocardiograms. Physiological Measurement. Physiol. Meas; 29(12):1351.

Allessie M.A., Bonke F.I, Schopman F.J., (1977). Circus movement in rabbit atrial muscle as a mechanism of tachycardia. The leading circle concept: a new model of circus movement in cardiac tissue without the involvement of an anatomical obstacle. Circ Res; 41:9-18.

Allessie M.A., Lammers W.J.E.P., Bonke F.I.M., Hollen J., (1985). Experimental evaluation of Moe's multiple wavelet hypothesis of atrial fibrillation. Cardiac Electropysiology and Arrhythmias; 265–275.

Alpert J.S., (2005). Cardiology for the primary care physician. Publisher Birkhauser; Edition 4, ISBN: 1573402125 and 9781573402125.

Anfinsen G., (2002). Non-pharmacological treatment of atrial fibrillation. Indian Pacing Electrophysiol Journal; 2(1): 4–14.

Arzeno N., Deng Z., Poon CH., (2008). Analysis of first-derivative based QRS detection algorithms. IEEE Trans Biomed Eng; 55(2): 478–484.

Barquero-Perez O., Rojo-Alvarez J.L., Requena-Carriion J., Alonso-Atienza. F., Everss E., Goya-Esteban R., Sanchez-Munoz J.J., Garcia-Alberola A., (2009). Cardiac arrhythmia spectral analysis of electrogram signals using Fourier organization analysis. Computers in Cardiology; 36:333−336.

Baykaner T., Clopton P., Krummen D., Shivkumar K., Sehra R., Miller J., Rappel W., Narayan S., (2012). Determinants of the number of localized sources for human atrial fibrillation. Journal of the American College of Cardiology; 59(3): E690.

Biffi M., and Boriani G., (2003). Atrial remodelling: evolving concepts. Indian Pacing Electrophysiol J; 3(2): 81–88.

Bollmann A., and Lombardi, F., (2006b). Electrocardiology of atrial fibrillation. IEEE Engineering in Medicine and Biology Magazine; 25(6):15-23.

Bollmann A., Husser D., Mainardi L., Lombardi F., Langley P., Murray A., Rieta J.J, Millet J., Olsson S.B., Stridh M. and Sörnmo L., (2006a). Analysis of surface electrocardiograms in atrial fibrillation: techniques, research, and clinical applications. Oxford Journals Medicine EP Europace; 8(11): 911-926.

Bollmann A., Kanuru N.K., McTeague K., Walter P., DeLurgio D., Langberg J., (1998). Frequency analysis of human atrial fibrillation using the surface electrocardiogram and its response to ibutilide. Am J Cardiol; 81:1439–1445.

Bollmann A., Klein H.U., Esperer H.D., (2000a). Determination of fibrillatory frequency for assessment of the atrial electrophysiologic state in human atrial fibrillation special consideration of a non-invasive approach. Herzschr Elektrophys; 11:77–87.

Bollmann A., Sonne K., Esperer H., Toepffer I., and Klein H., (2000b). Circadian variations in atrial fibrillatory frequency in persistent human atrial fibrillation. Pacing Clin. Electrophysiol; 23: 1867–1871.

Bond R.R, Finlay D.D., Nugent Ch.D, Moore G., (2010). A Web-based tool for processing and visualizing body surface potential maps. Journal of Electrocardiology; 43: 560–565.

Botteron G.W., Joseph M. Smith J.M., (1995). A Technique for measurement of the extent of spatial organization of atrial activation during atrial fibrillation in the intact human heart. IEEE Transactions on Biomedical Engineering; 42(6):579-586.

Botteron G.W., and Smith JM., (1996). Quantitative assessment of the spatial organization of atrial fibrillation in the intact human heart. Circulation; 93:513-518.

Calkins H. (Chair), and Brugada J., (co-Chair) (2007). European Heart Rhythm Association, European Cardiac Arrhythmia Society, American College of Cardiology, American Heart Association, Society of Thoracic Surgeons. HRS/EHRA/ECAS Expert consensus statement on catheter and surgical ablation of atrial fibrillation: recommendations for personnel, policy, procedures and follow-up. Heart Rhythm; 4:816-861.

Capucci A., Biffi M., Boriani G., Ravelli F., Nollo G., Sabbatani P., Orsi C., Magnani B., (1995). Dynamic electrophysiological behaviour of human atria during paroxysmal atrial fibrillation. Circulation; 92:1193–1202.

Castells F., Igual J., Millet J., Rieta J.J., (2005). Atrial activity extraction from atrial fibrillation episodes based on maximum likelihood source separation. Signal Processing; 85(3): 523–535.

Castells F., Mora C., Rieta J.J., Moratal-Perez D., Millet J., (2005a). Estimation of atrial fibrillatory wave from single-lead atrial fibrillation electrocardiograms using principal component analysis concepts. Medical and Biological Engineering and Computing; 43(5):557-560.

Castells F., Ruiz R., Rieta J.J., Millet J., (2003). An integral atrial wave identification approach based on spatiotemporal source separation: Clinical validation. IEEE Computers in Cardiology; 30:717–720.

Castells, F., Rieta, J.J., Millet, J., Zarzoso, V., (2005b). Spatiotemporal Blind Source Separation approach to atrial activity estimation in atrial tachyarrhythmias. IEEE Trans. Biomed. Eng; 52(2): 258- 267.

Chiarugi F., Sakkalis V., Emmanouilidou D., Krontiris T., Varanini M., Tollis I., (2007a). Adaptive threshold QRS detector with best channel selection based on a noise rating system. Computers in Cardiology; 34:157−160.

Chiarugi F., Varanini M., Cantini F., Conforti F. and Vrouchos G., (2007b). Non-invasive ECG as a tool for predicting termination of paroxysmal atrial fibrillation IEEE Trans. Biomed. Eng; 54:1399–1406.

Chilukuri k., Dukes J., Calkins H., (2010). Outcomes in patients requiring cardioversion following catheter ablation of atrial fibrillation. J Cardiovasc Electrophysiol. Blackwell Publishing; 21(1):27-32.

Chouhan V.S., and Mehta S.S., (2008). Detection of QRS complexes in 12-lead ECG using adaptive quantized threshold. International Journal of Computer Science and Network Security; 8(1): 155-163.

Cohn L. H., (2008). Cardiac surgery in the adult. Publisher McGraw-Hill Professional. Edition 3, ISBN 0071469133 and 9780071469135.

Corino V., Mainardi L.T., Bollmann A., Husser D., Stridh M. Sörnmo L., (2007). A gaussian mixture model for time–frequency analysis of atrial fibrillation electrocardiograms. IEEE Conf. Eng. Med. Biol; 271–274.

Cotter P.E., Martin P.J,. Ring L., Warburton E.A., Belham M., Pugh P.J., (2013). Incidence of atrial fibrillation detected by implantable loop recorders in unexplained stroke. Neurology; 80(17):1546-1550.

Cox J.L., Boineau J.P., Schuessler R.B., Ferguson T.B., Cain M.E., Lindsay B.D., Corr P.B., Kater K.M., Lappas D.G., (1991). Successful surgical treatment of atrial fibrillation. Review and clinical update. JAMA; 266:1976-1980.

Cox J.L., Boineau J.P., Schuessler R.B., Kater K.M., Lappas D.G., (1993). Five-year experience with the maze procedure for atrial fibrillation. Ann. Thorac. Surg; 56, 814-824.

Cox J.L., Jaquiss R.D., Schuessler R.B., Boineau J.P., (1995). Modification of the maze procedure for atrial flutter and atrial fibrillation. II. Surgical technique of the maze III procedure. J. Thorac. Cardiovasc. Surg; 110: 485-495.

Di Marco L., Bourke J.P., Langley P., (2012). Spatial complexity and spectral distribution variability of atrial activity in surface ECG recordings of atrial fibrillation. Medical & Biological Engineering & Computing; 50(5):439-46.

Di Marco, L.Y King S., Borke J., Chiari L., Murray A., Langley P., (2011). Time-frequency analysis of atrial fibrillation comparing morphology-clustering based QRS-T cancellation with blind source separation in multi-lead surface ECG recordings. Computing in Cardiology; ISBN: 978-1-4577-0612-7: 269 – 272.

Donnelly M.P., Finlay D.D., Nugent Ch.D., Black N.D., (2008).
Lead selection: old and new methods for locating the most electrocardiogram information. Journal of Electrocardiology; 41: 257–263.

Donnelly M.P., Nugent Ch. D., Finlay D.D., Rooney N.F., Black N.D., (2006). Diagnosing old MI by searching for a linear boundary in the space of principal components. IEEE Transactions on Information Technology in Biomedicine; 10: 3.

Do-Un J., Se-Jin K., (2008). Development of a technique for cancelling motion artifact in ambulatory ECG monitoring system. Third international conference on convergence and hybrid information technology. ISBN: 978-0-7695-3407-7, 954-961.

Elgendi M., Jonkman M., Boer D., (2009). Improved QRS detection algorithm using dynamic thresholds. International Journal Of Hybrid Information Technology; 2:1.

Elvan A., Linnenbank A. C., Beukema W.P., De Bakker M.T., (2009). Dominant frequency of atrial fibrillation correlates poorly with atrial fibrillation CL. Circ Arrhythm Electrophysiol; 2: 634-644.

Everett TH., Kok L.C., Vaughn R.H., Moorman J.R., Haines D.E., (2001). Frequency domain algorithm for quantifying atrial fibrillation organization to increase defibrillation efficacy. IEEE Trans. Biomed. Eng; 48 (9): 969–978.

Faes L., Nollo G., Antolini R., Gaita F., Ravelli F., (2002). A method for quantifying atrial fibrillation organization based on wave-morphology similarity. IEEE transactions on biomedical engineering; 49:12.

Faes L., Nollo G., Kirchner M., Olivetti E., Gaita F., Riccardi R., Antolini R., (2001). Cluster analysis for measuring the local organisation of human atrial fibrillation. Med. Biol. Eng. Comput; 39: 656-663.

Fagan T.P. (2002). The cardiovascular system. Edition 2. Elsevier Spain: Health Sciences. ISBN 072343249X.

Finlay D.D., Nugent Ch.D., Donnelly M.P., Lux R.L., McCullagh P.J., Black N.D., (2006). Selection of optimal recording sites for limited lead body surface potential mapping: A sequential selection based approach. BMC Medical Informatics and Decision Making; 6:9.

Finlay D.D., Nugent Ch.D., McCullagh P.J., Black N.D., (2005). Mining for diagnostic information in body surface potential maps: A comparison of feature selection techniques. BioMedical Engineering OnLine; 4:51.

Furlanello F., Lupo P., Pittalis M., Foresti S., Vitali-Serdoz L., Francia P., De Ambroggi G., Ferrero P., Nardi S., Inama G., De Ambroggi L., Cappato R., (2008). Radiofrequency catheter ablation of atrial fibrillation in athletes referred for disabling symptoms preventing usual training schedule and sport competition. J Cardiovasc Electrophysiol; 19:457-462.

Fuster V., Ryden L.E., Cannom D.S., (2006). ACC/AHA/ESC guidelines for the management of patients with atrial fibrillation: a report of the American College of Cardiology/American Heart Association Task Force on Practice Guidelines and the European Society of Cardiology Committee for Practice Guidelines. Circulation; 114 (7): e257–354.

Ganz L., and Saperia G., (2012). Catheter ablation of cardiac arrhythmias: Overview and technical aspects. Up to date for patients. Available from; www.uptodate.com.

Garrey W.E., (1914). The nature of fibrillary contraction of the heart: its relation to tissue mass and form. Am J Physiol; 33: 397-414.

Griffin B.P., Kapadia S.R., Rimmerman C.M., (2012). The cleveland clinic cardiology board review. Lippincott Williams & Wilkins. ISBN 13: 9781451177404, ISBN 10: 1451177402.

Guillem M.S., Climent A.M., Millet J., Arenal A., Fernandez-Aviles F., Jalife J., Atienza F., Berenfeld O., (2013). Non-invasive localization of maximal frequency sites of atrial fibrillation by body surface potential mapping. Circ Arrhythm Electrophysiol; 6(2): 294-301.

Guillem M.S., Quesadab A., Donisa V., Climenta A.M., Mihib N., Millet J., Castellsa F., (2009). Surface wavefront propagation maps: non-invasive characterization of atrial flutter circuit. International Journal of Bioelectromagnetism; 11(1): 22-26.

Habel N., Znojkiewicz P., Thompson N., Muller J.G., Mason B., Calame J., Spector P, (2010). The temporal variability of dominant frequency and complex fractionated atrial EGM constrains the validity of sequential mapping in human atrial fibrillation. HeartRhythm; 7(5): 586-593.

Hamilton P., (2002). Open source ECG analysis software documentation. Available from: www.eplimited.com.

Hanninen H., Takala P., Makjijarvi M., Katila T., Toivonen L., (2001). Recording locations in multichannel magnetocardiography and body surface potential mapping sensitive for regional exercise-induced myocardial ischemia. Basic Res Cardiol; 96: 405 -414.

Hargittai S., (2008). Efficient and fast ECG baseline wander reduction without distortion of important clinical information. Computers in Cardiology; 35: 841−844.

Hayn D., Kollmann A., Schreier G., (2007). Predicting initiation and termination of atrial fibrillation from the ECG Biomed. Tech; 52:5–10.

Hoekema R, Uijen G., van Oosterom A., (1999a). On selecting a body surface mapping procedure. Journal of Electrocardiology; 32(2): 93-101.

Hoekema R., Uijen G., Van Oosterom A., (1999b). The number of independent signals in body surface maps. Method Inform. Med; 38(2): 119–124.

Hoekstra B.P. T., Diks C.G. H., Allessie M.A., DeGoede J., (1995). Nonlinear analysis of epicardial atrial electrograms of electrically induced atrial fibrillation in man. J. Cardiovasc. Electrophysiol; 6: 419–40.

Hoekstra B.P., Diks C.G., Allessie M.A., DeGoede J., (1997). Nonlinear analysis of the pharmacological conversion of sustained atrial fibrillation in conscious goats by the class Ic drug cibenzoline. Chaos; 7(3):430-446.

Hoekstra B.P.T., Diks C.G.H., Allessie M.A., DeGoede J., (2000). Spatial correlation analysis of atrial activation patterns during sustained atrial fibrillation in conscious goats. Archives of Physiology and Biochemistry; 108(4): 313–331.

Holm M., Pehrson S., Ingemansson M., So¨rnmo L., Johansson R., Sandhall L., Sunemark M., Smideberg B., Olsson Ch., Olsson S.B., (1998). Non-invasive assessment of the atrial cycle length during atrial fibrillation in man: introducing, validating and illustrating a new ECG method. Cardiovascular Research; 38: 69–81.

Houben R., and Allessie M., (2006). Processing of intracardiac electrograms in atrial fibrillation. Engineering in Medicine and Biology Magazine, IEEE; 25:6.

Hsu N.W., Lin Y.J., Tai C.T., Kao T., Chang S.L., Wongcharoen W., Lo L.W., Udyavar A.R., Hu Y.F., Tso H.W., Chen Y.J., Higa S., Chen S.A., (2008). Frequency analysis of the fibrillatory activity from surface ECG lead V1 and intracardiac recordings: implications for mapping of AF. Europace; 10:438–43.

Husser D., Stridh M., Cannom D.S., Bhandari A.K., Girsky M.J., Kang S., Sörnmo L., Olsson S.B., Bollmann A., (2007). Validation and clinical application of time–frequency analysis of atrial fibrillation electrograms. J. Cardiovasc. Electrophysiol;18:41–6.

Husser D., Stridh M., Sörnmo L., Bertil Olsson S., Bollmann A., (2004). Frequency analysis of atrial fibrillation from the surface electrocardiogram. Indian Pacing and Electrophysiology Journal; ISSN: 0972-6292, 4(3):122-136.

Husser D., Stridh M., Sornmo L., Geller Ch., Klein H.U., Bollmann A., (2005). Corresponding author contact information, E-mail the corresponding authorTime–frequency analysis of the surface electrocardiogram for monitoring antiarrhythmic drug effects in atrial fibrillation. The American Journal of Cardiology; 95 (4): 526–528.

Husser D., Stridh M., Sörnmo L., Toepffer I, Bollmann A., (2006). Electroatriography time-frequency analysis of atrial fibrillation from modified 12-Lead ECG configurations for improved diagnosis and therapy. Medical Hypotheses; 68: 568–573.

Ihara Z.,Van Oosterom A., Jacquemet V., Hoekema R., (2007). Adaptation of the standard 12-lead electrocardiogram system dedicated to the analysis of atrial fibrillation. Journal of Electrocardiology; 68.e1– 68.e8.

Jacek M., Norbert H., (2005). ECG baseline wander and power line interference reduction using nonlinear filter bank. Signal Processing; 85(4): 779–781.

Jarman J.W., Wong T., Kojodjojo P., Spohr H., Davies J.E., Roughton M., Francis D.P., Kanagaratnam P., Markides V., Davies D.W., Peters N.S., (2012). Spatiotemporal behaviour of high dominant frequency during paroxysmal and persistent atrial fibrillation in the human left atrium. Circ Arrhythm Electrophisiology; 5(4): 650-658.

Kandori A., Hosono T., Kanagawa T., Miyashita S., Chiba Y., Murakami M., Miyashita T., Tsukada K., (2002). Detection of atrial-flutter and atrial-fibrillation waveforms by fetal magnetocardiogram. Med Biol Eng Comput; 40(2): 213-217.

Karimifard S., Ahmadian A., (2011). A robust method for diagnosis of morphological arrhythmias based on Hermitian model of higher-order statistics. BioMedical Engineering OnLine; 10: 22.

Karthikeyan P., Murugappan M., Yaacob S., (2012). ECG Signal denoising using wavelet thresholding techniques in human stress assessment. InternationalJournal on Electrical Engineering and Informatics; 4:2.

Kenneth M., (1995). From delirium cordis to atrial fibrillation: historical development of a disease concept. Ann Intern Med.; 122(11): 867-873.

Kim H., Min C., and Kim T., (2006). Adaptable noise reduction of ECG signals for feature extraction. School of Information, Communications and Electronics Engineering, Catholic University of Korea, LNCS 3973; 586-591.

Kim M., (2012). Catheter Ablation of Atrial Fibrillation in Octogenarians: The Right “Medicine?”. Journal of Cardiovascular Electrophysiology; 23(7): 694–696.

Klabunde R. E., (2005). Cardiovascular physiology concepts. Lippincott Williams and Wilkins; Second Edition, ISBN: 978-1-4511-1384-6.

Klamor C., Grimmel K., Lentz N., Bolz A., (2011). Spatiotemporal QRST cancellation method for 3-lead ECGs. IFMBE Proceedinds; 43: 61-64.

Kohler B.U., Hennig C., Orlgmeister R., (2002). The principles of software QRS detection. IEEE Trans Eng. Med Biol Mag; 21(1):42–57.

Kornreich F., (1997). Appropriate electrode placement in evaluating varied cardiac pathology. In Liebman J (ed) Electrocardiology ‘96. From the cell to the body surface. publ World Scientific; 83-92.

Kornreich F., MacLeod R.S., Lux R.L., (2008). Supplemented standard 12-lead electrocardiogram for optimal diagnosis and reconstruction of significant body surface map patterns. Journal of Electrocardiology; 41: 251–256.

Kozakevicius A., (2004). Adaptive ECG filtering and QRS detection using orthogonal wavelet transform. Universidade Federal de Santa Maria-Camobi, Santa Maria. Biomedical Engineering; 485.

Kozlikova K., (2007). P-Wave body surface iso-integral maps in children and in young adults. Physiol. Res; 56: S123-S128.

Kozlikova K., Martinka J., Murin J., Bulas J., (2011). The opposite polarity of the PQ segment compared to the P-Wave isointegral maps. Physiol. Res; 60: 777-784.

Krandycheva V.V., Kharin S.N., Shmakov D.N., (2006). P-wave body surface potential distribution in rats. J Electrocardiol; 39(1): 88-92.

Laguna P., (1992). Adaptive filtering of ECG baseline wander. International Conference of the IEEE; 2: 508 – 509.

Langley P., Bourke J.P., Murray A., (2000). Frequency analysis of atrial fibrillation. Computers in Cardiology; 27:65-68.

Langley P., Rieta J.J., Stridh M., Millet J., Sörnmo L., Murray A., (2006). Comparison of atrial signal extraction algorithms in 12-lead ECGs with atrial fibrillation. IEEE Trans Biomed Eng; 53(2): 343-6.

Langley P., Stridh M., Rieta J.J.,Sörnmo L.,Millet-Roig J.,Murray A., (2002). Comparison of atrial rhythm extraction techniques for the estimation of the main. atrial frequency from the 12-lead electrocardiogram in atrial fibrillation. Comput. Cardiol; 29: 29–32.

Lazar S., Dixit S., Marchlinski F.E., Callans D.J., Gerstenfeld E.P., (2004). Presence of left-to-right atrial frequency gradient in paroxysmal but not persistent atrial fibrillation in humans. Circulation; 110: 3181-3186.

Lemay M., Jacquemet V., Forclaz A., Vesin J., Kappenberger L., (2005). Spatiotemporal QRST cancellation method using separate QRS and T-Waves templates. IEEE; 32: 611−614.

Lemay M., Vesin J., Van Oosterom A., Jaquemet V., Kappenberger L., (2007). Cancellation of ventricular activity in the ECG: evaluation of novel and existing methods IEEE Trans. Biomed. Eng; 54(3): 542–546.

Leski J.M, Henzel N., (2005). ECG baseline wander and power line interference reduction using nonlinear filter bank. Signal Processing ; 85: 781–793.

Levkon Ch., Mihov G., Ivanov R., Daskalov I., Christon I., Dotsinsky I., (2005). Removal of power-line interference from the ECG: a review of the subtraction procedure. BioMedical Engineering OnLine; 4:50.

Lian J., Li G., Cheng J., Avitall B., He B., (2002). Body surface laplacian mapping of atrial depolarization in healthy human subjects. Med. Bio. Eng. Comput; 40: 650-659.

Lickfett L., Schwab J., Lewalter Th., (2008). Advanced mapping techniques in atrial fibrillation. J Interv Card Electrophysiol; 22:155–159.

Liem, L.B., Downar, E. (2001). Progress in catheter ablation: clinical application of new mapping and ablation technology. The Netherlands: Kluwer Academic Publishers. ISBN:1402001479.

Lin Y., Tai C., Kao T., Tso H.W., , Higa S., Tsao H.M., Chang S.L., Hsieh M.H., Chen S.A., (2006). Frequency analysis in different types of paroxysmal atrial fibrillation. Journal of the American College of Cardiology; ISSN: 0735-1097/06. 47:7.

Lip G.Y., Beevers D.G. (1996). ABC of atrial fibrillation. BMJ; ISBN 0727910701.

MacFarlane P.W., Van Oosterom A., Pahlm O., (2010). Comprehensive electrocardiology. Springer-Verlag London Limited. ISBN: 978184882046.

Mainardi L .T., Porta A., Calcagnini G., Bartolini P., Michelucci A., Cerutti S., (2001). Linear and non-linear analysis of atrial signals and local activation period series during atrial-fibrillation episodes Med. Biol. Eng. Comput; 39:249–254.

Mak, J. N.F., Hu Y., , Luk, K. D.K., (2010). An automated ECG-Artifact removal method for trunk muscle surface EMG recordings. Medical Engineering & Physics; 32(8): 840-848.

Mansour M., (2006). Highest dominant frequencies in atrial fibrillation a new target for ablation? Am Coll Cardiol; 47(7):1408-1409.

McCarthy P.M., Castle L.W., Maloney J.D., Trohman R.G., Simmons T.W., White R.D., Klein A.L., Cosgrove D.M., (1993). Initial experience with the maze procedure for atrial fibrillation. J. Thorac. Cardiovasc. Surg; 105:1077-1087.

Medvegy M., Duray G., Pinter A., Prkda I., (2002). Body surface potential mapping: historic backpound, present possibilities, diagnostic A.N.E; 7:2.

Meurling C., Waktare J., Holmqvist F., Hedman A., Camm A., Olsson S., Malik M., (2001). Diurnal variations of the dominant cycle length of chronic atrial fibrillation. Am. J. Physiol; 280: 401–406.

Meurling C.J., Waktare J.E , Holmqvist F., Hedman A., Camm A.J., Olsson S.B., Malik M., (2001). Diurnal variations of the dominant cycle length of chronic atrial fibrillation. The American Physiological Society; 280: H401-H406.

Milnor W. R., (1990). Cardiovascular physiology. Publisher: Oxford University Press US, ISBN: 0195058844 and 9780195058840.

Moe G.K., (1962). Multiple wavelet hypothesis of atrial fibrillation. Arch. Int. Pharmacodyn. Ther. 140: 183–188.

Moe G.K., and Abildskov J.A., (1959). Atrial fibrillation as a self-sustaining arrhythmia independent of focal discharge. Am Heart J; 58: 59-70. (Reference from: Steinberg J.S, Zelenkofske S., Wong S.C., Gelernt M., Sciacca R., Menchavez E., (1993). Value of the P-wave signal-averaged ECG for predicting atrial fibrillation after cardiac surgery. Circulation; 88:2618-2622)

Morganroth J., Horowitz L.N., Josephson M.E., Kastor and J.A., (1979). Relationship of atrial fibrillatory wave amplitude to left atrial size and etiology of heart disease. An old generalization re-examined. Amer. Heart J.; 97: 184–186.

National Clinical Guideline Centre (NCGC).National Clinical Guideline of Royal College of Physician, (2010). National Clinical Guideline for Management of AF: Royal College of Physicians. Available online: www.guidance.nice.org.uk/CG36.

Nattel S., (2002a). New ideas about atrial fibrillation 50 years on Macmillan Magazines Ltd. Nature; Vol. 415.

Nattel S., (2002b). Therapeutic implications of atrial fibrillation mechanisms: can mechanistic insights be used to improve AF management? Cardiovascular Research; 54: 347–360.

Ng J., Borodyanskiy A.I., Chang E.T., Villuendas R., Dibs S., Kadish A.H., Goldberger J.J., (2010). Measuring the complexity of atrial fibrillation electrograms. J Cardiovasc Electrophysiol; 21(6): 649-655.

Ng J., Borodyanskiy A.L., Chang E.T., Villuendas R., Samer Dibs, Kadish A.H., Goldberger J.J., (2010). Measuring the Complexity of Atrial Fibrillation Electrograms. Journal of Cardiovascular Electrophysiology; 21(6): 649–655.

Ng J., Goldberger J.J., (2007). Understanding and Interpreting dominant frequency analysis of AF electrograms. J Cardiovasc Electrophysiol; 18(6): 680-685.

Ng J., Passman R.S., Arora R., Kadish A.H., Goldberger J.J., (2012). Paradoxical change in atrial fibrillation dominant frequencies with baroreflex-mediated parasympathetic stimulation with phenylephrine infusion. J Cardiovasc Electrophysiol; 23(10): 1045-1050.

Ng J., Villuendas R., Cokic I., Schliamser J.E., Gordon D., Koduri H., Benefield B., Simon J., Murthy S.N., Lomasney J.W., Wasserstrom J.A., Goldberger J.J., Aistrup G.L., Arora R., (2011). Autonomic remodelling in the left atrium and pulmonary veins in heart failure: creation of a dynamic substrate for atrial fibrillation. Circ Arrhythm Electrophysiol; 4(3): 388-396.

Nguyen M., Schilling Ch., Dossel O., (2009). A new approach for frequency analysis of complex fractionated atrial electrograms. 31st Annual International Conference of the IEEE EMBS; ISBN: 978-1-4244-3296-7.

Nilsson F., Stridh M., Bollmann A., Sörnmo L., (2006). Predicting spontaneous termination of atrial fibrillation using the surface ECG. Med. Eng. Physics; 28: 802–808.

Nollo G., Marconcini M., Faes L., Bovolo F., Ravelli F., Bruzzone L., (2008). An automatic system for the analysis and classification of human atrial fibrillation patterns from intracardiac electrograms. IEEE Trans. Biomed. Eng; 55: 2275–2285.

Petrutiu S., Jason N.G., Nijm Grace M., Al-angari H., (2006). Atrial fibrillation and waveform characterization. IEEE Engineering In Medicine And Biology Magazine; 25:6.

Petrutiu S., Sahakian A.V., Fisher W., Swiryn S., (2009). Manifestation of left atrial events and inter-atrial frequency gradients in the surface electrocardiogram during atrial fibrillation: contributions from posterior leads. J. Cardiovasc. Electrophysiol; 20: 1231–1236.

Petrutiu S., Sahakian A.V., Swiryn S., (2007). Short-term dynamics in fibrillatory wave characteristics at the onset of paroxysmal atrial fibrillation in humans. J. Electrocardiol; 40: 155–160.

Phlypo R., Zarzoso V., Lemahieu I,. (2010). Atrial activity estimation from atrial fibrillation ECGs by blind source extraction based on a conditional maximum likelihood approach. Med Biol Eng Comput; 48(5): 483-488.

Portet F., Hernandez A.I., Carrault G., (2005). Evaluation of real-time QRS detection algorithms in variable contexts. Med Biol Eng Comput ; 43(3): 379–385.

Prinzmetal M., Corday E., Brill I.C., (1950). Mechanism of the auricular arrhythmias. Circulation; 1:241-245.

Rahman M., (2009). An efficient noise cancellation technique to remove noise from the ecg signal using normalized signed regressor. LMS Algorithm; ISBN: 9780769538853, 257-260.

Raine D., Langley P., Murray A., Dunuwille A., Bourke J.P., (2004). Fibrillation: A Tool For Evaluating the Effects of Intervention. Cardiovasc Electrophysiol; 15:1021-1026.

Raitt M.H, and Kusumoto W., (2012). Correlations among the frequencies of atrial activity on the surface electrocardiogram, intracardiac atrial electrograms,

and the atrial effective refractory period in patients with atrial fibrillation. J Electrocardiol; 45(3): 296-303.

Ravi K.C., Krummen D.E., Tran A.J., Bullinga J.R., Narayan S.M, (2009). Electrocardiographic measurements of regional atrial fibrillation cycle length. Pacing Clin Electrophysiol; 32(1): S66–S71.

Richman J.S., and Moorman J.R., (2002). Physiological time-series analysis using approximate entropy and sample entropy, Am. J. Physiol. Heart Circ. Physiol; 278: H2039–H2049.

Richter U., Faes L., Cristoforetti A., Mase M., Ravelli F., Stridh M., Sörnmo L., (2011). A novel approach to propagation pattern analysis in intracardiac atrial fibrillation signals. Annals of Biomedical Engineering; 39:1.

Rieta J.J., (2004). Atrial activity extraction for atrial fibrillation analysis using blind source separation. Biomedical Engineering, IEEE Transactions; 51:7.

Rooijakkers M.J, Rabotti Ch., Oei S.G., Mischi M., (2012). Low-complexity R-peak detection for ambulatory fetal monitoring. Physiol. Physiological Measurement; 33:7.

Salinet Jr J.L., Ahmad A., Brown P.D., Stafford P., Ng G.A., Schlindwein F.S., (2010). Three-dimensional Frequency mapping from the noncontact unipolar electrograms in atrial fibrillation. Computing in cardiology; ISSN: 0276-6547, P: 745 – 748.

Sanchez C., Millet J; Rieta J.J; Castells F., Francisco J.;Rodenas J.; Ruiz-Granel R., Ruiz, V. (2002). Packet wavelet decomposition: An approach for atrial activity extraction. Computers in Cardiology; ISBN: 0-7803-7735-4, 33 – 36.

Sanchez J., Marin F., Roldan V., Lip G.Y., (2008). The impact of statin use on atrial fibrillation. QJM: An International Journal of Medicine; 101(11):845-861.

Sandberg F., (2007). Time-Frequency analysis of atrial fibrillation. Thesis for the degree of licentiate in engineering. Printed in Sweden by Tryckeriet.

Sandberg F., Bollmann A., Husser D., Stridh1 M., Sörnmo1 L., (2010). Circadian variation in dominant atrial fibrillation frequency in persistent atrial fibrillation. Centre for Integrative Electrocardiology (CIEL), Lund University, Sweden. Department of Electrophysiology, Heart Centre, University Leipzig, Germany. IOP PUBLISHING. Physiol. Meas; 31: 531–542.

Sanders P., Nalliah Ch. J., Takahashi Y., Hocini M., Rotter M., Rostock Th., Sacher F., Hsu L., HaIssaguerre M., (2006). Frequency mapping of the pulmonary veins in paroxysmal versus permanent atrial fibrillation. J Cardiovasc Electrophysiol; 17: 965-972.

Sheldon M., and Mansour M., (2009). The relationship between electrogram CL and dominant frequency in patients with persistent atrial fibrillation. J Cardiovasc Electrophysiol; 20: 1336-1342.

Shimizu A., Yoshiga Y., Yamagata T., Esato M., Doi M., Kakugawa H., Matsuzaki M., (2003). New method of determining the atrial fibrillation cycle length during human atrial fibrillation. J Cardiovasc Electrophysiol; 14: 965-970.

Shkurovich S., Sahakian A.V., Swiryn S., (1998). Detection of atrial activity from high-voltage leads of implantable ventricular defibrillators using a cancellation technique. IEEE Transactions On Biomedical Engineering; 45:2.

Shusterman V., Ismail Shah S., Beigel A., Anderson K.P., (2000). Enhancing the precision of ECG baseline correction: selective filtering and removal of residual error. Computers and Biomedical Research; 33(2): 144–160.

Sih H.J., Zipes D.P., Berbari E.J., Olgin J.E., (1999). A high-temporal resolution algorithm for quantifying organization during atrial fibrillation. IEEE Trans. Biomed. Eng; 46 (4): 440–450.

Slocum J., Byrom E., McCarthy L., Sahakian A., Swiryn S., (1985). Computer detection of atrioventricular dissociation from surface electrocardiograms during wide QRS complex tachycardia. Circulation; 72:1028–1036.

Sörnmo L., (1998). Time-varying digital filtering of ECG baseline wanders. Medical & Biological Engineering & Computing; 31: 503-508.

Sörnmo L., Stridh M., Husser D., Bollmann A., Olsson S.B., (2009). Analysis of atrial fibrillation: from electrocardiogram signal processing to clinical measurement. Phil. Trans. R. Soc; 367: 235-253.

Stridh M., and Sörnmo L., (2001). Spatiotemporal QRST cancellation techniques for analysis of atrial fibrillation. Biomedical Engineering, IEEE Transactions on; 48(1): 105 – 111.

Stridh M., Sörnmo L., Meurling C., Olsson S., (2004). Sequential characterization of atrial tachyarrhythmias based on ECG time–frequency analysis. IEEE Trans. Biomed. Eng; 51:100–114.

Takahashi Y., O'Neill M.D., Haïssaguerre M., (2008). Characterization of electrograms associated with termination of chronic atrial fibrillation by catheter ablation. Journal of the American College of Cardiology; 51:10.

Thurmann M., (1965). Coarse atrial fibrillation in congenital heart disease. Circulation; 32: 290-292.

Trahanias P.E., (1993). An approach to QRS complex detection using mathematical morphology. Biomedical Engineering, IEEE Transactions on; 40(2): 201 – 205.

Trobec R., (2003). Computer analysis of multichannel ECG. Computers in Biology and Medicine; 33: 215–226.

Tso HW., Kao T., Lin YJ., Tai CT., Chen SA., (2005). Role of sinus node during atrial fibrillation: a novel insight from regional frequency analysis. Computers in Cardiology; 32: 65−68.

Van Oosterom A., Ihara Z, Jacquemet V., Hoekema R., (2007). Vectorcardiographic lead systems for the characterization of atrial fibrillation . Journal of Electrocardiology; 40: 343.e1– 343.e11.

Vaya C., and Rieta J.J., (2009). Time and frequency series combination for non-invasive regularity analysis of atrial fibrillation. Med Biol Eng Comput; 47:687–696.

Vaya C., Rieta J.J., Sanchez C., Moratal D., (2007). Convolutive blind source separation algorithms applied to the electrocardiogram of atrial fibrillation: study of performance. IEEE Trans. Biomed. Eng; 54 (8):1530–1533.

Waktare J., Hnatkova K., Murgatroyd F., Guo X., Camm A.J., Malik M., (1998). Atrial ectopics prior to atrial fibrillation onset. Annals of Noninvasive Electrocardiology; 3(2):115–118.

Walsh S., and King E., (2007). Pulse diagnosis: a clinical guide. Publisher Elsevier Health Sciences; ISBN: 0443102481 and 9780443102486.

Wanger, G.S., (2008). Marriott's practical electrocardiography. Edition 11. USA: Lippincott Williams & Wilkins. ISBN: 9780781797382.

Watanabe Y., Kohgame Y., Nakano H., Abo Y., Mizuno Y., (1988). P-wave changes in body surface potential maps due to increasing heart rate during exercise in normals. Jpn Circ J; 52(4): 349-356.

Wattigney W.A., Mensah G.A., Croft J.B ., (2002). Increased atrial fibrillation mortality: United States, 1980-1998. Am. J. Epidemiol; 155 (9): 819–26.

Wijffels M.C., Kirchhof C.J., Dorland R., Allessie M.A., (1995). Atrial fibrillation begets atrial fibrillation: a study in awake chronically instrumented goats. Circulation 92: 1954–1968.

Xi Q., Sahakian A., Frohlich T.G., Ng J., Swiryn S., (2004b). Relationship between patterns of occurrence of atrial fibrillation and surface electrocardiographic fibrillatory wave characteristics. Heart Rhythm; 1: 656–663.

Xi Q., Sahakian A.V., Ng J., Swiryn S., (2004a). Atrial fibrillatory wave characteristics on surface electrogram: ECG to ECG repeatability over twenty-four hours in clinically stable patients. J. Cardiovasc. Electrophysiol; 15: 911–919.

Xi Q., Sahakian A.V., Swiryn S., (2003). The effect of QRS cancellation on atrial fibrillatory wave signal characteristics in the surface electrocardiogram. Journal of Electrocardiology; 36(3): 243-249.

Xua L., Zhangb D., Wanga K., Lia N., Wangc X., (2007). Computers in biology and medicine 37 (2007) 716 – 731, 0010-4825, 2006 Elsevier Ltd.

Yamada T., Fukunami M., Shimonagata T., Kumagai K., Sanada S., Ogita H., Asano Y., Hori M., Hoki N., (1999). Dispersion of signal-averaged P-wave duration on precordial body surface in patients with paroxysmal atrial fibrillation. Eur Heart J; 20(3): 211-220.

Yoshida K., Tada H., Ogata K., Sekiguchi Y., Inaba T., Ito Y., Sato Y., Sato A., Seo, Y., Kandori A., Aonuma K., (2012). Electrogram organization predicts left atrial reverse remodelling after the restoration of sinus rhythm by catheter ablation in patients with persistent atrial fibrillation. Heart Rhythm 2012; 9:1769 –1778.

Ziad F., Issa M., Douglas P., (2008). Clinical arrhythmology and electrophysiology: a companion to Braunwald's heart disease. Publisher Elsevier Health Sciences; ISBN 1416059989 and 9781416059981.

Zimetbaum P.J., and Josephson M.E., (2003). Use of the electrocardiogram in acute myocardial infarction. N Engl J Med; 348: 993-940.